Gene regulation dynamics of the flagellar master regulatory operon *flhDC* in *Salmonella enterica* serovar Typhimurium

Von der Fakultät für Lebenswissenschaften

der Technischen Universität Carolo-Wilhelmina zu Braunschweig

zur Erlangung des Grades

einer Doktorin der Naturwissenschaften

(Dr. rer. nat.)

genehmigte

D i s s e r t a t i o n

von Caroline Kühne

aus Halle (Saale)

1. Referentin: Professorin Dr. Petra Dersch
2. Referentin: Professorin Dr. Susanne Engelmann
eingereicht am: 19.12.2016
mündliche Prüfung (Disputation) am: 23.02.2017

Druckjahr 2017

Vorveröffentlichungen der Dissertation

Teilergebnisse aus dieser Arbeit wurden mit Genehmigung der Fakultät für Lebenswissenschaften, vertreten durch die Mentorin der Arbeit, in folgenden Beiträgen vorab veröffentlicht:

Publikationen

Singer H. M., Kühne C., Deditius J. A., Hughes K. T., and Erhardt M. (2014): The *Salmonella* Spi1 virulence regulatory protein HilD directly activates transcription of the flagellar master operon *flhDC*. *Journal of Bacteriology* 196(7): 1448–1457.

Kühne C., Singer H. M., Grabisch E., Codutti L., Carlomagno T., Scrima A., and Erhardt M. (2016): RflM mediates target specificity of the RcsCDB phosphorelay system for transcriptional repression of flagellar synthesis in *Salmonella enterica*. *Molecular Microbiology* 101(5): 841–855.

Tagungsbeiträge

Kühne C., Singer H. M., and Erhardt M. (2013): HilD is a transcriptional activator of the flagellar master regulator *flhDC* (Poster). EMBO|EMBL Symposium: New Approaches and Concepts in Microbiology, Heidelberg.

Singer H. M., Kühne C., Deditius J. A., Hughes K. T., and Erhardt M. (2014): The *Salmonella* Spi1 virulence regulatory protein HilD directly activates transcription of the flagellar master operon *flhDC* (Poster). North Regio Day on Infection, NoRDI V, Braunschweig.

Kühne C., Bergmiller T., Guet C. C., and Erhardt M. (2016): Bistable expression of the flagellar master regulator FlhDC in *Salmonella enterica* serovar Typhimurium (Poster). Gordon Research Conference Sensory Transduction in Microorganisms, Signaling Diversity in Microbial Systems. Ventura, CA, USA.

Table of Contents

List of Figures

List of Tables

List of Abbreviations

A	adenine
Amp^R	ampicillin resistance
AMP	adenosine-3´-5´-monophosphate
APS	ammonium persulfate
Ara	arabinose
ASM	American Society for Microbiology
Asp; D	aspartic acid; aspartate
AnTc	anhydrotetracycline
BLAST	Basic Local Alignment Search Tool
BP	band-pass filter
bp	base pair
BSA	bovine serum albumin
C	cytosine
°C	degree Celsius
cAMP-CRP	cyclic AMP receptor protein complex
CARD	caspase activation and recruitment domain
CCD	charge-coupled device
c-di-GMP	3´-5´-cyclic-diguanosine monophosphate
Cm^R	chloramphenicol resistance
CoA	coenzyme A
Ct	threshold cycle
CTAB	cetyl trimethylammonium bromide
CTD	C-terminal domain
Cy5	sulfoindocyanine succinimidyl ester 5
Dam	DNA adenine methylase
DAPI	4',6-diamidino-2-phenylindole
ddH_2O	double distilled water
DIG	digoxigenin
DMF	dimethylformamide
DMSO	dimethylsulfoxide
DNA	desoxyribonucleic acid
dNTP	desoxyribonucleosid-triphosphate
dsDNA	double stranded DNA
ΔpH	delta pH; proton gradient
$\Delta\Psi$	delta psi; membrane potential
E	glutamic acid
ECM	extracellular matrix protein
EDTA	ethylenediaminetetraacetic acid
eGFP	enhanced green fluorescent protein
EMSA	electrophoretic mobility shift assay
F	Farad
FCF	FRT-chloramphenicol-FRT cassette
FKF	FRT-kanamycin-FRT cassette
FRT	Flp recombination target
fT3SS	flagellar-associated type-III secretion system
G	guanine
g	gram

h	hour
HA	hemagglutinin
HBB	hook-basal-body
HEPES	2-(4-(2-hydroxyethyl)-1-piperazinyl)-ethansulfon acid
HF	high-fidelity
His; H	histidine
H-NS	histone-like nucleoid structuring protein
Hpt	histidine-containing transmitter domain
HRP	horseradish peroxidase
HTH	helix-turn-helix
IHF	integration host factor
IL-1β	interleukin 1 beta
IPTG	isopropyl-β-D-thiogalactopyranoside
kb	kilo base
K_D	dissociation constant
kDa	kilo Dalton
Km^R	kanamycin resistance
L	leucine
l	liter
LB	lysogeny broth
LED	light-emitting diode
LP	low-pass filter
LPS	lipopolysaccharide
M	molar mass
MALS	multi-angle light scattering
MBP	maltose-binding protein
M cell	microfold cell
min	minute
mRNA	messenger RNA
MST	microscale thermophoresis
N	asparagine
n	number of biological replicates
NA	numerical aperture
NAIP5	NLR family apoptosis inhibitory factor 5
NCBI	National Centre for Biotechnology Information
ND8	neutral density filter factor 8
NEB	New England Biolabs
NLR	nucleotide-binding oligomerization domain (NOD)-like receptor
NLRC4	NLR family CARD domain-containing protein 4
NTA	nitriloacetic acid
NTD	N-terminal domain
OD	optical density
ONPG	O-nitrophenyl-β-D-galactopyranoside
Ω	Ohm
PAGE	polyacrylamide gel electrophoresis
PBS(T)	phosphate buffered saline (tween)
PCR	polymerase chain reaction
PFA	paraformaldehyde
pfu	plaque forming unit
poly-(dI-dC)	poly-(deoxyinosinic-deoxycytidylic acid)

PVDF	polyvinylidene fluoride
qRT-PCR	quantitative real-time PCR
RBS	ribosomal binding site
RI	refraction index
RNA	ribonucleic acid
RNAP	RNA polymerase
rpm	revolutions per minute
SCV	*Salmonella*-containing vacuole
SD	SDS-denaturing
SDS	sodiumdodecylsulfate
SEC	size exclusion chromatography
sec; s	second
Sif	*Salmonella*-induced filament
Spc^R	spectinomycin resistance
Spi	*Salmonella* pathogenicity island
spp.	species pluralis
subsp.	subspecies
SUMO	small ubiquitin-related modifier
T	thymine
t	time
$t_{1/2}$	half-life
T3SS	type-III secretion system
TAE	tris-acetate EDTA
Taq	DNA polymerase of *Thermus aquaticus*
TBE	tris-borate EDTA
TBS(T)	tris-buffered saline (tween)
Tc^R	tetracycline resistance
TCA	trichloracetic acid
TEMED	tetramethylethylenediamine
TLR5	Toll-like receptor 5
T-POP	Tn*10d*Tc[*del-25*] transposon
Tris	tris-(hydroxymethyl)-aminomethan
tRNA	transfer RNA
UDP	uridine 5´-diphosphate
URS	upstream repressing sequence
UspC	universal stress protein C
UTR	untranslated region
UV	ultraviolett
V	Volt
vT3SS	virulence-associated type-III secretion system
W	Watt
WT	wildtype
w/v	weight/volume percentage solution
x*g*	multiple of acceleration of gravity

Summary

The bacterial flagellum is of great importance for *Salmonella enterica* serovar Typhimurium in order to establish a successful infection by enabling directed movement in liquid environments, attachment to host cells, and stimulation of the host immune system. The biosynthesis of flagella is tightly regulated in a transcriptional hierarchy of three promoter classes. The flagellar master regulatory operon *flhDC* resides on top of the flagellar synthesis cascade and is under extensive transcriptional and post-transcriptional control. Furthermore, cross-regulation between the flagellar regulon and other virulence systems exist, including the *Salmonella* pathogenicity island 1 (Spi-1)-encoded injectisome that facilitates host cell invasion. Recently, two novel regulators of *flhDC* transcription were discovered, RflM and HilD, which are involved in autogenous control of *flhDC* and cross-regulation with the virulence-associated Spi-1 injectisome, respectively.

In the first part of this thesis, the RflM-dependent repression of *flhDC* transcription and the role of RcsB in this process was investigated. The RcsB protein is the response regulator of the RcsCDB phosphorelay system and known to interact with auxiliary proteins in order to regulate target gene expression upon binding. Accordingly, results of this thesis demonstrated that RcsB and RflM form a stable, heterodimeric protein complex. The RcsB-RflM protein complex coordinately represses *flhDC* transcription by binding to a RcsB/RflM box downstream of the $P1_{flhDC}$ transcriptional start site. Thereby, RflM mediates target specificity of unphosphorylated RcsB for *flhDC* repression and significantly increases its binding affinity, whereas RcsB serves to stabilize RflM protein. Since $FlhD_4C_2$ itself controls transcription of *rflM*, RcsB/RflM-dependent repression of *flhDC* transcription is proposed to constitute a mechanism that fine-tunes the initiation of flagellar biosynthesis independent of external stimuli.

The aim of the second part of this thesis was to investigate the mode of action of HilD-dependent activation of *flhDC* transcription. HilD belongs to a family of DNA-binding proteins and is a major activator of the Spi-1 injectisome. Here, it was demonstrated that HilD operates by binding upstream of the $P5_{flhDC}$ transcriptional start site, which adds another level of cross-talk between the flagellar and Spi-1 regulons.

In the third part of this thesis, the gene regulation dynamics of RcsB/RflM- and HilD-mediated transcriptional regulation of *flhDC* was addressed in respect of different growth phases. Single cell analyses showed that *flhDC* is heterogeneously expressed in a growth phase-dependent manner, resulting in two distinct subpopulations: $flhDC^{ON}$ and $flhDC^{OFF}$. Thereby, the negative $FlhD_4C_2$-RflM feedback loop enables downregulation of the $P1_{flhDC}$-dependent $flhDC^{ON}$ subpopulation during early exponential growth. In contrast, a double positive $FlhD_4C_2$-FliZ-HilD feedback loop facilitates expression of *flhDC* during late exponential growth from the $P5_{flhDC}$ transcriptional start site.

Taken together, this regulation allows *S.* Typhimurium to rapidly adapt to changing environmental conditions during the infection process. Furthermore, this enables fine-tuning of flagella-mediated motility, Spi-1-mediated host cell invasion, and other pathogenic strategies that might be associated with late flagellar gene expression.

Zusammenfassung

Das bakterielle Flagellum spielt für *Salmonella enterica* serovar Typhimurium eine große Rolle bei der Etablierung einer erfolgreichen Infektion, da es eine zielgerichtete Bewegung in flüssiger Umgebung, die Anheftung an Wirtszellen und die Stimulation des Immunsystems ermöglicht. Die Biosynthese von Flagellen ist durch eine transkriptionelle Hierarchie bestehend aus drei Promoterklassen streng reguliert. Das *flhDC* Operon, welches den Hauptregulator der Flagellensynthese kodiert, befindet sich am Anfang dieser Kaskade und ist auf transkriptioneller sowie post-transkriptioneller Ebene umfassend kontrolliert. Darüber hinaus besteht eine gegenseitige Regulation zwischen dem Flagellum und anderen Virulenzsystemen. Dazu gehört das auf der *Salmonella* Pathogenitätsinsel 1 (Spi-1) kodierte Sekretionssystem, welches die Invasion der Wirtszelle ermöglicht. Vor kurzem wurden zwei neue Regulatoren der *flhDC* Transkription entdeckt: RflM und HilD. RflM ist an der autogenen Kontrolle von *flhDC* beteiligt, wohingegen HilD eine Schnittstelle zwischen der Regulation von Flagellen und Spi-1 darstellt.

Im ersten Teil dieser Arbeit wurden die RflM-abhängige Repression der *flhDC* Transkription und die Rolle von RcsB in diesem Prozess untersucht. Das RcsB Protein ist der Responseregulator des RcsCDB Phosphorelays und bekannt dafür zusammen mit Hilfsproteinen die Expression von Zielgenen nach erfolgter Bindung zu regulieren. Dementsprechend zeigten Ergebnisse dieser Arbeit, dass RcsB und RflM einen stabilen heterodimeren Proteinkomplex bilden. Der RcsB-RflM Komplex bindet downstream des $P1_{flhDC}$ Transkriptionsstarts, um die *flhDC* Transkription koordiniert zu hemmen. Dabei vermittelt RflM dem unphosphorylierten RcsB Protein die Spezifität für eine gezielte *flhDC* Repression und steigert signifikant dessen Affinität. Im Gegensatz dazu dient RcsB der Stabilisierung des RflM Proteins. Da $FlhD_4C_2$ selbst die Transkription von *rflM* kontrolliert, wurde die Hypothese aufgestellt, dass die RcsB/RflM-abhängige Repression der *flhDC* Transkription ein Mechanismus darstellt, um die Initiation der Flagellen-Biosynthese unabhängig von externen Stimuli genau abzustimmen.

Das Ziel des zweiten Teils dieser Arbeit war es die Wirkungsweise der HilD-abhängigen Aktivierung der *flhDC* Transkription zu untersuchen. HilD gehört zu einer Familie von DNA-Bindeproteinen und ist ein Hauptaktivator des Spi-1 Sekretions-systems. In dieser Arbeit wurde gezeigt, dass HilD seine Funktion durch eine Bindung upstream des $P5_{flhDC}$ Transkriptionsstarts ausübt. Dies trägt auf einer weiteren Ebene zur gegenseitigen Regulation zwischen dem flagellaren und Spi-1 System bei.

Im dritten Teil dieser Arbeit wurden die Dynamiken der Genregulation aufgrund der RcsB/RflM- und HilD-vermittelten Regulation der *flhDC* Transkription in Hinblick auf verschiedene Wachstumsphasen untersucht. Einzelzellanalysen zeigten, dass *flhDC*

wachstumsphasenabhängig heterogen exprimiert ist, wodurch zwei Subpopulationen resultierten: *flhDC*^{ON} und *flhDC*^{OFF}. Dabei führt der negative $FlhD_4C_2$-RflM Rückkopplungskreislauf zu einer Herunterregulation der $P1_{flhDC}$-abhängigen *flhDC* positiven Subpopulation während des frühen exponentiellen Wachstums. Im Gegensatz dazu dient der $FlhD_4C_2$-FliZ-HilD Rückkopplungskreislauf der $P5_{flhDC}$-abhängigen Expression von *flhDC* während des späten exponentiellen Wachstums.

Zusammengenommen ermöglicht diese Regulation *S.* Typhimurium eine Feinabstimmung der flagellaren Motilität, der Spi-1-abhängigen Invasion von Wirtszellen und anderen pathogenen Strategien, welche mit einer späten Genexpression von Flagellen assoziiert sein könnten. Daraus ergibt sich eine schnelle Anpassung an wechselnde Umweltbedingungen während des Infektionsprozesses.

1 Introduction

Bacterial infections are still a worldwide problem with great health and economic relevance. In 2015, around 90 000 cases of foodborne diseases were reported in Germany, including 13 823 cases of *Salmonellosis*, which usually resulted in gastroenteritis, but caused death in some rare cases (Infektionsepidemiologisches Jahrbuch 2015, Robert Koch Institut). For many pathogenic bacteria, such as *Salmonella enterica* serovar Typhimurium, movement through the environment is of great importance to survive and establish successful infections (Duan *et al.*, 2013). Several different forms of motility exist, such as passive sliding, twitching via type IV pili, and flagella-mediated swimming through liquid environments and swarming over surfaces (Henrichsen, 1972). Bacterial flagella, long helical, rotary filaments that protrude from the cell body, facilitate directed movement towards favorable conditions and away from harmful substances in a chemotactic process (Adler and Templeton, 1967). Environmental stimuli are sensed by chemoreceptors and transmitted via a two-component system to the flagellar motor in order to determine the rotational direction. Counterclockwise rotation enables the formation of a flagellar bundle that propels the bacterium forward and results in a run phase. Upon a change in rotational direction to clockwise, the flagellar bundle is disrupted and the bacterium tumbles. These alternating run and tumble phases facilitate a so-called biased random walk along a chemical gradient (Eisenbach, 1996). This not only enables directed movement, but also affects host cell invasion (Jones *et al.*, 1992). Additional roles of flagella during the infection process have been discovered in recent years, such as attachment to host cells, biofilm formation, and stimulation of the host immune system (Rossez *et al.*, 2015). In the light of emerging antibiotic and multidrug resistance of pathogenic bacteria, the bacterial flagellum has been discussed as target for novel drugs to block bacterial pathogenesis (Erhardt, 2016). Many regulators of flagellar synthesis, assembly, and functionality that act on transcriptional and post-transcriptional levels are known and characterized (reviewed in Erhardt and Dersch, 2015). However, fine-tuning of flagellar regulation in *S.* Typhimurium during host cell infection and the complex cross-regulatory network with other pathogenic strategies are still not completely understood and thus addressed in this thesis.

1.1 The genus *Salmonella*

Salmonellae are Gram-negative, facultative anaerobic, rod-shaped, peritrichously flagellated bacteria that belong to the family of Enterobacteriaceae and are closely related to *Escherichia coli* (Fàbrega and Vila, 2013). The genus *Salmonella* was named after Daniel Elmer Salmon, whose assistant Theobald Smith discovered the novel species *Salmonella choleraesuis* in 1885 (Schultz, 2008). Currently, this genus comprises the species *S. bongori* and the species *S. enterica* that is subdivided into the six subspecies *enterica*, *salamae*, *arizonae*, *diarizonae*, *houtenae*, and *indica*. Furthermore, subspecies are classified into more than 2 500 serovars according to their antigenic properties of somatic (O) and flagellar (H1 and H2) antigens (listed in the Kauffmann-White classification). In the case of *S. enterica* subsp. *enterica*, serovars are designated according to their associated diseases, origins or habitats (Su and Chiu, 2007). The typhoidal serovars *S. enterica* serovar Typhi and *S. enterica* serovar Paratyphi A and B are host-restricted to humans and transmitted by the faeco-oral route via contaminated food or water. Infections cause enteric fever, which is a systemic disease leading to bacteremia, osteomyelitis, meningitis, and organ damages with a fatal outcome if not treated. In contrast, infections with non-typhoidal serovars are associated with food poisoning (*Salmonellosis*) and result in usually self-limiting gastroenteritis with abdominal cramps, diarrhea, nausea, and vomiting. Most frequently, *S. enterica* serovar Typhimurium and *S. enterica* serovar Enteritidis are the causative agents of *Salmonellosis*, which have a broad host range, including humans, poultry, swine, and cattle. However, in rare cases infections can cause enteric fever, especially in immunocompromised people, children, and the elderly. Generally, a high bacterial load ($> 10^6$ bacteria) must be ingested to establish disease (Hohmann, 2001; de Jong *et al.*, 2012; Chen *et al.*, 2013). The genomes of *S.* Typhi and *S.* Typhimurium are 90 % identical and differ mainly in virulence genes, such as the Vi antigen that is only present in *S.* Typhi, which results in the different course of disease upon infection (de Jong *et al.*, 2012).

1.2 Pathogenesis of *S.* Typhimurium

For successful infection of host cells, *S.* Typhimurium utilizes several pathogenic strategies and virulence factors. These strategies include flagella-mediated motility, adhesins, and the delivery of effector proteins into host cells through two needle-like injectisomes that harbor a virulence-associated type-III secretion system (vT3SS) and are encoded on *Salmonella* pathogenicity islands (Spi) (Haraga *et al.*, 2008). The gastrointestinal route of infection, host cell invasion, and intracellular survival and replication are shown schematically in Fig. 1.1. After ingestion of contaminated food or water, *S.* Typhimurium survives the stomach using an acid tolerance response (Foster and

Hall, 1990). Subsequently, bacteria enter the small intestine and traverse the intestinal mucus layer in order to reach the underlying intestinal epithelium. In this early stage of infection, flagella-mediated motility facilitates movement towards epithelial host cells, near surface swimming, and attachment to the site of infection (Crawford *et al.*, 2010; Misselwitz *et al.*, 2012). Additionally, various adhesins, including fimbrial and non-fimbrial structures, enable intimate contact by binding to extracellular matrix proteins and glycostructures of eukaryotic host cells (Wiedemann *et al.*, 2014). Following intimate contact, *S.* Typhimurium invades non-phagocytic epithelial host cells, preferentially microfold (M) cells, dependent on the secretion of effector molecules through the Spi-1-encoded injectisome (Zhou *et al.*, 1999). M cells are specialized cells in the follicle-associated epithelium of the Peyer's patches that exhibit reduced glycocalyx and transport engulfed bacteria to immune cells in the underlying lymphoid tissue by transcytosis (Jones *et al.*, 1994). The invasion process is characterized by induction of cytoskeletal rearrangements, membrane ruffling, and internalization of the bacteria in a trigger-like mechanism by macropinocytosis (Francis *et al.*, 1993; Sansonetti, 2002). After crossing the intestinal epithelium via M cell-mediated transcytosis, the bacteria are taken up by phagocytes, preferentially macrophages, and can disseminate into deeper organs, such as liver and spleen (Johansson *et al.*, 2006). Additionally, submucosal dendritic cells are able to pass tight junctions between intestinal epithelial cells and take up bacteria directly from the intestinal lumen (Rescigno *et al.*, 2001). Upon invasion of epithelial host cells or phagocytosis, *S.* Typhimurium is incorporated in modified phagosomes, so-called *Salmonella*-containing vacuoles (SCV). Inside the SCV, secretion of effector molecules through the Spi-2-encoded injectisome facilitates bacterial survival and replication, but also Spi-1 effectors and other molecules are involved. The SCV is characterized by a maturation process, which involves remodeling of the endosomal membrane (Waterman and Holden, 2003; Steele-Mortimer, 2008). Additionally, the SCV migrates along the microtubule network to the perinuclear region near the Golgi apparatus of the epithelial host cell, which presumably allows for the delivery of membrane components and nutrients (Ramsden *et al.*, 2007). At this position, vacuole-associated actin polymerization causes the formation of a F-actin meshwork around the SCV, followed by the formation of long *Salmonella*-induced filaments (Sif) along microtubules that extend from the SCV throughout the whole epithelial host cell (Méresse *et al.*, 2001; Drecktrah *et al.*, 2008). Importantly, SCV-lysosome fusions and lysosomal destruction of incorporated bacteria are blocked, either directly or by affecting and delaying endosomal trafficking and lysosome fusion (Steele-Mortimer, 2008).

During infection of eukaryotic host cells, *S.* Typhimurium stimulates the host immune system via bacterial virulence factors, which results in production of proinflammatory cytokines and caspases, recruitment of phagocytic immune cells, and

intestinal inflammation in the host (Hobbie *et al.*, 1997; Rydstrom and Wick, 2007). Most importantly, flagellar filament subunits are recognized as pathogen-associated molecular patterns and effectively stimulate the innate immune response via two pathways. Extracellular flagellin is detected by the Toll-like receptor 5 (TLR5), which induces the secretion of proinflammatory cytokines and antiapoptotic factors (Hayashi *et al.*, 2001; Vijay-Kumar *et al.*, 2006). In contrast, intracellular flagellin is detected by the NLRC4 inflammasome via the mammalian receptors Ipaf and NAIP5, which results in activation of caspase 1, secretion of interleukin IL-1β, and programmed macrophage cell death (Franchi *et al.*, 2006; Zhao *et al.*, 2011). *S.* Typhimurium has evolved several strategies to evade the host immune system and to dampen the immune response, such as downregulation of flagella production upon host cell invasion or modification of flagellar filament structures (Rossez *et al.*, 2015). However, stimulation of intestinal inflammation and macrophage cell death allows *S.* Typhimurium to successfully outcompete the intestinal microbiota and to disseminate in order to establish a systemic infection, respectively (Guiney, 2005; Stecher *et al.*, 2007). Hence, spatiotemporal fine-tuning of flagellar synthesis in *S.* Typhimurium is important for the successful infection of the host.

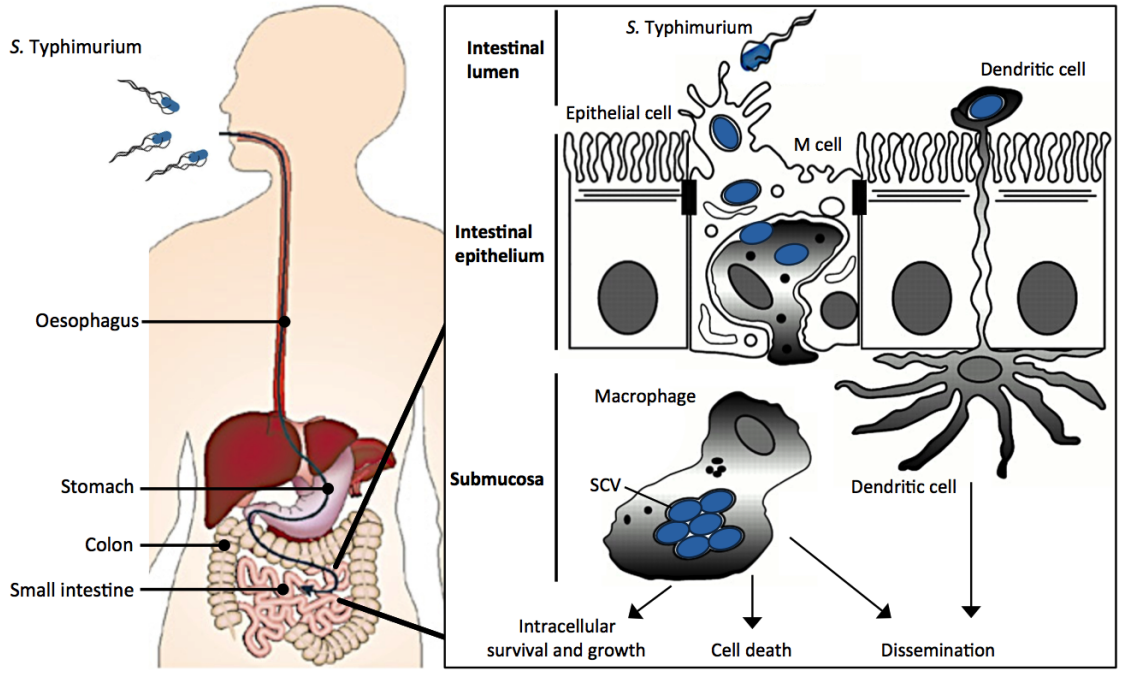

Fig. 1.1 Infection route of *S.* Typhimurium.
S. Typhimurium is taken up with contaminated food or water and travels through the gastrointestinal tract to the small intestine. Flagella-mediated motility enables movement to the intestinal epithelium. Subsequently, bacteria invade epithelial host cells, preferably M cells, dependent on the secretion of effector molecules through the Spi-1-encoded injectisome. M cell-mediated transcytosis facilitates crossing of the epithelial barrier and bacteria are taken up by phagocytes. Alternatively, dendritic cells take up bacteria directly from the intestinal lumen. The secretion of effector molecules through the Spi-2-encoded injectisome enables survival and replication in *Salmonella*-containing vacuoles (SCV) inside macrophages. *S.* Typhimurium can induce host cell death or disseminate into deeper organs to cause a systemic infection. Figure modified from Sansonetti, 2002 and Haraga *et al.*, 2008.

1.3 Structure and assembly of the bacterial flagellum

The flagellum of *S.* Typhimurium is a sophisticated macromolecular nanomachine that is made of more than 30 different proteins and comprises three structural parts: the basal body, the hook, and the filament (Fig. 1.2 A). The membrane-embedded basal body contains four ring structures that are located in the lipopolysaccharide layer in the outer membrane (L-ring; FlgH), the peptidoglycan layer (P-ring; FlgI), the inner membrane (MS-ring; FliF), and the cytoplasmic region (C-ring). The C-ring is composed of the rotor protein complex (FliGMN) that is attached to the MS-ring and involved in flagellar rotation (Blair, 2006; Chevance and Hughes, 2008). As mentioned above, the direction of flagellar filament rotation is determined by a two-component system, the CheA-CheY phosphorelay. In presence of repellents, the sensor kinase CheA is autophosphorylated and the phosphoryl group is transferred to the response regulator CheY. Upon phosphorylation, CheY binds to FliM and changes the rotational direction from counterclockwise to clockwise (Toker and Macnab, 1997). Additionally, the stator protein complex (MotAB), which is located in the inner membrane and periplasm, serves as an ion-conductor and motor-force generator (Berg, 2003). The torque of the rotary motor is transmitted to the hook and filament via a tubular rod (FlgBCFG) that traverses the periplasmic space through the stabilizing P- and L-rings in the basal body (Jones and Macnab, 1990). Outside the bacterial cell, the hook (FlgE) serves as flexible linking structure between the basal body and the filament to allow the formation of a propulsive bundle out of flagellar filaments that are distributed all over the cell (peritrichous flagellation) (Samatey *et al.*, 2004). The propeller-like filament is connected to the hook via two junction proteins (FlgKL) and consists of up to 20 000 subunits of one single protein named flagellin (FliC or FljB). The filament forms a 10–15 μm long helical tube, which is capped by a scaffold made of the FliD protein (Yonekura *et al.*, 2003). In order to secrete structural components of the flagellum outside the cytoplasm, the basal body contains a flagellar-associated type-III secretion system (fT3SS). Except for the proteins that form the P- and L-rings, which are secreted via the Sec system, all proteins that make up the extra-cytoplasmic parts of the flagellum are exported through the fT3SS. (Jones *et al.*, 1989; Macnab, 2004). The membrane-bound components of the fT3SS that correspond to the export gate (FlhAB FliOPQR) are located in the MS-ring of the basal body. Several chaperones in the cytoplasm prevent degradation of substrates prior to fT3SS-dependent translocation, such as the substrate-specific chaperones FlgN, FliS, and FliT (Macnab, 2004). Additionally, an ATPase complex (FliHIJ) is located in the cytoplasm, which directs the entry of substrates in the export gate and is believed to facilitate unfolding and chaperone release for efficient secretion via the fT3SS. However, the ATPase has been shown to be dispensable, and the actual substrate export is energized by the proton

motive force, which consists of the membrane potential ΔΨ and the proton gradient ΔpH (Minamino and Namba, 2008; Paul *et al.*, 2008; Erhardt *et al.*, 2014).

The flagellar-specific fT3SS has several homologous proteins in terms of sequence and/or function in the virulence-associated vT3SS of the injectisome that presumably evolved from an exaptation of the bacterial flagellum due to gene losses and acquisitions. The vT3SS not only exports structural components of the injectisome outside the cytoplasm, but also translocates effector proteins into host cells (Blocker *et al.*, 2003; Abby and Rocha, 2012). Moreover, the flagellum and the injectisome display several structural similarities (Fig. 1.2, compare A and B), especially in the basal part, which have been identified over the past years in electron microscopy studies. The few structures that differ include the flagellar P- and L-rings, which are substituted in the injectisome by a single secretin-type ring; the C-ring that actually constitutes a cytosolic 'pod' in the injectisome; and the extracellular parts. Compared to the flagellar hook and filament, the injectisome comprises a needle and pore-forming translocon (Diepold and Wagner, 2014). The length of both the needle and the hook is controlled during assembly by an intrinsic mechanism using a secreted molecular ruler, respectively (Erhardt *et al.*, 2010; Wee and Hughes, 2015). *S.* Typhimurium harbors two different injectisome complexes with respective vT3SS that are encoded on Spi-1 and Spi-2 and fulfill distinct functions during the infection process as described above (Zhou *et al.*, 1999; Waterman and Holden, 2003).

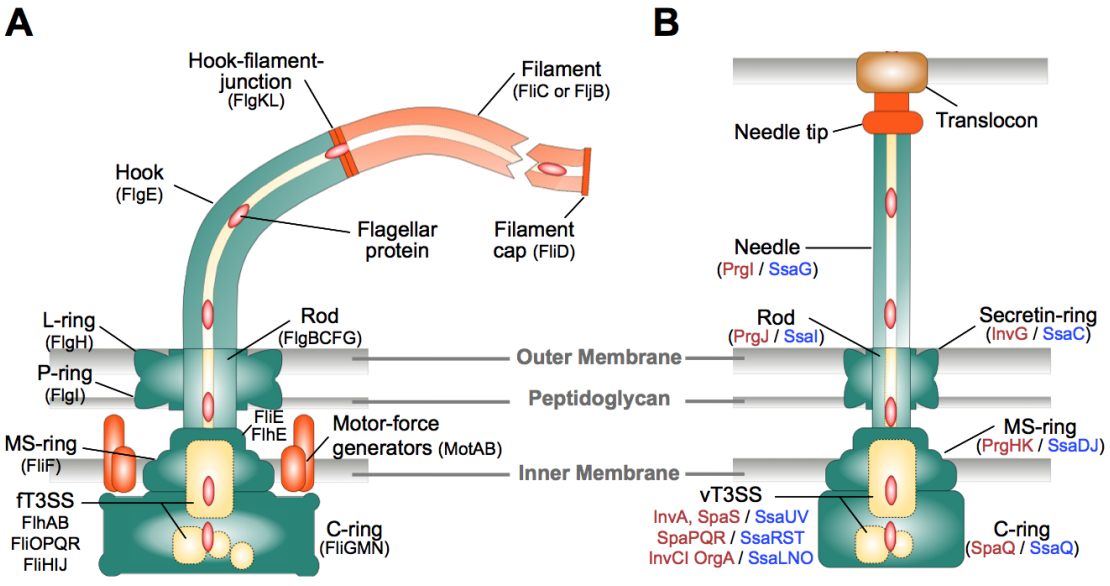

Fig. 1.2 Schematic structure of the bacterial flagellum and injectisome in *S.* Typhimurium.
(A) The flagellum consists of three structural parts: the basal body, the hook, and the filament. The membrane-embedded basal body comprises four ring structures (L-, P-, MS-, and C-ring), a rotary motor, a rod that serves as driveshaft, and a flagellar-specific type-III secretion system (fT3SS). **(B)** The injectisome is structurally related to the flagellum and harbors a virulence-associated type-III secretion system (vT3SS) and, instead of the hook and filament, a needle and translocon. **(A+B)** Proteins are indicated in brackets (black: flagellum; red: Spi-1-encoded; blue: Spi-2-encoded). Figure modified from Erhardt *et al.*, 2016.

The synthesis and assembly of the bacterial flagellum is strictly regulated in a temporal manner and coupled to the flagellar assembly state due to a transcriptional hierarchy of three promoter classes that drive expression of more than 60 genes (Fig. 1.3) (Chilcott and Hughes, 2000; Chevance and Hughes, 2008). The flagellar master operon *flhDC* is on top of the flagellar synthesis cascade and is transcribed from a single class 1 promoter. This results in the formation of a heteromultimeric $FlhD_4C_2$ complex, which directs σ^{70}-RNA polymerase to activate transcription of genes from flagellar class 2 promoters (Liu and Matsumura, 1994; Wang *et al.*, 2006). Genes expressed from class 2 promoters encode proteins that are required for structural parts and assembly of the hook-basal-body (HBB) complex. Additionally, two regulatory proteins, the alternative sigma factor σ^{28} (encoded by *fliA*) and the cognate anti-sigma factor FlgM, are expressed (Ikebe *et al.*, 1999). Flagellar assembly is initiated at the basal parts, which self-assemble in the inner membrane and the cytoplasmic region and include the MS-ring, the C-ring, and the components of the fT3SS. Next, the rod proteins are exported through the fT3SS and assemble together with the P- and L-rings in the periplasm and outer membrane. Then, the fT3SS exports hook components that polymerize outside the cell until the hook has reached its physiological length of around 55 nm (Macnab, 2003). In *S.* Typhimurium, the hook length is controlled by an intrinsic mechanism using an infrequent molecular ruler, FliK. The FliK protein is intermittently secreted during hook assembly and facilitates interaction with FlhB, an integral membrane component of the fT3SS, once the hook has reached its optimal length. This results in autocleavage of FlhB and a switch in the export specificity of the fT3SS from early HBB substrates to late substrates (Kutsukake *et al.*, 1994; Williams *et al.*, 1996; Minamino and Macnab, 2000; Erhardt *et al.*, 2010). Among those late substrates is the anti-sigma factor FlgM, which interacts with the alternative sigma factor σ^{28} in the cytoplasm before HBB completion and FlgM secretion. The σ^{28}-FlgM interaction dissociates the σ^{28}-RNA polymerase holoenzyme that is specific for transcription from flagellar class 3 promoters (Ohnishi *et al.*, 1990; Chadsey *et al.*, 1998). Hence, only genes from class 2 promoters are transcribed at that time. Upon HBB completion and the fT3SS substrate specificity switch, the FlgM protein is secreted outside the cell leaving active σ^{28} in the cytoplasm. Subsequently, σ^{28}-dependent transcription from flagellar class 3 promoters occurs, which include genes that encode the filament, motor-force generators, and chemotaxis proteins (Kutsukake, 1994; Karlinsey *et al.*, 2000). Additionally, chaperones of late secretion substrates negatively regulate flagellar gene expression in response to a completed HBB and the fT3SS export specificity switch. Upon secretion of the hook-filament junction proteins FlgKL, the cognate chaperone FlgN increases translation of FlgM providing a negative feedback on flagellar class 3 transcription (Aldridge *et al.*, 2003). After export of the filament cap protein FliD, the FliT protein no longer serves as chaperone, but represses transcription from flagellar class 2 promoters by interfering with

the flagellar master regulator $FlhD_4C_2$ (Yamamoto and Kutsukake, 2006b). Another important step in flagellar assembly is the polymerization of the filament, which is composed of either FliC or FljB. A genetic switch facilitates the alternate expression between FliC and FljB flagellins in a process referred to as flagellar phase variation (Iino, 1969). The *fljB* gene is encoded in one operon together with *fljA*, and transcription from the *fljBA* promoter results in formation of a FljB filament and expression of the inhibitor FljA, which represses translation of the alternative flagellin *fliC* (Yamamoto and Kutsukake, 2006a; Aldridge *et al.*, 2006). However, the *fljB* promoter is flanked by two recombination sites that can be flipped by the Hin recombinase, which prevents transcription of *fljBA* and leads to the formation of a FliC filament (Johnson and Simon, 1985). Altogether, this hierarchical and complex regulation enables *S.* Typhimurium to achieve a correct spatiotemporal assembly of the bacterial flagellum.

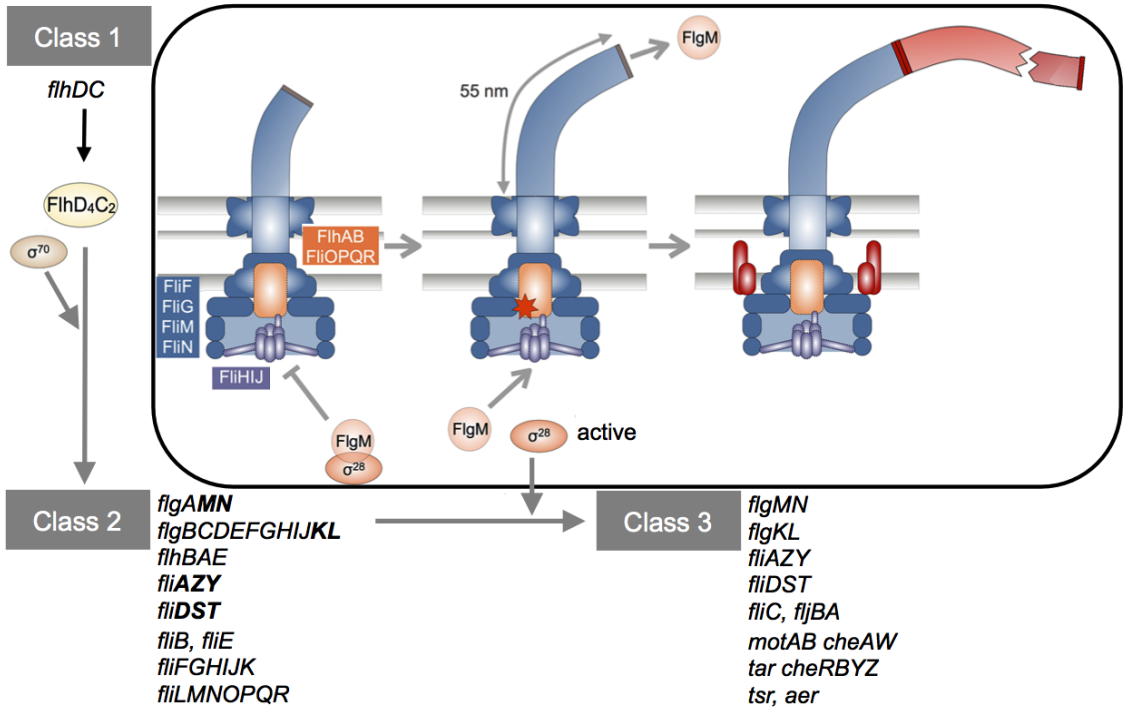

Fig. 1.3 Transcriptional hierarchy of flagellar synthesis and assembly in *S.* Typhimurium.
Flagellar synthesis is organized into a transcriptional hierarchy of three promoter classes. The single class 1 promoter resides on top of the hierarchy and drives expression of the flagellar master regulatory operon *flhDC*. The $FlhD_4C_2$ complex directs σ^{70}-RNA polymerase for transcription from class 2 promoters, whose gene products are components of the hook-basal-body (HBB; blue), including the flagellar-specific type-III-secretion system (fT3SS) with the export gate (orange) and the ATPase (purple). Additionally, the alternative σ^{28} factor and the anti-sigma factor FlgM are expressed, which interact with each other in the cytoplasm. As soon as the physiological hook length is reached (about 55 nm), there is a switch in the export specificity of the fT3SS from early HBB subunits to late subunits (star) enabling secretion of FlgM. Subsequently, σ^{28}-dependent transcription from class 3 promoters occurs including genes that encode the filament, motor-force generators, and chemotaxis proteins (red). Operons and genes that are under control of flagellar class 1, 2, and 3 promoters are indicated. Bold typed genes are under control of hybrid flagellar class 2/3 promoters. Figure modified from Erhardt *et al.*, 2014.

1.3.1 The flagellar master regulator is under extensive control

In *S.* Typhimurium, many environmental signals as well as positive and negative regulatory mechanisms are integrated at the level of the flagellar master regulator $FlhD_4C_2$ in order to tightly control the initiation of flagellar biosynthesis. Transcription of the *flhDC* operon is driven from a promoter that constitutes a complex structure with multiple transcriptional start sites (compare Fig. 1.4). Originally, six start sites were identified by primer extension and annotated $P1_{flhDC}$ through $P6_{flhDC}$ (Yanagihara *et al.*, 1999). However, recent transcriptome analyses detected only four of them under diverse environmental conditions ($P1_{flhDC}$, $P4_{flhDC}$, $P5_{flhDC}$, and $P6_{flhDC}$) (Kröger *et al.*, 2012). Additional studies showed that *flhDC* transcription is primarily driven from the $P1_{flhDC}$ and $P5_{flhDC}$ transcriptional start sites under standard laboratory growth conditions (Mouslim and Hughes, 2014). Several DNA-binding proteins have been described that act on the *flhDC* promoter to regulate expression of *flhDC*. Transcriptional activators include global regulators, such as the cyclic AMP receptor protein complex (cAMP-CRP), the iron-uptake regulator Fur, and the histone-like proteins H-NS and Fis (Kutsukake, 1997; Campoy *et al.*, 2002; Kelly *et al.*, 2004). Known repressors of *flhDC* transcription are the virulence-associated proteins SlyA and RcsB, the RtsB protein, which is encoded in the *rtsAB* operon together with the Spi-1 activator RtsA, and the fimbrial regulators FimZ and PefI-SrgD (Clegg and Hughes, 2002; Ellermeier and Slauch, 2003; Wang *et al.*, 2007; Wozniak *et al.*, 2009; Erhardt and Hughes, 2010). The LysR-type regulator LrhA is involved in *flhDC* repression as well, and has been shown to bind to the *flhDC* promoter in *E. coli* (Lehnen *et al.*, 2002; Erhardt and Hughes, 2010). Furthermore, a negative feedback is initiated by $FlhD_4C_2$-dependent activation of *rflM* that encodes the RflM protein, which in turn represses transcription of *flhDC* (Singer *et al.*, 2013).

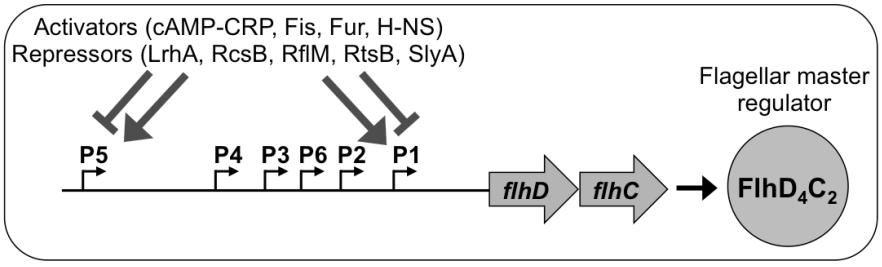

Fig. 1.4 Schematic promoter structure of the flagellar master regulatory operon *flhDC*.
The *flhDC* operon is transcribed from a promoter that comprises six transcriptional start sites annotated P1 through P6. However, expression is primarily driven from P1 and P5 (Mouslim and Hughes, 2014), which are under control of several positive and negative regulators as described in the text. Operon transcription results in the formation of the heteromultimeric $FlhD_4C_2$ complex, which serves as flagellar master regulator.

Regulation of *flhDC* on the post-transcriptional level includes ClpXP-mediated proteolytical degradation of the $FlhD_4C_2$ complex via two mechanisms. When $FlhD_4C_2$ is not bound to target DNA, FliT specifically interacts with the FlhC subunit to selectively increase the affinity for the ClpXP protease and to prevent DNA binding (Aldridge *et al.*, 2010; Sato *et al.*, 2014). However, DNA-bound $FlhD_4C_2$ is resistant against FliT, but is displaced by the nutrient response regulator YdiV, which is highly expressed under low nutrient conditions. YdiV specifically binds to a motif comprising the L22 amino acid in the FlhD subunit in order to direct the $FlhD_4C_2$ complex to ClpXP-dependent degradation (Wada *et al.*, 2011; Takaya *et al.*, 2012). This negative regulation can be counteracted by the flagellar protein FliZ, which serves as post-transcriptional activator of $FlhD_4C_2$ due to repression of *ydiV* transcription (Saini *et al.*, 2008; Wada *et al.*, 2011). Additionally, the carbon storage regulator CsrA, which is a small RNA binding protein, is indispensable for flagellar motility presumably via stabilizing *flhDC* transcript levels and due to regulation of the c-di-GMP metabolic network (Lawhon *et al.*, 2003; Jonas *et al.*, 2010). However, to fully activate the $FlhD_4C_2$ complex, the DnaK chaperone machinery has been shown to be important (Takaya *et al.*, 2006).

1.4 Other virulence factors of *S.* Typhimurium

Besides flagella, *S.* Typhimurium exhibits several other pathogenic strategies and virulence factors, including adhesins and effector molecules that modulate eukaryotic host cells. Most genes encoding virulence-associated proteins are clustered within the five *Salmonella* pathogenicity islands, including Spi-1 and Spi-2 that are necessary for host cell invasion and intracellular survival and replication, respectively. However, other virulence factors are encoded on the virulence plasmid pSLT or on the chromosome (Fàbrega and Vila, 2013). Overall, *S.* Typhimurium exhibits 13 fimbrial operons including *fim* (type 1 fimbriae), *csg*/*agf* (curli fimbriae), *lpf* (long polar fimbriae), *bcf*, *pef*, *saf*, *stb*, *stc*, *std*, *stf*, *sth*, *sti*, and *stj*, which contribute to host cell attachment, intestinal persistence in mice, and biofilm formation (Bäumler *et al.*, 1997; McClelland *et al.*, 2001; Weening *et al.*, 2005; Jain and Chen, 2007). The most important fimbrial structures are type 1 fimbriae, which bind to α-D-mannose residues on glycoproteins and the extracellular matrix protein (ECM) laminin of epithelial host cells (Korhonen *et al.*, 1980; Kukkonen *et al.*, 1993). In contrast, Pef and Std fimbriae adhere to the Lewis X blood group antigen and α1-2 fucosylated receptors, respectively (Chessa *et al.*, 2008; Chessa *et al.*, 2009). Additionally, the non-fimbrial autotransporter proteins ShdA and MisL bind to another ECM protein, fibronectin (Kingsley *et al.*, 2002; Dorsey *et al.*, 2005). The giant adhesin SiiE is required for subsequent invasion upon lectin-like adhesion to epithelial cells (Wagner *et al.*, 2014).

The Spi-1-encoded injectisome translocates effector molecules inside host cells in order to induce bacterial uptake. The OmpR/ToxR family member HilA is the master regulator of structural components of the Spi-1 injectisome and effectors (Bajaj *et al.*, 1995). Upon binding to the promoters, HilA activates transcription of the *prg/org* and *inv/spa* operons, which encode components of the needle complex and the regulator InvF. Simultaneously, this results in a readthrough into the *sic/sip* operon that encodes the translocon, chaperones, and effector proteins. However, transcription of *sic/sip* genes and additional effectors encoded outside Spi-1 (i. e. *sopE, sopB* (*sigD*), and *sptP*) is mainly activated by the AraC-like regulator InvF together with the chaperone SicA (Darwin and Miller, 1999; Eichelberg and Galán, 1999; Darwin and Miller, 2000). On top of the Spi-1 regulon resides a feed-forward loop comprising HilD, HilC, and RtsA (Fig. 1.5). Each of the proteins in this loop is capable to independently activate expression of *hilA*, their own, and each other (Ellermeier *et al.*, 2005). Additionally these three regulators can directly activate *invF* transcription independent of HilA (Akbar *et al.*, 2003). The integration of environmental signals and regulatory inputs into the Spi-1 regulon is described in detail in Chapter 3.1. The effector molecules that induce host cell invasion including cytoskeletal rearrangements, membrane ruffling, and macropinocytosis are well characterized. SopE, SopE2, and SopB (SigD) activate Rho GTPases leading to actin polymerization (Friebel *et al.*, 2001; Patel and Galán, 2006). Additionally, SipA and SipC stabilize and bundle the actin filaments, respectively (Zhou *et al.*, 1999; Hayward and Koronakis, 1999). Upon complete engulfment of bacteria, the SptP effector protein is secreted to inactivate Rho GTPases and reverse the cytoskeletal changes (Fu and Galán, 1999).

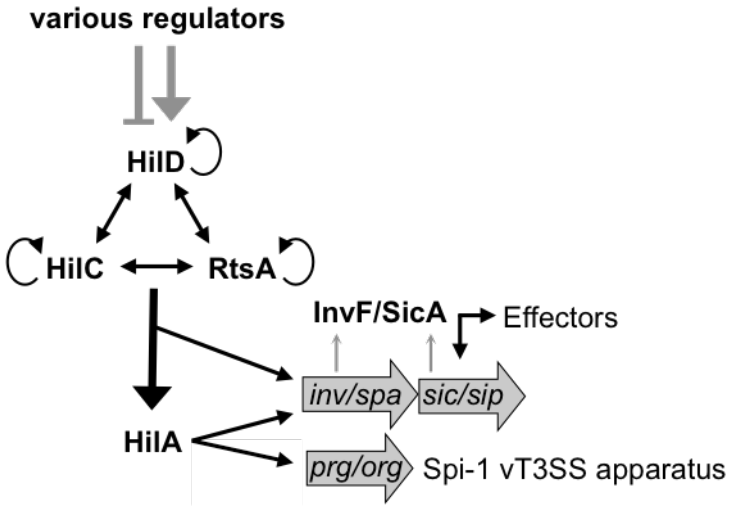

Fig. 1.5 Regulon of the Spi-1 injectisome in *S.* Typhimurium.
HilD, HilC, and RtsA constitute a feed-forward loop activating expression of the Spi-1 master regulator HilA, which in turn activates transcription of genes encoding structural components of the vT3SS and the regulator InvF. Subsequently, InvF and the chaperone SicA induce expression of the *sic/sip* operon and other effectors. Additionally, transcription of *invF* can be activated directly by HilD, HilC, and RtsA. The various regulators affecting HilD are described in detail in Chapter 3.1. For simplification, genes encoding HilD, HilC, RtsA, and HilA are not shown. Figure adapted from Ellermeier *et al.*, 2005.

In contrast, effector molecules that are translocated through the Spi-2-encoded injectisome facilitate survival and replication in SCVs. The SsrA/SsrB two-component system serves as Spi-2 master regulator that responds to low osmolarity, acidic pH or low calcium via the sensor kinase SsrA. Subsequently, the response regulator SsrB activates transcription of all gene clusters located within Spi-2 that encode structural components (*ssa*), regulators (*ssr*), chaperones (*ssc*), the translocon and effectors (*sse*). Additionally, SsrB induces transcription of effectors encoded outside Spi-2 (i. e. *sifA*). The two-component systems EnvZ/OmpR and PhoP/PhoQ sense acidic pH and low magnesium, respectively, and activate transcription of *ssrA*/*ssrB*. Other positive regulators include SlyA, HilD, and the nucleoid-associated proteins IHF (integration host factor) and Fis. Negative regulation occurs via H-NS-mediated silencing of Spi-2 gene expression, which is strengthened by YdgT and Hha (Garmendia *et al.*, 2003; Walthers *et al.*, 2007; Fass and Groisman, 2009). Several effectors, such as SseJ and SifA, are involved in the SCV maturation process via modulating the endosomal membrane (Ruiz-Albert *et al.*, 2002). However, a final and detrimental phagosome-lysosome fusion is prevented by SpiC (Uchiya *et al.*, 1999). Furthermore, the secretion of SifA, SseF, and SseG facilitates the correct intracellular positioning of the SCV in epithelial host cells (Deiwick *et al.*, 2006).

1.5 Aim of this study

In a previous transposon mutagenesis study, two novel regulators of the *S.* Typhimurium flagellar master operon *flhDC* were identified, RflM and HilD. On the one hand, RflM has been shown to be responsible for the formerly described negative auto-regulatory feedback loop of the flagellar master regulator $FlhD_4C_2$ on *flhDC* transcription. The $FlhD_4C_2$ complex activates transcription of *rflM*, and the RflM protein in turn represses transcription of *flhDC* (Singer *et al.*, 2013). However, the RflM-mediated effect on flagellar regulation is dependent on the RcsB protein, the response regulator of the RcsCDB phosphorelay system (Wozniak *et al.*, 2009), but the molecular mechanism is unknown. On the other hand, HilD is the main activator of the Spi-1-encoded injectisome and seems to be additionally involved in activation of *flhDC* expression. Furthermore, a recent study demonstrated that *flhDC* expression is controlled in a growth phase-dependent manner (Mouslim and Hughes, 2014). Thus, the overall aim of this thesis was to investigate the mode of action of RflM/RcsB- and HilD-dependent regulation of *flhDC* transcription and to dissect the consequential gene regulation dynamics of the flagellar master operon throughout the bacterial growth phase.

2 RflM mediates target specificity of RcsB for transcriptional repression of the flagellar master regulatory operon *flhDC* in *Salmonella* Typhimurium

This chapter focuses on the RcsCDB phosphorelay system, in particular the response regulator RcsB, and the novel flagellar regulator RflM in *S.* Typhimurium. The current state of research is given in the background section (see 2.1), and new results in context to the current knowledge are highlighted (see 2.2 Results and 2.3 Discussion).

Findings of this thesis about the heterodimeric RcsB-RflM protein complex that represses transcription of the flagellar master regulatory operon *flhDC* and its role in regulation of motility in *S.* Typhimurium are presented in this section and have been partially published before in the following peer-reviewed publication:

Kühne C., Singer H. M., Grabisch E., Codutti L., Carlomagno T., Scrima A. and Erhardt M. (2016): "RflM mediates target specificity of the RcsCDB phosphorelay system for transcriptional repression of flagellar synthesis in *Salmonella enterica*".
In: *Molecular Microbiology* vol. 101(5) pp. 841–855, doi: 10.1111/mmi.13427.

Contributions:

I performed all experiments and analyzed all data presented in this chapter of this thesis except the following. Bacterial-two-hybrid experiments (shown in Fig. 2.6) and the experiment for Fig. 2.12 C were performed by EG under my supervision. For SEC-MALS analyses, I prepared the protein samples and performed the experiments together with LC at the Centre for Biomolecular Drug Research Hannover. SEC-MALS data were analyzed by LC (shown in Fig. 2.7 A).
Author contributions to the publication are explained in the chapter "Declaration of Author Contributions".

2.1 Background

2.1.1 The RcsCDB phosphorelay system

The Rcs phosphorelay is involved in many regulatory processes in bacteria as a global regulatory system. It contains the sensor kinase RcsC, which is located in the bacterial membrane via two transmembrane domains and integrates environmental stimuli at the periplasmic input domain. Another transmembrane protein, RcsD (formerly designated YojN), serves as transmitter. The response regulator RcsB is located in the cytoplasm and has DNA-binding activity via the C-terminal LuxR-type helix-turn-helix (HTH) domain (Stout and Gottesman, 1990; Takeda *et al.*, 2001). On the chromosome, *rcsC* and the *rcsDB* operon are encoded in convergent directions (NCBI; compare Fig. 2.1 A). The Rcs phosphorelay system belongs to the histidine-aspartate (His-Asp) phosphotransfer systems that are characterized by transfer of the phosphoryl group from histidine to aspartate. Likewise, the RcsC, RcsD, and RcsB proteins contain a His-kinase (H1) and Asp-receiver domain (D1), a His-containing transmitter (Hpt, H2) domain, and an Asp-receiver domain (D2), respectively (Takeda *et al.*, 2001; Majdalani and Gottesman, 2005). The domain structure is illustrated schematically in Fig. 2.1 B.

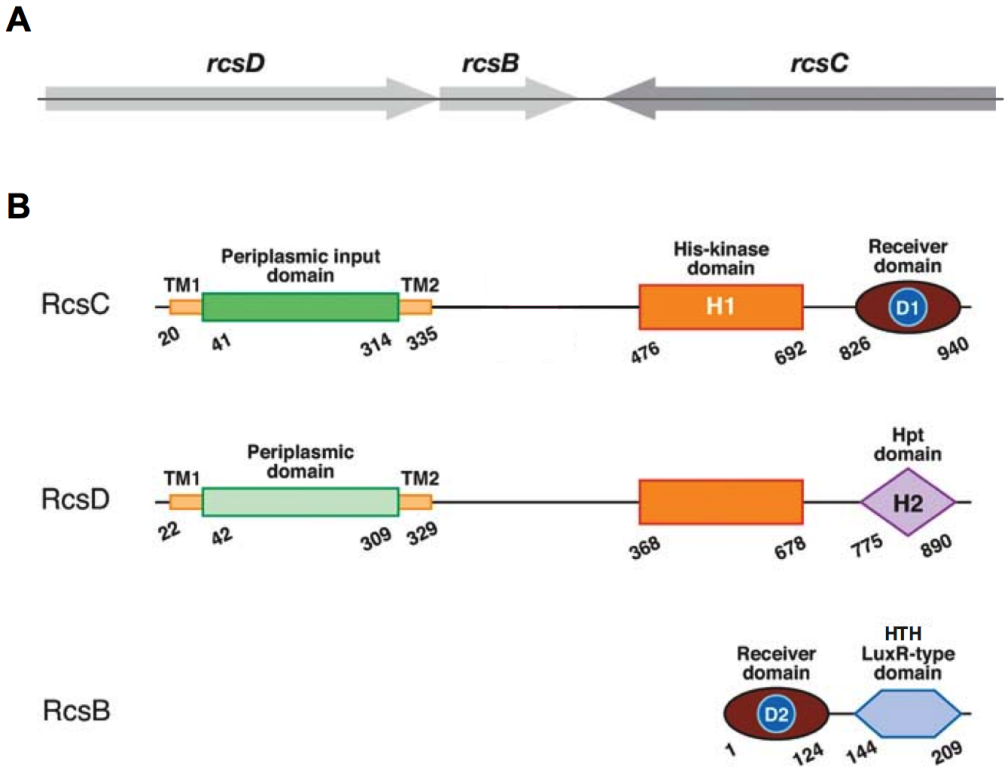

Fig. 2.1 Structural organization of the RcsCDB phosphorelay system.
(A) Orientation of the *rcsDB* operon and *rcsC* gene on the chromosome. **(B)** Domains of the RcsCDB proteins characterizing them as His-Asp phosphorelay members. TM: transmembrane domain; H: histidine; D: aspartate; Hpt: histidine-containing transmitter; HTH: helix-turn-helix. Numbers indicate start and end positions of the respective domains. Figure modified from Majdalani and Gottesman, 2005.

The phosphorelay cascade is initiated by autophosphorylation of the sensor kinase RcsC in the His-kinase domain (H1), followed by transfer of the phosphoryl group to the Asp-receiver domain in RcsC (D1) and the Hpt domain (H2) of the intermediate molecule RcsD. Finally, the phosphoryl group is transferred to the Asp-receiver domain (D2) of the response regulator RcsB (compare Fig. 2.2). Upon phosphorylation, RcsB is able to bind to target gene DNA as a homodimer or after heterodimerization with auxiliary proteins and thereby regulates target gene expression (Huang *et al.*, 2006). Alternative but less efficient pathways of RcsB phosphorylation are discussed via direct phosphoryl group transfer from RcsC or without involvement of RcsC, but RcsD serves both as sensor kinase and transmitter (Pescaretti *et al.*, 2013). In *S. enterica*, the RcsCDB phosphorelay is activated by changes in environmental conditions that affect the integrity of the bacterial cell envelope, osmolarity or result in increased oxidative stress (Huang *et al.*, 2006). Envelope stress can be induced by amphipathic cationic antimicrobial peptides, which are sensed by the outer membrane lipoprotein RcsF leading to activation of RcsC autophosphorylation (Farris *et al.*, 2010). Changes in environmental osmolarity due to variation of salt concentration activate the Rcs system and lead to differential regulation of target genes, dependent on high or low osmolarity (Arricau *et al.*, 1998). In addition to RcsF, another regulator of the Rcs system is the intracellular growth attenuator IgaA, which attenuates the RcsCDB phosphorelay cascade by preventing RcsB phosphorylation (Mariscotti and García-del Portillo, 2009). Furthermore, mutations in *igaA* or mutants leading to outer membrane perturbations, such as deletion of *pmrA* in presence of Fe^{3+} and low Mg^{2+} or deletion of *tolB*, result in activation of the RcsCDB system (Cano *et al.*, 2002; Mouslim and Groisman, 2003; Mouslim *et al.*, 2003).

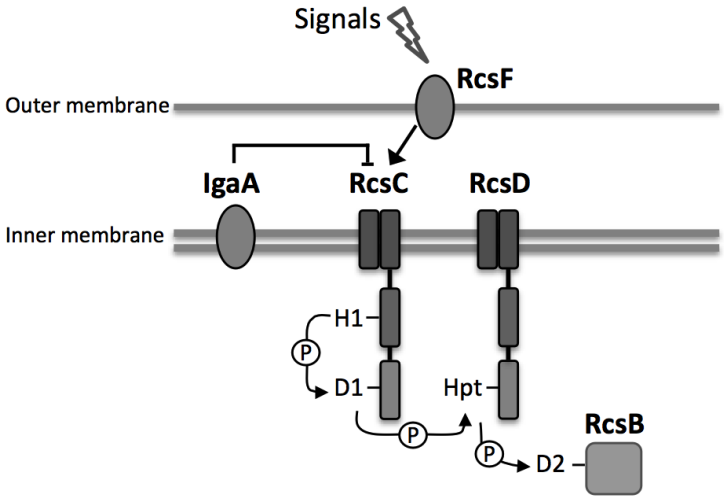

Fig. 2.2 The RcsCDB phosphorelay cascade.
The His-Asp phosphorelay is generally activated by environmental signals leading to autophosphorylation of the RcsC sensor kinase H1 domain, followed by transfer of the phosphoryl group via the D1 domain to the Hpt domain of the intermediate protein RcsD to the D2 domain of the response regulator RcsB. Positive (RcsF) and negative (IgaA) regulators of the Rcs system are shown.

The RcsCDB regulon in *S. enterica* comprises a variety of target genes that are involved in biosynthesis of the bacterial cell envelope, motility, virulence, survival and other physiological processes. As mentioned above, RcsB regulates target genes by binding alone or together with auxiliary proteins, such as RcsA, to target DNA. After heterodimerization of RcsB with RcsA, the RcsB-RcsA complex binds to a conserved RcsAB box in the target DNA region (Wehland and Bernhard, 2000). Originally, RcsB emerged as a positive regulator of colanic acid capsule synthesis upon osmotic shock in *E. coli* (Sledjeski and Gottesman, 1996). Comparably, the RcsAB proteins jointly activate transcription of biosynthetic genes of the cell envelope in *S.* Typhimurium. Under RcsB activating conditions and in presence of RcsA, transcription of the capsule synthesis operon *cps* is increased. RcsAB-dependent expression was also reported for the *ugd* gene, which encodes the UDP-glucose-dehydrogenase enzyme and facilitates production of lipopolysaccharide (LPS) 4-aminoarabinose and colanic acid (Mouslim *et al.*, 2003). Independent of RcsA, RcsB activates transcription of the wzz_{st} gene that encodes a regulator of LPS O-antigen chain length, which ensures correct O-antigen formation (Delgado *et al.*, 2006). Additionally, RcsB regulates physiological processes, such as oxidative stress resistance by activating the *dps* gene (Farizano *et al.*, 2014). The biofilm master regulatory gene *csgD* is activated by unphosphorylated RcsB, but repressed by phosphorylated RcsB (Latasa *et al.*, 2012). Concerning virulence regulation, RcsB displays a dual regulatory activity. Upon RcsB activation, transcription of Spi-1 and Spi-2 genes, such as the *srfABC* operon and *srfJ*, which encodes a Spi-2 effector molecule, is repressed (García-Calderón *et al.*, 2007; Lin *et al.*, 2008; Cordero-Alba *et al.*, 2012). Moreover, constitutive activation of the RcsCDB system results in attenuated virulence (Mouslim *et al.*, 2004; García-Calderón *et al.*, 2005). In contrast, RcsB activates transcription of several Spi-2 genes, and thus the Rcs system is required for Spi-2-dependent intracellular survival and late infection stages in mice (Detweiler *et al.*, 2003; Wang *et al.*, 2007). Likewise, flagellar motility is differentially regulated by RcsB. Negative regulation occurs at the level of the flagellar master regulatory operon *flhDC*. In *E. coli*, the RcsB-RcsA complex binds to a RcsAB box of the *flhDC* promoter leading to repression of motility (Francez-Charlot *et al.*, 2003). In *S.* Typhimurium, however, RcsB-dependent repression of *flhDC* transcription does not require RcsA (Wang *et al.*, 2007). Positive regulation occurs at the level of the *fliPQR* operon, which encodes integral membrane components of the flagellar export apparatus. Anti-sense transcription upstream of the *fliPQR* genes induced by RcsB leads to improved motility due to control of the correct FliPQR stoichiometry by the anti-sense *fliPQR* transcript (Wang *et al.*, 2007; Wang and Harshey, 2009).

2.1.2 The role of RflM in flagellar regulation

RflM (regulator of flagellar master operon; formerly designated EcnR) was identified in a transposon screen for novel flagellar regulators in *S.* Typhimurium (Wozniak *et al.*, 2009). Due to its chromosomal location near to the *ecnAB* genes that encode for bacteriolytic entericidins, it was thought to act as an entericidin regulator and was originally named EcnR. The entericidin genes are positively regulated by σ^S and negatively regulated by the two-component system EnvZ/OmpR (Bishop *et al.*, 1998), but there is no indication that RflM is involved in regulation of *ecnAB*. In contrast, *rflM* transcription is activated by the flagellar master regulator $FlhD_4C_2$. RflM, in turn, is a negative regulator of *flhDC* transcription, and participates together with the RcsCDB system in a negative auto-regulatory feedback loop presumably fine-tuning *flhDC* expression (Wozniak *et al.*, 2009; Singer *et al.*, 2013). RflM homologs exist in other Enterobacteriaceae species, such as *E. coli*, *Yersinia pseudotuberculosis*, *Burkholderia pseudomallei*, *Legionella pneumophila*, *Clostridium colicanis*, *Vibrio paraheamolyticus*, *Bdellovibrio bacteriovorus* and *Bacillus subtilis*. The RflM protein contains a C-terminal LuxR-type helix-turn-helix DNA-binding motif, which is not present in *E. coli* EcnR. In *S.* Typhimurium, RflM exhibits amino acid sequence similarities to RcsA, the auxiliary protein of RcsB (NCBI; compare Fig. 2.3).

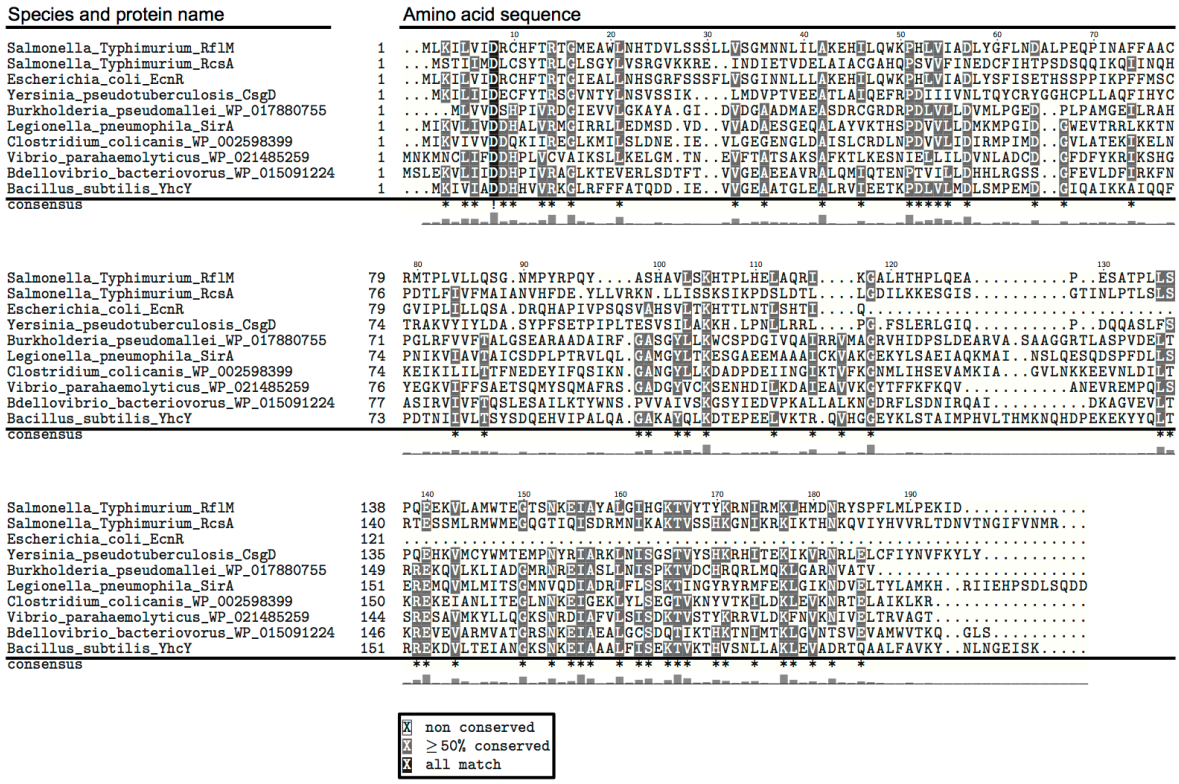

Fig. 2.3 Multiple sequence alignment of RflM.
Homologous RflM sequences were identified using Basic Local Alignment Search Tool and compared by multiple sequence alignment. Species, protein names, amino acid sequences, and conservations (consensus) are shown. Identical amino acids (all match) are highlighted in black and marked with an exclamation mark. Conserved amino acids (≥ 50 %) are highlighted in gray and marked with an asterisk. The degree of conservation is indicated by bar heights below the sequence. Figure modified from Kühne *et al.*, 2016.

2.2 Results

2.2.1 RflM- and RcsB-dependent motility defect in *S.* Typhimurium

Previous studies identified RflM as a novel flagellar regulator in *S.* Typhimurium responsible for repression of transcription of the flagellar master operon *flhDC*. Transcription of *rflM*, in turn, is activated by the $FlhD_4C_2$ complex, which results in a $FlhD_4C_2$-RflM auto-regulatory feedback loop. Additionally, the RcsCDB phosphorelay system was implicated in this regulation (Wozniak *et al.*, 2009; Singer *et al.*, 2013). To confirm the inhibitory effect of RflM on motility and the role of RcsB in this process, swimming motility analyses were performed on motility agar plates (0.3 % agar) with a strain that enabled *rflM* overexpression from the arabinose promoter upon addition of arabinose (P_{araBAD}::*rflM*$^+$). Additionally, known flagellar regulators were deleted to test a putative epistatic effect. Overexpression of *rflM* abolished swimming motility in a wildtype background and in absence of the flagellar regulators *slyA*, *rtsB*, *lrhA*, *fliZ*, and the Spi-1 region *prgH-hilDA*, but not in a *rcsB* deletion strain (Fig. 2.4, compare A and B). Moreover, the *rcsB* deletion strain displayed increased swimming motility with and without *rflM* overexpression. These results confirmed that the RcsCDB phosphorelay system is involved in *rflM*-dependent repression of motility.

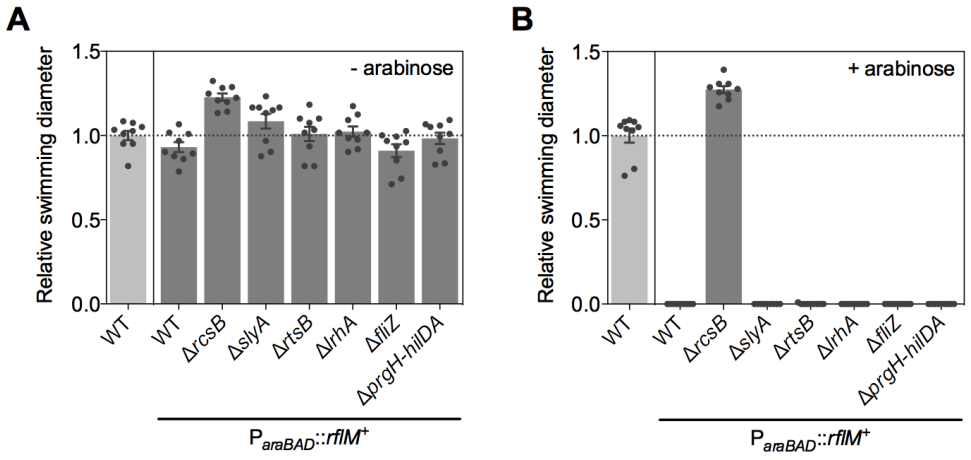

Fig. 2.4 The RflM-mediated motility defect depends on RcsB.
Swimming motility of strains deleted for *flhDC*-specific regulators (Δ*rcsB*, Δ*slyA*, Δ*rtsB*, Δ*lrhA*, Δ*fliZ*, and Δ*hilD* in the Δ*prgH-hilDA* region) that contained *rflM* under control of the arabinose promoter (P_{araBAD}::*rflM*$^+$) was determined under **(A)** non-inducing (- arabinose) or **(B)** inducing conditions (+ arabinose) after incubation on 0.3 % motility agar plates. Swimming diameters are shown relative to the P_{araBAD}::FRT wildtype control (WT, light gray) with *rflM* expressed from its native promoter. **(A+B)** Bars represent mean values of nine biological replicates shown as individual data points (circles). Error bars represent the standard error of the mean. Figure adapted from Kühne *et al.*, 2016 with permission from John Wiley & Sons Ltd.

Next, the RcsB-dependent motility defect was analyzed in more detail. Activation of the RcsCDB phosphorelay cascade by environmental signals leads to RcsB phosphorylation (Huang *et al.*, 2006). The RcsB phosphorylation site is located at the aspartate residue D56, and chromosomal mutations in *rcsB* were constructed that resulted in a more active RcsB variant mimicking phosphorylation ($RcsB_{D56E}$, aspartate changed to glutamate) or a less active protein that cannot be phosphorylated ($RcsB_{D56N}$, aspartate changed to asparagine) (Gupte *et al.*, 1997). These RcsB mutants were analyzed for their capability to influence swimming motility in comparison to a wildtype and a *rcsB* deletion strain (Fig. 2.5). Motility of the phosphomimetic $RcsB_{D56E}$ mutant was significantly decreased in comparison to the wildtype, whereas motility of the phosphorylation-deficient $RcsB_{D56N}$ mutant was increased. The greatest motility increase was observed for the *rcsB* deletion strain. These results verified the functionality of the phosphorylation mutants and indicated that RcsB needs to be phosphorylated for repression of motility.

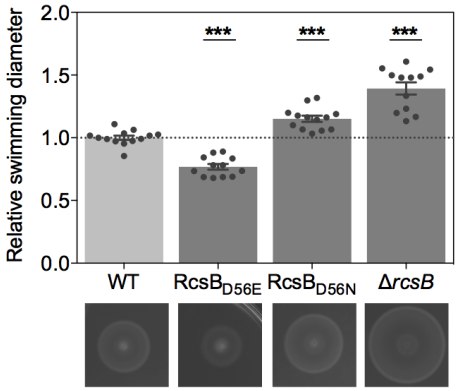

Fig. 2.5 The RcsB-mediated motility defect depends on the RcsB phosphorylation status.
Swimming motility was determined for RcsB phosphorylation mutants ($RcsB_{D56E}$: phosphomimetic; $RcsB_{D56N}$: phosphorylation-deficient) and a *rcsB* deletion strain (Δ*rcsB*) after incubation on 0.3 % motility agar plates. Swimming diameters are shown relative to the RcsB wildtype control (WT) with exemplary images of the motility phenotypes. Bars represent mean values of ≥ 12 biological replicates shown as individual data points (circles). Error bars represent the standard error of the mean and asterisks indicate significant difference to the WT according to Student's *t*-test (*** $P < 0.0005$). Figure adapted from Kühne *et al.*, 2016 with permission from John Wiley & Sons Ltd.

2.2.2 RcsB and RflM proteins form a heterodimeric protein complex

The RcsB protein is a previously described negative regulator of the flagellar master regulatory operon *flhDC* that represses transcription together with the auxiliary co-regulator RcsA in *E. coli* (Francez-Charlot *et al.*, 2003). Since RflM and RcsA display sequence similarity in *S.* Typhimurium (see Chapter 2.1.2), the hypothesis was proposed that RflM could act as a novel auxiliary protein for RcsB regarding *flhDC* repression in *S.* Typhimurium. A potential functional link between RflM and RcsB in this context was confirmed with an unbiased genetic screen using the Tn*10d*Tc[*del-25*] transposon (T-POP) for a random transposon mutagenesis (Kühne *et al.*, 2016). In a strain harboring a transcriptional *flhC-lac* reporter fusion and arabinose-dependent *rflM* overexpression, one class of T-POP insertions was identified that was linked to *rcsCDB* probably due to disruption of genes belonging to the RcsCDB phosphorelay and thus resulting in de-repression of *flhC-lac*. In fact, insertions were identified by DNA sequencing, which were located in the *rcsDB* operon (Kühne *et al.*, 2016).

The next step was to analyze a potential link between RflM and RcsB on protein level. Protein-protein interactions were determined using a transcription-based bacterial-two-hybrid analysis. Therefore, RflM and RcsB proteins were fused to the bait (pBT) and target (pTRG) plasmids, and expression of a *lacZ* reporter gene was determined upon co-expression of the fusion proteins in an *E. coli* reporter strain. In order to prevent any unspecific interaction with the promoter that drives reporter gene expression, RflM and RcsB were truncated for their respective C-terminal helix-turn-helix DNA-binding domains. Co-expression of truncated RflM and RcsB resulted in increased *lacZ* expression above the levels observed for the positive control, whereas no increased transcription of *lacZ* was determined for co-expression of empty plasmids that served as negative control and for RflM or RcsB expressed alone (Kühne *et al.*, 2016). These results indicated interaction between RcsB and RflM proteins, but no self-interaction of RflM or RcsB under the tested conditions. In order to narrow down the potential interaction site, RcsB was co-expressed with RflM amino acid length variants (Fig. 2.6). According to the results described above, increased *lacZ* expression was detected for the positive control (pBT-LGF2 pTRG-Gal11P; 10-fold increase) and co-expression of RcsB and RflM lacking their DNA-binding domains (pTRG-RcsB pBT-RflM (16-fold increase) or pBT-RcsB pTRG-RflM (10-fold increase)). However, interaction between RcsB and the RflM length variants was detected only for $RflM_{1–120}$ due to 5-fold increase of *lacZ* expression, but not for any shorter construct (Fig. 2.6). These results indicated that interaction of RcsB and RflM proteins involves the RflM C-terminus preceding the DNA-binding domain.

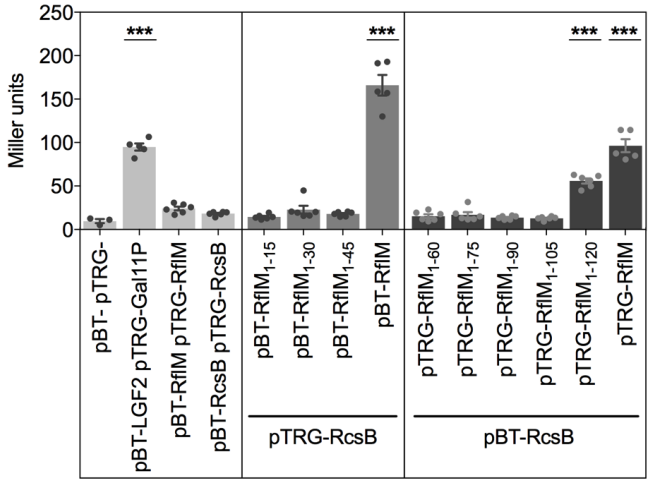

Fig. 2.6 Interaction between RcsB and RflM involves the RflM C-terminus.
Protein-protein interactions were studied in a transcription-based bacterial-two-hybrid assay using pBT and pTRG plasmids that enabled expression of a *lacZ* reporter gene upon interaction of fusion proteins. RcsB and RflM proteins lacking their respective DNA-binding domains were fused to pBT and pTRG and co-expressed in an *E. coli* reporter strain with addition of 20 μM IPTG. β-galactosidase activity was determined for negative controls (pBT- pTRG-; empty vectors), positive controls (pBT+ pTRG+; pBT-LGF2 pTRG-Gal11P fusions), RcsB and RflM expressed alone (pBT-RflM pTRG-RflM; pBT-RcsB pTRG-RcsB) or combined (pTRG-RcsB pBT-RflM; pBT-RcsB pTRG-RflM). Analyzed RflM length variants comprise amino acids 1–15 to 1–120. Bars represent mean values of three to six biological replicates shown as individual data points (circles). Error bars represent the standard error of the mean and asterisks indicate significant difference to the negative controls (pBT- pTRG-) according to Student's *t*-test (*** $P < 0.0005$).

After demonstrating that the RcsB and RflM proteins have the potential to interact with each other, the stoichiometry of the RcsB-RflM protein complex was investigated by size exclusion chromatography (SEC) coupled with multi-angle light scattering (MALS). Since RflM in absence of RcsB was unstable and was not successfully purified alone (own observation), the RcsB and RflM proteins were co-expressed from the pSUMO plasmid (pSUMO-His_6-SUMO-RflM-RBS-RcsB; including an additional ribosomal binding site (RBS) for efficient expression of RcsB) and co-purified resulting in the His_6-SUMO-RflM/RcsB protein complex. The His_6-SUMO-RflM/RcsB complex eluted in one prominent protein peak from SEC separation with an apparent molar mass distribution of 57.96 kDa (± 0.573 %) as determined by MALS and refraction index signals (Fig. 2.7 A). SDS-PAGE analysis of elution fractions from SEC confirmed the existence of both proteins (His_6-SUMO-RflM: 34 kDa; RcsB: 24 kDa) in the peak fractions (Fig. 2.7 B). Based on the predicted molecular mass of the His_6-SUMO-RflM/RcsB complex of 58 kDa (NCBI; Andréasson *et al.*, 2008), these results correlated with a 1:1 stoichiometry of His_6-SUMO-RflM and RcsB and suggested heterodimerization for RflM and RcsB proteins.

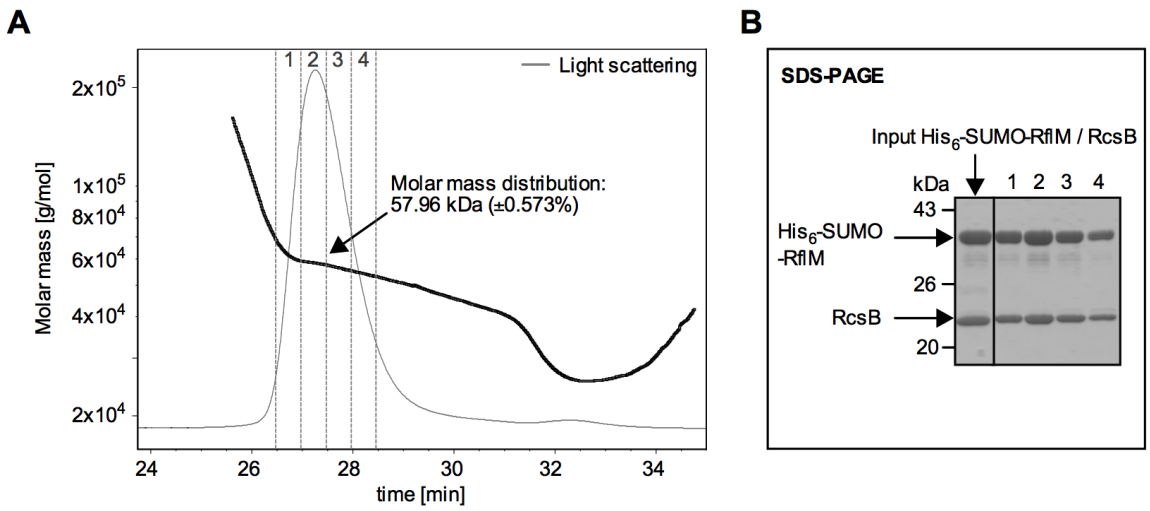

Fig. 2.7 Co-purified His_6-SUMO-RflM/RcsB forms a heterodimeric protein complex.
(A) Elution profile (gray line) and molar mass distribution (black line) of the His_6-SUMO-RflM/RcsB protein complex upon separation by size exclusion chromatography (SEC) and molar mass determination using on-line multi-angle light scattering (MALS). Vertical lines indicate elution fractions taken for further analysis. **(B)** SDS-PAGE of elution fractions (1–4) from SEC-MALS analysis. The first lane contains the input sample used for SEC-MALS. Horizontal arrows indicate His_6-SUMO-RflM (34 kDa) and RcsB (24 kDa) proteins. Figure modified from Kühne *et al.*, 2016 with permission from John Wiley & Sons Ltd.

Since RflM was unstable without RcsB, as noticed during protein purification procedures, the stability of RflM protein was determined in presence and absence of RcsB by analyzing protein levels of epitope-tagged RflM-HA after inhibition of protein synthesis. Functionality of chromosomal RflM-HA expressed from its native promoter (*rflM*$_{HA}$) was confirmed by swimming motility assay (Fig. 2.8 A). Compared to the wildtype control, no effect on motility was observed that would indicate disruption of RflM protein due to the HA-tag and thus disruption of the $FlhD_4C_2$-RflM negative feedback loop described above. Functionality of RflM-HA expressed from the chromosomal arabinose promoter was confirmed by a β-galactosidase assay using a transcriptional *flhC-lac* fusion (Fig. 2.8 B). Arabinose-induced overexpression of *rflM*-HA (P_{araBAD}::*rflM*$_{HA}$) resulted in 4-fold decreased *flhC-lac* expression level, similar to the non-tagged *rflM* version (P_{araBAD}::*rflM*).

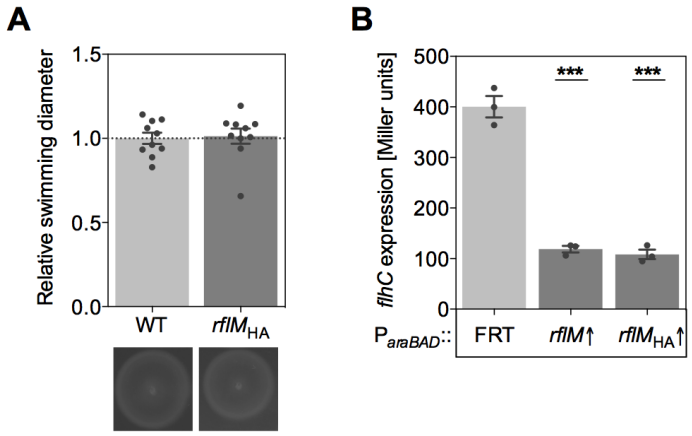

Fig. 2.8 Chromosomal, epitope-tagged RflM-HA protein is functional.
(A) Swimming motility was determined for HA-tagged RflM under control of its native promoter ($rflM_{HA}$) after incubation on 0.3 % motility agar plates. Swimming diameters are shown relative to the wildtype control (WT) with exemplary images of the motility phenotypes. n=10. **(B)** Expression of *flhC-lac* was determined according to β-galactosidase activity upon arabinose-induced overexpression of non-tagged (P_{araBAD}::*rflM*↑) or HA-tagged RflM (P_{araBAD}::$rflM_{HA}$↑) compared to a P_{araBAD}::FRT control. n=3. **(A+B)** Bars represent mean values of n biological replicates shown as individual data points (circles). Error bars represent the standard error of the mean and asterisks indicate significant difference to the WT according to Student's *t*-test (*** $P < 0.0005$).

De novo protein synthesis was stopped and protein levels of RflM-HA expressed from the arabinose promoter were determined by western blot analyses in absence or presence of *rcsB* to determine RflM stability. DnaK served as loading control and RflM-HA levels were normalized to the corresponding DnaK amounts. RflM-HA protein degraded faster in a *rcsB* deletion mutant compared to the wildtype strain background, but no difference was observed upon anhydrotetracycline (AnTc)-induced *rcsB* overexpression from the tetracycline promoter P_{tetA} (Fig. 2.9). These results indicated that interaction with RcsB stabilizes RflM protein.

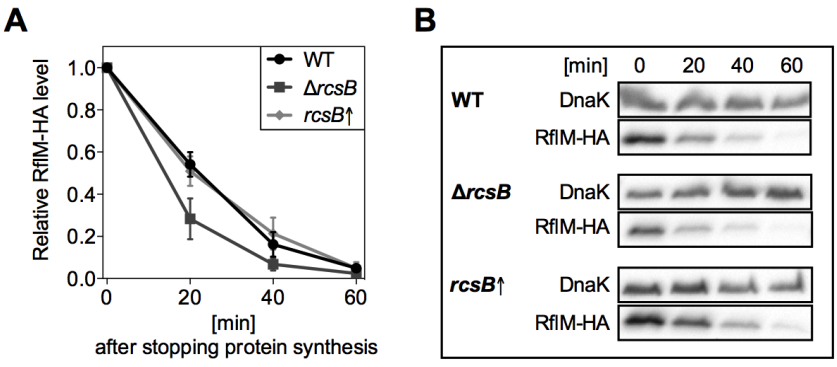

Fig. 2.9 RcsB stabilizes RflM protein level.
Stability of RflM-HA expressed from the arabinose promoter was determined in a *rcsB* deletion strain (Δ*rcsB*, dark gray line) or upon AnTc-induced *rcsB* overexpression (*rcsB*↑, light gray line) in comparison to a wildtype strain (WT, black line). Protein levels were determined 0, 20, 40, and 60 min after stopping of protein synthesis. **(A)** RflM-HA levels are shown relative to the corresponding DnaK control and $t = 0$ min. Data points represent mean values of three biological replicates with connection lines, and error bars represent the standard error of the mean. **(B)** Exemplary western-blots of DnaK and RflM-HA protein levels. Panels A+B adapted from Kühne *et al.*, 2016 with permission from John Wiley & Sons Ltd.

Next, the protease responsible for the rapid degradation of RflM was investigated. Protein synthesis was stopped and protein levels of RflM-HA expressed from its native promoter were determined by western blot analyses in strains deleted for the major proteases Lon, ClpXP, and the ATPases ClpX and ClpA driving proteolysis. RflM-HA protein levels were more stable in the *clpXP-lon* and *lon* deletion mutants 20 and 40 minutes after stopping of protein synthesis (Fig. 2.10). For the wildtype strain and other deletion mutants (Δ*clpXP*, Δ*clpX*, and Δ*clpA*), hardly any amounts of RflM-HA protein were detected 40 minutes after stopping of *de novo* protein synthesis. These results indicated that Lon is the protease mainly responsible for degradation of the RflM protein.

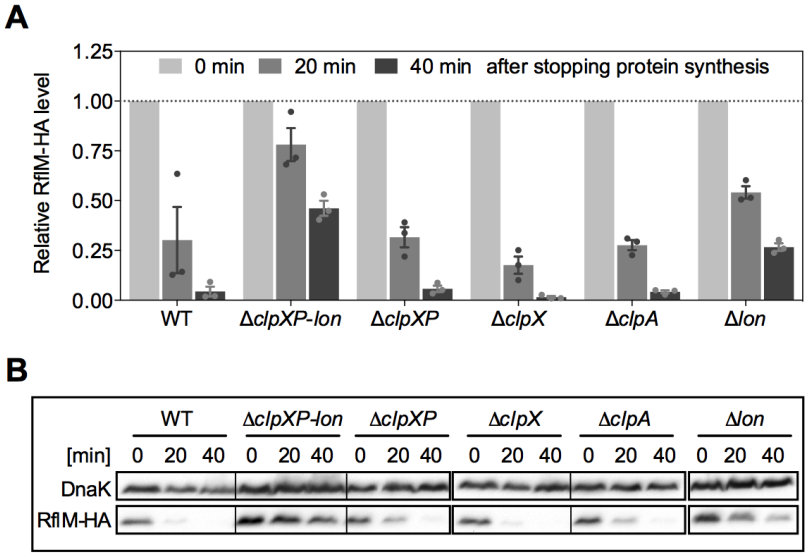

Fig. 2.10 The Lon protease is mainly responsible for RflM degradation.
Stability of RflM-HA expressed from its native promoter was determined in various protease deletion strains (Δ*clpXP-lon*, Δ*clpXP*, Δ*clpX*, Δ*clpA*, and Δ*lon*) in comparison to a wildtype control (WT). Protein levels were determined 0, 20, and 40 min after stopping of protein synthesis. **(A)** RflM-HA levels are shown relative to the respective DnaK control and $t = 0$ min. Bars represent mean values of three biological replicates shown as individual data points (circles). Error bars represent the standard error of the mean. **(B)** Exemplary western-blots of DnaK and RflM-HA protein levels. Panels A+B modified from Kühne *et al.*, 2016 with permission from John Wiley & Sons Ltd.

2.2.3 The RcsB-RflM complex coordinately represses *flhDC* transcription

Since RcsB and RflM interact with each other forming a stable heterodimeric RcsB-RflM protein complex, the hypothesis was proposed that RflM could act as an auxiliary protein for RcsB to promote target specificity for transcriptional repression of *flhDC*. The specificity of RflM in promoting RcsB-dependent repression of *flhDC* transcription was tested by analyzing transcript levels of various known RcsB targets in presence and absence of *rflM* by qRT-PCR. Analyzed target genes of RcsB that belong to the flagellar regulon include *flhD* and genes downstream of the flagellar synthesis cascade such as *aer* and *hilD*. Arabinose-induced overexpression of either *rflM* or *rcsB* from the arabinose

promoter P_{araBAD} resulted in repression of the flagellar targets (Fig. 2.11 A). Notably, *rflM*-mediated regulation was dependent on the presence of RcsB due to the instability of RflM in absence of RcsB as described above. In contrast, target genes that belong to the RcsCDB regulon (*wzzB*, *dps*, and *csgD*) were regulated by *rcsB* overexpression or deletion, whereas overexpression of *rflM* had no effect on target gene expression (Fig. 2.11 B), suggesting that RflM is not involved in their regulation. These results indicated that RflM specifically promotes RcsB-dependent regulation only for flagellar targets with *flhDC* on top and not for RcsB targets in general.

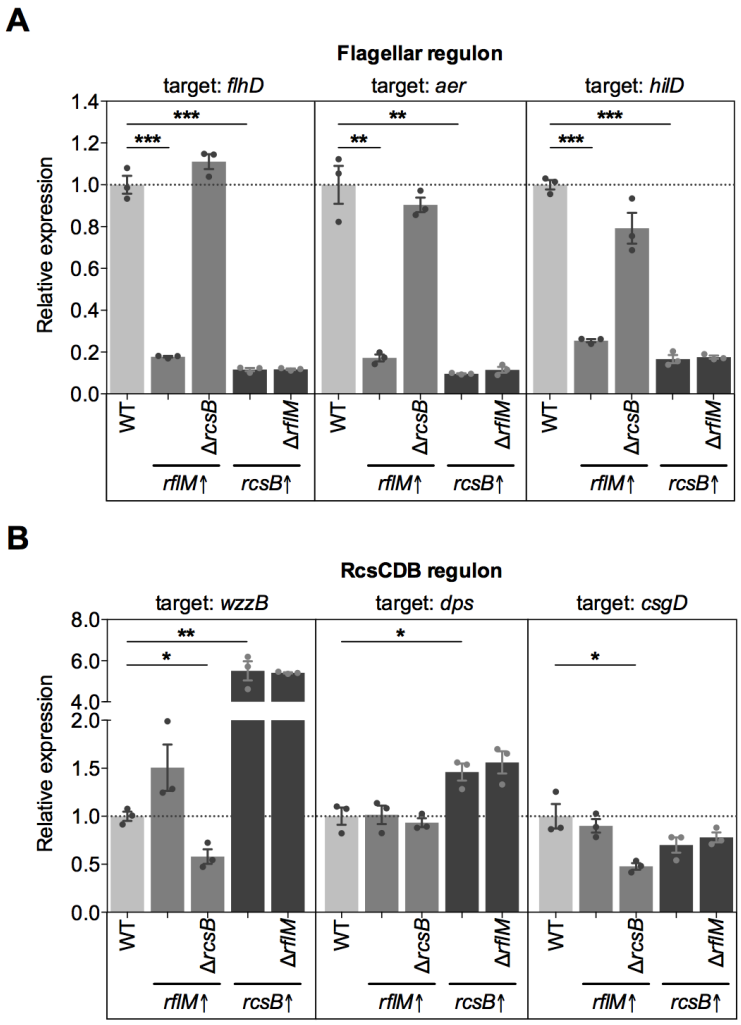

Fig. 2.11 RflM regulates RcsB targets that belong to the flagellar regulon.
Expression levels of genes that belong **(A)** to the flagellar (*flhD*, *aer*, and *hilD*) or **(B)** to the RcsCDB regulon (*wzzB*, *dps*, and *csgD*) were determined by qRT-PCR. Strains with arabinose-induced *rflM* overexpression (*rflM*↑) in presence or absence of *rcsB* (Δ*rcsB*), or *rcsB* overexpression (*rcsB*↑) in presence or absence of *rflM* (Δ*rflM*) were compared to a P_{araBAD}::FRT wildtype control (WT). Transcript levels were normalized to reference genes (*gmk*, *gyrB*, and *rpoD*) and the WT. **(A+B)** Bars represent mean values of three biological replicates shown as individual data points (circles). Error bars represent the standard error of the mean and asterisks indicate significant difference to the WT according to Student's *t*-test (* $P < 0.05$; ** $P < 0.005$; *** $P < 0.0005$). Figure modified from Kühne *et al*., 2016 with permission from John Wiley & Sons Ltd.

Next, the mode of action of the RcsB-RflM protein complex in repression of *flhDC* transcription was analyzed in a β-galactosidase assay using a transcriptional *flhC-lac* fusion (Fig. 2.12 B). It is important to note that strains harboring the *flhC-lac* fusion do not produce a functional $FlhD_4C_2$ protein complex and accordingly do not express *rflM* from its native promoter, since $FlhD_4C_2$ is required for *rflM* expression as mentioned above (Singer *et al.*, 2013). Thus, expression of *rflM* was controlled from the chromosomal, arabinose-inducible promoter (P_{araBAD}::*rflM*), and in absence of arabinose, *rflM* was not expressed. Upon arabinose-induced *rflM* overexpression, transcription of *flhC-lac* was approximately 4-fold reduced, but only in presence of *rcsB* and not in a *rcsB* deletion strain (compare columns 1 + 2 and 9 + 10). This demonstrated that RcsB is indispensable for *rflM*-dependent repression of *flhDC* transcription, which is consistent with previous observations (Wozniak *et al.*, 2009). The role of RcsB in *flhDC* repression was analyzed using various *rcsB* mutants. Overexpression of *rcsB* was induced with AnTc from the chromosomal tetracycline promoter (P_{tetA}::*rcsB*), and RcsB activity was modulated by chromosomal mutations of the RcsB phosphorylation site D56 ($RcsB_{D56E}$: phosphomimetic; $RcsB_{D56N}$: phosphorylation-deficient). In absence of *rflM*, overexpression of *rcsB* resulted in 2-fold decreased *flhC-lac* expression (compare column 1 and 3). However, *flhC-lac* transcription was not reduced to the level observed under *rflM* overexpressing conditions (column 2). Likewise, the phosphomimetic $RcsB_{D56E}$ mutant decreased *flhC-lac* expression comparable to the level upon *rcsB* overexpression (compare column 3 and 5). In contrast, the phosphorylation-deficient $RcsB_{D56N}$ mutant did not affect *flhC-lac* expression (compare column 1 and 7), indicating that RcsB needs to be phosphorylated for *flhDC* repression as already suggested above. Simultaneous overexpression of *rflM* and *rcsB* reduced *flhC-lac* expression to the level observed for *rflM* overexpression under wildtype *rcsB* conditions (compare columns 1 + 2 and 3 + 4). Notably, additional overexpression of *rflM* in the $RcsB_{D56N}$ strain resulted in decreased *flhC-lac* level and thus seemed to restore the ability of RcsB to repress *flhDC* (compare column 7 and 8). These results indicated that the presence of RcsB, but not the RcsB phosphorylation status, is essential for *rflM*-mediated *flhDC* repression.

The cooperative effect of RcsB and RflM on *flhDC* repression was confirmed in a β-galactosidase assay under constant *rcsB* overexpression (P_{tetA}::*rcsB*) and simultaneous titration of *rflM* expression (P_{araBAD}::*rflM*) using increasing amounts of arabinose. With increasing expression of *rflM*, the expression levels of the *flhC-lac* fusion decreased, providing further evidence for coordinated repression of *flhDC* transcription by the RcsB-RflM protein complex (Fig. 2.12 C). As mentioned above, phosphorylation of RcsB is indispensable for RcsB-mediated repression of *flhDC* in absence of *rflM*. However, overexpression of *rcsB* appeared to be sufficient to bypass the need for RcsB phosphorylation. To test this hypothesis, any possibility for phosphorylation of RcsB was

excluded by deleting the RcsCDB phosphorelay cascade (Δ*rcsDBC*) or by analyzing the effect of overexpression of the phosphorylation-deficient $RcsB_{D56N}$ mutant. In absence of *rflM*, overexpression of *rcsB* from the chromosomal arabinose promoter retained the ability to repress *flhC-lac* expression even in strain backgrounds that prevented RcsB phosphorylation (Fig. 2.12 D). Furthermore, any potential regulation of *rcsB* expression by *rflM* and vice versa was excluded (Kühne *et al.*, 2016).

In summary, the results above demonstrated that the heterodimeric RcsB-RflM protein complex is formed to cooperatively repress *flhDC* transcription.

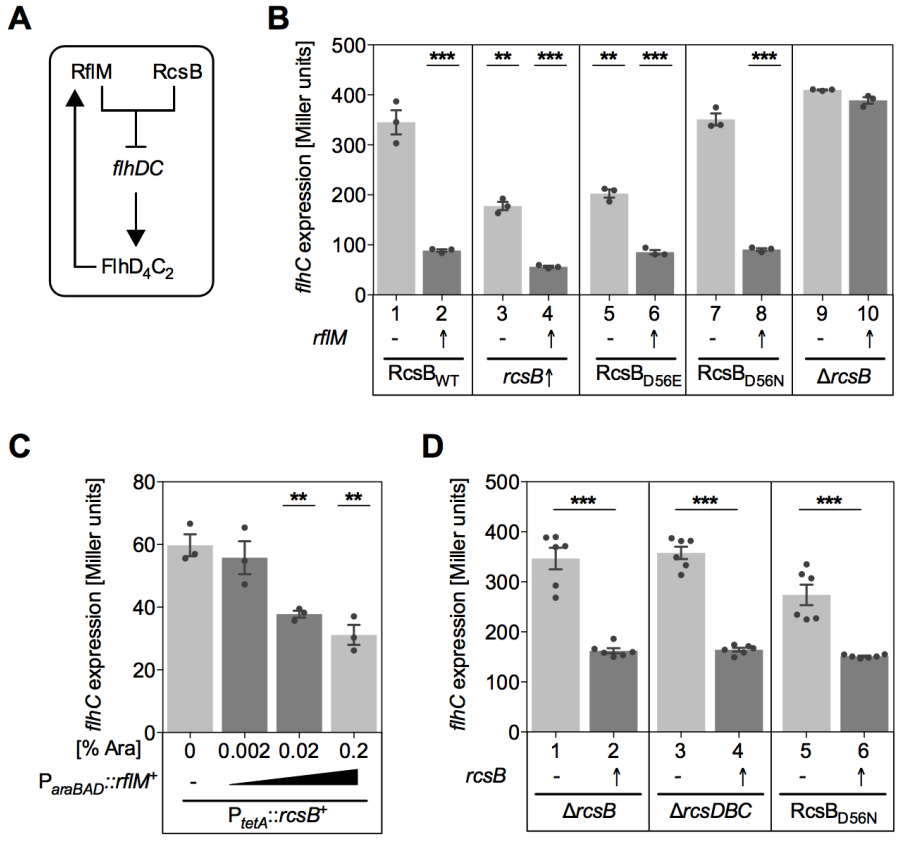

Fig. 2.12 RcsB and RflM coordinately repress *flhDC* transcription.
(A) Schematic regulation of *flhDC* by RcsB and RflM including the negative $FlhD_4C_2$-RflM feedback loop. **(B-D)** Expression of *flhC-lac* was determined according to β-galactosidase activity in *rcsB* and *rflM* mutants. In all strains, *rflM* was not expressed from its native promoter due to the *flhC-lac* fusion, which resulted in non-functional $FlhD_4C_2$. Instead, *rflM* expression was controlled from the arabinose promoter. **(B)** Strains with *rflM* overexpression (*rflM*↑) that contained either *rcsB* wildtype ($RcsB_{WT}$), *rcsB* overexpressed from an AnTc-inducible promoter (*rcsB*↑), a phosphomimetic mutant ($RcsB_{D56E}$), a phosphorylation-deficient mutant ($RcsB_{D56N}$) or a *rcsB* deletion (Δ*rcsB*) were compared to control strains without *rflM* expression (*rflM*-). n=3. **(C)** Cooperativity of RcsB and RflM was determined upon AnTc-induced *rcsB* overexpression (P_{tetA}::$rcsB^+$) and simultaneous titration of *rflM* expression (P_{araBAD}::$rflM^+$) using the indicated arabinose concentrations [% Ara]. n=3. **(D)** Phosphorylation of RcsB was excluded using a strain deleted for the RcsCDB phosphorelay (Δ*rcsDBC*) and the phosphorylation-deficient $RcsB_{D56N}$ mutant. Strains with arabinose-induced *rcsB* overexpression (*rcsB*↑) were compared to control strains that did not express *rcsB* (*rcsB*-). n=6. **(B-D)** Bars represent mean values of n biological replicates shown as individual data points (circles) and error bars represent the standard error of the mean. Asterisks indicate significant difference to the wildtype control without *rflM* expression (A: column 1; B: 0 % Ara) or to the corresponding control without *rcsB* expression (C: *rcsB*-) according to Student's *t*-test (** $P < 0.005$; *** $P < 0.0005$). Panels A–D adapted from Kühne *et al.*, 2016 including rearrangements (D) with permission from John Wiley & Sons Ltd.

Transcription of *flhDC* is primarily driven from the $P1_{flhDC}$ and $P5_{flhDC}$ transcriptional start sites of the *flhDC* promoter (Mouslim and Hughes, 2014). Using chromosomal, transcriptional *luxCDABE* fusions to the *flhDC* promoter, the transcriptional start sites affected by RcsB- and RflM-dependent repression of *flhDC* transcription were determined. The analyzed constructs retained either the wildtype promoter ($P1\text{-}6_{flhDC}$) or a functional $P1_{flhDC}$ or $P5_{flhDC}$ promoter due to mutations in the -10 boxes of the other transcriptional start sites. Furthermore, a *flhDC* promoter duplication following the P_{flhDC}-*luxCDABE* fusion ensured production of a functional $FlhD_4C_2$ complex and maintenance of the flagellar regulon. Arabinose-induced *rcsB* or *rflM* overexpression from the P_{araBAD} promoter resulted in reduced *flhDC* expression levels for all tested promoter fusions compared to a control strain, as determined by a luminescence assay (Fig. 2.13 A). Notably, repression of the $P1_{flhDC}$ transcriptional start site was substantially greater than repression of $P5_{flhDC}$, which indicated that the $P1_{flhDC}$ promoter is the primary target for *rcsB*- and *rflM*-dependent repression of *flhDC* transcription. Time-course analyses of the $P1_{flhDC}$ promoter fusion to *luxCDABE* demonstrated continuous *flhDC* repression upon *rcsB* or *rflM* overexpression after entry in the exponential growth phase (3 h post inoculation) (Fig. 2.13 B).

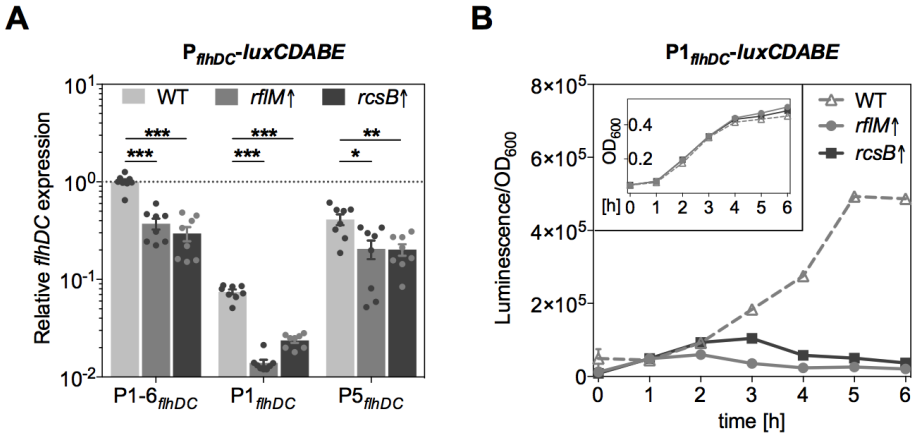

Fig. 2.13 RcsB and RflM repress *flhDC* transcription from the $P1_{flhDC}$ promoter.
Expression of *flhDC* was determined from luminescence activity of P_{flhDC}-*luxCDABE* fusions relative to the bacterial growth (OD_{600}) in strains with arabinose-induced overexpression of *rflM* (*rflM*↑) or *rcsB* (*rcsB*↑) in comparison to a P_{araBAD}::FRT wildtype control (WT). A *flhDC* promoter duplication (P_{flhDC}-*luxCDABE*-Km-P_{flhDC}-*flhDC*) enabled functional *flhDC* expression. For expression from $P1_{flhDC}$ or $P5_{flhDC}$, the -10 boxes of the other transcriptional start sites were mutated. **(A)** Expression from $P1\text{-}6_{flhDC}$ or individual start sites $P1_{flhDC}$ or $P5_{flhDC}$ was determined after 3 h growth and is shown relative to the $P1\text{-}6_{flhDC}$ WT. Bars represent mean values of eight biological replicates shown as individual data points (circles). Error bars represent the standard error of the mean and asterisks indicate significant difference to the WT control according to Student's *t*-test (* $P < 0.05$; ** $P < 0.005$; *** $P < 0.0005$). **(B)** Expression from $P1_{flhDC}$ was monitored over time (1–6 h post inoculation). Data points represent mean values of 10 biological replicates with connection lines, and error bars represent the standard error of the mean. The inlay shows the bacterial growth (OD_{600}). Panels A+B adapted from Kühne *et al*., 2016 with permission from John Wiley & Sons Ltd.

RcsB regulates target genes by binding to the target DNA via its C-terminal LuxR-type helix-turn-helix DNA-binding motif (Huang *et al.*, 2006). In order to confirm the requirement of the RcsB-specific DNA-binding domain for RcsB/RflM-dependent repression of *flhDC* transcription, the functionality of a RcsB mutant lacking its helix-turn-helix domain was investigated. The domain was exchanged with the helix-turn-helix domain of either RflM or SdiA, a *Salmonella* LuxR homolog. The effect of P_{araBAD}-dependent overexpression of these *rcsB* mutants on *flhC-lac* expression in absence and presence of *rflM* was analyzed in a β-galactosidase assay (Fig. 2.14). Comparable to the results described above, overexpression of *rflM* from the AnTc-inducible promoter (compare column 1 and 2) and overexpression of wildtype *rcsB* in presence and absence of *rflM* (compare columns 1 and 5–8) resulted in reduced *flhC-lac* transcription. In contrast, overexpression of *rcsB* harboring either the RflM or the SdiA helix-turn-helix domain prevented *flhC-lac* repression in absence of *rflM* (compare columns 1, 9 and 13). Overexpression of *rflM* in these strains enabled reduction of *flhC-lac* expression only in presence of additional wildtype *rcsB*, indicating that not only presence of RcsB, but also specific interaction of RcsB with the *flhDC* target DNA is necessary for *rflM*-mediated *flhDC* repression.

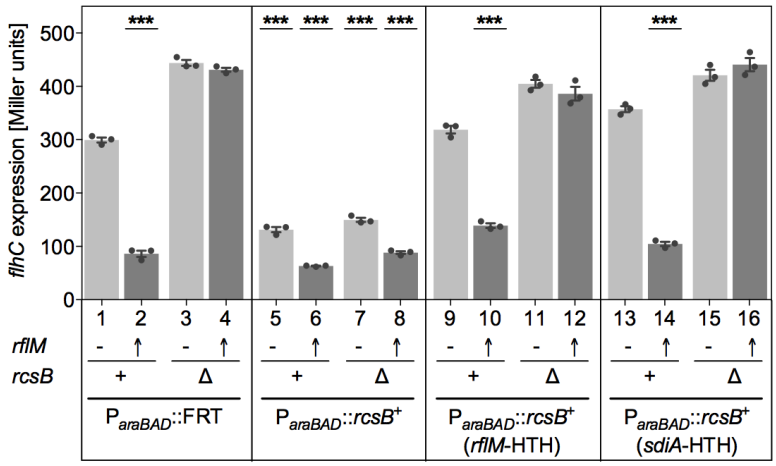

Fig. 2.14 RcsB-dependent *flhDC* repression requires the RcsB DNA-binding domain.
Expression of *flhC-lac* was determined according to β-galactosidase activity in strains that expressed *rcsB* with different helix-turn-helix (HTH) DNA-binding domains from the arabinose promoter (P_{araBAD}). Strains with AnTc-dependent *rflM* overexpression (*rflM*↑) in presence (*rcsB*+) or absence of native *rcsB* (Δ*rcsB*) were compared with a P_{araBAD}::FRT control and strains that do not express *rflM* (*rflM*-). The RcsB HTH domain was either wildtype (P_{araBAD}::$rcsB^+$) or replaced with the RflM HTH domain (P_{araBAD}::$rcsB^+$ (*rflM*-HTH)) or the SdiA HTH domain (P_{araBAD}::$rcsB^+$ (*sdiA*-HTH)). Bars represent mean values of three biological replicates shown as individual data points (circles). Error bars represent the standard error of the mean and asterisks indicate significant difference to the P_{araBAD}::FRT control (column 1) according to Student's *t*-test (*** $P < 0.0005$).

BLAST analysis revealed that RflM contains a C-terminal LuxR-type helix-turn-helix domain, such as RcsB and its co-regulator RcsA (see Chapter 2.1.2). To test if the RflM helix-turn-helix domain is required for RcsB/RflM-dependent *flhDC* repression, the functionality of a RflM mutant lacking its DNA-binding domain was analyzed. P_{araBAD}-induced overexpression of *rflM* containing the helix-turn-helix domain of RcsB resulted in reduced *flhC-lac* level in presence of *rcsB*, but repression was less as observed upon overexpression of native *rflM* (Fig. 2.15, compare columns 1, 4 + 5 and 7 + 8). In contrast, replacement with the SdiA DNA-binding domain or deletion of the RflM helix-turn-helix domain prevented repression of *flhC-lac* transcription (compare columns 1, 10 and 13). Additional overexpression of *rcsB* in these strains decreased *flhC-lac* expression, probably due to RcsB-mediated *flhDC* repression. However, only a slight repression was observed for the RflM mutant without any helix-turn-helix domain, indicating that interaction of RflM with the *flhDC* target DNA is necessary for efficient repression of *flhDC* transcription by the RcsB-RflM complex.

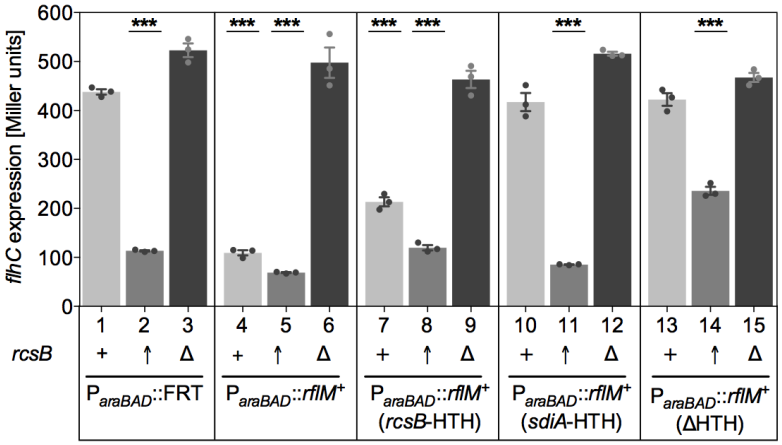

Fig. 2.15 RcsB/RflM-dependent *flhDC* repression requires the RflM DNA-binding domain.
Expression of *flhC-lac* was determined according to β-galactosidase activity in strains that expressed *rflM* with different helix-turn-helix (HTH) DNA-binding domains from the arabinose promoter (P_{araBAD}). Strains in presence of *rcsB* (*rcsB*+), upon AnTc-induced *rcsB* overexpression (*rcsB*↑) or without *rcsB* (Δ*rcsB*) were compared with a P_{araBAD}::FRT control, which does not express *rflM* due to the *flhC-lac* fusion. The RflM HTH domain was either wildtype (P_{araBAD}::$rflM^+$), replaced with the RcsB HTH domain (P_{araBAD}::$rflM^+$ (*rcsB*-HTH)), replaced with the SdiA HTH domain (P_{araBAD}::$rflM^+$ (*sdiA*-HTH)) or deleted (P_{araBAD}::$rflM^+$ (ΔHTH)). Bars represent mean values of three biological replicates shown as individual data points (circles). Error bars represent the standard error of the mean and asterisks indicate significant difference to the P_{araBAD}::FRT control (column 1) according to Student's *t*-test (*** $P < 0.0005$). Figure adapted from Kühne *et al.*, 2016 including additional data (columns 7–9) with permission from John Wiley & Sons Ltd.

2.2.4 The RcsB-RflM complex binds to the RcsB box in the P1$_{flhDC}$ promoter

The results above demonstrated that both the RcsB and RflM DNA-binding domains are indispensable for repression of *flhDC* transcription, suggesting that the RcsB-RflM protein complex binds to the *flhDC* promoter DNA to regulate expression. This led to the hypothesis that heterodimerization of RflM with RcsB could stabilize binding and increase target specificity of RcsB to the *flhDC* promoter. To test this hypothesis, *in vitro* protein-DNA interaction studies were performed with *flhDC* promoter fragments and recombinantly expressed and purified RcsB protein, phosphomimetic RcsB$_{D56E}$ and co-expressed His$_6$-SUMO-RflM/RcsB protein complex, respectively. As mentioned above, RflM in absence of RcsB was not stably purified and was therefore not included. First, *in vivo* functionality of fusion proteins that were used for protein purification was confirmed with a β-galactosidase assay in *S.* Typhimurium strains that enabled propagation of the overexpression plasmids (Fig. 2.16). IPTG-dependent induction of His$_6$-SUMO-RcsB (exemplary for both RcsB and RcsB$_{D56E}$) and His$_6$-SUMO-RflM/RcsB expression from the respective pSUMO plasmids resulted in reduced *flhC-lac* levels compared to an empty vector control. Deletion of chromosomally encoded *rcsB* resulted in higher *flhC-lac* level in the control strain and repression of *flhC-lac* upon additional His$_6$-SUMO-RcsB and His$_6$-SUMO-RflM/RcsB expression comparable to the levels observed before. Notably, *flhC-lac* repression was also observed for the His$_6$-SUMO-RflM protein in presence of chromosomal wildtype *rcsB*, but not in the chromosomal *rcsB* deletion strain.

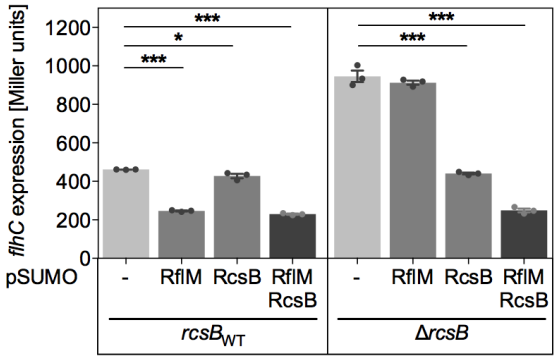

Fig. 2.16 His$_6$-SUMO fusion proteins are functional in *S.* Typhimurium.
In vivo expression of *flhC-lac* was determined according to β-galactosidase activity upon IPTG-induced (0.2 mM) overexpression of fusion proteins His$_6$-SUMO-RflM, His$_6$-SUMO-RcsB, His$_6$-SUMO-RflM/RcsB in presence (*rcsB*$_{WT}$) or absence of chromosomal *rcsB* (Δ*rcsB*). The used strain background expressed T7 RNA polymerase constitutively to enable expression of fusion proteins from the T7 promoter of the pSUMO plasmid. Chromosomal *rflM* is not expressed due to the *flhC-lac* fusion. Bars represent mean values of three biological replicates shown as individual data points (circles). Error bars represent the standard error of the mean and asterisks indicate significant difference to the empty plasmid control (pSUMO-) according to Student's *t*-test (* $P < 0.05$; ** $P < 0.005$; *** $P < 0.0005$). Figure adapted from Kühne *et al.*, 2016 with permission from John Wiley & Sons Ltd.

Next, protein-DNA interactions were studied by electrophoretic mobility shift assay (EMSA) analyses. Previously, a conserved RcsB binding box has been predicted downstream of the $P1_{flhDC}$ transcriptional start site in the *flhDC* promoter (Wang *et al.*, 2007). In order to confirm the existence of this RcsB binding site, different fragments of the *flhDC* promoter were tested that comprised either the whole promoter region (P_{flhDC}, -560 to -90 nucleotides upstream of the *flhD* start codon) or only the $P1_{flhDC}$ or $P5_{flhDC}$ transcriptional start site ($P1_{flhDC}$, -271 to -71; $P5_{flhDC}$, -588 to -388 nucleotides upstream of the *flhD* start codon) or neither the $P1_{flhDC}$ nor $P5_{flhDC}$ transcriptional start site ($P4/6_{flhDC}$, -431 to -231 nucleotides upstream of the *flhD* start codon) as illustrated in Fig. 2.17.

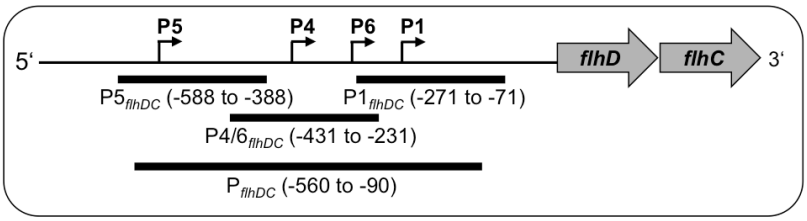

Fig. 2.17 EMSA probes used for RcsB/RflM-P_{flhDC} interaction studies.
DNA fragments covering the *flhDC* promoter region used for protein-DNA binding studies and their positions relative to the *flhD* ATG start codon are illustrated schematically. Arrows labeled P1, P4, P5, and P6 indicate the respective transcriptional start sites. Figure adapted from Kühne *et al.*, 2016 with permission from John Wiley & Sons Ltd.

The different *flhDC* promoter fragments were incubated with increasing amounts of purified RcsB protein and a negative control DNA fragment (*gyrA*), to which RcsB should not bind (Fig 2.18 A). A shift of the whole P_{flhDC} promoter region was observed, but not of *gyrA*, indicating specific binding of the RcsB protein to the *flhDC* promoter (left column). RcsB seemed to bind weakly to the $P1_{flhDC}$ promoter fragment, which contained the predicted annotated RcsB box. In contrast, no binding was observed for the $P4/6_{flhDC}$ and $P5_{flhDC}$ promoter fragments. The phosphomimetic $RcsB_{D56E}$ mutant was described to be more active (Gupte *et al.*, 1997). Comparably, purified $RcsB_{D56E}$ protein displayed higher binding affinity to the P_{flhDC} and $P1_{flhDC}$ promoter regions leading to a shift of the respective DNA fragments (right column). However, weak binding was also observed to the $P4/6_{flhDC}$ and $P5_{flhDC}$ promoter regions indicating overall higher binding activity, but reduced target specificity of the phosphomimetic $RcsB_{D56E}$ protein. The purified His_6-SUMO-RflM/RcsB protein complex resulted in a specific shift of the whole P_{flhDC} promoter region and the $P1_{flhDC}$ promoter fragment with apparent higher binding affinity than RcsB protein alone or the phosphomimetic $RcsB_{D56E}$ mutant (middle column). Additionally, the His_6-SUMO-RflM/RflM protein complex formed a faster migrating second protein-DNA species that was not observed for RcsB alone or $RcsB_{D56E}$ and might be due to a tighter interaction of the protein complex to the target DNA region. No binding was detected for the promoter fragments comprising $P4/6_{flhDC}$ and $P5_{flhDC}$,

demonstrating increased target specificity of the RcsB-RflM protein complex. Purified protein samples (RcsB, $RcsB_{D56E}$ and His_6-SUMO-RflM/RcsB) used for EMSA experiments contained comparable levels of RcsB protein as determined by SDS-PAGE analyses of the corresponding samples (Fig. 2.18 B).

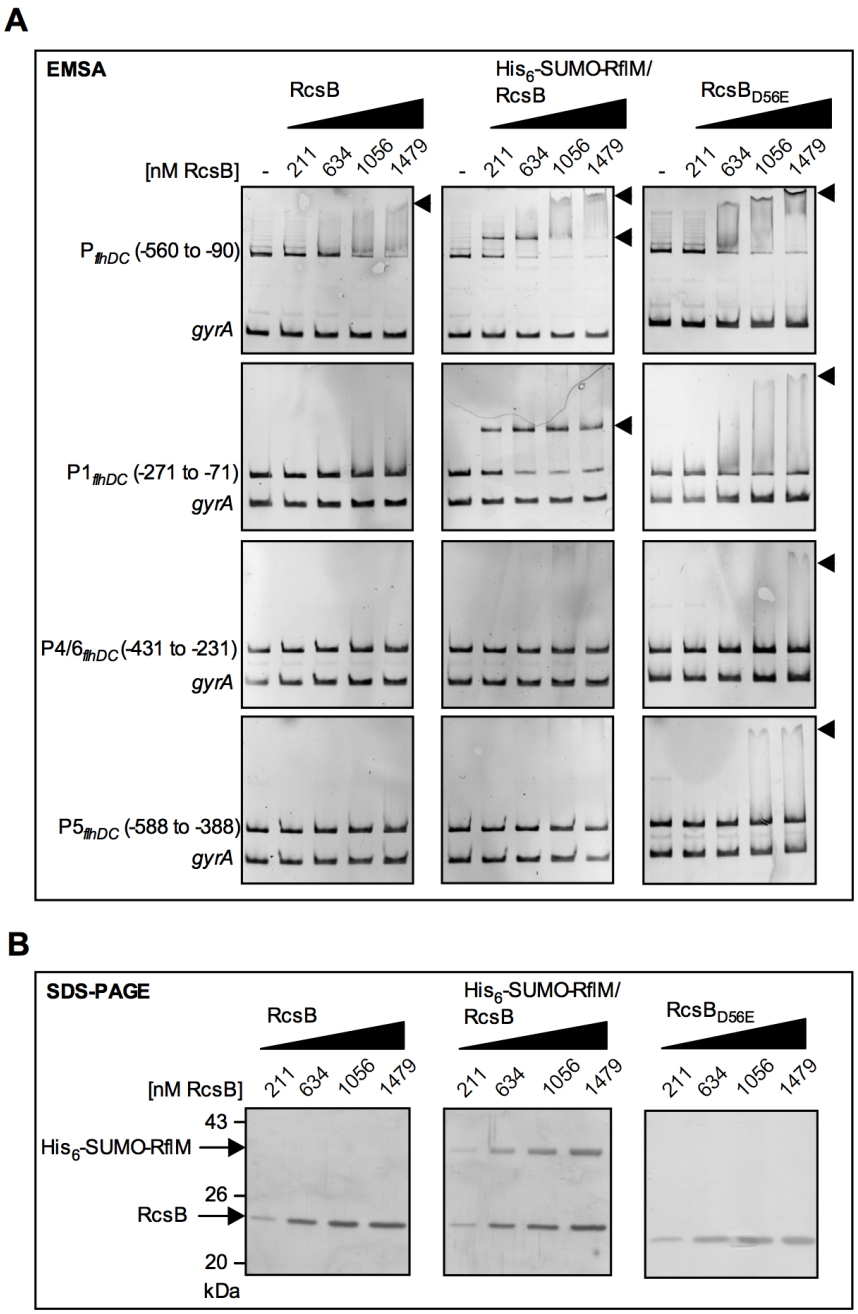

Fig. 2.18 Co-purified RcsB-RflM protein complex binds to the $P1_{flhDC}$ promoter.
(A) Electrophoretic mobility shift assays (EMSA) were performed with increasing amounts of purified RcsB, phosphomimetic $RcsB_{D56E}$ or co-expressed His_6-SUMO-RflM/RcsB complex and *flhDC* promoter fragments P_{flhDC}, $P1_{flhDC}$, $P4/6_{flhDC}$, and $P5_{flhDC}$. Numbers in brackets indicate positions relative to the *flhD* start site. Equal amounts of RcsB protein were used for all samples as indicated above the lanes [nM RcsB] and incubated with 100 ng promoter DNA and *gyrA* as negative control DNA. Arrowheads on the right indicate protein-DNA complexes. **(B)** Samples used for EMSA were analyzed by SDS-PAGE. The RcsB concentration is given above the lanes and horizontal arrows indicate His_6-SUMO-RflM (34 kDa) and RcsB (24 kDa) proteins. Panels A+B adapted from Kühne *et al.*, 2016 with permission from John Wiley & Sons Ltd.

In order to confirm that efficient binding of the RcsB-RflM protein complex to the *flhDC* target promoter DNA required the DNA-binding domain of RflM, a mutated RcsB-RflM protein complex lacking the C-terminal RflM helix-turn-helix (HTH) domain was analyzed by electrophoretic mobility shift assay (Fig. 2.19). The His_6-SUMO-RflM(ΔHTH)/RcsB protein complex was successfully expressed and purified as determined by SDS-PAGE (Fig. 2.19 A). However, only weak binding to the $P1_{flhDC}$ promoter fragment was observed compared to the full-length His_6-SUMO-RflM/RcsB protein complex (Fig. 2.19 B). These results indicated that the RflM-dependent increase in target specificity for RcsB/RflM-mediated *flhDC* repression requires interaction of both RcsB and RflM helix-turn-helix DNA-binding domains with the *flhDC* promoter DNA.

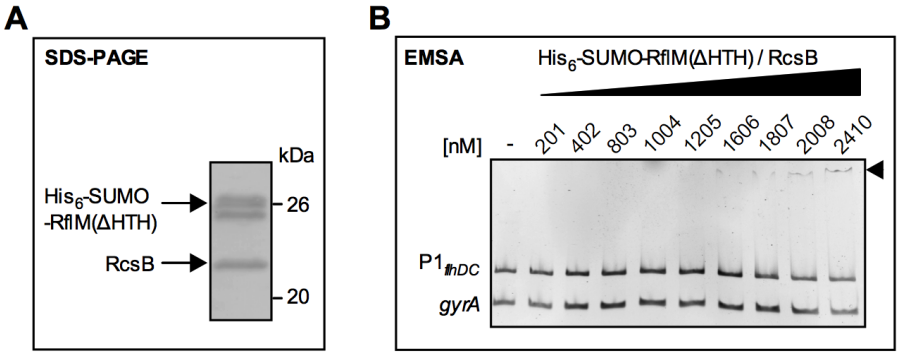

Fig. 2.19 The RcsB-RflM complex requires the RflM DNA-binding domain for efficient binding to $P1_{flhDC}$. **(A)** Co-expressed His_6-SUMO-RflM(ΔHTH)/RcsB complex lacking the RflM helix-turn-helix (HTH) DNA-binding domain was analyzed on SDS-PAGE. Arrows indicate His_6-SUMO-RflM(ΔHTH) (26 kDa) with a potential degradation product and RcsB (24 kDa) proteins. **(B)** EMSA was performed with increasing amounts of purified His_6-SUMO-RflM(ΔHTH)/RcsB complex as indicated above the lanes [nM], 100 ng $P1_{flhDC}$ promoter DNA and *gyrA* as negative control. The arrowhead on the right indicates protein-DNA complexes. Figure adapted from Kühne *et al*., 2016 with permission from John Wiley & Sons Ltd.

Next, the exact binding site of the RcsB-RflM protein complex to the $P1_{flhDC}$ promoter fragment was investigated by DNaseI footprinting. Therefore, increasing amounts of purified His_6-SUMO-RflM/RcsB protein complex were incubated with 5′-DIG-labeled $P1_{flhDC}$ promoter fragment, subsequently digested with DNaseI and analyzed on a sequencing gel. Binding of the His_6-SUMO-RflM/RcsB complex to the $P1_{flhDC}$ promoter DNA would protect this region from DNaseI degradation. A completely protected region was identified corresponding to nucleotides +2 to +27 downstream of the +1 transcriptional start site of the $P1_{flhDC}$ promoter (Fig. 2.20). This region contained the predicted, conserved RcsB binding box (nucleotides +5 to +19) (Wang *et al*., 2007). This binding site was referred to as the RcsB/RflM binding box in the following.

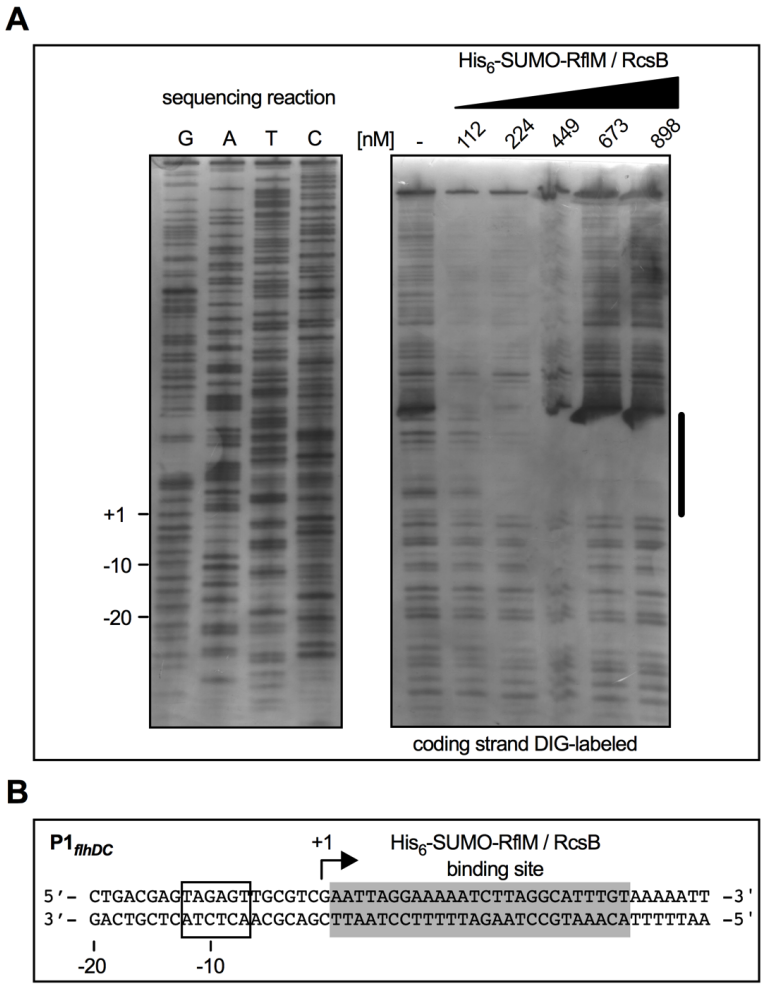

Fig. 2.20 The RcsB-RflM complex binds to the RcsB box downstream of P1$_{flhDC}$.
(A) DNaseI footprinting was performed with increasing amounts of purified His$_6$-SUMO-RflM/RcsB complex as indicated above the lanes [nM] and 100 ng 5′-DIG-labeled P1$_{flhDC}$ promoter DNA (coding strand DIG-labeled). The vertical line on the right indicates the protected region due to binding of the His$_6$-SUMO-RflM/RcsB complex. Lanes G, A, T, C show the sequencing reactions of the P1$_{flhDC}$ fragment. **(B)** Partial DNA sequence of the P1$_{flhDC}$ promoter fragment with -10 box and +1 transcriptional start site. The His$_6$-SUMO-RflM/RcsB binding site is highlighted in gray. Figure modified from Kühne *et al*., 2016 with permission from John Wiley & Sons Ltd.

Binding kinetics and affinities of RcsB protein alone and in complex with RflM to the RcsB/RflM box were quantified using microscale thermophoresis (MST). Therefore, increasing amounts of purified RcsB protein or His$_6$-SUMO-RflM/RcsB protein complex were incubated with a 5′-Cy5-labeled *flhDC* promoter fragment comprising the identified RcsB/RflM box (-1 to +29 nucleotides relative to the +1 transcriptional start site of P1$_{flhDC}$), and fluorescence changes were recorded (Fig. 2.21 A). Increased fluorescence was detected with increasing amounts of RcsB or His$_6$-SUMO-RflM/RcsB due to an enhancement of the fluorescence intensity upon DNA binding. Specificity of the binding was confirmed upon protein denaturation. Due to the release of labeled promoter DNA from protein binding, this resulted in comparable fluorescence intensities (< 15 %

difference) of MST samples comprising the lowest and highest protein concentrations. The determined dissociation constant of the His_6-SUMO-RflM/RcsB protein complex (K_D = 378 ± 25 nM) was approximately tenfold lower than for the RcsB protein (K_D = 3316 ± 32 nM), demonstrating higher binding affinity for the His_6-SUMO-RflM/RcsB complex to the RcsB/RflM box than for the RcsB protein in absence of RflM. Binding of purified RcsB and His_6-SUMO-RflM/RcsB complex to the 5′-Cy5-labeled *flhDC* promoter DNA was confirmed by EMSA of the samples used for MST analyses (Fig. 2.21 B). A shift of the DNA fragment was observed for both proteins, but the His_6-SUMO-RflM/RcsB complex demonstrated apparent higher binding affinity than the RcsB protein alone. Furthermore, a faster-migrating second protein-DNA species was observed as already detected above.

Taken together, the results above demonstrated that the His_6-SUMO-RflM/RcsB protein complex represses *flhDC* transcription efficiently by binding to a RcsB/RflM box downstream of the $P1_{flhDC}$ promoter with high affinity.

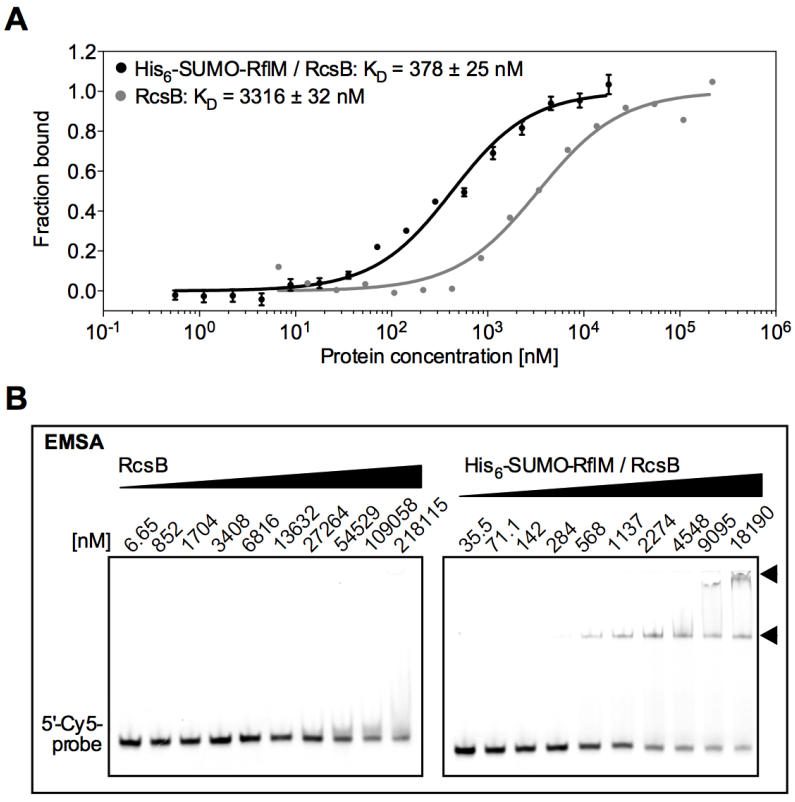

Fig. 2.21 The RcsB-RflM complex binds with high affinity to the RcsB/RflM box.
(A) Microscale thermophoresis (MST) was performed with 100 nM 5′-Cy5-labeled *flhDC* promoter DNA comprising the RcsB/RflM box (5′-Cy5-probe) and 1:2 dilution series of purified His_6-SUMO-RflM/RcsB (black line and data points) or RcsB (gray line and data points). Protein concentrations are plotted on the X axis [nM]. The fraction bound was determined from fluorescence changes of the 5′-Cy5-probe. Data points with error bars represent mean values and standard deviations of three technical replicates from a representative experiment. Lines represent the corresponding curve fit. **(B)** EMSA of samples used for MST analysis. Concentrations of RcsB and His_6-SUMO-RflM/RcsB proteins are indicated above the lanes [nM]. Arrowheads on the right indicate protein-DNA complexes. Figure adapted from Kühne *et al.*, 2016 with permission from John Wiley & Sons Ltd.

2.3 Discussion

The global RcsCDB phosphorelay system is involved in regulation of flagellar motility in both *E. coli* and *S.* Typhimurium. However, regulation differs between both species. In *E. coli*, RcsB-dependent repression of the flagellar master regulatory operon *flhDC* is potentiated by the auxiliary co-regulator RcsA (Francez-Charlot *et al.*, 2003). In contrast, RcsA is not involved in RcsB-dependent repression of *flhDC* transcription in *S.* Typhimurium (Wang *et al.*, 2007). The flagellar master regulator $FlhD_4C_2$ is under negative auto-regulatory control. The $FlhD_4C_2$ complex activates transcription of *rflM* that encodes the RflM protein, which in turn represses *flhDC* transcription. Previous studies indicated an additional role of the RcsCDB phosphorelay system in *flhDC* auto-regulation (Wozniak *et al.*, 2009; Singer *et al.*, 2013). The flagellar specific regulator RflM shares sequence similarity to RcsA, the well-known auxiliary co-regulator of RcsB, and both display structural homologies. RflM and RcsA, as well as RcsB, contain a LuxR-type helix-turn-helix DNA-binding domain at the C-terminus (Henikoff *et al.*, 1990). RcsA and RflM are conserved in many Enterobacteriaceae species, such as *E. coli, S.* Typhimurium and *S.* Typhi, *Yersinia* spp., *Shigella flexneri, Klebsiella pneumoniae*, *Erwinia* spp., *Proteus mirabilis* (Huang *et al.*, 2006; compare Fig. 2.3). Besides RcsA, several other auxiliary co-regulators of RcsB have been described that are involved in RcsB-dependent regulation of target genes. In *E. coli*, the BglJ-RcsB complex acts as a pleiotropic transcriptional activator and coordinates H-NS-, CRP-, and LeuO-mediated regulation (Salscheider *et al.*, 2014). Together with GadE, RcsB enables acid stress resistance against glutamate, arginine, and lysine (Krin *et al.*, 2010). Recently, MatA has been identified as a novel co-regulator of RcsB leading to repression of motility in meningitic *E. coli* (Pannen *et al.*, 2016). In *S.* Typhi, TviA is an auxiliary protein of RcsB that functions to activate synthesis of the capsular polysaccharide Vi antigen and to repress *flhDC* in response to osmolarity together with RcsB (Virlogeux *et al.*, 1996; Winter *et al.*, 2009).

In this thesis, RflM was identified as a novel auxiliary co-regulator of RcsB to mediate target specificity of unphosphorylated RcsB for repression of the flagellar master regulatory operon *flhDC* in *S.* Typhimurium. The findings summarized in this chapter demonstrate that RcsB and RflM proteins interact with each other forming a stable heterodimeric RcsB-RflM protein complex in order to coordinately repress *flhDC* transcription by binding to a RcsB/RflM box downstream of the transcriptional start site of the $P1_{flhDC}$ promoter.

2.3.1 Mode of action of RcsB/RflM-dependent *flhDC* repression

Without RflM, a phosphomimetic $RcsB_{D56E}$ mutant was able to repress *flhDC*, but less efficiently than in presence of RflM. The need for RcsB phosphorylation in *flhDC* repression was bypassed by overexpression of *rcsB*, indicating that RcsB needs to be in a somehow activated state in order to regulate *flhDC* expression in absence of RflM. However, RcsB-mediated repression of *flhDC* transcription increased significantly in the presence of RflM irrespective of the RcsB phosphorylation status. In contrast, presence of RcsB was indispensable for RflM-mediated repression of *flhDC*. This dependency has been described before for other auxiliary proteins that are involved in RcsB target gene regulation, such as BglJ, GadE, and MatA (Castanié-Cornet *et al.*, 2010; Venkatesh *et al.*, 2010; Pannen *et al.*, 2016). The RcsA protein is generally unstable due to rapid degradation by the Lon protease, but stabilized by RcsB (Torres-Cabassa and Gottesman, 1987; Stout *et al.*, 1991). Likewise, results of this chapter demonstrated that RcsB is required for stabilizing RflM protein, since RflM was unstable in absence of RcsB and was not successfully purified upon recombinant expression without simultaneous co-expression of RcsB. Moreover, RflM was mainly subjected to Lon-dependent proteolytical degradation, and a previous study showed that after reaching a maximum in the early exponential growth phase, RflM protein level decline quickly (Mouslim and Hughes, 2014).

For target gene regulation, RcsB binds as homodimer or after heterodimerization with auxiliary co-regulators (Majdalani and Gottesman, 2005). Bacterial-two-hybrid and SEC-MALS analyses demonstrated that the RcsB and RflM proteins interact with each other forming a stable, heterodimeric protein complex. Analyses of various RflM length variants indicated that the C-terminus preceding the helix-turn-helix DNA-binding domain of RflM is involved in the interaction of RcsB and RflM. However, an involvement of N-terminal parts of RflM was not necessarily excluded. The functionality of the truncated RflM variants for repression of *flhDC* transcription needs to be verified in order to exclude that improper protein folding, which would result in non-functional RflM protein, prevented interaction with RcsB. Additionally, truncations of the RflM N-terminus could be analyzed in order to gain more information about the RcsB-RflM interaction. Recently, the interaction between RcsB and auxiliary co-regulators was investigated with emphasis on the RcsB protein. Mutations in proximity to the RcsB D56 phosphorylation site impair the activity of phosphorylation-dependent RcsB/co-regulator dimers, whereas these mutations have only minor effects on phosphorylation-independent heterodimers of RcsB and co-regulator (Pannen *et al.*, 2016). In this thesis, self-interaction of neither RcsB nor RflM was detected. The lack of homodimerization has been reported for other RcsB co-regulators, such as RcsA and BglJ (Venkatesh *et al.*, 2010). The presence of target DNA or RcsB phosphorylation would presumably promote RcsB

homodimer formation. Alternatively, a simple single-plasmid-based bacterial-two-hybrid approach could be used in order to study homodimerization of proteins, such as the LexA-based assay. In this assay, homodimer formation of the protein of interest fused to the LexA DNA-binding domain enables binding to the *sulA* promoter and repression of *lacZ* target gene expression (Dmitrova *et al.*, 1998; Venkatesh *et al.*, 2010).

Phosphorylation of RcsB was indispensable for repression of *flhDC* transcription in absence of RflM, probably due to its requirement for RcsB dimerization. In contrast, RcsB phosphorylation was not essential for *flhDC* repression in presence of RflM. This indicated that RflM mediates RcsB target specificity for the *flhDC* promoter independent of external stimuli that would activate the Rcs phosphorelay cascade and would result in RcsB phosphorylation. Similarly, the BglJ-RcsB complex activates transcription of target genes, such as *bgl* (aryl-β,D-glucoside) or the pleiotropic virulence regulator *leuO*, independent of RcsB phosphorylation (Venkatesh *et al.*, 2010; Stratmann *et al.*, 2012).

2.3.2 Binding of the RcsB-RflM complex to the *flhDC* target DNA

The mode of action of RcsB/RflM-mediated repression of *flhDC* transcription was further analyzed in more detail. Protein-DNA interaction studies with recombinantly expressed and co-purified RcsB-RflM protein complex demonstrated that the complex bound to a *flhDC* promoter fragment comprising the $P1_{flhDC}$ transcriptional start site. Upon binding of the RcsB-RflM protein complex, transcription is blocked. In comparison to the RcsB-RflM complex, purified RcsB protein in absence of RflM bound with tenfold lower affinity to the same *flhDC* promoter fragment. Since recombinantly expressed RcsB was presumably not phosphorylated, efficient binding to the *flhDC* target DNA was not expected due to the described need of RcsB phosphorylation for *flhDC* repression in absence of RflM. However, the recombinantly expressed and purified phosphomimetic $RcsB_{D56E}$ mutant displayed increased binding affinity compared to wildtype RcsB protein, but showed reduced target specificity due to additional binding to other *flhDC* promoter fragments. Comparably, overexpression of *rcsB* or *rflM* resulted in slightly reduced transcription of *flhDC* from the $P5_{flhDC}$ promoter according to the P_{flhDC}-*luxCDABE* promoter studies, which indicated reduced target specificity. This could be due to unspecific interaction of activated RcsB variants with target DNA. Notably, no binding of the purified RcsB-RflM complex to the *flhDC* promoter fragment comprising the $P5_{flhDC}$ transcriptional start site and not $P1_{flhDC}$ was detected. Additionally, the observed effect on $P5_{flhDC}$-dependent *flhDC* expression could be an indirect consequence of RcsB- and RflM-dependent repression of *hilD* transcription, which is a transcriptional activator of *flhDC* (Mouslim and Hughes, 2014; compare Chapter 3).

Efficient binding of the RcsB-RflM protein complex to the *flhDC* target DNA required the C-terminal RflM helix-turn-helix DNA-binding domain. A mutated complex lacking the helix-turn-helix domain of RflM was presumably not able to interact tightly with the *flhDC* promoter, since no additional faster-migrating protein-DNA species was observed like for the full-length RcsB-RflM complex. Furthermore, RflM-mediated repression of *flhDC* transcription was not facilitated with RcsB protein lacking the RcsB-specific helix-turn-helix domain, and indicated that RflM is not able to bind properly to target DNA without cooperative binding of RcsB. In *E. coli* and *Erwinia amylovora* it has been shown that the RcsB co-regulator RcsA is not able to bind to target DNA without RcsB (Kelm *et al.*, 1997; Wehland and Bernhard, 2000). Hence, the RflM protein appears to modulate binding affinity of RcsB for the *flhDC* promoter target DNA, and facilitates a fast and stable binding of the heterodimeric RcsB-RflM complex leading to repression of *flhDC* transcription from the P1 transcriptional start site.

In enteric bacteria, the sequence of the binding site for RcsB and its auxiliary co-regulator RcsA in target promoter DNA for exopolysaccharide biosynthesis genes is conserved (consensus: TAAGAATATTCCTA) and thus named the RcsAB box (Wehland and Bernhard, 2000). The same sequence can be found in the *flhDC* promoter of both *E. coli* and *S.* Typhimurium at similar locations (TAGGAAAAATCTTA; nucleotides +5 to +19 relative to the +1 transcriptional start site of $P1_{flhDC}$). Since RcsA is not required for RcsB-mediated repression of *flhDC* transcription in *S.* Typhimurium, this binding site is referred to as the RcsB box (Francez-Charlot *et al.*, 2003; Wang *et al.*, 2007). Binding of the RcsB-RflM protein complex to a region comprising the predicted RcsB box downstream of the $P1_{flhDC}$ transcriptional start site was confirmed by electrophoretic mobility shift assay, DNaseI footprinting, and microscale thermophoresis. In the present study, this binding site was referred to as the RcsB/RflM box, because the identified binding sequence was slightly larger than proposed (+2 to +27 downstream of the $P1_{flhDC}$ +1 start site), which is probably due to different steric effects of the analyzed His_6-SUMO-RflM/RcsB complex compared to RcsB/RcsA. A previous study identified suppressor mutations that abrogated RflM-mediated repression of motility, which were mainly located in the RcsB box or close to it (Wozniak *et al.*, 2009). Consistently, the co-purified RcsB-RflM heterodimer bound specifically to fragments of the *flhDC* promoter comprising the RcsB/RflM box and not to any other *flhDC* promoter fragment.

2.3.3 Model of *flhDC* repression by the RcsB-RflM complex

Based on the findings summarized in this chapter, a novel regulatory mechanism controlling expression of the flagellar master regulatory operon *flhDC* and flagellar synthesis in response to environmental signals can be proposed (Fig. 2.22). The Rcs

system responds to changes in environmental conditions that are generally associated with cellular stress by activating the phosphorelay cascade, which results in phosphoryl group transfer to RcsB. Phosphorylated RcsB is able to bind with low affinity and specificity to the RcsB box downstream of the $P1_{flhDC}$ transcriptional start site in the *flhDC* promoter leading to repression of *flhDC* transcription. However, in absence of environmental signals the RcsCDB phosphorelay system is not activated, and the flagellar-specific novel auxiliary protein RflM is able to mediate target specificity of an existing pool of unphosphorylated RcsB to the *flhDC* promoter. The resulting heterodimeric RcsB-RflM protein complex binds with high affinity to the RcsB/RflM box in the *flhDC* promoter and blocks *flhDC* transcription. The crucial determinant in this complex is the availability of RflM. Initial expression of *flhDC* activates $FlhD_4C_2$-dependent transcription of *rflM*, which enables fine-tuning of flagellar synthesis in an early stage of flagellar synthesis by the RcsB-RflM protein complex.

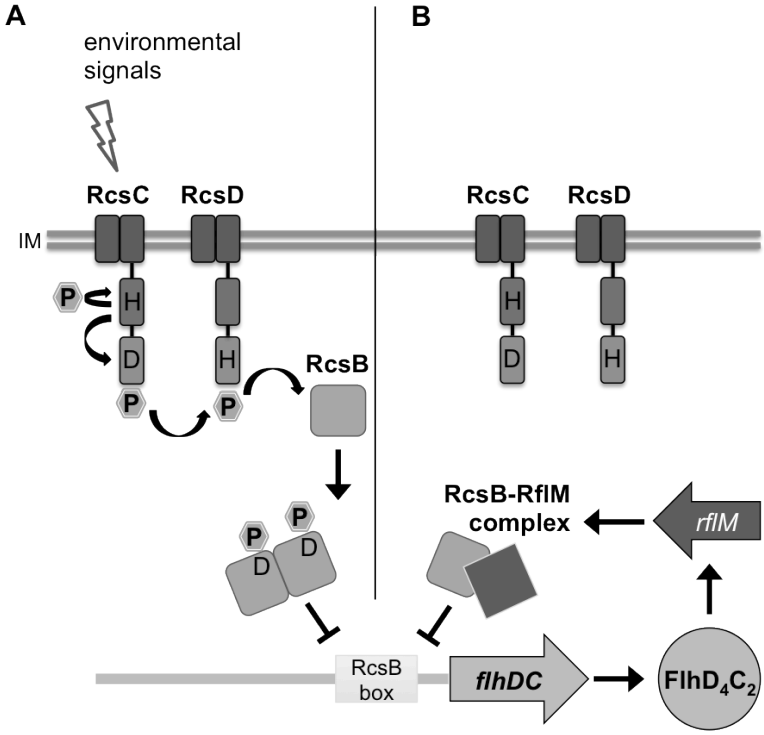

Fig. 2.22 Model for repression of *flhDC* transcription by the RcsB-RflM complex.
(A) The Rcs phosphorelay cascade is activated by environmental signals leading to RcsC autophosphorylation and phosphoryl group transfer via RcsD to RcsB. Upon phosphorylation, RcsB binds with low affinity as homodimer to the RcsB box in the *flhDC* promoter. **(B)** When RcsB phosphorylation is not possible due to absence of environmental signals, and upon $FlhD_4C_2$-dependent *rflM* expression, the RcsB-RflM heterodimeric protein complex is formed that binds with high affinity to the RcsB box in order to block *flhDC* transcription after initial expression of *flhDC* and initiation of the flagellar synthesis cascade. Figure adapted from Kühne *et al.*, 2016 with permission from John Wiley & Sons Ltd.

3 The Spi-1 virulence regulator HilD activates transcription of the flagellar master regulatory operon *flhDC* in *Salmonella* Typhimurium

This chapter focuses on HilD, the main activator of the *Salmonella* pathogenicity island 1 (Spi-1)-encoded injectisome controlling host cell invasion, and its role in cross-regulation of motility, invasion, intracellular survival, and replication. The current state of research is given in the background section (see 3.1), and new results in context to the current knowledge are highlighted (see 3.2 Results and 3.3 Discussion).

Findings of this thesis about HilD-mediated transcriptional activation of the flagellar master regulatory operon *flhDC* and its role in regulation of motility in *S.* Typhimurium are presented in this section and have been partially published before in the following peer-reviewed publication:

Singer H. M., **Kühne C.**, Deditius J. A., Hughes K. T. and Erhardt M. (2014): "The *Salmonella* Spi1 virulence regulatory protein HilD directly activates transcription of the flagellar master operon *flhDC*"
In: *Journal of Bacteriology* vol. 196(7) pp. 1448-1457, doi: 10.1128/JB.01438-13.

Contributions:

I performed all experiments and analyzed all data presented in this chapter of this thesis.
Author contributions to the publication are explained in the chapter "Declaration of Author Contributions".

3.1 Background

3.1.1 HilD – the predominant activator of the Spi-1 injectisome

The injectisome encoded on the *Salmonella* pathogenicity island 1 (Spi-1) facilitates secretion of effector molecules into epithelial host cells, which enable invasion of non-phagocytic epithelial host cells as described in more detail in Chapters 1.2 and 1.4. Briefly, a regulatory feed-forward loop composed of the three DNA-binding proteins HilD, HilC, and RtsA resides on top of the Spi-1 regulon. Each of the proteins in this loop is capable to independently activate expression of the Spi-1 master regulator *hilA*, their own, and each other. Thereby, HilD plays a predominant role, whereas HilC and RtsA amplify activation of *hilA* transcription. Subsequently, HilA activates expression of structural components and effector proteins of the Spi-1 injectisome (Ellermeier *et al.*, 2005).

The 309 amino acids long HilD protein belongs to the AraC/XylS family of primarily positive transcriptional regulators that are characterized by a conserved domain of a 99-amino-acid stretch at the C-terminus and a non-conserved domain at the N-terminus, which are connected via a linker region. The conserved domain contains typically two helix-turn-helix DNA-binding motifs, whereas the non-conserved domain is involved in DNA recognition and possesses a dimerization domain and functional activity (Gallegos *et al.*, 1997). Comparably, HilD comprises two helix-turn-helix DNA-binding motifs separated by 27 amino acids that enable binding to target promoters and regulation of transcription (Schechter and Lee, 2001). In general, members of the AraC/XylS protein family are involved in carbon metabolism, stress response, and virulence regulation (Gallegos *et al.*, 1997).

The Spi-1 injectisome is regulated by various environmental conditions, and many global regulatory inputs act at the level of HilD (Golubeva *et al.*, 2012). On the transcriptional level, *hilD* expression is activated by the ferric uptake regulator Fur via two pathways. In the metal-bound form, Fur binds to an AT-rich sequence in the *hilD* promoter leading to a direct activation of *hilD* transcription. Furthermore, binding of Fur to the *hns* promoter leads to repression of *hns* and indirect activation of *hilD* (Teixidó *et al.*, 2011; Troxell *et al.*, 2011). The nucleoid-associated proteins H-NS and Hha repress transcription of all regulators of the feed-forward loop, *hilD*, *hilC*, and *rtsA* (Olekhnovich and Kadner, 2007). In contrast, the nucleoid-binding protein Fis activates Spi-1 gene expression presumably via transcriptional activation of *hilD*, either directly or indirectly via the upstream regulator OmpR (Wilson *et al.*, 2001; Wang *et al.*, 2013). The two-component regulatory system EnvZ/OmpR, which is responsible for osmoregulation, and BarA/SirA activate HilD (Ellermeier *et al.*, 2005). SirA acts through the Csr system and thereby controls *hilD* mRNA levels. CsrA blocks *hilD* translation by binding to the mRNA near the ribosomal binding site, but is counteracted by SirA-mediated activation of the

two non-coding regulatory RNAs CsrB and CsrC that sequester CsrA (Martinez *et al.*, 2011). Additionally, *hilD* mRNA levels are stabilized by the DNA adenine methylase (Dam) and several other regulators (López-Garrido and Casadesús, 2010; Golubeva *et al.*, 2012). The activity of the HilD protein is affected upon binding by HilE, which has been shown to result in negative regulation of *hilA* expression (Baxter *et al.*, 2003). Expression of *hilE* is activated by the global virulence regulator LeuO and by the fimbrial regulator FimZ (Baxter and Jones, 2005; Espinosa and Casadesús, 2014). Recently, it has been demonstrated that the two-component regulators PhoB/PhoR and PhoP/PhoQ are involved in HilD repression via induction of *fimZ* expression and post-transcriptional stabilization of FimZ, respectively (Baxter and Jones, 2015). Moreover, the stability of HilD is affected by Lon-dependent degradation and upon growth in presence of propionate (such as propionyl-CoA) presumably via post-translational modification of the HilD protein (Takaya *et al.*, 2005; Hung *et al.*, 2013).

3.1.2 Cross-regulation of virulence systems at the level of HilD

Besides being the main regulator of the Spi-1 injectisome, HilD is additionally involved in cross-regulation between the virulence systems of *S.* Typhimurium including motility, fimbriae, Spi-1-mediated invasion, and Spi-2-mediated intracellular survival and replication. Under *in vitro* conditions it has been demonstrated that HilD regulates timing of the Spi-1 and Spi-2 injectisomes by activating Spi-2 gene expression in a later phase during stationary growth in LB medium than expression of Spi-1 genes. In contrast, HilD was not required for Spi-2 gene expression under growth conditions that mimicked the intracellular environment (Bustamante *et al.*, 2008). Cross-regulation has also been reported between HilD and fimbriae, which facilitate adhesion to host cells. StdE and StdF, encoded within the *std* fimbrial operon, downregulate *hilD* mRNA levels resulting in attenuation of eukaryotic host cell invasion and virulence in mice. This effect can be counteracted upon repression of *std* genes by Dam (López-Garrido and Casadesús, 2012). As mentioned above, the activity of HilD is regulated indirectly by the type 1 fimbrial regulator FimZ. Moreover, it has been shown that flagella, the Spi-1 injectisome, and type 1 fimbriae are regulated in a temporal hierarchy (Saini *et al.*, 2010c). Flagella and fimbriae are inversely regulated via FliZ-mediated repression of FimZ on the post-transcriptional level and via FimZ-mediated repression of *flhDC* transcription (Clegg and Hughes, 2002; Saini *et al.*, 2010c). A positive regulator of HilD activity is the flagellar protein FliZ, which thereby constitutes cross-regulation between the bacterial flagellum and the Spi-1 injectisome (Chubiz *et al.*, 2010). FliZ levels are affected indirectly by ClpXP-mediated proteolytical degradation of the flagellar master regulator $FlhD_4C_2$, and thereby the ClpXP protease indirectly influences HilD protein levels (Kage *et al.*, 2008).

3.2 Results

In a previous study, the negative auto-regulatory feedback loop of the flagellar master regulatory operon *flhDC* was investigated, and random transposon mutagenesis identified RflM as repressor of *flhDC* transcription that, in turn, is activated by $FlhD_4C_2$ (Singer *et al.*, 2013). In the same screen, one class of transposon insertions was identified that resulted in de-repression of negative *flhDC* auto-regulation only upon addition of tetracycline. The employed Tn*10d*Tc[*del-25*] transposon (T-POP) comprising the *tetRA* genes is deleted for the terminator of the *tetA* gene. Upon addition of tetracycline, this enables P_{tetA}-dependent transcription of chromosomal genes adjacent to the insertion site of the T-POP element (Rappleye and Roth, 1997). Thus, tetracycline addition resulted presumably in P_{tetA}-dependent expression of a *flhDC* activator, and DNA sequencing identified the T-POP insertion upstream of the *hilD* gene (Singer *et al.*, 2014). As mentioned above, HilD is a DNA-binding protein and known as a transcriptional activator of the master regulator of the Spi-1 injectisome, HilA (Olekhnovich and Kadner, 2002). The *hilD*-mediated positive effect on *flhDC* expression could be due to direct effects or due to indirect effects via HilD-dependent activation or repression of a positive or negative regulator of *flhDC*, respectively. However, negative effects on *rflM*, which encodes a repressor of *flhDC* transcription as described above, could be ruled out. In contrast, *hilD* overexpression resulted in increased transcript levels of *rflM* and *flhDC* (Singer *et al.*, 2014). This led to the hypothesis that HilD directly activates *flhDC* transcription.

3.2.1 The main Spi-1 activator HilD activates *flhDC* transcription

In order to confirm that HilD activates transcription of *flhDC*, expression levels of a transcriptional *flhC-lac* fusion were analyzed in a β-galactosidase assay (Fig. 3.1 A). Overexpression of *hilD* from the arabinose-inducible promoter P_{araBAD} resulted in 2.5-fold increased expression of *flhC-lac* in the non-virulent *S.* Typhimurium LT2 strain background compared to a control strain. Similarly, *flhC-lac* levels were increased upon *hilD* overexpression in the virulent strain backgrounds SL1344 and ST14028. It is important to note that all strain backgrounds were deleted for the chromosomal Spi-1 region (*ΔinvH-sprB* = Δ*spi-1*), since HilD-mediated induction of Spi-1 gene expression has been shown to result in growth retardation due to the energy-consuming expression of translocon and/or effector proteins of the injectisome (Sturm *et al.*, 2011). The use of *spi-1* deletion strains compensated this growth defect and ensured better comparison. Since no strain-specific differences in HilD-mediated activation of *flhDC* transcription were observed (Fig. 3.1 A), further experiments were performed using the non-virulent LT2 strain background.

Next, the transcriptional start site of the *flhDC* promoter affected by HilD-dependent activation of *flhDC* transcription was determined. As described before, transcription of *flhDC* is primarily driven from the $P1_{flhDC}$ and $P5_{flhDC}$ transcriptional start sites of the *flhDC* promoter (Mouslim and Hughes, 2014). Therefore, the *flhDC* promoter was fused to the *luxCDABE* cassette, and expression was determined from either the wildtype promoter ($P1\text{-}6_{flhDC}$) or individual promoters $P1_{flhDC}$ or $P5_{flhDC}$ due to -10 box mutations of the other transcriptional start sites. Overexpression of *hilD* from the arabinose promoter resulted in increased expression levels for the $P1\text{-}6_{flhDC}$ promoter fusion and for $P5_{flhDC}$ compared to a control strain, but no difference was observed for $P1_{flhDC}$ (Fig. 3.1 B). These results indicated that only the $P5_{flhDC}$ promoter is affected by HilD-mediated activation of *flhDC* transcription.

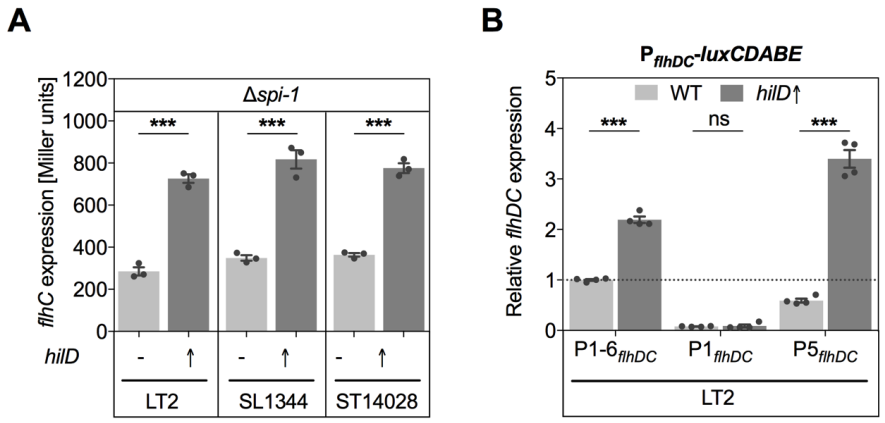

Fig. 3.1 HilD activates *flhDC* transcription from the $P5_{flhDC}$ promoter.
(A) Expression of *flhC-lac* was determined according to β-galactosidase activity upon arabinose-induced overexpression of *hilD* (↑) in comparison to a P_{araBAD}::FRT control without *hilD* expression (-) due to deletion of Spi-1 (Δ*spi-1* = Δ*invH-sprB*). The non-virulent LT2 strain background and the virulent strains SL1344 and ST14028 were analyzed. n=3. **(B)** Expression of *flhDC* was determined from luminescence activity of P_{flhDC}-*luxCDABE* fusions relative to the bacterial growth (OD_{600}) in strains with arabinose-induced overexpression of *hilD* (*hilD*↑) in comparison to a P_{araBAD}::FRT control (WT). For expression from $P1_{flhDC}$ or $P5_{flhDC}$, the -10 boxes of the other transcriptional start sites were mutated. Expression from $P1\text{-}6_{flhDC}$ or individual start sites $P1_{flhDC}$ or $P5_{flhDC}$ was determined after 3 h growth, and is shown relative to the $P1\text{-}6_{flhDC}$ WT. n=4. **(A+B)** Bars represent mean values of n biological replicates shown as individual data points (circles). Error bars represent the standard error of the mean and asterisks indicate significant difference to the respective control strains according to Student's *t*-test (ns: non significant; *** $P < 0.0005$). Panel B shows data from Singer, Kühne *et al.*, 2014 with permission from ASM.

3.2.2 Other Spi-1 regulators are not involved in HilD-mediated activation of *flhDC* transcription

After demonstrating that *hilD* overexpression activates transcription of the flagellar master regulator *flhDC*, which resides on top of the flagellar synthesis cascade, the effect on downstream flagellar genes was determined in a β-galactosidase assay (Fig. 3.2 A). Expression levels of transcriptional *lac* fusions to flagellar class 2 (*fliL-lac*) and class 3 (*fljB-lac*) promoters significantly increased upon arabinose-induced *hilD* overexpression. Since the Spi-1 genes were not deleted in this case, the activating effect on *flhC-lac* was not as pronounced as observed above (compare Fig. 3.1 A). In addition, an involvement of the Spi-1 master regulator HilA was investigated to exclude that the observed HilD-mediated activation of flagellar gene expression was not due to indirect effects via HilA. Contradictory results have been reported concerning HilA-mediated flagellar regulation. Initially, it has been shown that HilA has no effect on transcriptional *luxCDABE* fusions to *flhD* and *motA* (flagellar class 3) during growth in motility agar (Teplitski *et al.*, 2003). Later, a genome-wide location and transcriptome analysis showed *hilA*-dependent downregulation of *flhD* transcription under invasive conditions and binding of a HilA$^+$ protein extract to the *flhD* promoter (Thijs *et al.*, 2007). However, analyses of transcriptional *lac* fusions to all three classes of flagellar promoters (*flhC-*, *fliL-*, and *fljB-lac*) demonstrated that overexpression of *hilA* from the arabinose promoter had no effect on flagellar gene expression (Fig. 3.2 B). These results indicated that HilA is not involved in regulation of *flhDC* expression and flagellar synthesis, and further supports the hypothesis that HilD directly activates *flhDC* transcription.

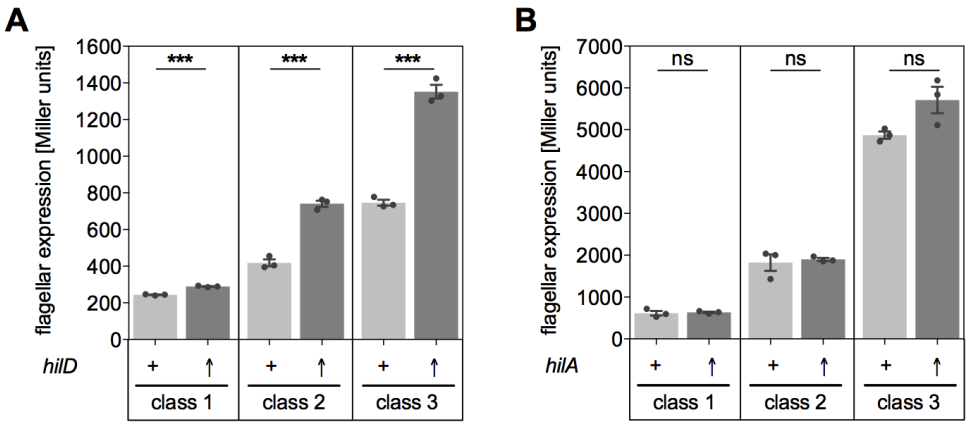

Fig. 3.2 HilD activates transcription of flagellar class 1, 2, and 3, whereas HilA has no effect.
Expression of *lac* fusions to flagellar class 1 (*flhC*), class 2 (*fliL*), and class 3 (*fljB*) promoters was determined according to β-galactosidase activity upon arabinose-induced overexpression (↑) of **(A)** *hilD* or **(B)** *hilA* in comparison to P_{araBAD}::FRT control strains (+). **(A+B)** Bars represent mean values of three biological replicates shown as individual data points (circles). Error bars represent the standard error of the mean and asterisks indicate significant difference to controls according to Student's *t*-test (ns: non significant; *** $P < 0.0005$). Panel B modified from Singer, Kühne *et al.*, 2014 with permission from ASM.

Several other DNA-binding proteins are known to regulate *flhDC* transcription (compare Chapter 1.3.1). HilD together with HilC and RtsA constitute a feed-forward loop in order to activate transcription of the Spi-1 master regulator *hilA*. The RtsB protein is encoded within the *rtsAB* operon and has been shown to repress *flhDC* transcription by binding to a region downstream of the $P1_{flhDC}$ promoter (-4 to +106 nucleotides relative to the +1 transcriptional start site of $P1_{flhDC}$) (Ellermeier and Slauch, 2003). RtsB-mediated repression of *flhDC* transcription from the $P1_{flhDC}$ promoter was confirmed in a luminescence assay (Fig. 3.3 A). Arabinose-dependent overexpression of *rtsB* resulted in decreased expression of the P1-6_{flhDC} and $P1_{flhDC}$ promoter fusions, but not of $P5_{flhDC}$. In order to test any dominant effects between HilD and RtsB in regulation of *flhDC* transcription, expression levels of a *flhC-lac* fusion were determined in a β-galactosidase assay upon overexpression of *hilD* and *rtsB* (Fig. 3.3 B). Individual overexpression of *hilD* significantly increased *flhC-lac* expression, whereas *rtsB* overexpression resulted in repression (compare column 2 and 3). However, simultaneous overexpression of *hilD* from the arabinose-inducible P_{araBAD} promoter and overexpression of *rtsB* from the AnTc-inducible P_{tetA} promoter had no effect on *flhC-lac* expression compared to a control strain (compare column 1 and 4). These results indicated that HilD and RtsB have the potential to act simultaneously, but independently, as activator and repressor of *flhDC* transcription on the $P5_{flhDC}$ and $P1_{flhDC}$ promoter, respectively.

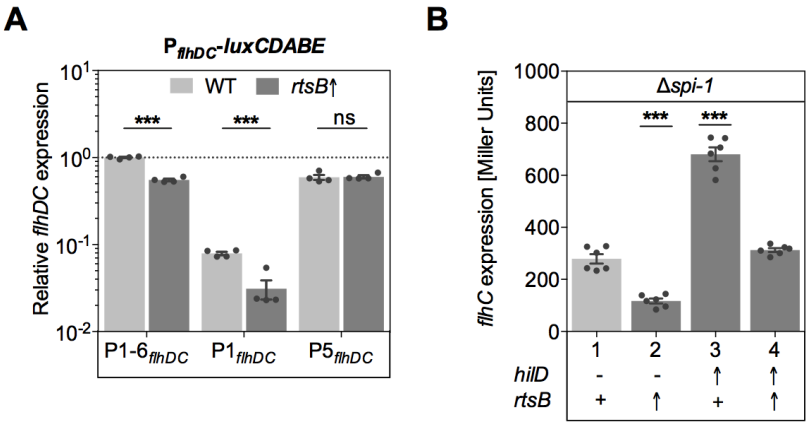

Fig. 3.3 HilD and RtsB act on different promoters to activate and repress *flhDC* transcription.
(A) Expression of *flhDC* was determined from luminescence activity of P_{flhDC}-*luxCDABE* fusions relative to the bacterial growth (OD_{600}) in strains with arabinose-induced overexpression of *rtsB* (*rtsB*↑) in comparison to a P_{araBAD}::FRT control (WT). Expression was determined after 3 h growth from the P1-6_{flhDC} promoter and from $P1_{flhDC}$ or $P5_{flhDC}$, and is shown relative to the P1-6_{flhDC} WT. n=4. **(B)** Expression of *flhC-lac* was determined according to β-galactosidase activity upon overexpression (↑) of *hilD* from P_{araBAD} or *rtsB* from P_{tetA} in comparison to a control strain (1). Due to deletion of Spi-1 (Δ*spi-1* = Δ*invH-sprB*), *hilD* was not expressed from its native promoter (-). The *rtsB* gene was present (+), but probably not expressed due to the absence of the activator HilD. n=6. **(A+B)** Bars represent mean values of n biological replicates shown as individual data points (circles). Error bars represent the standard error of the mean and asterisks indicate significant difference to the controls according to Student's *t*-test (ns: non significant; *** $P < 0.0005$). Panels A+B adapted and modified from Singer, Kühne *et al.*, 2014 with permission from ASM.

3.2.3 The HilD protein binds to a region upstream of the P5$_{flhDC}$ promoter

Since HilD is a DNA-binding protein and the results above demonstrated that HilD activates transcription of *flhDC*, the hypothesis was proposed that HilD directly binds to the *flhDC* promoter. Moreover, this hypothesis was supported by a HilD deletion mutant lacking its helix-turn-helix DNA-binding motif, which was no longer able to activate *flhDC* transcription (Singer *et al.*, 2014). To test this hypothesis, protein-DNA binding studies were performed with recombinantly expressed and purified HilD protein and 5'-biotin-labeled fragments of the *flhDC* promoter. Analyzed fragments comprised either the P1$_{flhDC}$ or P5$_{flhDC}$ transcriptional start site (P1$_{flhDC}$ -271 to -71; P5$_{flhDC}$ -588 to -388; P5'$_{flhDC}$ -688 to -462 nucleotides upstream of the *flhD* start codon) or neither the P1$_{flhDC}$ nor P5$_{flhDC}$ transcriptional start site (P4/6$_{flhDC}$, -431 to -231 nucleotides upstream of the *flhD* start codon) as illustrated in Fig. 3.4. A DNA fragment of the *flhDC* coding region (+403 to +672 nucleotides of *flhD*) and *gyrA* DNA served as negative controls.

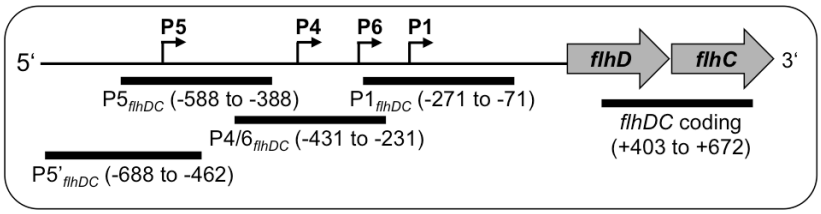

Fig. 3.4 EMSA probes used for HilD-P$_{flhDC}$ interaction studies.
DNA fragments covering the *flhDC* promoter region used for electrophoretic mobility shift assays (EMSAs) and their positions relative to the *flhD* ATG start codon are shown schematically. Arrows labeled P1, P4, P5, and P6 indicate the respective transcriptional start sites.

Biotin-labeled *flhDC* promoter fragments were incubated with increasing amounts of purified HilD protein, and binding of HilD to these fragments was analyzed using electrophoretic mobility shift assays (EMSAs). A shift of promoter fragments comprising the P5$_{flhDC}$ transcriptional start site (P5$_{flhDC}$ and P5'$_{flhDC}$) was observed (Fig. 3.5). Upon addition of excess amounts of unlabeled competitor DNA of the respective promoter fragment, the shift of biotin-labeled DNA was released indicating specific binding of HilD protein to these *flhDC* promoter fragments. In contrast, no binding was observed for other *flhDC* promoter fragments or the negative controls *flhDC* coding and *gyrA* DNA.

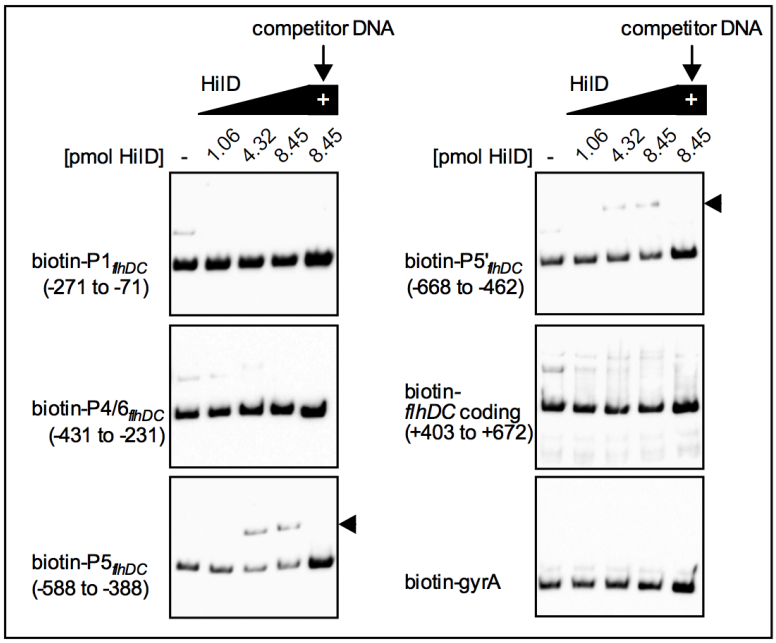

Fig. 3.5 Purified HilD protein binds to a *flhDC* promoter fragment comprising P5$_{flhDC}$.
Electrophoretic mobility shift assays (EMSAs) were performed with increasing amounts of purified HilD protein as indicated above the lanes [pmol] and 0.01 pmol of each 5'-biotin-labeled *flhDC* promoter DNA and control fragment (*flhDC* coding, *gyrA*). Numbers in brackets indicate the position of each P$_{flhDC}$ fragment relative to the *flhD* start codon. Specific binding was demonstrated upon addition of excess amounts (250-fold) of unlabeled competitor DNA of the respective promoter fragment to the highest HilD protein concentration (+). Arrowheads on the right indicate HilD-DNA complexes. Figure modified from Singer, Kühne *et al*., 2014 with permission from ASM.

Next, the precise binding site of HilD protein to the *flhDC* promoter region comprising the P5$_{flhDC}$ transcriptional start site was investigated by DNaseI footprint analysis (Fig. 3.6). Increasing amounts of purified HilD protein were incubated with a 5'-DIG-labeled *flhDC* promoter fragment (-668 to -388 upstream of the *flhD* start codon; non-coding strand labeled), which contained the putative binding site as determined by EMSAs. After partial digestion with DNaseI, the reactions were analyzed on a sequencing gel. A region from -68 to -24 nucleotides upstream of the +1 transcriptional start site of the P5$_{flhDC}$ promoter was protected from DNaseI digestion indicating binding of the HilD protein to this region. Furthermore, HilD binding to the *flhDC* promoter resulted in exposed nucleotides at positions -51, -33, -28, and -27 probably due to enhanced digestion. HilD-mediated DNA bending of the P5$_{flhDC}$ fragment could make these nucleotides more accessible to degradation by DNaseI.

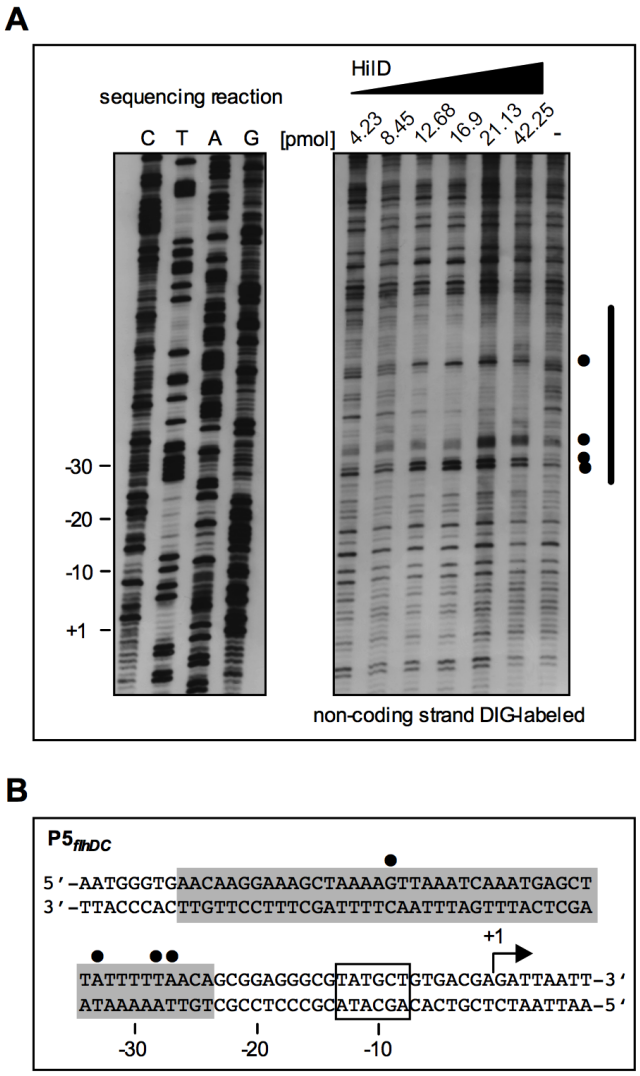

Fig. 3.6 HilD protein binds to a region upstream of the P5*flhDC* transcriptional start site.
(A) DNaseI footprinting was performed with increasing amounts of purified HilD protein as indicated above the lanes [pmol] and 100 ng 5'-DIG-labeled *flhDC* promoter DNA (non-coding strand DIG-labeled) comprising P5*flhDC* (-668 to -388 upstream of the *flhD* start codon). The vertical line on the right indicates the protected region, and dots indicate exposed nucleotides. Lanes C, T, A, and G show the sequencing reactions of the P5*flhDC* fragment. **(B)** Partial DNA sequence of the P5*flhDC* promoter with -10 box and +1 transcriptional start site. The HilD binding site is highlighted in gray and exposed nucleotides are marked with dots. Panels A+B modified from Singer, Kühne *et al*. with permission from ASM.

3.3 Discussion

The HilD protein is the predominant transcriptional activator of *hilA*, the master regulator of the Spi-1-encoded injectisome. HilA activates synthesis of structural components of the injectisome and effector molecules, which facilitate invasion of non-phagocytic epithelial host cells (Ellermeier *et al.*, 2005). Besides activating the Spi-1 injectisome, HilD has been reported to be involved in cross-regulation between the virulence systems of *S.* Typhimurium (Bustamante *et al.*, 2008; Saini *et al.*, 2010c; Chubiz *et al.*, 2010). Recently, transcriptome analyses from differential RNA sequencing data discovered activation of transcriptional start sites of *S.* Typhimurium strain SL1344 under several infection-relevant conditions. Spi-1 inducing conditions (i. e. anaerobic growth (Bajaj *et al.*, 1996)) have been shown to activate *flhDC* expression from the $P5_{flhDC}$ transcriptional start site (Kröger *et al.*, 2013), indicating a link between Spi-1 and the flagellar master regulator. Previously, an unbiased transposon mutagenesis screen was performed in order to investigate the negative auto-regulation of the flagellar master regulatory operon *flhDC*, which identified RflM as novel negative regulator of *flhDC* expression generating the negative $FlhD_4C_2$-RflM feedback loop (Singer *et al.*, 2013). Additionally, this screen suggested an involvement of HilD in *flhDC* regulation. Indeed, initial investigations demonstrated increased expression level of a transcriptional *flhC-lac* fusion upon overexpression of *hilD* from the arabinose promoter (Singer *et al.*, 2014). The HilD protein belongs to the AraC/XylS family of transcriptional activators and comprises two helix-turn-helix DNA-binding motifs for regulation of target gene expression upon binding (Schechter and Lee, 2001).

In this thesis, the mode of action of HilD-mediated transcriptional activation of the flagellar master regulatory operon *flhDC* in *S.* Typhimurium was elucidated. The findings summarized in this chapter demonstrate that HilD activates *flhDC* transcription by directly binding to a region upstream of the transcriptional start site of the $P5_{flhDC}$ promoter. This provides another level of cross-regulation between the Spi-1 injectisome and flagellar motility.

3.3.1 Mode of action of HilD-dependent *flhDC* activation

The HilD-mediated activation of *flhDC* transcription was observed in all tested strain backgrounds, which represent different virulence characteristics. Strain LT2 is attenuated in virulence due to suboptimal translation of the RpoS sigma factor (Hoiseth and Stocker, 1981). The virulent strain SL1344 is histidine auxotroph, but more virulent compared to ST14028 due to the presence of the additional Spi-1 effector SopE (Wilmes-Riesenberg *et al.*, 1997; Clark *et al.*, 2011). However, no strain-specific differences were detected upon *hilD*-mediated activation of *flhDC* transcription. Overexpression of *hilD* not only resulted

in transcriptional activation of the flagellar master regulatory operon *flhDC*, but also in activation of downstream genes that are under control of flagellar class 2 (*fliL*) and class 3 (*fljB*) promoters. Thus, HilD activates the whole flagellar synthesis cascade, which has been shown to ultimately result in flagellar assembly and rotation (J. A. Deditius, Master's thesis; J. A. Horstmann, unpublished). In this process, *flhDC* transcription from the $P5_{flhDC}$ transcriptional start site seems to play an important role. In accordance to the transcriptome analyses described above (Kröger *et al.*, 2013), binding of HilD upstream of the +1 transcriptional start site of the $P5_{flhDC}$ promoter activates flagellar master operon transcription.

The identified HilD binding site in the *flhDC* promoter region shares several conserved nucleotides with known HilD binding sites in the *hilD, hilA, hilC,* and *rtsA* promoters (Olekhnovich and Kadner, 2007) (compare Fig. S1). Additionally, the location of the HilD binding site within the entire *flhDC* promoter region is comparable to the one in the *invF* promoter. The promoter region of *invF*, which encodes an activator of Spi-1 effector proteins, has two transcriptional start sites that are differentially regulated. Usually, transcription of *invF* is activated upon binding of the Spi-1 master regulator HilA. In order to activate *invF* transcription independent of HilA, the HilD protein binds to a promoter that is far upstream of the HilA-controlled promoter and the *invF* open reading frame (Akbar *et al.*, 2003). Likewise, the transcriptional start site of *flhDC* that is activated by HilD, $P5_{flhDC}$, is located far upstream of the *flhD* open reading frame.

DNaseI footprinting identified a region of the *flhDC* promoter from nucleotides -68 to -24 relative to the +1 transcriptional start site of $P5_{flhDC}$ that is protected and partially exposed upon binding of HilD. Thereby, HilD seems to cover the -35 box of $P5_{flhDC}$ upon binding, which is usually recognized by the RNA polymerase to initiate transcription. This localization is in accordance with other members of the AraC/XylS family of transcriptional activators, whose binding sites have been reported to be adjacent to the -35 box or overlapping this region (Gallegos *et al.*, 1997). Comparably, the HilD binding sites in the *hilA* (-101 to -49), *hilC* (-91 to -47), *hilD* (-98 to -55), and *rtsA* (-74 to -34) promoters are located close to the -35 box of the respective transcriptional start sites in the promoter region (Schechter and Lee, 2001; Olekhnovich and Kadner, 2002; Olekhnovich and Kadner, 2007). Several DNA-bound regulators interact directly with the RNA polymerase at the C-terminal or N-terminal domain of the α-subunit (α-CTD or α-NTD) or the σ^{70} subunit to stabilize binding of the RNA polymerase to the promoter (Hochschild and Dove, 1998). However, for the *E. coli* AraC/XylS family members MarA, SoxS, and Rob it has been shown that they do not require interaction with the α-CTD for transcriptional activation from binding sites that overlap the -35 region. More important is the about 20 base pair distance between the interaction site and the -10 hexamer of the RNA polymerase (Martin *et al.*, 1999). The distance between the HilD binding site in the

$P5_{flhDC}$ promoter region and its -10 box is comparably short. Thus, HilD might interact with the α-NTD or the σ^{70} subunit of the RNA polymerase to stimulate transcription of *flhDC* from the $P5_{flhDC}$ transcriptional start site. Additionally, HilD might have conformation-dependent negative effects on *flhDC* transcription as already discussed earlier for HilD-mediated activation of *hilA* transcription (Schechter and Lee, 2001). One prominent example for this mechanism is the regulation of the arabinose promoter. Without arabinose, AraC represses transcription of the *araBAD* operon. Upon presence of arabinose, the AraC protein undergoes a conformational change, which enables activation of *araBAD* transcription (Schleif, 2010). Similarly, external or internal signals might modulate HilD binding to the *flhDC* promoter. However, there was no evidence for HilD-mediated repression of *flhDC* transcription, neither upon *hilD* overexpression nor deletion (Mouslim and Hughes, 2014), that would indicate such a regulation.

As mentioned above, binding of HilD to the $P5_{flhDC}$ promoter region generated exposed nucleotides in the DNaseI protection assay. Crystal structure analysis of the *E. coli* MarA protein in complex with target DNA has been shown to bend the DNA-binding site by an angle of 35°. This enables interaction of the two helix-turn-helix DNA-binding motifs of MarA with two adjacent major grooves of the target DNA region (Rhee *et al.*, 1998). Comparably, HilD seems to bend the region upstream of the transcriptional start site of the $P5_{flhDC}$ promoter. For MarA and Rob monomers, binding sites with a length of 20 nucleotides have been described to be sufficient (Martin *et al.*, 1999). Thus, the identified 45 base pair long HilD binding site in the $P5_{flhDC}$ promoter might be bound by two HilD monomers. Likewise, interaction of a HilD dimer with target promoter regions was proposed before (Olekhnovich and Kadner, 2007). The HilD-mediated DNA-bending might additionally influence interaction of the RNA polymerase with the $P5_{flhDC}$ promoter region to initiate *flhDC* expression.

Several studies assumed another model for HilD-dependent transcriptional activation of target genes: the displacement of negative regulators upon HilD binding. For expression of *hilA*, the so-called upstream repressing sequence (URS) plays an important role, since many negative regulators such as Hha and H-NS bind to this region. The binding site of HilD in the *hilA* promoter has been mapped inside this URS leading to the model that HilD counteracts and displaces negative regulators (Lucas and Lee, 2001; Schechter and Lee, 2001). However, HilD has been shown to be indispensable for *hilA* expression also in the absence of known repressors (Boddicker *et al.*, 2003). However, in absence of the repressors Hha and H-NS, expression of *rtsA* is no longer dependent on HilD, indicating that HilD binding to the *rtsA* promoter antagonizes Hha and H-NS (Olekhnovich and Kadner, 2007). Recently, HilD-mediated effective displacement of H-NS from target promoters was demonstrated for the Spi-2 operon *ssrAB*, which is activated upon HilD binding in the late stationary growth phase in LB medium (Martínez

et al., 2014). Comparably, HilD might counteract negative regulators of *flhDC* expression that bind to the $P5_{flhDC}$ promoter region. One such candidate could be the DNA-binding protein LrhA, which has been shown to repress *flhDC* transcription from the $P5_{flhDC}$ promoter during the initial growth phase, whereas HilD activates *flhDC* transcription from $P5_{flhDC}$ in a later growth phase (Mouslim and Hughes, 2014). Thus, HilD might displace bound LrhA from the *flhDC* promoter region in order to activate *flhDC* transcription. However, the so-far annotated LrhA binding site does not overlap with the identified HilD binding site, and further studies need to be conducted to analyze LrhA-mediated repression of *flhDC* transcription in *S.* Typhimurium in more detail.

Taken together, both the displacement of negative regulators and the recruitment and stabilization of the RNA polymerase upstream of the $P5_{flhDC}$ transcriptional start site might contribute to HilD-mediated activation of *flhDC* transcription from the $P5_{flhDC}$ promoter.

3.3.2 Cross-regulation between the Spi-1 and flagellar regulons

The characterized HilD-mediated transcriptional activation of the flagellar master regulatory operon *flhDC* adds another level of cross-talk between flagellar motility and the invasion-relevant Spi-1 injectisome. Both HilD and $FlhD_4C_2$ constitute master regulators of the respective virulence system and enable cross-regulation at the initiation of virulence gene expression. The regulatory network between both virulence systems is illustrated schematically in Fig. 3.7. The flagellar master regulator $FlhD_4C_2$ activates transcription of *rflM*, which forms the RcsB-RflM complex in order to repress *flhDC* transcription from the $P1_{flhDC}$ promoter as described in Chapter 2. Additionally, $FlhD_4C_2$ activates transcription of flagellar genes from class 2 promoters, such as the *fliAZ* operon. The FliZ protein positively regulates activity of HilD on the post-transcriptional level and thereby indirectly promotes expression of the Spi-1 injectisome (Iyoda *et al.*, 2001; Chubiz *et al.*, 2010). Besides activating the Spi-1 injectisome, HilD activates transcription of *flhDC* from the $P5_{flhDC}$ promoter. Negative regulation of *flhDC* expression from the Spi-1 regulon occurs via RtsB, which is encoded in the *rtsAB* operon and represses *flhDC* transcription from the $P1_{flhDC}$ promoter independent of HilD (Ellermeier and Slauch, 2003). A previously proposed negative effect of HilA on flagellar gene transcription was not observed in this thesis. Studies performed by Thijs *et al.* showed binding of $HilA^+$ protein extract to the *flhDC* promoter (Thijs *et al.*, 2007). However, the use of extracts instead of purified proteins could result in false positive results, and the observed binding could be due to the presence of another *flhDC* regulator in this protein extract, such as HilD.

The most significant role of cross-regulation between the different virulence systems in *S.* Typhimurium is timing during the infection process. The role of flagella and cross-regulation with other virulence systems during the infection process is discussed in more detail in the conclusion section in Chapter 5.

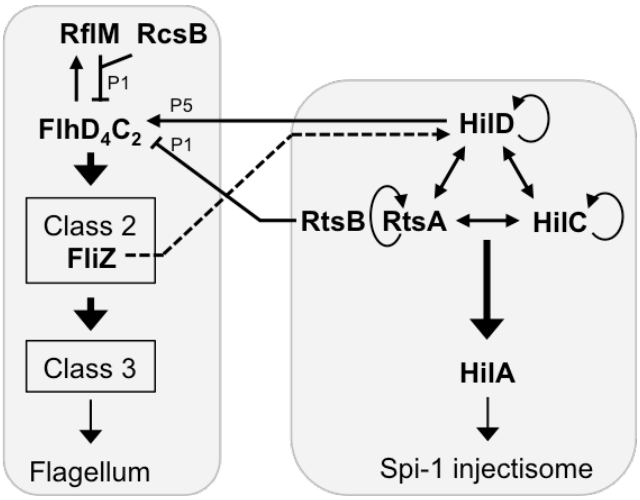

Fig. 3.7 Model of cross-regulation between the flagellar and Spi-1 synthesis cascades.
The flagellar master regulator $FlhD_4C_2$ constitutes a negative feedback leading to repression of *flhDC* transcription from the $P1_{flhDC}$ promoter by the RcsB-RflM complex. Additionally, $FlhD_4C_2$ initiates the flagellar synthesis cascade. The flagellar protein FliZ activates the main Spi-1 regulator HilD on the post-transcriptional level (dashed line). The HilD protein, in turn, and the Spi-1-related protein RtsB independently activate and repress transcription of the *flhDC* from the $P5_{flhDC}$ and $P1_{flhDC}$ promoters, respectively. For simplification, encoding genes are not shown.

4 Growth phase-dependent heterogeneous expression of the flagellar master regulatory operon *flhDC* in *Salmonella* Typhimurium

This chapter focuses on heterogeneous expression and bistability in *S.* Typhimurium, in particular bistable regulation of flagellar gene expression. The current state of research is given in the background section (see 4.1), and new results in context to the current knowledge are highlighted (see 4.2 Results and 4.3 Discussion). In this section, findings of this thesis about heterogeneous expression of the flagellar master regulatory operon *flhDC* and its role in regulation of motility in *S.* Typhimurium are presented.

Contributions:

I performed all experiments and analyzed all data presented in this chapter of this thesis except the following. For single-cell time-lapse fluorescence microscopy experiments, I constructed strains, prepared samples and performed the experiments together with Dr. Tobias Bergmiller at the Institute of Science and Technology Austria.

4.1 Background

4.1.1 Phenotypic heterogeneity in bacteria

A bacterial population is not strictly clonal, but may display differences between individual cells as elucidated in the last decade by several single-cell-based analysis tools, such as fluorescence microscopy and flow cytometry (Brehm-Stecher and Johnson, 2004). Phenotypic heterogeneous bacterial populations contain individual cells that are genetically identical, but behave differently under the same growth conditions (Avery, 2006). The bifurcation of one population into two distinct subpopulations without any DNA mutation or rearrangement is termed bistability, which represents a special kind of phenotypic heterogeneity (Dubnau and Losick, 2006; Graumann, 2006). Two distinct subpopulations can be characterized by two stable expression states of a certain gene, like high or low/no expression, as illustrated schematically in Fig. 4.1. A prerequisite for phenotypic heterogeneity are stochastic fluctuations in gene expression, referred to as (intrinsic) noise. This intrinsic noise is influenced by the rates of transcription and translation, regulatory dynamics, and genetic factors. The bifurcation into two subpopulations is facilitated if some cells exceed a certain threshold, which results in expression of a certain gene in this subpopulation, whereas other cells do not express this gene (Ozbudak *et al.*, 2002; Elowitz, 2002). Thereby, positive and double negative feedback loops of regulatory networks together with a non-linear response play a major role, but also DNA methylation is involved (Ferrell, 2002; Casadesús and Low, 2013). Recently, another effect of noise and feedback loops has been described, namely pulsing. This kind of phenotypic heterogeneity is characterized by a pulse-like activation and deactivation of key regulators, which enables a temporal organization of genetic circuits (Levine *et al.*, 2013).

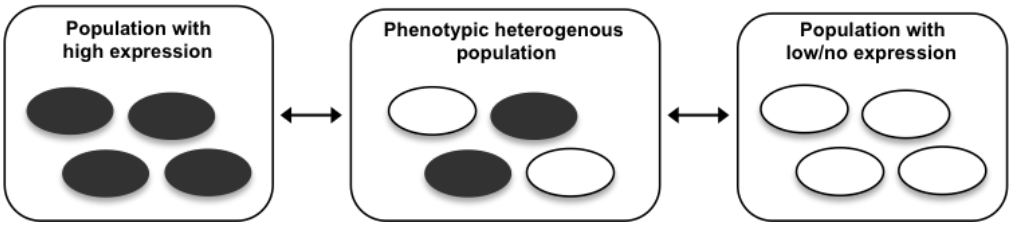

Fig. 4.1 Principle of phenotypic heterogeneous bacterial populations.
Genetically identical bacterial population may express a certain gene with either high (only black cells) or low/no levels (only white cells) resulting in homogeneous populations, respectively. Stochastic fluctuations in gene expression may result in phenotypic heterogeneous populations that contain individual cells with high or low/no expression levels of a certain gene at the same time under the same environmental conditions.

Phenotypic heterogeneity is widespread among Gram-negative and Gram-positive bacteria and can be found in many bacterial processes, such as persistence, antibiotic resistance, motility, biofilms, competence, sporulation, and quorum-sensing (Grote *et al.*, 2015). Compared to homogeneous populations, phenotypic heterogeneity displays several advantages for the entire bacterial population, which can be summarized as a kind of social behavior. On the one hand, it enables a form of bet-hedging and risk-spreading strategies by comprising one subpopulation that is optimized to the current environmental condition and another subpopulation that is pre-adapted to future conditions. This increases the fitness of the entire population, especially in unfavorable and fast changing environments (Veening *et al.*, 2008b). On the other hand, it provides the division of labor by comprising one subpopulation that is specialized to a cellular function and takes over the producing costs, but shares the benefits with the whole bacterial population (van Gestel *et al.*, 2015).

4.1.2 Examples of phenotypic heterogeneity in *S.* Typhimurium

S. Typhimurium utilizes both bet-hedging and the division of labor from phenotypic heterogeneous populations to enable efficient pathogenesis (Ackermann, 2015). The formation of biofilms is a well-studied example for the division of labor in bacterial populations (van Gestel *et al.*, 2015). In *S.* Typhimurium, the biofilm master regulator CsgD is bistably expressed, which results in one subpopulation of planktonic cells that express low level of CsgD. The other subpopulation expresses high level of CsgD, is associated with multicellular aggregates, and produces cellulose for the biofilm development of the bacterial community (Grantcharova *et al.*, 2010). Furthermore, transcriptome analyses revealed that the planktonic subpopulation is correlated with virulence, whereas aggregated cells enable persistence in harsh environments and thus provide a bet-hedging strategy (MacKenzie *et al.*, 2015). Another and extreme form of division of labor is self-destructive cooperation and can be found in bistable expression of the Spi-1-encoded virulence-associated type-III-secretion system (vT3SS-1). In this process, a vT3SS-1 positive subpopulation allows for host cell invasion, but is retarded in growth and rapidly cleared by the host immune system. However, a fast-growing vT3SS-1 negative subpopulation is able to outcompete the commensal microbiota due to the induced inflammatory response (Ackermann *et al.*, 2008; Sturm *et al.*, 2011; Diard *et al.*, 2013). As the vT3SS-1 positive subpopulation is retarded in growth, it additionally enables bet-hedging due to increased tolerance against antibiotic treatment (Arnoldini *et al.*, 2014). Such persistent subpopulations typically arise from preexisting heterogeneous populations and provide temporary tolerance to certain stresses and antibiotics. If cells from these populations regrow, they regain sensitivity (Balaban, 2004).

Phenotypic heterogeneity has also been described for many promoters that control flagellar synthesis in *S*. Typhimurium, which are characterized by high levels of noise in gene expression (Freed *et al.*, 2008). For instance, expression of the flagellar filament protein flagellin encoded by *fliC* is bistable, which results in the formation of a *fliC*-positive and a *fliC*-negative subpopulation during systemic infection. Moreover, the *fliC*-positive subpopulation is anatomically restricted to the Peyer's patches and not present in deeper organs, such as mesenteric lymph nodes and spleen (Cummings *et al.*, 2006). This enables both bet-hedging and the division of labor. The *fliC*-positive subpopulation is recognized by the host immune system and stimulates inflammation, whereas the *fliC*-negative subpopulation is able to evade the caspase-1-mediated immune response and to spread into deeper organs. This bistability is regulated by YdiV and FliZ, separately (Stewart *et al.*, 2011; Stewart and Cookson, 2014). Additionally, the FliZ-YdiV double negative feedback loop generates bistable expression of *flhB*, which is transcribed from a flagellar class 2 promoter and encodes the inner membrane protein of the flagellar T3SS. Thereby, phenotypic heterogeneity of flagellar motility is regulated in response to nutrients (Saini *et al.*, 2010b; Koirala *et al.*, 2014).

4.2 Results

In a previous study it has been demonstrated that expression of the flagellar master regulatory operon *flhDC* is regulated in a growth phase-dependent manner on the transcriptional level (Mouslim and Hughes, 2014). In order to analyze this growth phase-dependent regulation in more detail and in terms of the bacterial population, the *flhDC* promoter region was fused to an enhanced variant of the green fluorescent protein ($eGFP_{LVA}$) in the pKH70 plasmid (pKH70-P_{flhDC}-$egfp_{LVA}$). P_{flhDC}-$egfp_{LVA}$ expression enabled single-cell analyses to determine the expression dynamics of the *flhDC* promoter of individual cells within one bacterial population. Since the eGFP protein is very stable, the $eGFP_{LVA}$ variant was used, which contains a C-terminal degradation tag (amino acid sequence: RPAANDENYA-LVA) (Andersen *et al.*, 1998). This SsrA-like tag is rapidly degraded by tag-specific proteases and enables detection of rapid changes in gene expression. Degradation of $eGFP_{LVA}$ was reported to be dependent on the bacterial species and growth conditions (Andersen *et al.*, 1998). Therefore, the half-life of the $eGFP_{LVA}$ protein was determined in the virulent *S.* Typhimurium strain background ST14028 harboring the pKH70-P_{flhDC}-$egfp_{LVA}$ plasmid during growth in LB medium batch cultures at 37 °C, the standard growth conditions used. After stopping of *de novo* protein synthesis, the protein levels of $eGFP_{LVA}$ were determined by western blot analyses and normalized to the corresponding DnaK amounts, which served as loading control (Fig. 4.2). The slope constant of the $eGFP_{LVA}$ degradation was determined to be approximately -0.06219 min^{-1}, and the half-life was calculated as described before (Andersen *et al.*, 1998) with the following equation: $t_{1/2} = -\ln 2 / \text{slope}$. This resulted in an $eGFP_{LVA}$ half-life of approximately 4.8 min in the ST14028/pKH70-P_{flhDC}-$egfp_{LVA}$ strain under the tested growth conditions.

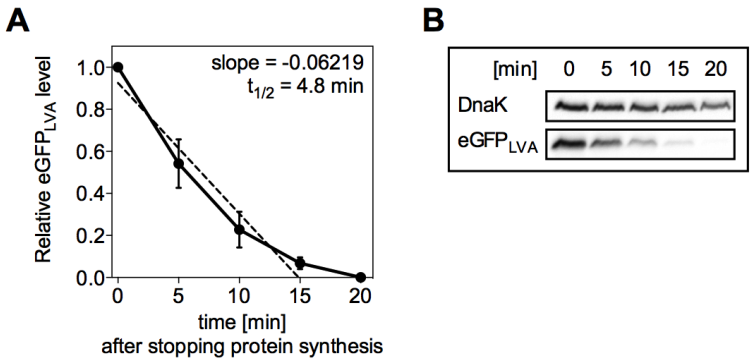

Fig. 4.2 Stability of the $eGFP_{LVA}$ fusion protein in *S.* Typhimurium ST14028.
Protein levels of $eGFP_{LVA}$ expressed from the pKH70-P_{flhDC}-$egfp_{LVA}$ fusion plasmid were determined 0, 5, 10, 15, and 20 min after stopping of protein synthesis. **(A)** $eGFP_{LVA}$ levels are shown relative to the corresponding DnaK control and $t = 0$ min. Data points represent mean values of three biological replicates with connection line, and error bars represent the standard error of the mean. The dashed line shows the linear regression determined using the software PRISM. The $eGFP_{LVA}$ half-life was calculated with $t_{1/2} = -\ln 2 / \text{slope}$. **(B)** Exemplary western-blots of DnaK and $eGFP_{LVA}$ protein levels.

Before analyzing P_{flhDC}-$egfp_{LVA}$ expression from the pKH70 fusion plasmid of individual *S.* Typhimurium ST14028 cells, growth phenotypes of all strains of interest were determined in LB medium batch cultures at 37 °C (Fig. 4.3). A strain harboring the wildtype *flhDC* promoter fused to $egfp_{LVA}$ in the pKH70 plasmid (pKH70-P_{flhDC}-$egfp_{LVA}$) required approximately two hours to adapt to the growth conditions. This lag phase was followed by exponential growth, which could be separated into an early exponential growth phase (2–3 h post inoculation) and a late exponential growth phase (5–6 h post inoculation). Strains harboring the pKH70-P_{flhDC}-$egfp_{LVA}$ plasmid with variants of the fused *flhDC* promoter or a constitutive active promoter instead ($P_{LtetO-1}$) displayed a similar growth phenotype (Fig. 4.3 A). Comparably, the absence of the *flhDC* regulators *rcsB*, *hilD*, and *fliZ* in a strain harboring the wildtype pKH70-P_{flhDC}-$egfp_{LVA}$ fusion plasmid did not affect bacterial growth (Fig. 4.3 B). In contrast, deletion of *rflM*, which encodes the negative regulator of *flhDC* transcription, RflM, resulted in slower growth compared to the wildtype strain background (Fig. 4.3 B). Preliminary experiments were performed with mutant strains that prevented YdiV-mediated degradation of FlhD protein via the ClpXP protease (Fig. 4.3 C). Deletion of *ydiV* had no effect on bacterial growth. However, a strain with a $FlhD_{L22H}$ point mutation that prevented binding of YdiV to the FlhD protein resulted in slower growth, which was additionally reduced with simultaneous deletion of *rflM*. This indicated that an appropriate (low) level of flagellar expression is necessary to enable an optimal distribution of the cell's biosynthetic resources for other physiological processes, such as bacterial growth.

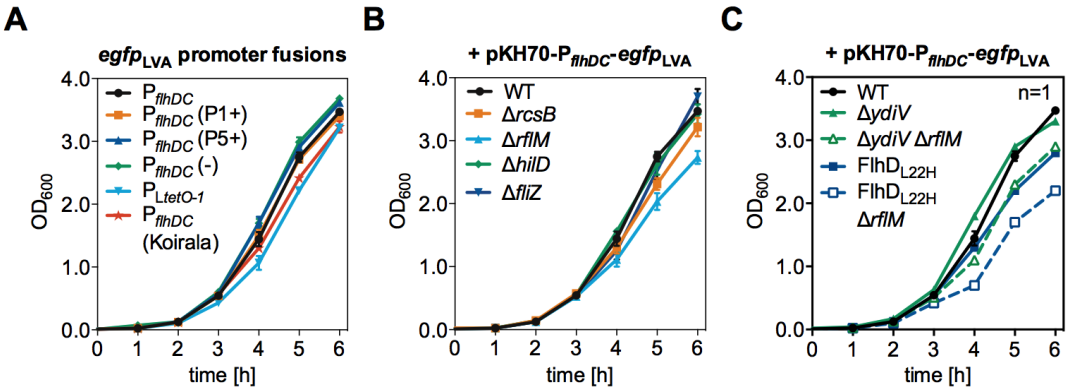

Fig. 4.3 Growth curves of strains expressing $egfp_{LVA}$ promoter fusions.
Bacterial growth was determined by measuring the optical density at 600 nm (OD_{600}) 1–6 h post inoculation from batch cultures grown in LB medium at 37 °C. **(A)** Growth curves of ST14028 wildtype strains harboring the pKH70-P_{flhDC}-$egfp_{LVA}$ plasmid with different P_{flhDC} variants (P1+, P5+, Koirala, and -) or pKH70-$P_{LtetO-1}$-$egfp_{LVA}$. n = 6. **(B)** Growth curves of ST14028 wildtype (WT) and mutant strains (Δ*rcsB*, Δ*hilD*, and Δ*fliZ*) harboring the pKH70-P_{flhDC}-$egfp_{LVA}$ plasmid or Δ*rflM* with pKH70-P_{flhDC} (P+1)-$egfp_{LVA}$. n = 6. **(C)** Preliminary growth curves of ST14028 wildtype (WT) and mutant strains (Δ*ydiV* ± Δ*rflM*, $FlhDC_{L22H}$ ± Δ*rflM*) harboring the pKH70-P_{flhDC}-$egfp_{LVA}$ plasmid. n = 1. **(A–C)** Data points represent mean values of n biological replicates with connection lines, and error bars represent the standard error of the mean.

4.2.1 Expression of *flhDC* is growth phase-dependent heterogeneous

Next, P_{flhDC}-*egfp*$_{LVA}$ expression from the pKH70 fusion plasmid (pKH70-P_{flhDC}-*egfp*$_{LVA}$) was determined at different growth phases (1–6 h post inoculation) for the ST14028 wildtype strain (Fig. 4.4). Flow cytometry analyses of batch cultures grown in LB medium at 37 °C revealed two co-existing, distinct subpopulations (Fig. 4.4 A): one subpopulation that was $eGFP_{LVA}$-positive and another subpopulation that was $eGFP_{LVA}$-negative. The proportion of these subpopulations was growth phase-dependent. After an adaptation during the lag phase, the percentage of $eGFP_{LVA}$-positive cells increased during early exponential growth (2 h post inoculation) due to activation of $eGFP_{LVA}$ expression from the pKH70-P_{flhDC}-*egfp*$_{LVA}$ plasmid. The initial surge of transcription was followed by a decrease in expression (3 h post inoculation). During late exponential growth (5 h post inoculation), the percentage of $eGFP_{LVA}$-positive cells additionally increased, but to a minor extent than observed in the earlier growth phase. However, the $eGFP_{LVA}$ fluorescence intensities were stronger during late exponential growth compared to the early exponential growth phase. This led to the hypothesis that different promoters within P_{flhDC} drive the growth phase-dependent heterogeneous expression of $eGFP_{LVA}$ from the pKH70-P_{flhDC}-*egfp*$_{LVA}$ fusion plasmid.

In order to follow the growth phase-dependent P_{flhDC}-*egfp*$_{LVA}$ expression of individual cells in more detail, live-cell imaging was performed using single-cell time-lapse fluorescence microscopy. Therefore, the ST14028 wildtype strain harboring the pKH70-P_{flhDC}-*egfp*$_{LVA}$ plasmid and a constitutively expressed plasmid (pFS48-mCherry) was grown in batch cultures to mid-exponential growth phase and analyzed on LB agarose pads under the microscope for two hours at 37 °C. Consistent with the growth phase-dependent phenotypic heterogeneity of the *flhDC* promoter determined for batch cultures using flow cytometry, the bacterial population displayed phenotypic heterogeneous P_{flhDC}-*egfp*$_{LVA}$ expression (Fig. 4.4 B). Some cells were $eGFP_{LVA}$-positive, whereas others were $eGFP_{LVA}$-negative. Moreover, cells switched between these two states quickly within approximately 8–12 minutes, instead of maintaining one expression state all the time. The $eGFP_{LVA}$ fluorescence signal intensities of the P_{flhDC}-*egfp*$_{LVA}$ construct varied for single cells during growth, similar to what has been observed for early and late exponential growth phases using flow cytometry.

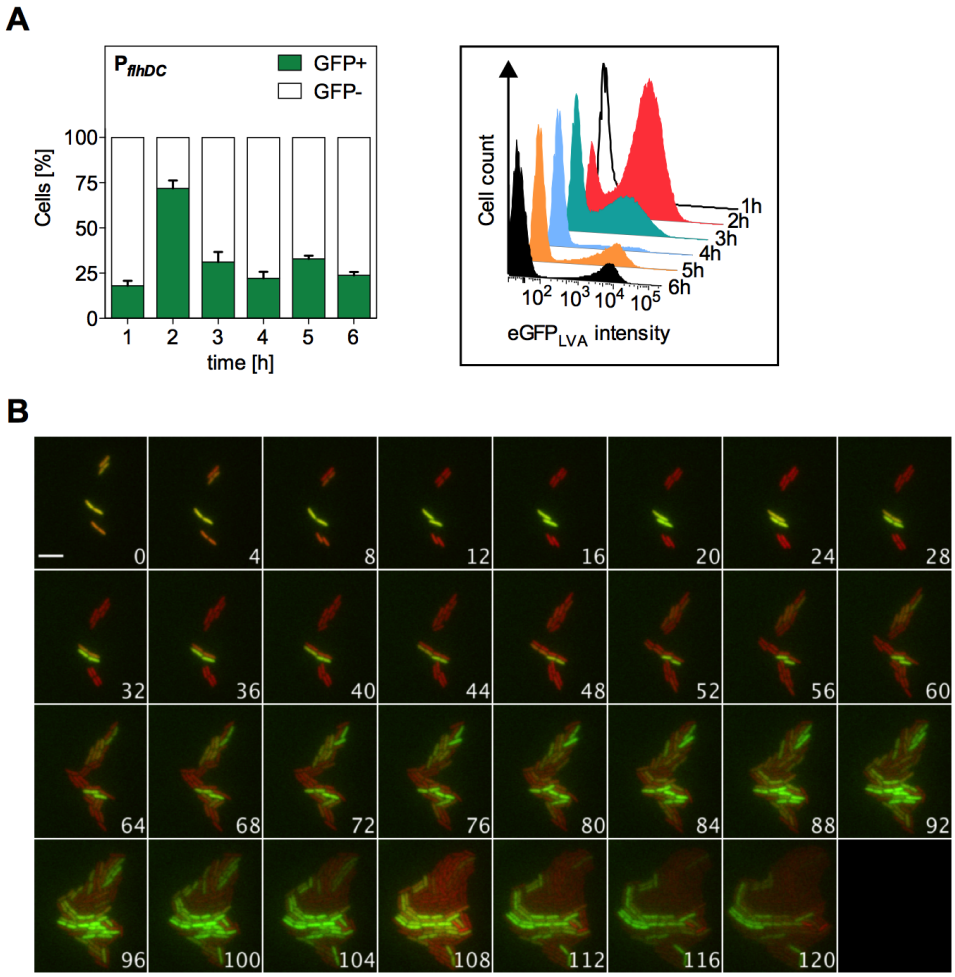

Fig. 4.4 Expression of P_{flhDC}-*egfp*$_{LVA}$ displays growth phase-dependent phenotypic heterogeneity resulting in two distinct subpopulations.
(A) The percentage of eGFP$_{LVA}$-positive (GFP+) and eGFP$_{LVA}$-negative (GFP-) cells was determined by flow cytometry from batch cultures of a ST14028 wildtype strain harboring pKH70-P_{flhDC}-*egfp*$_{LVA}$. For growth phase-dependent analyses, samples were taken 1–6 h post inoculation. Left: Bars represent mean values of six biological replicates, and error bars represent the standard error of the mean. Right: Exemplary histogram of eGFP$_{LVA}$ fluorescence intensities. **(B)** Single-cell expression dynamics were determined by time-lapse fluorescence microscopy of a ST14028 wildtype strain harboring pKH70-P_{flhDC}-*egfp*$_{LVA}$ (green) and pFS48-mCherry (red, constitutive). Cells from mid exponential growth phase batch cultures were grown on agarose pads under the microscope at 37 °C. Images were taken every 4 min for 120 min in total as indicated by inlay numbers. The scale bar size corresponds to 5 μm.

In a previous study, a different *flhDC* promoter fusion to a fluorescence reporter was analyzed by flow cytometry, which did not display phenotypic heterogeneity in minimal medium supplemented with different concentrations of yeast extract (Koirala *et al.*, 2014). Here, this promoter fragment was termed P_{flhDC} (Koirala), fused to $egfp_{LVA}$ in the pKH70 plasmid (pKH70-P_{flhDC} (Koirala)-$egfp_{LVA}$) and analyzed at different growth phases (1–6 h post inoculation) from batch cultures using flow cytometry. Compared to the *flhDC* promoter region used above (-628 to +9 nucleotides relative to the *flhD* start codon), the P_{flhDC} (Koirala) fusion (-1013 to -112 nucleotides upstream of the *flhD* start codon) comprised a larger upstream, but shorter downstream part of the *flhDC* promoter region. In accordance with the previously published results (Koirala *et al.*, 2014), almost all cells expressing the P_{flhDC} (Koirala)-$egfp_{LVA}$ construct were $eGFP_{LVA}$-positive during the early exponential growth phase (2–3 h post inoculation) and not heterogeneously expressed (Fig. 4.5). In contrast, in the late exponential growth phase (4–5 h post inoculation), some cells were additionally $eGFP_{LVA}$-negative. At 6 h post inoculation, P_{flhDC} (Koirala)-$egfp_{LVA}$ expression was heterogeneous with a ratio of $eGFP_{LVA}$-positive and -negative cells as observed for the wildtype P_{flhDC}-$egfp_{LVA}$ promoter fusion analyzed above. These results indicated that a binding site of a putative negative regulator was not present in the P_{flhDC} (Koirala) promoter fusion, but which might be essential for the growth phase-dependent heterogeneous P_{flhDC}-$egfp_{LVA}$ expression during early exponential growth.

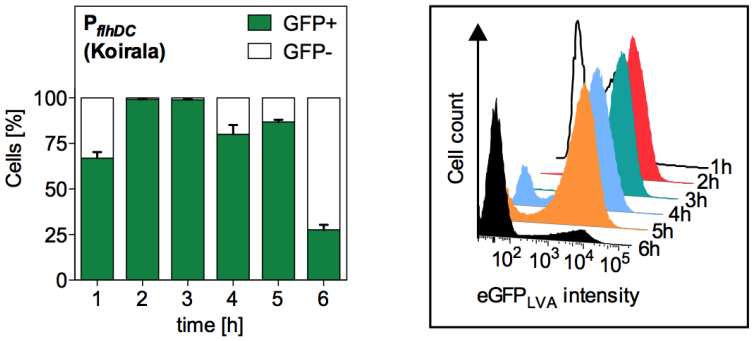

Fig. 4.5 The *flhDC* promoter region is important for growth phase-dependent heterogeneous expression. The percentage of $eGFP_{LVA}$-positive (GFP+) and $eGFP_{LVA}$-negative (GFP-) cells was determined by flow cytometry from batch cultures of a ST14028 wildtype strain harboring pKH70-P_{flhDC} (Koirala)-$egfp_{LVA}$. For growth phase-dependent analyses, samples were taken 1–6 h post inoculation. The designated P_{flhDC} (Koirala) promoter variant excluded a P_{flhDC} region preceding the *flhD* start codon (Koirala *et al.*, 2014), which is important for heterogeneous P_{flhDC}-$egfp_{LVA}$ expression. Left: Bars represent mean values of six biological replicates, and error bars represent the standard error of the mean. Right: Exemplary histogram of $eGFP_{LVA}$ fluorescence intensities.

In order to confirm that the observed growth phase-dependent heterogeneous expression of P_{flhDC}-*egfp*$_{LVA}$ is specific to the P_{flhDC} promoter fusion and not due to growth phase-dependent synthesis or degradation of eGFP$_{LVA}$, control promoters were fused to *egfp*$_{LVA}$ in the pKH70 plasmid and analyzed by flow cytometry. First, the *egfp*$_{LVA}$ reporter gene was fused to a non-functional P_{flhDC} promoter that contained -10 box mutations of all transcriptional starts sites, which was termed P_{flhDC} (-) and served as negative control. As expected, no eGFP$_{LVA}$-positive cells were detected throughout all analyzed growth phases (1–6 h post inoculation) of batch culture samples (Fig. 4.6 A). Next, the *egfp*$_{LVA}$ reporter was fused to a constitutive active promoter $P_{LtetO-1}$ that served as positive control. In contrast to the negative control, predominantly eGFP$_{LVA}$-positive cells were detected throughout all tested growth phases for the $P_{LtetO-1}$-*egfp*$_{LVA}$ fusion construct (Fig. 4.6 B). These results demonstrated that the observed phenotypic heterogeneity was specific to growth phase-dependent heterogeneous P_{flhDC}-*egfp*$_{LVA}$ expression.

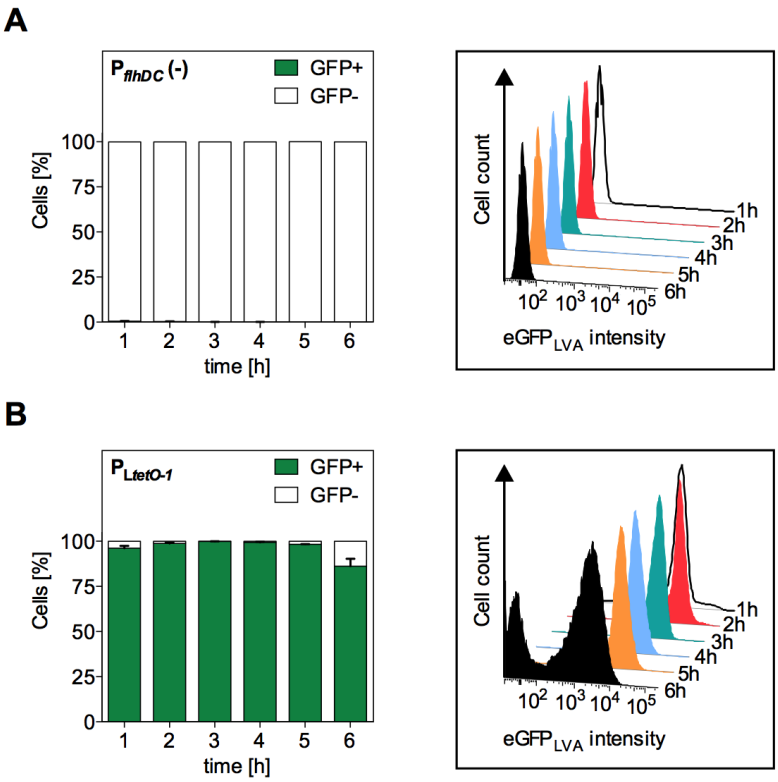

Fig. 4.6 Expression of *egfp*$_{LVA}$ fused to control promoters.
The percentage of eGFP$_{LVA}$-positive (GFP+) and eGFP$_{LVA}$-negative (GFP-) cells was determined by flow cytometry from batch cultures of a ST14028 wildtype strain harboring **(A)** pKH70-P_{flhDC}(-)-*egfp*$_{LVA}$ or **(B)** pKH70-$P_{LtetO-1}$-*egfp*$_{LVA}$. For growth phase-dependent analyses, samples were taken 1–6 h post inoculation. P_{flhDC}(-) was non-functional due to -10 box mutations of all P_{flhDC} transcriptional start sites. $P_{LtetO-1}$ was constitutively expressed. **(A+B)** Left: Bars represent mean values of six biological replicates, and error bars represent the standard error of the mean. Right: Exemplary histograms of eGFP$_{LVA}$ fluorescence intensities.

4.2.2 Role of P1$_{flhDC}$ and P5$_{flhDC}$ in heterogeneous *flhDC* expression

In order to test the hypothesis that different promoters within P$_{flhDC}$ drive the observed growth phase-dependent heterogeneous expression of P$_{flhDC}$-*egfp*$_{LVA}$ at different growth phases, *flhDC* promoter variants of pKH70-P$_{flhDC}$-*egfp*$_{LVA}$ were analyzed by flow cytometry. Of the six originally annotated transcriptional start sites in the *flhDC* promoter region, two major start sites drive *flhDC* expression, P1$_{flhDC}$ and P5$_{flhDC}$ (Mouslim and Hughes, 2014). Thus, the analyzed *flhDC* promoter mutants retained only one functional transcriptional start site, either P1$_{flhDC}$ or P5$_{flhDC}$. The -10 boxes of the other start sites in the *flhDC* promoter region were mutated, except of P2$_{flhDC}$ and P6$_{flhDC}$, which overlap with the binding site of CRP that is necessary for *flhDC* transcription from P1$_{flhDC}$ (Yanagihara *et al.*, 1999). For simplification, these *flhDC* promoter mutations were designated P$_{flhDC}$ (P1+) and P$_{flhDC}$ (P5+).

Flow cytometry analyses of a ST14028 wildtype strain expressing P$_{flhDC}$ (P1+)-*egfp*$_{LVA}$ revealed eGFP$_{LVA}$-positive cells only during the early exponential growth phase (1–4 h post inoculation), but not during late exponential growth (5–6 h post inoculation) (Fig. 4.7 A). This indicated that transcription from P1$_{flhDC}$ drives early expression of P$_{flhDC}$-*egfp*$_{LVA}$. Thereby, the heterogeneous expression pattern observed for the wildtype pKH70-P$_{flhDC}$-*egfp*$_{LVA}$ construct during early exponential growth was maintained. The percentage of eGFP$_{LVA}$-positive cells increased upon 2 h growth, followed by a decrease 3 h post inoculation. In contrast, for P$_{flhDC}$ (P5+)-*egfp*$_{LVA}$ hardly any eGFP$_{LVA}$-positive cell was detected during early exponential growth (1–3 h post inoculation), but during the late exponential growth phase (4–6 h post inoculation) (Fig. 4.7 B). This indicated that transcription from P5$_{flhDC}$ drives later expression of P$_{flhDC}$-*egfp*$_{LVA}$. As observed for the *flhDC* wildtype promoter fusion, the percentage of eGFP$_{LVA}$-positive cells slightly increased 5 h post inoculation. Furthermore, the eGFP$_{LVA}$ fluorescence intensity from P$_{flhDC}$ (P5+) in the late exponential growth phase (5 h) was approximately three times higher than from P$_{flhDC}$ (P1+) during early exponential growth (2 h) (median fluorescence intensity of P$_{flhDC}$ (P1+)-*egfp*$_{LVA}$ = 1172 ± 104; P$_{flhDC}$ (P5+)-*egfp*$_{LVA}$ = 3080 ± 130). This indicated that expression from P5$_{flhDC}$ is stronger than expression from P1$_{flhDC}$. Taken together, both P1$_{flhDC}$- and P5$_{flhDC}$-dependent expression contributed to the growth phase-dependent heterogeneous expression of wildtype P$_{flhDC}$-*egfp*$_{LVA}$. Moreover, these results suggested that regulators of *flhDC* transcription that act on the P1$_{flhDC}$ or P5$_{flhDC}$ transcriptional start sites are involved in heterogeneous expression in the early or late growth phase, respectively.

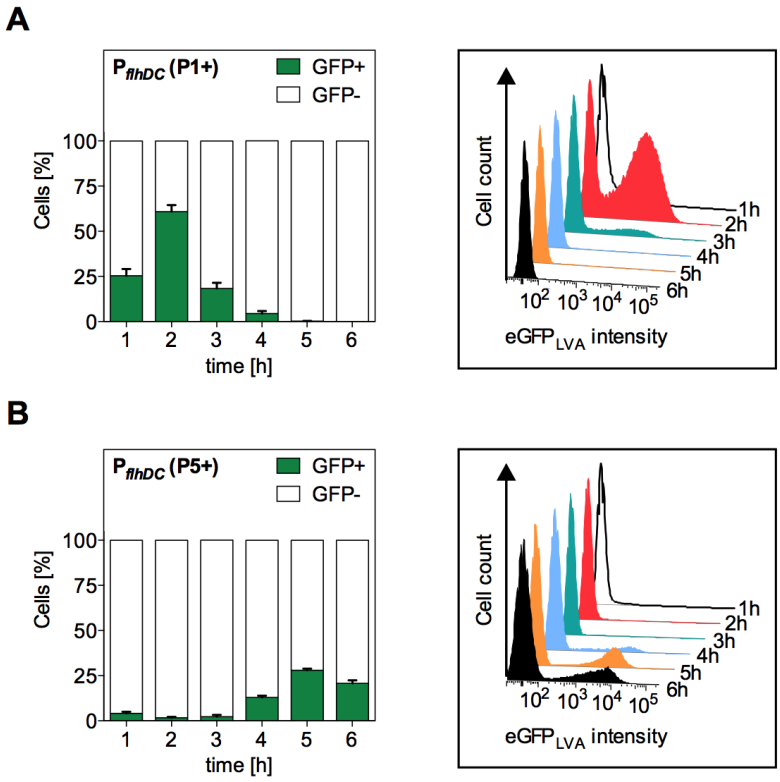

Fig. 4.7 P1$_{flhDC}$ and P5$_{flhDC}$ drive heterogeneous P$_{flhDC}$-*egfp*$_{LVA}$ expression at different growth phases. The percentage of eGFP$_{LVA}$-positive (GFP+) and eGFP$_{LVA}$-negative (GFP-) cells was determined by flow cytometry from batch cultures of a ST14028 wildtype strain harboring **(A)** pKH70-P$_{flhDC}$ (P1+)-*egfp*$_{LVA}$ or **(B)** pKH70-P$_{flhDC}$ (P5+)-*egfp*$_{LVA}$. For growth phase-dependent analyses, samples were taken 1–6 h post inoculation. For expression from P1$_{flhDC}$ or P5$_{flhDC}$, the -10 boxes of the other transcriptional start sites were mutated, except for P2$_{flhDC}$ and P6$_{flhDC}$ as described in the text. **(A+B)** Left: Bars represent mean values of six biological replicates, and error bars represent the standard error of the mean. Right: Exemplary histograms of eGFP$_{LVA}$ fluorescence intensities.

Next, the physiological role of P1$_{flhDC}$- and P5$_{flhDC}$-dependent *flhDC* expression for flagellar motility was analyzed. A previous study showed that a functional P1$_{flhDC}$ transcriptional start site was indispensable for motility, whereas a non-functional P5$_{flhDC}$ transcriptional start site did not affect swimming motility (Mouslim and Hughes, 2014). In order to confirm the specific roles of P1$_{flhDC}$ and P5$_{flhDC}$ for flagellar motility, swimming motility analyses were performed on motility agar plates (0.3 % agar) with strains comprising chromosomal *flhDC* promoter mutations P$_{flhDC}$ (P1+) or P$_{flhDC}$ (P5+) (including functional P2$_{flhDC}$ and P6$_{flhDC}$ as described above). The P$_{flhDC}$ (P1+) mutant, which drives *flhDC* expression solely from P1$_{flhDC}$, did not affect swimming motility compared to a wildtype control (Fig. 4.8 A). In contrast, the P$_{flhDC}$ (P5+) mutant, which drives expression of *flhDC* solely from P5$_{flhDC}$, resulted in a non-motile phenotype. These results confirmed that P1$_{flhDC}$ is indispensable for flagellar motility.

In order to test if the P_{flhDC} (P5+) mutant was non-motile due to the lack of flagellar filament formation, the number of flagella per cell was determined from cultures grown to mid exponential phase using anti-FliC immunostaining in strains locked for the FliC filament. On average, the wildtype strain assembled two flagella per cell (mean = 2.1 ± 1.7) (Fig. 4.8 B). A comparable flagellar number per cell was determined for the P_{flhDC} (P1+) mutant (mean = 2.3 ± 2.0) (Fig. 4.8 C). In contrast, the P_{flhDC} (P5+) mutant assembled only a small number of flagella (mean = 0.3) (Fig. 4.8 D), which is in accordance with the observed motility defect in swimming motility agar.

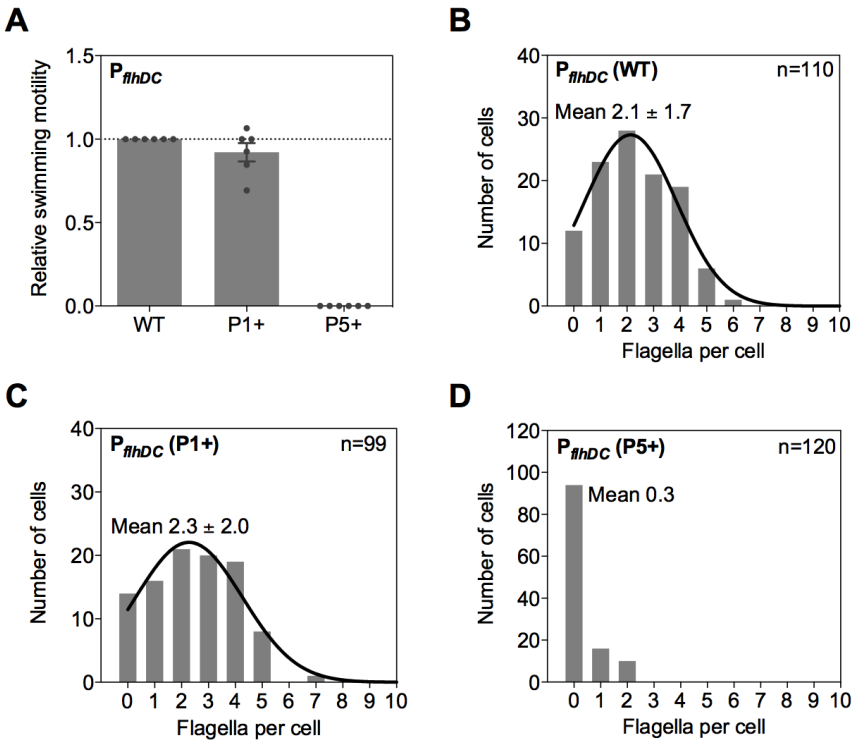

Fig. 4.8 $P1_{flhDC}$-driven *flhDC* transcription is indispensable for flagellar motility.
(A) Swimming motility was determined for chromosomal *flhDC* promoter mutations that drive expression either from $P1_{flhDC}$ or $P5_{flhDC}$ after incubation on 0.3 % motility agar plates. Swimming diameters are shown relative to the wildtype control (WT). Bars represent mean values of six biological replicates, and error bars represent the standard error of the mean. **(B–D)** Flagellar filaments per cell body were determined using anti-FliC immunostaining in FliC-locked strains that comprised following chromosomal *flhDC* promoter variants: **(B)** P_{flhDC} wildtype (WT), **(C)** P_{flhDC} (P1+) or **(D)** P_{flhDC} (P5+). Bars represent the counted number of cells with indicated flagellar number per cell body. Gaussian non-linear regression analyses were performed using the software PRISM (black lines) and averaged flagella numbers per cell body are given (mean ± SD). n = total number of cells. **(A–D)** For *flhDC* expression from either $P1_{flhDC}$ or $P5_{flhDC}$, the -10 boxes of the other transcriptional start sites were mutated, except for $P2_{flhDC}$ and $P6_{flhDC}$ as described in the text.

4.2.3 Role of the $FlhD_4C_2$-RflM feedback loop in heterogeneous *flhDC* expression

It has been shown previously that expression of $FlhD_4C_2$ initiates a negative auto-regulatory feedback loop by activating transcription of *rflM* that encodes RflM, which in turn represses *flhDC* (Singer *et al.*, 2013). RflM-mediated repression of *flhDC* transcription requires the formation of a heterodimeric protein complex with RcsB, the response regulator of the RcsCDB phosphorelay (see Chapter 2). Since regulatory feedback loops are required for phenotypic heterogeneity (Casadesús and Low, 2013), a potential participation of the RcsB-RflM complex in the observed growth phase-dependent heterogeneous P_{flhDC}-$egfp_{LVA}$ expression was investigated. Therefore, flow cytometry analyses of strains deleted for the components of the RcsB-RflM complex were performed. Expression of P_{flhDC}-$egfp_{LVA}$ from the pKH70 plasmid in a strain deleted for *rcsB* resulted in delayed downregulation of the $eGFP_{LVA}$-positive subpopulation during early exponential growth (3 h post inoculation) (Fig. 4.9 A) compared to a wildtype strain background. This suggested that the RcsB-RflM complex affected heterogeneous P_{flhDC}-$egfp_{LVA}$ expression from the $P1_{flhDC}$ transcriptional start site, which is the primary target for RcsB/RflM-dependent repression of *flhDC* transcription (see Chapter 2). In order to disrupt the above-mentioned auto-regulatory $FlhD_4C_2$-RflM feedback loop directly, *rflM* was deleted and expression of the P_{flhDC} (P1+)-$egfp_{LVA}$ fusion was analyzed by flow cytometry in this strain background (Fig. 4.9 B). As determined in absence of *rcsB*, a strain deleted for *rflM* resulted in delayed downregulation of the $eGFP_{LVA}$-positive subpopulation during early exponential growth upon expression from pKH70-P_{flhDC} (P1+)-$egfp_{LVA}$. Additionally, a significant percentage of $eGFP_{LVA}$-positive cells was detected in the late exponential growth phase (4–5 h post inoculation) that was not present upon expression of P_{flhDC} (P1+)-$egfp_{LVA}$ in the wildtype strain background (compare Fig. 4.7 A). Comparison of $eGFP_{LVA}$ fluorescence intensities 3 h post inoculation in the *rcsB*/*rflM* deletion strains with the wildtype strain background revealed approximately four times increased levels, which indicated a stronger P_{flhDC}-$egfp_{LVA}$ expression in the deletion strains (median fluorescence intensity of wildtype = 901 ± 27; Δ*rcsB* = 4531 ± 104; Δ*rflM* = 4196 ± 84).

Next, expression dynamics of individual cells in the *rflM* deletion strain harboring pKH70-P_{flhDC} (P1+)-$egfp_{LVA}$ and the constitutive pFS48-mCherry plasmid were determined using single-cell time-lapse fluorescence microscopy (Fig. 4.9 C). Consistent with the flow cytometry results, the majority of bacteria were $eGFP_{LVA}$-positive. In contrast to the heterogeneous P_{flhDC}-$egfp_{LVA}$ expression observed in the wildtype background, no switching from the $eGFP_{LVA}$-positive to the $eGFP_{LVA}$-negative state was detected in absence of *rflM*. Thus, the switching rate seemed to be impaired. Taken together, these results indicated that the $FlhD_4C_2$-RflM feedback loop is involved in regulation of $P1_{flhDC}$-dependent phenotypic heterogeneity of P_{flhDC}-$egfp_{LVA}$ in early exponential growth phases.

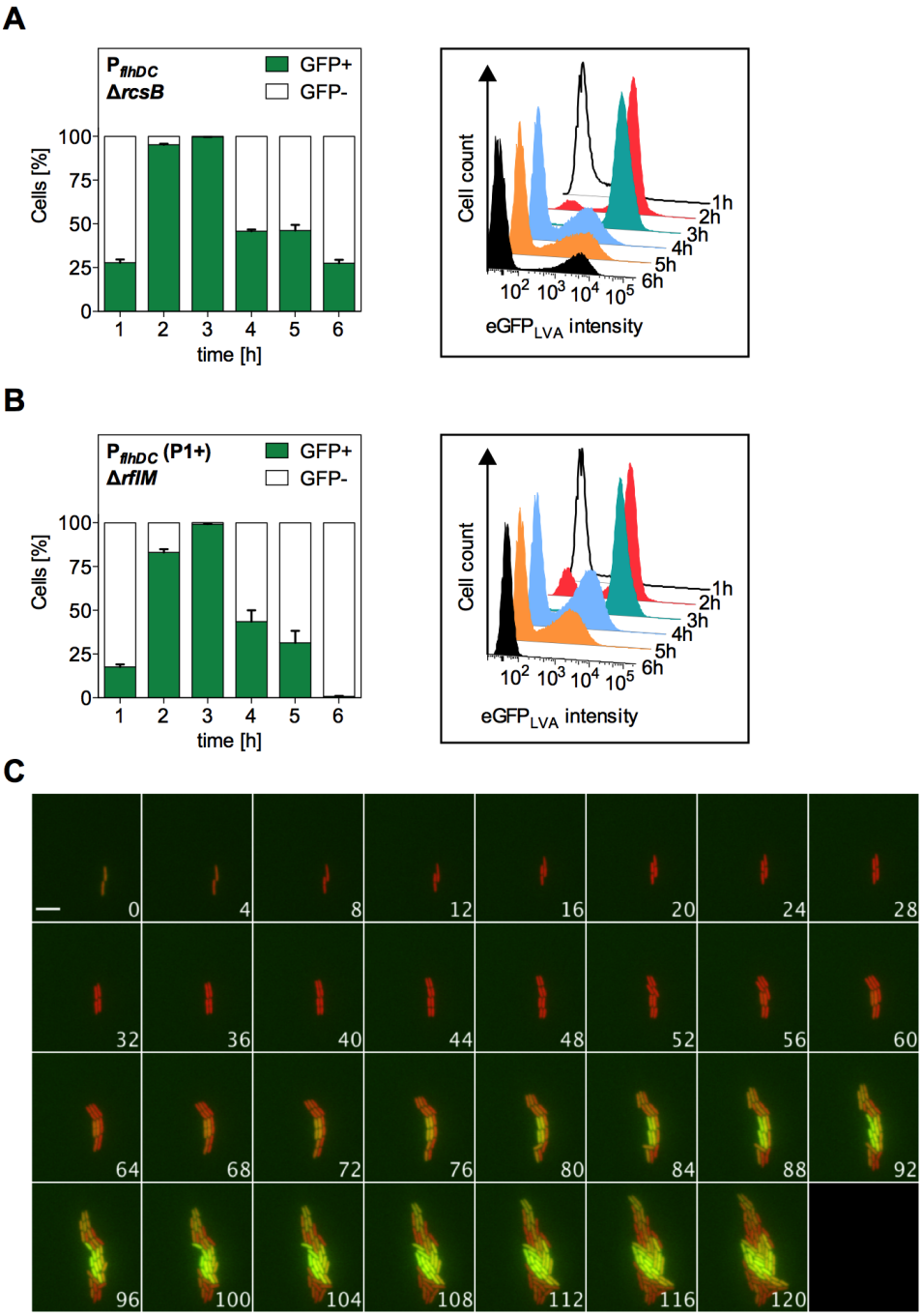

Fig. 4.9 $FlhD_4C_2$-RflM feedback regulation enables heterogeneous P_{flhDC}-*egfp*$_{LVA}$ expression in the early exponential growth phase.
(A+B) The percentage of $eGFP_{LVA}$-positive (GFP+) and $eGFP_{LVA}$-negative (GFP-) cells was determined by flow cytometry from batch cultures of **(A)** a *rcsB* deletion strain harboring pKH70-P_{flhDC}-*egfp*$_{LVA}$ or **(B)** a *rflM* deletion strain harboring pKH70-P_{flhDC} (P1+)-*egfp*$_{LVA}$. For growth phase-dependent analyses, samples were taken 1–6 h post inoculation. Left: Bars represent mean values of six biological replicates, and error bars represent the standard error of the mean. Right: Exemplary histograms of $eGFP_{LVA}$ fluorescence intensities. **(C)** Single-cell expression dynamics were determined by time-lapse fluorescence microscopy of a *rflM* deletion strain harboring pKH70-P_{flhDC} (P1+)-*egfp*$_{LVA}$ (green) and pFS48-mCherry (red, constitutive). Cells from mid exponential growth phase batch cultures were grown on agarose pads under the microscope at 37 °C. Images were taken every 4 min for 120 min in total as indicated by inlay numbers. The scale bar size corresponds to 5 μm.

In order to confirm that switching between the $eGFP_{LVA}$-positive and $eGFP_{LVA}$-negative state of individual cells within one bacterial population expressing P_{flhDC}-$egfp_{LVA}$ is controlled by the $FlhD_4C_2$-RflM feedback loop, bacteria were tested for their ability to remember the expression state of their recent ancestors. Therefore, the *flhDC* expression status of a bacterial population was controlled from the chromosomal, inducible P_{tetA} promoter, which disrupted the chromosomally native *flhDC* promoter and allowed for induction of *flhDC* expression upon addition of anhydrotetracycline (AnTc). Non-induced and induced ancestors were designated the OFF and ON pre-culture, respectively. For flow cytometry analyses, cells from the ON and OFF pre-cultures harboring the pKH70-P_{flhDC}-$egfp_{LVA}$ plasmid were sub-cultured at different AnTc concentrations (0–10 ng/ml) and further grown to the early exponential growth phase (2 h post inoculation).

In a wildtype strain background, different proportions of $eGFP_{LVA}$-positive and $eGFP_{LVA}$-negative subpopulations were detected depending on the respective pre-culture and recent ancestors (Fig. 4.10 A). Cells from the OFF pre-culture were predominantly $eGFP_{LVA}$-positive at the lowest AnTc concentrations, whereas cells from the ON pre-culture started with heterogeneous P_{flhDC}-$egfp_{LVA}$ expression and contained both subpopulations ($eGFP_{LVA}$-positive and $eGFP_{LVA}$-negative cells). With increasing AnTc concentration, bacterial populations from both pre-cultures shifted to an increasing $eGFP_{LVA}$-negative subpopulation, whereas cells from the ON pre-culture displayed faster kinetics than cells from the OFF pre-culture. It is important to note that P_{tetA}-dependent activation of *flhDC* expression resulted in increased $FlhD_4C_2$-mediated transcription of *rflM*, which in turn represses *flhDC* transcription from the $P1_{flhDC}$ transcriptional start site due to the negative $FlhD_4C_2$-RflM feedback loop mentioned above. The flow cytometry analyses demonstrated that P_{flhDC}-$egfp_{LVA}$ expression exhibits history-dependency known as hysteresis.

Next, a *rflM* deletion mutant that disrupted the $FlhD_4C_2$-RflM feedback loop was analyzed for its ability to remember the P_{flhDC}-$egfp_{LVA}$ expression status of ancestor cells (Fig. 4.10 B). Irrespective of the expression status of recent ancestors (ON or OFF pre-culture), hardly any $eGFP_{LVA}$-negative cell was observed, indicating that the *rflM* deletion mutant does not exhibit hysteresis. Hence, the negative auto-regulatory $FlhD_4C_2$-RflM feedback loop is indispensable for heterogeneous P_{flhDC}-$egfp_{LVA}$ expression from the $P1_{flhDC}$ transcriptional start site during early exponential growth.

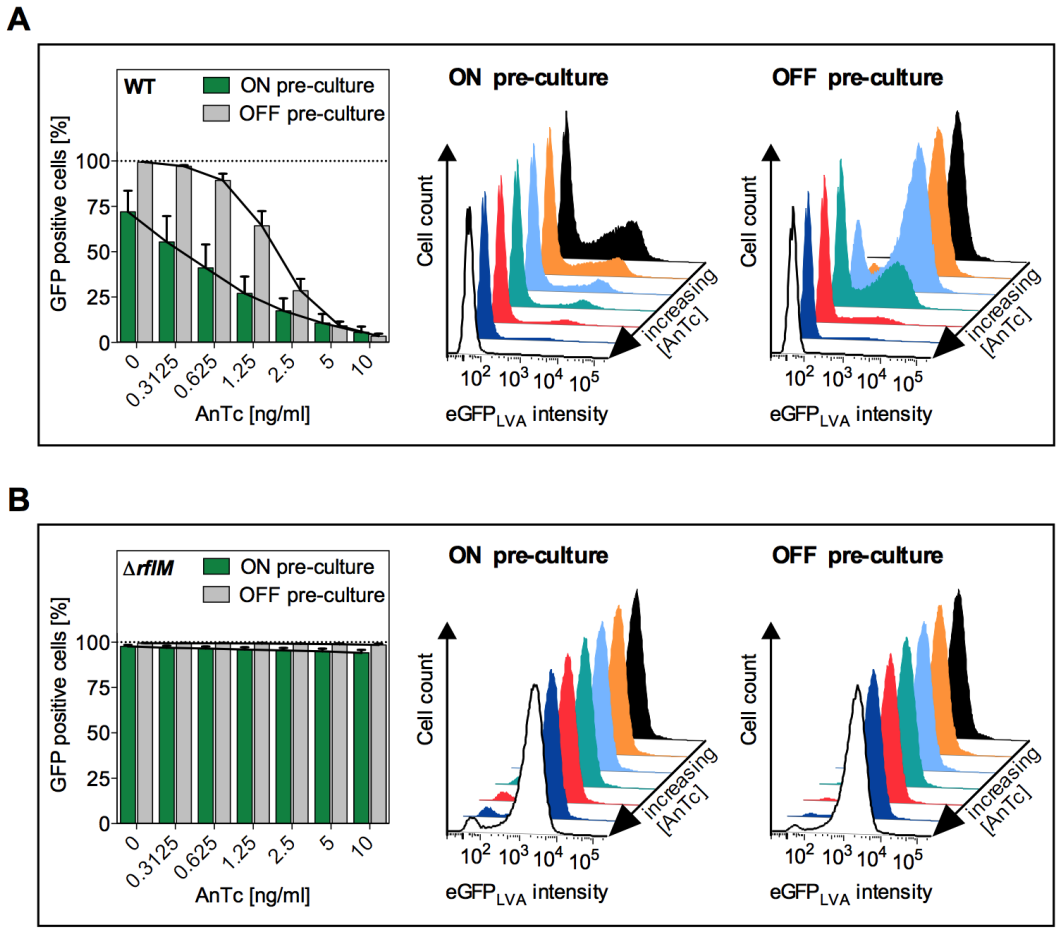

Fig. 4.10 Expression of P_{flhDC}-*egfp*$_{LVA}$ leads to hysteresis.
The percentage of $eGFP_{LVA}$-positive cells was determined by flow cytometry from strains with chromosomally inducible *flhDC* expression (P_{flhDC}::T-POP) that harbor pKH70-P_{flhDC}-*egfp*$_{LVA}$ in a **(A)** wildtype or **(B)** *rflM* deletion strain. Ancestor cells were either induced with 100 ng/ml anhydrotetracycline (AnTc) (ON pre-culture, P_{tetA}-dependent *flhDC* expression) or non-induced (OFF pre-culture, no *flhDC* expression), sub-cultured at different AnTc concentrations (0–10 ng/ml) and grown to early exponential phase (2 h post inoculation) before analyses. Left: Bars and connection lines represent mean values of three biological replicates, and error bars represent the standard error of the mean. Middle and right: Exemplary histograms of $eGFP_{LVA}$ fluorescence intensities from ON and OFF pre-cultures, respectively.

4.2.4 Role of the $FlhD_4C_2$-FliZ-YdiV feedback loop in heterogeneous *flhDC* expression

A recent study demonstrated that the FliZ-YdiV double negative feedback loop is responsible for bistable expression of *flhB*, which is under control of a flagellar class 2 promoter, in response to nutrients (Koirala *et al.*, 2014). YdiV targets the FlhD protein to ClpXP-dependent proteolytic degradation by binding to a motif comprising the L22 amino acid of FlhD and thereby regulates cellular levels of $FlhD_4C_2$ (Takaya *et al.*, 2012). Thus, the hypothesis emerged that the YdiV-dependent post-transcriptional regulation of $FlhD_4C_2$ affected the identified growth phase-dependent heterogeneous expression of P_{flhDC}-*egfp*$_{LVA}$. YdiV could influence the $FlhD_4C_2$-RflM feedback loop, which is responsible for phenotypic heterogeneity in the early exponential growth phase, by tuning the amounts of the $FlhD_4C_2$ complex and thereby affecting *rflM* expression. Initial flow cytometry analyses were performed with strains that prevented YdiV-mediated degradation of FlhD. Preliminary results demonstrated that expression of P_{flhDC}-*egfp*$_{LVA}$ from the pKH70 fusion plasmid in a strain deleted for *ydiV* decreased the eGFP$_{LVA}$-positive subpopulation in the early exponential growth phase (2–3 h post inoculation) (Fig. 4.11 A) compared to a wildtype strain background. This deregulation seemed to be RflM-dependent, since the observed effect could be reversed upon additional deletion of *rflM* (Fig. 4.11 B). This resulted in a primarily eGFP$_{LVA}$-positive population during early exponential growth as observed for the *rflM* or *rcsB* deletion strains. Comparably, a mutation in the FlhD protein, which prevented YdiV-binding ($FlhD_{L22H}$, lysine changed to histidine), showed an eGFP$_{LVA}$ expression pattern in presence and absence of *rflM* (Fig. 4.11 C + D) like the *ydiV* deletion strain. These preliminary results indicated that YdiV-dependent tuning of $FlhD_4C_2$ levels is involved in the $FlhD_4C_2$-RflM regulatory feedback loop and thus influences heterogeneous P_{flhDC}-*egfp*$_{LVA}$ expression. Further experiments need to be performed to confirm this indication.

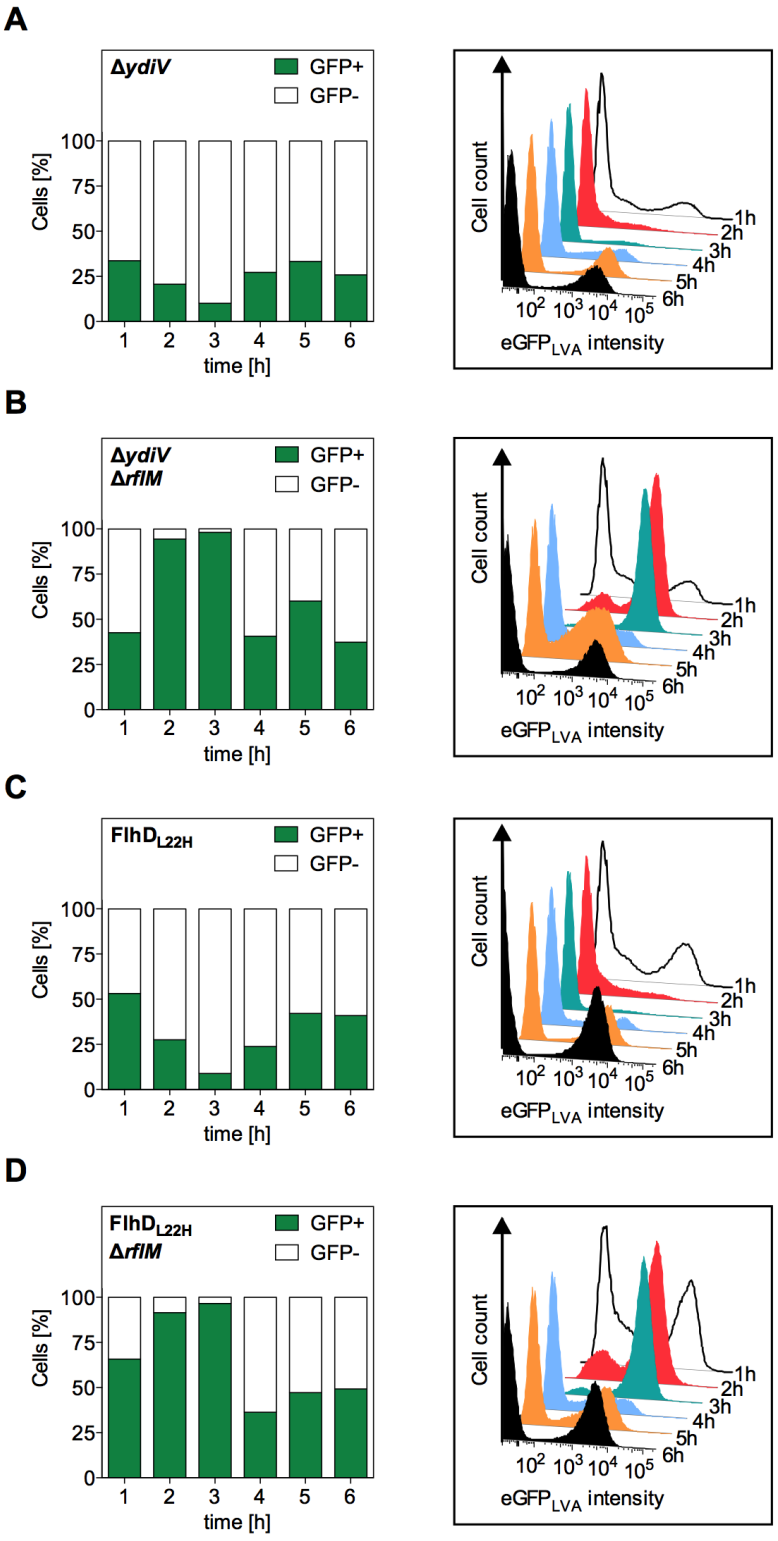

Fig. 4.11 Disruption of YdiV-mediated $FlhD_4C_2$ degradation deregulates $FlhD_4C_2$-RflM-dependent phenotypic heterogeneity.
The percentage of $eGFP_{LVA}$-positive (GFP+) and $eGFP_{LVA}$-negative (GFP-) cells was determined by flow cytometry from batch cultures of strains harboring pKH70-P_{flhDC}-*egfp*$_{LVA}$ and **(A)** a *ydiV* deletion, **(B)** a *ydiV rflM* double deletion, **(C)** a $FlhD_{L22H}$ point mutation or **(D)** a $FlhD_{L22H}$ point mutation and *rflM* deletion. For growth phase-dependent analyses, samples were taken 1–6 h post inoculation. Left: Bars represent data of one biological replicate. Right: Histograms of $eGFP_{LVA}$ fluorescence intensities. It is important to note that this figure shows preliminary results.

4.2.5 Role of the $FlhD_4C_2$-FliZ-HilD feedback loop in heterogeneous *flhDC* expression

Another auto-regulatory feedback loop that is involved in expression of *flhDC* contains the regulatory proteins FliZ and HilD. $FlhD_4C_2$ activates transcription of *fliZ* from the flagellar class 2 promoter and the FliZ protein post-transcriptionally promotes activity of the Spi-1 regulator HilD (Chubiz *et al.*, 2010). The HilD protein in turn activates transcription of *flhDC* from the $P5_{flhDC}$ transcriptional start site (see Chapter 3; Singer *et al.*, 2014). A potential involvement of the double positive $FlhD_4C_2$-FliZ-HilD regulatory feedback loop in growth phase-dependent heterogeneous expression of P_{flhDC}-$egfp_{LVA}$ was analyzed by flow cytometry. In a strain deleted for *hilD*, expression of P_{flhDC}-$egfp_{LVA}$ from the pKH70 plasmid was abolished in the late exponential growth phase (5–6 h post inoculation) (Fig. 4.12 A). Likewise, expression of P_{flhDC}-$egfp_{LVA}$ in a *fliZ* deletion strain resulted in a primarily $eGFP_{LVA}$-negative population during late exponential growth (Fig. 4.12 B). Thus, the effect was more pronounced in the *hilD* deletion strain than in the *fliZ* deletion strain, indicating that HilD is the primary regulator that is responsible for activation of *flhDC* transcription from the $P5_{flhDC}$ transcriptional start site during late exponential growth. Furthermore, a small percentage of $eGFP_{LVA}$-positive cells was observed in the *fliZ* deletion strain 5 h post inoculation. This indicated that HilD-mediated activation of *flhDC* expression from $P5_{flhDC}$ is not completely dependent on FliZ-mediated post-transcriptional activation of HilD.

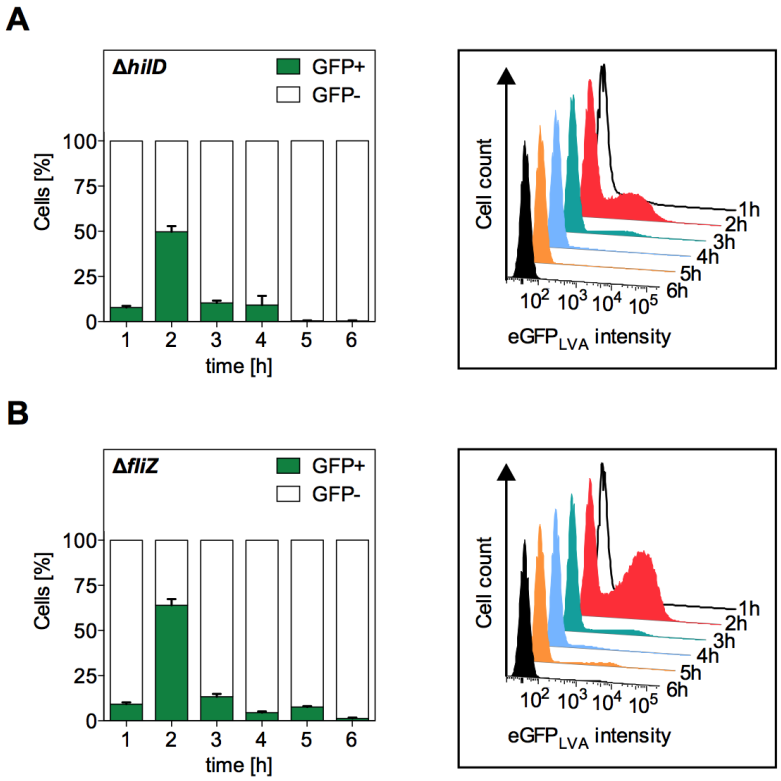

Fig. 4.12 $FlhD_4C_2$-FliZ-HilD feedback regulation enables heterogeneous P_{flhDC}-*egfp*$_{LVA}$ expression in the late exponential growth phase.
The percentage of $eGFP_{LVA}$-positive (GFP+) and $eGFP_{LVA}$-negative (GFP-) cells was determined by flow cytometry from batch cultures of strains harboring pKH70-P_{flhDC}-*egfp*$_{LVA}$ and deleted for **(A)** *hilD* or **(B)** *fliZ*. For growth phase-dependent analyses, samples were taken 1–6 h post inoculation. Left: Bars represent mean values of six biological replicates, and error bars represent the standard error of the mean. Right: Exemplary histograms of $eGFP_{LVA}$ fluorescence intensities.

4.3 Discussion

In *S.* Typhimurium, expression of the flagellar master operon *flhDC* is regulated in a growth phase-dependent manner (Mouslim and Hughes, 2014). During exponential growth in LB medium, *flhDC* expression is initially low followed by activation and subsequent downregulation. In the late exponential growth phase, *flhDC* expression is increased again, followed by another downregulation when cells enter the stationary growth phase. Several DNA-binding proteins (LrhA, RcsB/RflM, HilD, SlyA, and RtsB) are implicated in this growth phase-dependent regulation of *flhDC* transcription (Mouslim and Hughes, 2014). The non-coding region upstream of the *flhDC* operon is very long (787 nucleotides upstream of the *flhD* start codon), and the *flhDC* promoter comprises several transcriptional start sites (Kröger *et al.*, 2013), additionally indicating a complex regulation of *flhDC* expression. The entire *flhDC* promoter region is weakly conserved (< 20 %) among Enterobacteriaceae species including *S.* Typhimurium, *E. coli*, *Yersinia* spp., *Shigella dysenteriae*, *Erwinia amylovora*, *Proteus mirabilis*, and *Xenorhabdus nematophila* (compare Fig. S2). However, the RcsB binding site in the *flhDC* promoter is conserved in enteric bacteria, and the HilD binding site is conserved within *S.* Typhimurium target genes (Wehland and Bernhard, 2000; Olekhnovich and Kadner, 2007). Several flagellar promoters exhibit a high level of noise in gene expression, which is a prerequisite for heterogeneous gene expression (Freed *et al.*, 2008). In a recent study, the *flhDC* promoter was investigated for its ability to generate phenotypic heterogeneous populations in response to nutritional control yet revealing homogeneous expression of *flhDC* (Koirala *et al.*, 2014).

In this thesis, however, growth phase-dependent heterogeneous expression of the flagellar master regulatory operon *flhDC* in *S.* Typhimurium was identified, and the regulatory feedback loops involved in this process were discovered. The findings summarized in this chapter demonstrate that expression of *flhDC* results in two distinct subpopulations within a bacterial population: one subpopulation that is *flhDC* positive (*flhDC*^{ON}) and another subpopulation that is *flhDC* negative (*flhDC*^{OFF}). The fraction of the *flhDC*^{ON} and *flhDC*^{OFF} cells correlated with the growth phase-dependent pattern of *flhDC* expression as described above. The percentage of *flhDC*^{ON} cells increased during early exponential growth in LB medium and again during the late exponential growth phase.

Phenotypic heterogeneity was discovered for a *flhDC* promoter region that contained nucleotides -628 to +9 upstream of the *flhD* start codon. In contrast, a P_{flhDC} fragment comprising nucleotides -1013 to -112 upstream of the *flhD* start codon, designated P_{flhDC} (Koirala), displayed homogeneous expression during the early exponential growth, which confirmed the results determined previously (Koirala *et al.*, 2014). This indicated that a binding site of a repressor of *flhDC* transcription is disrupted in the construct used by Koirala *et al.*, which would allow for a *flhDC*^{OFF} subpopulation.

Accordingly, the binding site of the RcsB-RflM repressor complex (RcsB/RflM box: -202 to -177 nucleotides upstream of the *flhD* start codon; see Chapter 2) is located in proximity to the 3'-end of the P_{flhDC} (Koirala) promoter construct. This presumably affects binding of the RcsB-RflM complex to this promoter fusion and prevents RcsB/RflM-mediated repression of *flhDC* transcription resulting in a homogeneous $flhDC^{ON}$ phenotype. Moreover, the expression profile determined by flow cytometry in the early exponential growth phase closely resembled the homogeneous $flhDC^{ON}$ state observed in the *rcsB* deletion strain harboring the wildtype P_{flhDC}-$egfp_{LVA}$ fusion and in the *rflM* deletion strain harboring P_{flhDC} (P+1)-$egfp_{LVA}$. In addition to the shorter downstream part of the *flhDC* promoter, the P_{flhDC} (Koirala) construct contains a larger upstream part than the heterogeneously expressed P_{flhDC} fragment. Thereby, P_{flhDC} (Koirala) partially includes the promoter and coding region of *yecG*. The *yecG* gene encodes the universal stress protein C (UspC), which has been shown to be essential for flagellar motility in *E. coli* (Nachin *et al.*, 2005). Comparably, UspC could be involved in regulation of flagellar synthesis in *S.* Typhimurium. Additional expression of an UspC peptide from the P_{flhDC} (Koirala) construct might positively affect *flhDC* expression contributing to the determined homogeneous $flhDC^{ON}$ expression profile.

P_{flhDC}-$egfp_{LVA}$ expression from the pKH70 plasmid resulted in growth phase-dependent phenotypic heterogeneous populations comprising $eGFP_{LVA}$-positive and $eGFP_{LVA}$-negative cells, which led to the deductive reasoning that *flhDC* is heterogeneously expressed leading to $flhDC^{ON}$ and $flhDC^{OFF}$ subpopulations, respectively. The specificity of growth phase-dependent heterogeneous expression was confirmed with positive and negative control promoters. Additionally, $FlhD_4C_2$ protein levels could be determined to substantiate the correlation between the P_{flhDC}-$egfp_{LVA}$ expression profile and heterogeneous *flhDC* expression. Since no antibodies against FlhD or FlhC are available, protein levels need to be determined from chromosomal, epitope-tagged FlhD or FlhC versions. Initial western blot analyses with FlhC-3xFLAG revealed a correlation between chromosomal FlhC protein levels and the $eGFP_{LVA}$ profile determined by flow cytometry (Fig. S3). However, the employed C-terminal 3xFLAG tag seemed to impair the functionality of the $FlhD_4C_2$ complex, since bacteria were non-motile. Hence, other epitope-tagged versions should be tested for their functionality and used instead.

4.3.1 Regulation of heterogeneous *flhDC* expression in the early growth phase

Growth phase-dependent heterogeneous *flhDC* expression is separately driven from two different transcriptional start sites dependent on the particular bacterial growth phase as determined by flow cytometry analyses. In the early exponential growth phase, *flhDC* is expressed from the $P1_{flhDC}$ transcriptional start site, which enables flagellar motility. The

$P5_{flhDC}$ transcriptional start sites drives *flhDC* expression in the late exponential growth phase, but is rather involved in other processes than flagellar motility, since cells were non-motile. Accordingly, a previous study proposed such a functional relationship, in which $P1_{flhDC}$ initiates flagellar synthesis in an early cell growth phase, and $P5_{flhDC}$ might play a role in virulence gene expression in a later cell growth phase (Mouslim and Hughes, 2014). Expression of *flhDC* from the $P1_{flhDC}$ promoter is controlled by the negative $FlhD_4C_2$-RflM auto-regulatory feedback loop (Singer *et al.*, 2013), which allows for phenotypic heterogeneity and the bifurcation into two distinct subpopulations ($flhDC^{ON}$ and $flhDC^{OFF}$).

Heterogeneous expression of *flhDC* from the $P1_{flhDC}$ promoter might be bistable. Bistability is characterized by two stable and distinct expression states within one bacterial population (Veening *et al.*, 2008a). Besides auto-regulatory feedback loops, history-dependency, known as hysteresis, is another characteristic of bistability (Ferrell, 2002). Dependent on the expression status of their recent ancestors, different response curves for heterogeneous *flhDC* expression were obtained upon titration of *flhDC* expression from the chromosomal P_{tetA} promoter. Importantly, the activation of $FlhD_4C_2$ production resulted in subsequent downregulation of *flhDC* expression due to the initiation of the negative $FlhD_4C_2$-RflM feedback loop, which represses $P1_{flhDC}$-mediated transcription (see Chapter 2). Thus, ancestors with AnTc-induced $FlhD_4C_2$ production from P_{tetA} (ON pre-culture) resulted in mixed populations with $flhDC^{ON}$ and $flhDC^{OFF}$ cells already without further induction of $FlhD_4C_2$ production. Without induction (OFF pre-culture), bacteria did not produce the activator complex $FlhD_4C_2$ due to disruption of the chromosomal *flhDC* promoter by the P_{tetA} promoter. Consequentially, *rflM* was not expressed and RflM-mediated repression of *flhDC* did not occur, resulting in a homogeneous $flhDC^{ON}$ population in absence of AnTc. Titration of $FlhD_4C_2$ production with increasing amounts of AnTc resulted in *rflM* expression and subsequently heterogeneous $flhDC^{ON}$ and $flhDC^{OFF}$ subpopulations. At higher levels of $FlhD_4C_2$ production, cells shifted to a homogeneous $flhDC^{OFF}$ population. The dynamics of the transition from $flhDC^{ON}$ to $flhDC^{OFF}$ populations was faster for cells originating from the ON pre-culture. This demonstrates that cells remembered the *flhDC* expression state of their recent ancestors and that *flhDC* expression exhibits hysteresis. Consistently, $flhDC^{OFF}$ cells were never detected in a *rflM* deletion strain under these experimental conditions.

As already demonstrated in the hysteresis experiments, expression states of subpopulations within heterogeneous populations do not necessarily need to be irreversible, but cells can also switch between states (Veening *et al.*, 2008a). Transition from an OFF to an ON state has been described for heterogeneous expression of *flhB*, which is under control of a flagellar class 2 promoter (Saini *et al.*, 2010b). Also other flagellar promoters, such as the bistable expressed promoter of *fliC*, have been shown to

switch between activity and inactivity (Freed *et al.*, 2008). Likewise, fast switching frequencies between the ON and OFF states were determined from the P_{flhDC}-*egfp*$_{LVA}$ reporter construct in live-cell analyses using single-cell time-lapse fluorescence microscopy. However, cells repeatedly switched from an OFF to an ON state and vice versa within a few minutes, which indicates an asynchronous pulse-like behavior of individual cells rather than bistability. Dynamic pulses leading to activation and deactivation of key regulators of genetic circuits facilitate temporal organization of critical physiological processes (Levine *et al.*, 2013). Comparably, a pulse-like activation and deactivation of the flagellar master regulatory operon *flhDC* might enable timing of flagellar synthesis during the bacterial cell cycle. Pulsing has been described for the general stress response and sporulation initiation in *Bacillus subtilis* (Locke *et al.*, 2011; Levine *et al.*, 2012). Here, in *S.* Typhimurium, one pulse of *flhDC* activation leading to a *flhDC*^{ON} subpopulation was observed, which was followed by a fast switch to the *flhDC*^{OFF} expression state that is facilitated by the negative $FlhD_4C_2$-RflM auto-regulatory feedback loop. Consistently, no switching from ON to OFF states was determined by time-lapse microscopy in the *rflM* deletion strain. Another round of *flhDC* expression from the $P1_{flhDC}$ promoter will be enabled by low $FlhD_4C_2$ levels that prevent further activation of *rflM* expression, and after degradation of the RflM protein, which has been reported to decay quickly (Mouslim and Hughes, 2014). Taken together, these findings highlight that the $FlhD_4C_2$-RflM feedback loop is responsible for the phenotypic heterogeneity of *flhDC* expression during early exponential growth. Fine-tuning of *flhDC* expression via the auto-regulatory feedback loop presumably allows controlling the amount of the $FlhD_4C_2$ activator complex and might prevent an overshooting of the resource-intensive flagellar production.

The levels of the $FlhD_4C_2$ complex can be tuned by several factors. Most importantly, $FlhD_4C_2$ itself controls *flhDC* expression via $FlhD_4C_2$-dependent activation of *rflM* as described above (Singer *et al.*, 2013). Additionally, RflM requires complex formation with the RcsB protein for repression of *flhDC* transcription. Phosphorylated RcsB alone is also capable of repressing *flhDC*, but with reduced target specificity (see Chapter 2). Moreover, YdiV-mediated ClpXP-dependent proteolytical degradation of FlhD tunes the level of the $FlhD_4C_2$ complex (Takaya *et al.*, 2012). Preliminary results demonstrated that this additionally feeds into the $FlhD_4C_2$-RflM feedback loop that enables heterogeneous *flhDC* expression. In strains that abolished YdiV-mediated $FlhD_4C_2$ degradation (deletion of *ydiV* or the $FlhD_{L22H}$ mutation that prevents YdiV binding), immediate downregulation of the *flhDC*^{ON} subpopulation was observed, which was RflM-dependent. Thus, YdiV seems to be important for generating different pools of $FlhD_4C_2$ in individual cells within a bacterial population that enable phenotypic heterogeneity and subsequently modulate RflM-dependent repression of *flhDC* transcription. Hence, post-

transcriptional regulation of $FlhD_4C_2$ plays an important role in heterogeneous *flhDC* expression in the early growth phase and need to be investigated further. Additionally, $FlhD_4C_2$ levels are tuned by FliT-mediated ClpXP-dependent proteolytical degradation of FlhC (Yamamoto and Kutsukake, 2006b; Sato *et al.*, 2014). However, this might rather play a role in later growth phases, since FliT-mediated degradation is coupled to completion of the flagellar hook-basal-body complex. Before, FliT is associated with the filament cap protein FliD, which prevents $FlhD_4C_2$ degradation (Aldridge *et al.*, 2010).

4.3.2 Regulation of heterogeneous *flhDC* expression in the late growth phase

As mentioned above, *flhDC* transcription from the $P5_{flhDC}$ transcriptional start site drives heterogeneous expression in the late exponential growth phase. However, motility analyses and flagellar immunostaining revealed that this results in a non-flagellated and non-motile phenotype. It is important to note that the flagellar filament formation was determined of a bacterial culture from mid exponential growth phase. Since $P5_{flhDC}$ drives expression of *flhDC* in later growth phases, the analyzed P_{flhDC} (P5+) mutant might assemble flagella at later time points that could enable swimming motility. Comparably, a previous study showed that $P5_{flhDC}$-dependent *flhDC* transcription activates transcription from flagellar class 2 promoters in later growth phases (Mouslim and Hughes, 2014).

Expression of *flhDC* from the $P5_{flhDC}$ promoter is induced by the Spi-1 regulatory protein HilD (Singer *et al.*, 2014), which allows for phenotypic heterogeneity during later growth phases due to the generation of a $flhDC^{ON}$ subpopulation. Moreover, expression from $P5_{flhDC}$ is completely dependent on HilD-mediated activation, since no $flhDC^{ON}$ cells were detected in the *hilD* deletion strain during late exponential growth. This potent activating effect of HilD on the $P5_{flhDC}$ transcriptional start site has been shown previously. Mouslim *et al.* isolated a suppressor mutation that restored the motility defect upon $P5_{flhDC}$-dependent *flhDC* expression, which was located in the *hilD* promoter region resulting in increased expression of *hilD* (Mouslim and Hughes, 2014). Moreover, the $P5_{flhDC}$ promoter seems to be stronger than the $P1_{flhDC}$ promoter, since higher $eGFP_{LVA}$ intensities were determined from the P_{flhDC} (P5+)-$egfp_{LVA}$ construct compared to the P_{flhDC} (P1+)-$egfp_{LVA}$ fusion. This might be associated with the longer 5'-UTR that is generated upon $P5_{flhDC}$-dependent *flhDC* transcription or with its putative role in virulence regulation. Heterogeneous *flhDC* expression in the late growth phase is strengthened by the double positive $FlhD_4C_2$-FliZ-HilD feedback loop. Upon $FlhD_4C_2$-dependent transcription of *fliZ* from the flagellar class 2 promoter, the FliZ protein enhances HilD activity on a post-transcriptional level (Chubiz *et al.*, 2010). In presence of *fliZ*, the $flhDC^{ON}$ subpopulation represents about 30 % of the entire bacterial population. However, upon *fliZ* deletion, a small fraction of $flhDC^{ON}$ cells (10 %) were detected, which indicates that

heterogeneous *flhDC* expression is not strictly dependent on the positive feedback loop via FliZ. Furthermore, FliZ contributes to the tuning of $FlhD_4C_2$ levels by repressing transcription of *ydiV* (Wada *et al.*, 2011). This might additionally influence the above-described $FlhD_4C_2$-RflM feedback regulation during early growth phases.

Heterogeneous expression of *flhDC* from the $P5_{flhDC}$ promoter is likely bistable. Genetic networks that include positive feedback loops in combination with a non-linear response are capable of generating bistability (Ferrell, 2002; Angeli *et al.*, 2004). In case of bistable *flhDC* expression, this non-linearity is likely introduced via the HilD protein. HilD together with HilC and RtsA constitute a feed-forward loop in order to activate their own and mutual gene expression (Ellermeier *et al.*, 2005). For initiation of positive auto-regulation and coupled positive feedback, expression of HilD requires to overcome a certain threshold. Thereafter, HilC and RtsA facilitate additional amplification of Spi-1 gene expression (Saini *et al.*, 2010a). This enables bistable expression of Spi-1-encoded genes and leads to phenotypic heterogeneity of the Spi-1 injectisome (Sturm *et al.*, 2011; Arnoldini *et al.*, 2014). Only cells that have overcome the threshold to express HilD facilitate activation of *flhDC* expression from the $P5_{flhDC}$ transcriptional start site, which is additionally amplified by the $FlhD_4C_2$-FliZ-HilD double positive feedback loop.

4.3.3 Model of heterogeneous *flhDC* expression during flagellar synthesis

The regulatory feedback loops that presumably contribute to the identified growth phase-dependent heterogeneous expression of the flagellar master regulatory operon *flhDC* are summarized in Fig. 4.13. During early exponential growth, the negative $FlhD_4C_2$-RflM auto-regulatory feedback loop results in downregulation of *flhDC* expression from the $P1_{flhDC}$ promoter in a subpopulation where $FlhD_4C_2$ levels were high enough to activate *rflM*. Activation of RflM enables formation of the RcsB-RflM repressor complex that represses *flhDC* transcription from the $P1_{flhDC}$ promoter to presumably prevent overproduction of flagella. Tuning of $FlhD_4C_2$ levels via YdiV-mediated FlhD degradation by the ClpXP protease additionally feeds into the $FlhD_4C_2$-RflM regulation. During late exponential growth, the double positive $FlhD_4C_2$-FliZ-HilD feedback loop activates *flhDC* transcription from the $P5_{flhDC}$ promoter, which might be involved in virulence regulation. The double negative FliZ-YdiV feedback has been shown previously to regulate bistable expression of the flagellar class 2 promoter of *flhB* in response to nutrients (Koirala *et al.*, 2014). Additionally, the $FlhD_4C_2$-FliZ-YdiV feedback loop might contribute the $FlhD_4C_2$-RflM-dependent heterogeneous *flhDC* expression by tuning the amounts of $FlhD_4C_2$. In summary, cross-talk between master regulators of two heterogeneously expressed systems, the Spi-1 injectisome and flagella, might allow *S.* Typhimurium to rapidly adapt

to changing environments during host cell infection. This might facilitate a fast switch between flagella-mediated motility and Spi-1-mediated host cell invasion.

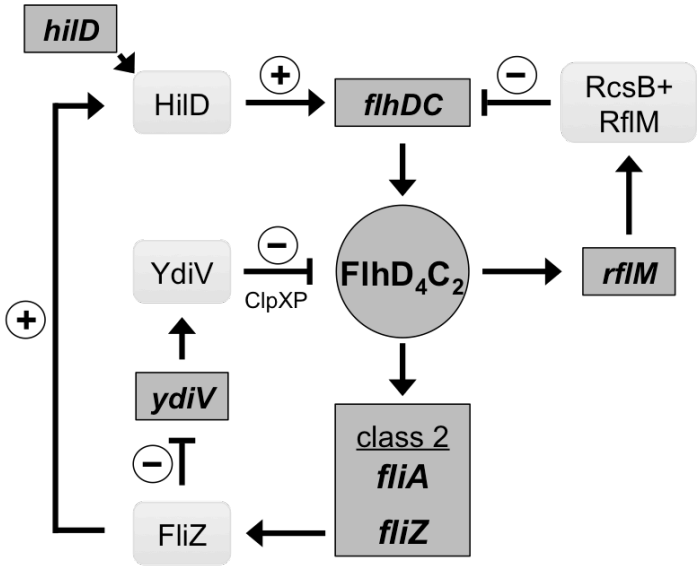

Fig. 4.13 Schematic model of feedback regulation leading to heterogeneous *flhDC* expression.
Heterogeneous expression of the flagellar master regulatory operon *flhDC* is presumably mainly controlled by two auto-regulatory feedback loops: 1) negative auto-regulation by $FlhD_4C_2$-dependent activation of *rflM* transcription that enables formation of the RcsB-RflM complex leading to *flhDC* repression ($FlhD_4C_2$-RflM feedback). 2) Positive auto-regulation by $FlhD_4C_2$-dependent activation of *fliAZ* operon transcription that enables FliZ-mediated increase in HilD activity to efficiently activate *flhDC* expression ($FlhD_4C_2$-FliZ-HilD feedback). Additionally, YdiV-mediated tuning of $FlhD_4C_2$ levels by ClpXP-dependent degradation of FlhD feeds into $FlhD_4C_2$-RflM regulation. FliZ might be additionally involved via the double negative FliZ-YdiV feedback loop ($FlhD_4C_2$-FliZ-YdiV feedback).

5 Conclusion and Future Perspectives

S. Typhimurium exhibits several pathogenic strategies that need to be regulated in a spatiotemporal manner during the infection process. Thereby, bacterial flagella play an important role not only by facilitating directed movement, but also via adherence to host cells and stimulation of the host immune system (Rossez *et al.*, 2015). Although flagella-mediated induction of an intestinal proinflammatory response and host cell death can be beneficial for *S.* Typhimurium under certain conditions, overexpression and deregulation of flagellar synthesis attenuates virulence in the mouse model (Yang *et al.*, 2012; Lai *et al.*, 2013). Thus, and due to the consumption of a significant amount of biosynthetic resources, flagellar synthesis and assembly needs to be tightly regulated and fine-tuned according to the environmental conditions and the bacterium's needs. Under high nutrient conditions, such as upon induction of the mucosal defense in the small intestine resulting in secretion of high-energy nutrients, flagella are expressed and *S.* Typhimurium is motile (Stecher *et al.*, 2008; Wada *et al.*, 2011). Inside epithelial host cells at early stages of infection, when bacteria are localized inside the SCV but do not replicate yet, flagellar gene expression is downregulated. However, *de novo* production of flagellin was detected at later infection stages when bacteria started replicating inside the SCV. At the same time, genes encoding the Spi-1 and Spi-2 injectisomes were upregulated (Hautefort *et al.*, 2008). Comparably, in the cytosol of epithelial cells, the presence of hyperreplicating bacteria that are flagellated and express the Spi-1 injectisome has been reported (Knodler *et al.*, 2010). Furthermore, flagellin expression was detected for 60 % of the bacterial population in the Peyer's patches that belong to the gut-associated lymphoid tissue underlying the intestinal epithelium (Cummings *et al.*, 2006). In deeper organs, such as spleen and mesenteric lymph nodes, however, flagellin is repressed in order to evade the $CD4^+$ T-cells of the adaptive host immune response (Cummings *et al.*, 2005; Cummings *et al.*, 2006). In case of macrophages, flagella-mediated motility is essential for efficient infection, but inside the host cell flagellar genes are downregulated throughout early and late infection stages (Eriksson *et al.*, 2003; Hautefort *et al.*, 2008; Achouri *et al.*, 2015). However, also in macrophages *de novo* synthesis of flagella seems to occur, since only flagellated cells facilitate escape from dying oncotic macrophages (Sano *et al.*, 2007).

In this thesis, it was discovered that the expression of the flagellar master regulatory operon is growth phase-dependent heterogeneous (Chapter 4), which could correspond to certain steps during the infection cycle as proposed hereinafter. During early exponential growth, most of the cells express *flhDC* from the $P1_{flhDC}$ transcriptional start site resulting in flagellar assembly and motility, which facilitates bacteria to seek for nutrients in the intestinal lumen and to reach the site of infection. Subsequently, the negative auto-regulatory $FlhD_4C_2$-RflM feedback loop (involving RcsB) leads to

downregulation of flagellar gene expression, which might coincide with the phase immediately after host cell invasion. Since inside host cells motility is presumably no longer required, the absence of flagella would allow *S.* Typhimurium to evade the host immune system and to use the biosynthetic resources for other bacterial processes than flagellar assembly and rotation. When bacteria start replicating and the cell number increases, the main Spi-1 activator HilD facilitates induction of *flhDC* transcription from the $P5_{flhDC}$ transcriptional start site for a bacterial subpopulation. This further results in flagellar assembly and rotation as determined recently in our laboratory, although cells were non motile. Thus, it is proposed in the present study that $P5_{flhDC}$-driven expression might be involved in other pathogenic strategies and virulence processes of *S.* Typhimurium. Likewise, flagellar filaments, but not motility, are important for biofilm formation on human cholesterol gallstones in presence of bile, indicating a role in persistence (Crawford *et al.*, 2010). In *E. coli* and *Y. enterocolitica*, mutants lacking flagella or flagellar rotation are impaired in biofilm formation (Wood *et al.*, 2006; Kim *et al.*, 2008). Furthermore, the presence of flagella during this late stage of infection might stimulate the host immune system in order to induce host cell death and release of *S.* Typhimurium. Subsequently, bacteria that have been in a state ready for flagella-mediated motility might be able to become motile and to seek further eukaryotic host cells for infection and dissemination. During the whole infection cycle, heterogeneous expression of *flhDC* provides another strategy to optimize fitness and survival of *S.* Typhimurium. The *flhDC* negative subpopulation would be able to evade the host immune system, whereas the *flhDC* positive subpopulation would produce flagella, which enable motility, stimulate the host immune response or induce other virulence processes. Thereby, the bacterial population will be optimized to fast changing conditions during host cell infection. The findings of this thesis add another regulatory layer to the flagellar synthesis cascade in addition to the already known bistable expression of genes under control of flagellar class 2 and class 3 promoters and coupling of the transcriptional hierarchy to the flagellar assembly status.

In future studies, the respective physiological role of *flhDC* transcription from the two distinct transcriptional start sites $P1_{flhDC}$ and $P5_{flhDC}$ should be investigated in more detail. Therefore, mutant strains expressing *flhDC* from either $P1_{flhDC}$ or $P5_{flhDC}$ could be analyzed in cell culture experiments and *in vivo* mouse studies. Using fluorescence or luminescence reporter fusions, $P1_{flhDC}$- and $P5_{flhDC}$-expressing bacteria could be monitored directly. Furthermore, $P1_{flhDC}$- or $P5_{flhDC}$-dependent specific stimulation of the host immune response leading to host cell death could be addressed in a cell culture-based cytotoxicity assay. In order to determine if the different roles of $P1_{flhDC}$ and $P5_{flhDC}$ can be assigned to the distinct transcriptional start sites or the timing of their expression, strains with modified expression dynamics could be analyzed. Overexpression of *hilD* in a

P_{flhDC} (P5+) strain will cause premature *flhDC* expression, whereas deletion of *rflM* in P_{flhDC} (P1+) leads to prolonged *flhDC* transcription. Such a temporal regulation indeed seems to play a role, since a previous study demonstrated that the $P5_{flhDC}$-dependent motility defect could be restored upon increased *hilD* expression in early growth phases (Mouslim and Hughes, 2014). A more detailed transcriptome analysis of the P_{flhDC} (P5+) mutant strain might uncover an additional link to other virulence systems of *S.* Typhimurium. Moreover, the role of the long 5′-UTR upon $P5_{flhDC}$-driven transcription of *flhDC* has to be elucidated further. The potential formation of secondary structures or processed 5′-UTR products might be involved in RNA-mediated regulation of *flhDC* expression and the flagellar synthesis cascade or other non flagellar-related genes.

In Chapter 2 and Chapter 3 of this thesis, the molecular mechanisms of RcsB/RflM-dependent repression and HilD-mediated activation of *flhDC* transcription were investigated, respectively. The flagellar master regulator $FlhD_4C_2$ activates transcription of its own repressor, RflM, which is, however, only functional in presence of RcsB, the response regulator of the RcsCDB phosphorelay system. RflM mediates target specificity of unphosphorylated RcsB for the *flhDC* promoter and RcsB/RflM-dependent repression of *flhDC* transcription. Environmental signals might modulate this intrinsic regulation upon phosphorylation of RcsB. The question remains if RflM is able to interact with phosphorylated RcsB protein for binding to the *flhDC* promoter, which should be investigated in future studies. Otherwise, phosphorylation of RcsB via external stimuli might rather result in self-dimerization or dimerization with other auxiliary proteins. Such a mechanism would allow the Rcs system to uncouple specific stimuli from flagellar regulation and to regulate other bacterial processes. The RflM protein, no longer in complex with RcsB, is most likely unable to bind to the *flhDC* promoter and will decay quickly according to the results of this thesis. However, in order to prove this hypothesis, stable purification of recombinantly expressed RflM without RcsB will be necessary. Thus, the expression and purification conditions need to be optimized. A different affinity purification tag could be used that enhances protein solubility, such as the tandem N-terminal His_6-maltose-binding protein (MBP) tag (Rocco *et al.*, 2008). Moreover, structural analyses of the RcsB-RflM protein complex as well as the RcsB-RflM heterodimer and HilD in complex with the cognate binding box in the *flhDC* promoter would provide further details about the respective interaction.

Besides the RcsCDB signal transduction system, *S.* Typhimurium harbors several two-component regulatory systems, including PhoP/PhoQ, EnvZ/OmpR, BarA/SirA, and QseC/QseB, which respond to various environmental signals and belong to partial overlapping regulons (Erhardt and Dersch, 2015). Together with several other (global) regulators, this facilitates a spatiotemporal regulation of the different virulence systems in *S.* Typhimurium according to the bacterium's needs. For instance, motility and

persistence are exclusive events and thus the transition from a motile to a sessile state is cross-regulated. High levels of the secondary signaling molecule c-di-GMP induce biofilm formation, but repress flagella-mediated motility via the biofilm master regulator CsgD, cellulose production as well as different di-guanylate cyclases, phosphodiesterases, and EAL-like proteins (Lamprokostopoulou *et al.*, 2010; Le Guyon *et al.*, 2014). Likewise, type 1 fimbriae, which contribute to intestinal persistence, and flagella are inversely regulated via mutual repression (Clegg and Hughes, 2002; Saini *et al.*, 2010c). Additionally, *S.* Typhimurium exhibits regulatory cross-talk between the flagellar regulon and the two virulence-associated injectisomes responsible for invasion (Spi-1) and intracellular survival and replication (Spi-2). Although simultaneous expression of flagella, Spi-1, and Spi-2 genes has been detected, cross-regulation facilitates temporal regulation and sequential expression (Hautefort *et al.*, 2008; Bustamante *et al.*, 2008; Saini *et al.*, 2010c). Thereby, the flagellar regulon promotes Spi-1 gene expression via FliZ-mediated increase of HilD activity. In turn, the Spi-1-related protein RtsB represses *flhDC* transcription from the $P1_{flhDC}$ transcriptional start site. However, the findings of this thesis uncovered another cross-regulation that is positive due to HilD-dependent activation of *flhDC* transcription from the $P5_{flhDC}$ transcriptional start site. Furthermore, recent studies identified extensive regulatory overlap of the main Spi-1 activators HilD, HilC, and RtsA, and cross-talk with other virulence systems, including flagella and Spi-2 (Smith *et al.*, 2016). Positive correlation between the Spi-2 injectisome and flagella is provided by the Spi-2 effector molecule SpiC, which is involved in survival of *S.* Typhimurium in macrophages and expression of *flhD* (Uchiya *et al.*, 2009). SpiC-mediated activation of flagellar synthesis is implicated in modulation of the host immune system (Uchiya and Nikai, 2008), which supports the hypothesis that expression of *flhDC* during late infection stages might be involved in other processes than motility. Taken together, this complex cross-regulatory network allows *S.* Typhimurium to rapidly adapt expression patterns of pathogenic strategies during host cell infection.

In order to gain more information about the gene regulation dynamics of the different virulence systems in *S.* Typhimurium, the expression profile of various regulators could be monitored simultaneously using single-cell time-lapse microscopy. Therefore, spectrally distinct fluorescence reporters could be used, such as the three-color scaffold described before (Cox *et al.*, 2010). Imaging during cell culture and *in vivo* experiments would provide further details about the spatiotemporal expression and possible role of these regulators in the infection cycle. Moreover, a microfluidic device would enable to study a large number of individual cells under constant *in vitro* conditions, which is currently under investigation for heterogeneous expression of *flhDC*. Future research should determine if phenotypic heterogeneity is a general strategy of *S.* Typhimurium to increase fitness during expression of different virulence factors.

Furthermore, mathematical modeling of the *flhDC* gene regulation dynamics and the role of the identified regulatory inputs from the $FlhD_4C_2$-RflM (including RcsB), $FlhD_4C_2$-FliZ-HilD and $FlhD_4C_2$-FliZ-YdiV feedback loops might illustrate their contributions to the heterogeneous expression of *flhDC*.

6 Materials and Methods

6.1 Strains and plasmids

All *Salmonella* Typhimurium (LT2, SL1344 and ATCC 14028S) and *Escherichia coli* K12 strains used in this study are listed in Tab. 6.1. Plasmid specifications are given in Tab. 6.2.

Tab. 6.1 Strains used in this study.

Strain	Genotype	Source or Reference
***Salmonella* Typhimurium LT2 strains**		
EM4	Δ*araBAD1065*::*hilD*$^+$ *flhC5213*::Mu*d*J Δ*invH-sprB*::FCF (Δ*spi-1*)	Singer *et al.*, 2014
EM43	Δ*araBAD1065*::*hilD*$^+$ *rtsB*::T-POP *flhC5213*::Mu*d*J Δ*invH-sprB*::FCF (Δ*spi-1*)	Singer *et al.*, 2014
EM221	Δ*araBAD1005*::FCF *flhC5213*::Mu*d*J *rcsB*::T-POP	Kühne *et al.*, 2016
EM222	Δ*araBAD996*::*rcsB*$^+$ *flhC5213*::Mu*d*J *rflM*2::T-POP	Lab collection
EM229	Δ*araBAD921*::*rflM*$^+$*flhC5213*::Mu*d*J *rcsB*::T-POP	Kühne *et al.*, 2016
EM477	Δ*araBAD1170*::*rflM*-(*rcsB*-HTH)$^+$ *flhC5213*::Mu*d*J	Lab collection
EM490	Δ*araBAD1170*::*rflM*-(*rcsB*-HTH)$^+$ *flhC5213*::Mu*d*J *rcsB*::T-POP	Lab collection
EM504	Δ*araBAD1005*::FRT *flhC5213*::Mu*d*J *rflM*2::T-POP	Kühne *et al.*, 2016
EM506	Δ*araBAD1171*::*rcsB-(rflM*-HTH)$^+$ *flhC5213*::Mu*d*J *rflM2*::T-POP	Lab collection
EM515	Δ*araBAD1005*::FRT *flhC5213*::Mu*d*J *rflM*2::T-POP Δ*rcsDBC*::FCF	Kühne *et al.*, 2016
EM517	Δ*araBAD1005*::FRT *flhC5213*::Mu*d*J	Singer *et al.*, 2014
EM521	Δ*araBAD996*::*rcsB*$^+$ *flhC5213*::Mu*d*J *rflM*2::T-POP Δ*rcsDBC*::FCF	Kühne *et al.*, 2016
EM541	Δ*araBAD1171*::*rcsB*-(*rflM*-HTH)$^+$ *flhC5213*::Mu*d*J *rflM2*::T-POP Δ*rcsDBC*::FCF	Lab collection
EM656	Δ*araBAD1165*::*rflM*-(*sdiA*-HTH)$^+$ *flhC5213*::Mu*d*J	Kühne *et al.*, 2016
EM676	Δ*araBAD1181*::*rflM*-(*sdiA*-HTH)$^+$ *flh5213*::Mu*d*J *rcsB*::T-POP	Kühne *et al.*, 2016
EM677	Δ*araBAD1180*::*rcsB*-(*sdiA*-HTH)$^+$ *flh5213*::Mu*d*J *rflM*::T-POP	Lab collection
EM704	Δ*araBAD1005*::FRT *flhC5213*::Mu*d*J *rcsB*::T-POP	Kühne *et al.*, 2016
EM705	Δ*araBAD1180*::*rcsB*-(*sdiA*-HTH)$^+$ *flh5213*::Mu*d*J *rflM*::T-POP	Lab collection
EM706	P_{flhDC}*8093* (P_{flhDC}-*luxCDABE*-Km-P_{flhDC}^+) Δ*araBAD1005*::FRT	Singer *et al.*, 2014
EM707	P_{flhDC}*8124* (P_{flhDC} P1+ (-10 of P2, P3, P4, P5, P6 changed to GTTGGT)-*luxCDABE*-Km-P_{flhDC}^+) Δ*araBAD1005*::FRT	Singer *et al.*, 2014
EM711	P_{flhDC}*8128* (P_{flhDC} P5+ (-10 of P1, P2, P3, P4, P6 changed to GTTGGT)-*luxCDABE*-Km-P_{flhDC}^+) Δ*araBAD1005*::FRT	Singer *et al.*, 2014
EM713	P_{flhDC}*8093* (P_{flhDC}-*luxCDABE*-Km-P_{flhDC}^+) Δ*araBAD1065*::*hilD*$^+$	Singer *et al.*, 2014
EM714	P_{flhDC}*8124* (P_{flhDC} P1+ (-10 of P2, P3, P4, P5, P6 changed to GTTGGT)-*luxCDABE*-Km-P_{flhDC}^+) Δ*araBAD1065*::*hilD*$^+$	Singer *et al.*, 2014
EM718	P_{flhDC}*8128* (P_{flhDC} P5+ (-10 of P1, P2, P3, P4, P6 changed to GTTGGT)-*luxCDABE*-Km-P_{flhDC}^+) Δ*araBAD1065*::*hilD*$^+$	Singer *et al.*, 2014
EM808	Δ*araBAD1005*::FRT	Lab collection
EM827	Δ*araBAD1005*::FRT *flhC5213*::Mu*d*J Δ*invH-sprB*::FCF (Δ*spi-1*)	Singer *et al.*, 2014
EM937	Δ*araBAD1005*::FRT *rtsB*::T-POP *flhC5213*::Mu*d*J Δ*invH-sprB*::FCF (Δ*spi-1*)	Singer *et al.*, 2014
EM1009	Δ*araBAD1183*::*hilA*$^+$ *fljB5001*::Mu*d*J Δ*hin-5718*::FRT (*fliC*^{OFF})	Singer *et al.*, 2014
EM1010	Δ*araBAD1005*::FRT *fljB5001*::Mu*d*J Δ*hin-5718*::FRT (*fliC*^{OFF})	Singer *et al.*, 2014
EM1011	Δ*araBAD1183*::*hilA*$^+$ *flhC5213*::Mu*d*J	Singer *et al.*, 2014
EM1018	Δ*araBAD1005*::FRT *fliL5100*::Mu*d*J	Singer *et al.*, 2014
EM1019	Δ*araBAD1183*::*hilA*$^+$ *fliL5100*::Mu*d*J	Singer *et al.*, 2014

Strain	Genotype	Source or Reference
EM1048	P_{flhDC}*8093* (P_{flhDC}-*luxCDABE*-Km-P_{flhDC}^{+}) Δ*araBAD1109*::*rtsB*$^{+}$	Singer *et al*., 2014
EM1049	P_{flhDC}*8124* (P_{flhDC} P1+ (-10 of P2, P3, P4, P5, P6 changed to GTTGGT)-*luxCDABE*-Km-P_{flhDC}^{+}) Δ*araBAD1109*::*rtsB*$^{+}$	Singer *et al*., 2014
EM1053	P_{flhDC}*8128* (P_{flhDC} P5+ (-10 of P1, P2, P3, P4, P6 changed to GTTGGT)-*luxCDABE*-Km-P_{flhDC}^{+}) Δ *araBAD1109*::*rtsB*$^{+}$	Singer *et al*., 2014
EM1055	P_{flhDC}*8093* (P_{flhDC}-*luxCDABE*-Km-P_{flhDC}^{+}) Δ*araBAD921*::*rflM*$^{+}$	Kühne *et al*., 2016
EM1056	P_{flhDC}*8124* (P_{flhDC} P1+ (-10 of P2, P3, P4, P5, P6 changed to GTTGGT)-*luxCDABE*-Km-P_{flhDC}^{+}) Δ*araBAD921*::*rflM*$^{+}$	Kühne *et al*., 2016
EM1060	P_{flhDC}*8128* (P_{flhDC} P5+ (-10 of P1, P2, P3, P4, P6 changed to GTTGGT)-*luxCDABE*-Km-P_{flhDC}^{+}) Δ*araBAD921*::*rflM*$^{+}$	Kühne *et al*., 2016
EM1062	P_{flhDC}*8093* (P_{flhDC}-*luxCDABE*-Km-P_{flhDC}^{+}) Δ*araBAD996*::*rcsB*$^{+}$	Kühne *et al*., 2016
EM1063	P_{flhDC}*8124* (P_{flhDC}P1+ (-10 of P2, P3, P4, P5, P6 changed to GTTGGT)-*luxCDABE*-Km-P_{flhDC}^{+}) Δ*araBAD996*::*rcsB*$^{+}$	Kühne *et al*., 2016
EM1067	P_{flhDC}*8128* (P_{flhDC} P5+ (-10 of P1, P2, P3, P4, P6 changed to GTTGGT)-*luxCDABE*-Km-P_{flhDC}^{+}) Δ*araBAD996*::*rcsB*$^{+}$	Kühne *et al*., 2016
EM1134	Δ*araBAD1005*::FRT *fljB5001*::Mu*d*J Δ*hin-5718*::FRT (*fliC*^{OFF})	Lab collection
EM1325	Δ*rcsB*	Kühne *et al*., 2016
EM1432	Δ*araBAD1005*::FRT *flhC5213*::Mu*d*J Δ*rcsB*	Kühne *et al*., 2016
EM1434	Δ*araBAD1005*::FRT *flhC5213*::Mu*d*J *rflM2*::T-POP Δ*rcsB*	Kühne *et al*., 2016
EM1435	Δ*araBAD996*::*rcsB*$^{+}$ *flhC5213*::Mu*d*J *rflM2*::T-POP Δ*rcsB*	Kühne *et al*., 2016
EM1740	*rflM33*::HA-FRT	Kühne *et al*., 2016
EM1766	Δ*araBAD1201::rflM*-HA-FRT^{+}	Kühne *et al*., 2016
EM1792	Δ*araBAD921*::*rflM*-HA-FRT^{+} *flhC5213*::Mu*d*J	This study
EM2004	$RcsB_{D56E}$ (mimics RcsB phosphorylation)	Kühne *et al*., 2016
EM2005	$RcsB_{D56N}$ (prevents RcsB phosphorylation)	Kühne *et al*., 2016
EM2423	Δ*araBAD1005*::FRT *flhC5213*::Mu*d*J Δ*rflM32* $RcsB_{D56E}$	Kühne *et al*., 2016
EM2424	Δ*araBAD1005*::FRT *flhC5213*::Mu*d*J Δ*rflM32* $RcsB_{D56N}$	Kühne *et al*., 2016
EM2426	Δ*araBAD921*::*rflM*$^{+}$ *flhC5213*::Mu*d*J Δ*rflM32* $RcsB_{D56E}$	Kühne *et al*., 2016
EM2427	Δ*araBAD921*::*rflM*$^{+}$ *flhC5213*::Mu*d*J Δ*rflM32* $RcsB_{D56N}$	Kühne *et al*., 2016
EM2486	Δ*araBAD921*::*rflM*$^{+}$ *flhC5213*::Mu*d*J Δ*rcsB*	Kühne *et al*., 2016
EM2504	Δ*araBAD1201*::*rflM*-HA-FRT^{+} Δ*rcsB*	Kühne *et al*., 2016
EM4358	*trp*::(Spc^{R} T7-RNAP *lacO lacP lacI*) *flhC5213*::Mu*d*A	Kühne *et al*., 2016
EM4365	Δ*araBAD921*::*rflM*$^{+}$ Δ*rcsB*	Kühne *et al*., 2016
EM4366	Δ*araBAD996*::*rcsB*$^{+}$ Δ*rflM32*	Kühne *et al*., 2016
EM4369	Δ*araBAD921*::*rflM*$^{+}$ Δ*lrhA*	Kühne *et al*., 2016
EM4370	Δ*araBAD921*::*rflM*$^{+}$ Δ*slyA*	Kühne *et al*., 2016
EM4372	Δ*araBAD921*::*rflM*$^{+}$ Δ*rtsB*	Kühne *et al*., 2016
EM4373	Δ*araBAD921*::*rflM*$^{+}$ Δ*fliZ*	Kühne *et al*., 2016
EM4420	*rflM33*::HA-FRT Δ*clpXP*::FRT	Kühne *et al*., 2016
EM4421	*rflM33*::HA-FRT Δ*clpX*	Kühne *et al*., 2016
EM4422	*rflM33*::HA-FRT Δ*clpA*	Kühne *et al*., 2016
EM4451	*rflM33*::HA-FRT Δ*clpXP-lon*::FRT	Kühne *et al*., 2016
EM4453	Δ*araBAD1005*::FRT *flhC5213*::Mu*d*J *rflM2*::T-POP $RcsB_{D56N}$	Kühne *et al*., 2016
EM4454	Δ*araBAD1211*::$rcsB_{D56N}$ *flhC5213*::Mu*d*J *rflM2*::T-POP Δ*rcsB*	Kühne *et al*., 2016
EM4470	Δ*araBAD921*::*rflM*$^{+}$ Δ*prgH-hilD-hilA7791*	Kühne *et al*., 2016
EM4528	*trp*::(Spc^{R} T7-RNAP *lacO lacP lacI*) *flhC5213*::Mu*d*A pEM95	Kühne *et al*., 2016
EM4529	*trp*::(Spc^{R} T7-RNAP *lacO lacP lacI*) *flhC5213*::Mu*d*A pEM775	Kühne *et al*., 2016
EM4530	*trp*::(Spc^{R} T7-RNAP *lacO lacP lacI*) *flhC5213*::Mu*d*A pEM4318	Kühne *et al*., 2016
EM4570	*trp*::(Spc^{R} T7-RNAP *lacO lacP lacI*) *flhC5213*::Mu*d*A pSUMO	Kühne *et al*., 2016
EM4586	Δ*araBAD1201*::*rflM*-HA-FRT^{+} *rcsB*::T-POP	Kühne *et al*., 2016
EM4598	*trp*::(Spc^{R} T7-RNAP *lacO lacP lacI*) *flhC5213*::Mu*d*A Δ*rcsB*::*tetRA* pEM95	Kühne *et al*., 2016

Strain	Genotype	Source or Reference
EM4599	*trp*::(Spc^R T7-RNAP *lacO lacP lacI*) *flhC5213*::Mu*d*A Δ*rcsB*::*tetRA* pEM775	Kühne *et al*., 2016
EM4600	*trp*::(Spc^R T7-RNAP *lacO lacP lacI*) *flhC5213*::Mu*d*A Δ*rcsB*::*tetRA* pEM4318	Kühne *et al*., 2016
EM4601	*trp*::(Spc^R T7-RNAP *lacO lacP lacI*) *flhC5213*::Mu*d*A Δ*rcsB*::*tetRA* pSUMO	Kühne *et al*., 2016
EM4655	*rflM33*::HA-FRT Δ*lon*	Kühne *et al*., 2016
EM4665	Δ*araBAD1170*::*rflM*-(*rcsB*-HTH)$^+$ *flhC5213*::Mu*d*J Δ*rcsB*	This study
EM4666	Δ*araBAD1181*::*rflM*-(*sdiA*-HTH)$^+$ *flhC5213*::Mu*d*J Δ*rcsB*	Kühne *et al*., 2016
EM4697	Δ*araBAD1213*::*rflM*-(ΔHTH)$^+$ *flhC5213*::Mu*d*J	Kühne *et al*., 2016
EM4711	Δ*araBAD1213*::*rflM*-(ΔHTH)$^+$ *flhC5213*::Mu*d*J *rcsB*::T-POP	Kühne *et al*., 2016
EM4727	Δ*araBAD1213*::*rflM*-(ΔHTH)$^+$ *flhC5213*::Mu*d*J Δ*rcsB*	Kühne *et al*., 2016
TH437	wildtype	J. Roth
TH2793	F'128 *pro*$^+$ *lac*$^+$ *ataA*::[P22 HT105/1 *int-201*]	Lab collection
TH4702	pKD46	Lab collection
TH9386	Δ*araBAD921*::*rflM*$^+$	J. Karlinsey
TH12883	Δ*araBAD996*::*rcsB*$^+$	K. T. Hughes
TH13069	Δ*araBAD921*::*rflM*$^+$ *flhC5213*::Mu*d*J	K. T. Hughes
TH13662	pSUB11	L. Bossi
TH13664	pSU315	L. Bossi
TH16385	Δ*araBAD1065*::*hilD*$^+$ *fliL5100*::Mu*d*J	Singer *et al*., 2014
TH16386	Δ*araBAD1065*::*hilD*$^+$ *flhC5213*::Mu*d*J	Singer *et al*., 2014
TH16423	Δ*araBAD1065*::*hilD*$^+$ *fljB5001*::Mu*d*J Δ*hin-5718*::FRT (*fliC*^{OFF})	Singer *et al*., 2014
	***Salmonella* Typhimurium SL1344 strains**	
EM1566	Δ*araBAD1065*::*hilD*$^+$ *flhC5213*::Mu*d*J Δ*invH-sprB*::FCF (Δ*spi-1*)	This study
EM1656	Δ*araBAD1055*::FRT *flhC5213*::Mu*d*J Δ*invH-sprB*::FCF (Δ*spi-1*)	This study
	***Salmonella* Typhimurium ATCC 14028S (ST14028) strains**	
EM667	Δ*araBAD1065*::*hilD*$^+$ *flhC5213*::Mu*d*J Δ*invH-sprB*::FCF (Δ*spi-1*)	Singer *et al*., 2014
EM674	Δ*araBAD1055*::FRT *flhC5213*::Mu*d*J Δ*invH-sprB*::FCF (Δ*spi-1*)	Singer *et al*., 2014
EM2180	pEM2055	This study
EM2182	pEM2133	This study
EM2370	P$_{flhDC}$*22349* (P$_{flhDC}$ P1+ P2+ P6+ (-10 of P3, P4, P5 changed to GTTGGT))	This study
EM2371	P$_{flhDC}$*22350* (P$_{flhDC}$ P2+ P5+ P6+ (-10 of P1, P3, P4 changed to GTTGGT))	This study
EM2420	P$_{flhDC}$*22349* (P$_{flhDC}$ P1+ P2+ P6+ (-10 of P3, P4, P5 changed to GTTGGT)) Δ*hin-5717*::FRT (*fliC*^{ON})	This study
EM2421	P$_{flhDC}$*22350* (P$_{flhDC}$ P2+ P5+ P6+ (-10 of P1, P3, P4 changed to GTTGGT)) Δ*hin-5717*::FRT (*fliC*^{ON})	This study
EM2625	pEM2474	This study
EM2626	pEM2475	This study
EM2627	pEM2506	This study
EM3102	Δ*rcsB* pEM2055	This study
EM3105	Δ*rflM32* pEM2055	This study
EM3517	Δ*hilD323* pEM2055	This study
EM3940	Δ*sseA-ssaU*::FKF (Δ*spi-2*) pEM2055 pFS48	This study
EM3949	Δ*rflM32* Δ*sseA-ssaU*::FKF (Δ*spi-2*) pEM2055 pFS48	This study
EM4353	pEM4319	This study
EM4800	Δ*fliZ5738*::FRT pEM2055	This study
EM4801	*flhC22735*::3xFLAG-FRT pEM2055	This study

Strain	Genotype	Source or Reference
EM4807	P_{flhDC}::T-POP pEM2055	This study
EM4808	Δ*rflM32* P_{flhDC}::T-POP pEM2055	This study
EM4977	$FlhD7915_{L22H}$ pEM2055	This study
EM4980	Δ*ydiV*::FRT pEM2055	This study
EM4981	$FlhD7915_{L22H}$ Δ*rflM6*::T-POP pEM2055	This study
EM4982	Δ*ydiV*::FRT Δ*rflM32* pEM2055	This study
TH6622	wildtype	B. Cookson
TH11175	pKD46	Lab collection
TH11252	Δ*hin-5717*::FCF ($fliC^{ON}$)	K. T. Hughes
***Escherichia coli* strains**		
EM104	BL21 (λDE3) pEM96	Singer *et al.*, 2014
EM105	BL21 (λDE3) pUlp1	Lab collection
EM567	BacterioMatch pBT- pTRG-	Kühne *et al.*, 2016
EM571	BacterioMatch pBT-RflM pTRG-RflM	Kühne *et al.*, 2016
EM572	BacterioMatch pBT-RflM pTRG-RcsB	Kühne *et al.*, 2016
EM574	BacterioMatch pBT-RcsB pTRG-RcsB	Kühne *et al.*, 2016
EM575	BacterioMatch pBT-RcsB pTRG-RflM	Kühne *et al.*, 2016
EM576	BacterioMatch pBT-LGF2 pTRG-Gal11P	Kühne *et al.*, 2016
EM577	BacterioMatch pBT-RcsB pTRG-Gal11P	Kühne *et al.*, 2016
EM578	BacterioMatch pBT-RflM pTRG-Gal11P	Kühne *et al.*, 2016
EM579	BacterioMatch pBT-LGF2 pTRG-RcsB	Kühne *et al.*, 2016
EM580	BacterioMatch pBT-LGF2 pTRG-RflM	Kühne *et al.*, 2016
EM765	BL21 (λDE3) pEM775	Kühne *et al.*, 2016
EM902	DH10β, F^- *endA1 recA1 galE15 galK16 nupG rpsL* Δ*lacX74* Φ80*lacZ*Δ*M15 araD139* Δ(*ara,leu*)7697 *mcrA* Δ(*mrr-hsdRMS-mcrBC*) λ^-	P. Dersch
EM1020	BL21 (λDE3) pEM4318	Kühne *et al.*, 2016
EM2122	BacterioMatch pBT-$RflM_{1–15}$ pTRG-RcsB	Kühne *et al.*, 2016
EM2123	BacterioMatch pBT-$RflM_{1–30}$ pTRG-RcsB	Kühne *et al.*, 2016
EM2124	BacterioMatch pBT-$RflM_{1–45}$ pTRG-RcsB	Kühne *et al.*, 2016
EM2125	BacterioMatch pBT-RcsB pTRG-$RflM_{1–60}$	Kühne *et al.*, 2016
EM2126	BacterioMatch pBT-RcsB pTRG-$RflM_{1–75}$	Kühne *et al.*, 2016
EM2127	BacterioMatch pBT-RcsB pTRG-$RflM_{1–90}$	Kühne *et al.*, 2016
EM2128	BacterioMatch pBT-RcsB pTRG-$RflM_{1–105}$	Kühne *et al.*, 2016
EM2129	BacterioMatch pBT-RcsB pTRG-$RflM_{1–120}$	Kühne *et al.*, 2016
EM3064	BL21 (λDE3) pEM3062	Kühne *et al.*, 2016
EM4413	BL21 (λDE3) pEM4357	Kühne *et al.*, 2016
TH3552	BL21 (λDE3), F^- *ompT gal dcm lon* $hsdS_B$ ($r_B^-m_B^-$) λ (DE3 [*lacI lacUV5-T7p07 ind1 sam7 nin5*]) [$malB^+$]$_{K\ 12}$ (λ^S)	K. Stephens
TH5313	XL1-Blue MRF′, Δ(*mcrA*)*183* Δ(*mcrCB-hsdSMR-mrr*)*173 endA1 supE44 thi-1 recA1 gyrA96 relA1 lac* [F′ *proAB* $lacI^q$ZΔ*M15 Tn*5 (Tet^R)]	Stratagene
TH5314	BacterioMatch reporter strain, Δ*mcrA183* Δ(*mcrCB-hsdSMR-mrr*)*173 endA1 supE44 thi-1 recA1 gyrA96 relA1 lac* [F′ $lacI^q$ *bla lacZ* Kan^R]	Stratagene

Tab. 6.2 Plasmids used in this study.

Name	Genotype	Source or Reference
pBT	bacterial-two-hybrid bait plasmid, P_{lacUV5}-λcI, p15A, Cm^R	Stratagene
pBT-LGF2	pBT positive control, P_{lacUV5}-λcI-LGF2 ($Gal4_{1–40}$)	Stratagene
pBT-RcsB	P_{lacUV5}-λcI-$RcsB_{1–150}$ (ΔHTH)	Kühne *et al.*, 2016
pBT-RflM	P_{lacUV5}-λcI-$RflM_{1–135}$ (ΔHTH)	Kühne *et al.*, 2016
pBT- $RflM_{1–15}$	P_{lacUV5}-λcI-$RflM_{1–15}$	This study
pBT- $RflM_{1–30}$	P_{lacUV5}-λcI-$RflM_{1–30}$	This study
pBT- $RflM_{1–40}$	P_{lacUV5}-λcI-$RflM_{1–40}$	This study
pCP20	Flp expression plasmid, $P_{λpR}$-λcI857-FLP, *repA101ts*, Cm^R, Amp^R, 30 °C	B. Wanner
pEM95	pSUMO-His_6-SUMO-RflM	Lab collection
pEM96	pSUMO-His_6-SUMO-HilD	Singer *et al.*, 2014
pEM775	pSUMO-His_6-SUMO-RcsB	Kühne *et al.*, 2016
pEM2055	pKH70-P_{flhDC} (-628 to +9)-$egfp_{LVA}$ [P_{rovA} (-622 to +170)-*rovA* replaced with P_{flhDC}]	This study
pEM2133	pEM2055, pKH70-P_{flhDC} (- [P_{flhDC} -10 of P1, P2, P3, P4, P5, P6 changed to GTTGGT])-$egfp_{LVA}$	This study
pEM2474	pEM2055, pKH70-P_{flhDC} (P1+ P2+ P6+ [P_{flhDC} -10 of P3, P4, P5 changed to GTTGGT])-$egfp_{LVA}$	This study
pEM2475	pEM2055, pKH70-P_{flhDC} (P2+ P5+ P6+ [P_{flhDC} -10 of P1, P3, P4 changed to GTTGGT])-$egfp_{LVA}$	This study
pEM2506	pKH70-P_{flhDC} (Koirala [P_{flhDC} -1013 to -112])-$egfp_{LVA}$ [P_{rovA} (-622 to +170)-*rovA* replaced with P_{flhDC}]	This study
pEM3062	pSUMO-His_6-SUMO-$RcsB_{D56E}$	Kühne *et al.*, 2016
pEM4318	pSUMO-His_6-SUMO-RfM-RBS-RcsB (RBS: AAGAAGGAGATATACAT)	Kühne *et al.*, 2016
pEM4319	pKH70-$P_{LtetO-1}$-$egfp_{LVA}$ [P_{rovA} (-622 to +170)-*rovA* replaced with $P_{LtetO-1}$]	This study
pEM4357	pSUMO-His_6-SUMO-$RflM_{1–124}$(ΔHTH)-RBS-RcsB	Kühne *et al.*, 2016
pFS48	$P_{LtetO-1}$-*mCherry*, p15A, Cm^R	F. Schuster, PhD thesis
pKD46	λ-Red recombinase plasmid, P_{ara}-λ *red* (γ, β, *exo*) tL3, *repA101ts*, *oriR101*, Amp^R, 30 °C	B. Wanner
pKH70	P_{rovA} (-622 to +170)-*rovA*-$egfp_{LVA}$, *ori*29807, Amp^R, ΔR6Kmob	K. Herbst, PhD thesis
pSU315	HA-tagging vector, R6k *oriV*, Amp^R, Km^R	Uzzau *et al.*, 2011
pSUB11	3xFLAG-tagging vector, R6k *oriV*, Amp^R, Km^R	Uzzau *et al.*, 2011
pSUMO	$P_{T7\text{-}lacO}$-His_6-SUMO-MCS, ColE1, Km^R	Andréasson *et al.*, 2008
pTRG	bacterial-two-hybrid target plasmid, $P_{llpp/lac\text{-}UV5}$-RNAPα, ColE1, Tet^R	Stratagene
pTRG-Gal11p	pTRG positive control, $P_{llpp/lac\text{-}UV5}$-RNAPα-Gal11p (mutant $Gal11_{1\text{-}90}$)	Stratagene
pTRG-RcsB	$P_{llpp/lac\text{-}UV5}$-RNAPα-$RcsB_{1–150}$ (ΔHTH)	Kühne *et al.*, 2016
pTRG-RflM	$P_{llpp/lac\text{-}UV5}$-RNAPα-$RflM_{1–135}$ (ΔHTH)	Kühne *et al.*, 2016
pTRG- $RflM_{1–60}$	$P_{llpp/lac\text{-}UV5}$-RNAPα-$RflM_{1–60}$	This study
pTRG- $RflM_{1–75}$	$P_{llpp/lac\text{-}UV5}$-RNAPα-$RflM_{1–75}$	This study
pTRG- $RflM_{1–90}$	$P_{llpp/lac\text{-}UV5}$-RNAPα-$RflM_{1–90}$	This study
pTRG- $RflM_{1–105}$	$P_{llpp/lac\text{-}UV5}$-RNAPα-$RflM_{1–105}$	This study
pTRG- $RflM_{1–120}$	$P_{llpp/lac\text{-}UV5}$-RNAPα-$RflM_{1–120}$	This study
pUlp1	pSUMO-His_6-Ulp1 (SUMO protease)	C. Andréasson

6.2 Chemicals and equipment

Chemicals and equipment used in this study were purchased from Acros Organics, Ambion, Amersham Biosciences, antibodies-online, Applichem, Axygen Scientific, BD (Becton, Dickinson and Company), BD Biosciences, Bellco Glass, Biometra, Bio-Rad, Brand, Conda pronadisa, Corning, Edmund Bühler, Embi Tec, Eppendorf, Fermentas, Fisher BioReagents, Fluka, GE Healthcare, G. Heinemann, Grant bio, Greiner Bio-One, Heidolph Instruments, Honeywell, Invitrogen, J. T. Baker, KNF, Macherey-Nagel, Merck, Mettler-Toledo, Millipore, Nalgene, New Brunswick Scientific, New England Biolabs (NEB), Qiagen, Promega, Ratiolab, Roche, Roth, Sanyo, Sarstedt, Schott, Scientific Industries, Serva, Sigma-Aldrich, Starlab, Stratagene, Thermo Scientific, VITLAB, VWR International, and WLD-Tec. Special chemicals and equipment are mentioned in the text.

6.3 Media and supplements

Compositions of liquid and solid media used for bacterial cultivation are given in Tab. 6.3. Media were supplemented with solutions given in Tab. 6.4 if needed.

Tab. 6.3 Media used in this study.

Medium	Composition (for 1 liter, in ddH_2O)
LB (lysogeny broth) (Bertani, 2004)	10 g tryptone, 5 g yeast extract, 5 g NaCl (12 g agar for plates)
Motility agar (0.3 %) plates (Gillen and Hughes, 1991)	10 g tryptone, 5 g NaCl, 3 g Bacto-agar
Green plates	7.4 g D-glucose, 7.9 g tryptone, 1 g yeast extract, 4.9 g NaCl, 12 g Bacto-agar, 65 mg methyl blue, 0.6 g alizarin yellow G
Minimal E (EDEX) plates	2 % Ex50, 12 g agar, 0.2 % glucose Ex50: 9.6 g/l $MgSO_4$ x 7 H_2O, 100 g/l citric acid, 655 g/l K_2HPO_4 x 3 H_2O, 175 g/l $NaNH_4PO_4$ x 4 H_2O, 2.5 % chloroform
Minimal NCE-arabinose plates	2 % NCEx50, 12 g agar, 1 mM $MgSO_4$, 0.2 % arabinose NCEx50: 19.7 g/l KH_2PO_4, 32.3 g/l K_2HPO_4 x 3 H_2O, 17.5 g/l $NaNH_4PO_4$ x 4 H_2O, 2.5 % chloroform
Tet-sensitive plates	5 g tryptone, 5 g yeast extract, 12 g agar, 10 g NaCl, 10 g NaH_2PO_4 x H_2O, 5 ml fusaric acid, 5 ml anhydrotetracycline, 0.1 mM $ZnCl_2$

Tab. 6.4 Supplements for media used in this study.

Solution	Stock concentration[a]	Final concentration
Ampicillin	20 mg/ml	100 µg/ml
Anhydrotetracycline	0.2 mg/ml in 50 % ethanol	0.1 µg/ml
Chloramphenicol	2.5 mg/ml	12.5 µg/ml
Fusaric acid	2.4 mg/ml in DMF	12 µg/ml
D-glucose	40 % (w/v)	0.2 %

Solution	Stock concentration[a]	Final concentration
Kanamycin	10 mg/ml	50 µg/ml
L-arabinose	20 % (w/v)	0.2 %
Tetracycline	3 mg/ml in 50 % ethanol	15 µg/ml

[a] Stock solutions were prepared in ddH_2O if not stated otherwise.

6.4 Oligonucleotides

DNA oligonucleotides and gBlock® gene fragments used in this study were purchased from IDT Integrated DNA Technologies and are listed in Tab. 6.5. Labeling at the 5′-end was constructed by the manufacturer and is indicated in the sequence.

Tab. 6.5 Oligonucleotides and gBlocks used in this study.

ID	Name	Sequence (5′ to 3′)
Oligonucleotides for strain constructions[a,b]		
10	*ara120*_rv	GGAAAAGCGTGGCAGGGACA
57	5′-SUMO-seq_52C-fw	CAGACCCCTGAAGATTTGG
58	3′-pSUMO-seq_52C-rv	AAGGGGTTATGCTAGTTATTGC
183	3′-*tetR*-out_54C-rv	CTAAGTCATCGCGATGGAGC
184	5′-*tetA*-out_54C-fw	GGTTGGCTTTTCATTAGCGG
187	K1-test	CAGTCATAGCCGAATAGCCT
268	*rtsA*_sequ_56C	CCAGAGTTGCCTTGCCTACC
337	5′-*Not*I-*ecnR*_bait-prey_49C-fw	ataagaatgcggccgcaATGTTGAAAATTTTAGTGATAGACC
341	5′-pBT-seq_52C-fw	TCCGTTGTGGGGAAAGTTATC
342	3′-pBT-seq_55C-rv	GGGTAGCCAGCAGCATCC
343	5′-pTRG-seq_52C-fw	GTCAGCCTGAAGTGAAAGAAG
344	3′-pTRG-seq_53C-rv	GATTCGTCGCCCGCCATAA
380	5′-*Bsa*I-*rcsB*_50C_fw	ccagtgggtctcaggtggtATGAACAATATGAACGTAATTATTGC
381	3′-*Hind*III-*rcsB*_54C_rv	tagcatgatcaagcttTTATTCTTTGTCTGTCGGACTCAG
397	5′-*rcsB*_ΔD56-*tetR*_fw	caacaacctgccgaaattagatgcgcatgtgttgatcactTTAAGACCCACTTTCACATT
398	3′-*rcsB*_ΔD56-*tetA*_rv	caaggtgatcccatcgccgtatttatctcccggcatggagagCTAAGCACTTGTCTCCTG
399	5′-*rcsB*_D56E_54C_fw	caacctgccgaaattagatgcgcatgtgttgatcact**gaa**CTCTCCATGCCGGGAGATAA
400	5′-*rcsB*_D56N_54C_fw	caacctgccgaaattagatgcgcatgtgttgatcact**aac**CTCTCCATGCCGGGAGATAA
401	3′-*rcsB*-internal_52C_rv	GATGGTCTTAATGCTGCGGT
402	5′-*rcsB*_sequ_54C_fw	GTACCCGGCAAGCAGTTATG
403	3′-*rcsB*_sequ_50C_rv	ACGTAAAACGCGGGCATAAA
404	3′-*Xho*I-*ecnR*_1–15_bait-prey_54C_rv	gatcccgctcgagTTACGTACGGGTAAAGTGGCATC
405	3′-*Xho*I-*ecnR*_1–30_bait-prey_50C_rv	gatcccgctcgagTTATGAAGAACTGAGCACATCAG
406	3′-*Xho*I-*ecnR*_1–45_bait-prey_49C_rv	gatcccgctcgagTTAATGTTCTTTCGCCAGTATAAG

ID	Name	Sequence (5′ to 3′)
407	3′-*Xho*I-*ecnR*_1–60_bait-prey_49C_rv	gatcccgctcgagTTAACCATATAAATCAGCGATAACC
408	3′-*Xho*I-*ecnR*_1–75_bait-prey_51C_rv	gatcccgctcgagTTAAAAAAATGCATTGATAGGCTGTTC
409	3′-*Xho*I-*ecnR*_1–90_bait-prey_49C_rv	gatcccgctcgagTTAATTCCCTGACTGTAATAATACC
410	3′-*Xho*I-*ecnR*_1–105_bait-prey_49C_rv	gatcccgctcgagTTATTTAGATAACACCGCATGACT
411	3′-*Xho*I-*ecnR*_1–125_bait-prey_50C_rv	gatcccgctcgagTTATAGCGCTCCTTTAATTCGTTG
478	5′-*Hind*III-RBS-*rcsB*_50C_fw	cccaagcttAAGAAGGAGATATACATATGAACAATATGAACGTAATTATTGC
479	3′-*Xho*I-*rcsB*_48C_rv	ccgctcgagTTATTCTTTGTCTGTCGGAC
480	5′-P_{araB}-seq_-240bp_50C-fw	CAAGACTTTGCGCTTGATGA
913	5′-*flhC*-FLAG_52C_fw	tattccacaactgctggatgaacagatcgaacaggctgttGACTACAAAGACCATGACGG
914	3′-*flhC*-FLAG_46C_rv	tgacttaccgctgctggagtgtttgtccacaccgtttcggCATATGAATATCCTCCTTAG
927	5′-P_{ara}-*rflM*-intern_52C_fw	TATGCCAGTCATGCGGTGTT
931	3′-P_{ara}-tagging_46C_rv	ttcatcaacgcgccccccatgggacgcgtttttagaggcaCATATGAATATCCTCCTTAG
967	5′-Δ*slyA*-*tetR*_fw	gcaagctaattataaggagatgaaattggaatcgccactaTTAAGACCCACTTTCACATT
968	3′-Δ*slyA*-*tetA*_rv	atggccacacgtatgcccctgcacctcaatcgtgagagtgCTAAGCACTTGTCTCCTG
969	5′-Δ*slyA*-clean_50C_fw	aagcaatgttcctttgcgtc
970	3′-Δ*slyA*-clean_48C_rv	atggccacacgtatgcccctgcacctcaatcgtgagagtgTAGTGGCGATTCCAATTTCA
971	5′-*slyA*-seq_48C_fw	aacatgagatcttgtaaggg
972	3′-*slyA*-seq_56C_rv	cagccaggttaccgtctctc
973	5′-Δ*rtsB*-*tetR*_fw	cttcctctcgtcatcaatatgttaattgagatatctgacaTTAAGACCCACTTTCACATT
974	3′-Δ*rtsB*-*tetA*_rv	cactctaccaacattttaggaaaaattacgtaatatcgacCTAAGCACTTGTCTCCTG
975	5′-Δ*rtsB*-clean_50C_fw	ctcattcagcgaagtttacc
976	3′-Δ*rtsB*-clean_44C_rv	cactctaccaacattttaggaaaaattacgtaatatcgacTGTCAGATATCTCAATTAAC
977	5′-*rtsB*-seq_48C_fw	CTCTATATGAGTTGTTCCAC
984	5′-Δ*rcsB*-*tetR*_fw	ttgctgtagcaaggtagcccaatacatgaacaatatgaacTTAAGACCCACTTTCACATT
985	3′-Δ*rcsB*-*tetA*_rv	tcaggctgggtaacataaaagcgatttattctttgtctgtCTAAGCACTTGTCTCCTG
986	5′-Δ*rcsB*-clean_53C_fw	aaccagcgatttcgctgcg
987	3′-Δ*rcsB*-clean_46C_rv	tcaggctgggtaacataaaagcgatttattctttgtctgtCATATTGTTCATGTATTGGG
988	5′-*fliZ*-seq_53C_fw	ACCTGCGACAGCGGGTAAT
989	3′-*fliZ*-seq_53C_rv	CTTTGGGGGACTCAGCCTA
1218	5′-*Sal*I-P_{flhDC}_54C_fw	gatcacgcgtcgacCACCACCCGGATGCTTCATT
1219	3′-*Eco*RI-P_{flhDC}_50C_rv	gatcgaattcTGTTCCCATCCAGAATAACC
1227	5′-*rflM*-HA_49C_fw	cggtattctccctttcttatgcttccggagaaaatcgatTATCCGTATGATGTTCCTGAT
1228	3′-*rflM*-HA_46C_rv	tcagcagtaatcatcaacggtacggcatggcgtcgtaccgCATATGAATATCCTCCTTAG

ID	Name	Sequence (5′ to 3′)
1358	5′-pKH70_seq_56C_fw	CGTATCACGAGGCCCTTTCG
1359	3′-pKH70_seq_48C_rv	CTCCAGTGAAAAGTTCTTCT
1534	5′-*Sal*I-P_{flhDC}(K)_54C_fw	gatcacgcgtcgacGCCTTTTCCCCCAGCATCTT
1535	3′-*EcoR*I-P_{flhDC}(K)_50C_rv	gatcgaattcGGACATTGTGACGTATAACG
2070	5′-*Sal*I-P_{tetO}_49C_fw	gatcacgcgtcgacTCCCTATCAGTGATAGAGATT
2071	3′-*EcoR*I-P_{tetO}_50C_rv	gatcgaattcGTGCTCAGTATCTCTATCAC
2255	5′-*Xba*I-pSUMO_47C_fw	tagcatgatcaagctttaTGGATGAGTATGTAGCGCTC
2256	3′-*Hind*III-RflM(P124)_52C_rv	ccctctagaAATAATTTTGTTTAA
2304	5′-P_{ara}-*rflM*(ΔHTH)-*tetR*_fw	gcttgcacaacgaattaaaggagcgctacatactcatccaTTAAGACCCACTTTCACATT
2305	3′-P_{ara}-*rflM*(ΔHTH)-*tetA*_rv	atcaacgcgccccccatgggacgcgtttttagaggcattaCTAAGCACTTGTCTCCTG
2306	3′-P_{ara}-*rflM*(ΔHTH)-clean_52C_rv	atcaacgcgccccccatgggacgcgtttttagaggcattaTGGATGAGTATGTAGCGCTC
VI636		ACGAGGCCCTTTCGTCTTCAC
Oligonucleotides for qRT-PCR		
537	*flhDC*-qPCR-fw	GTAGGCAGCTTTGCGTGTAG
538	*flhDC*-qPCR-rv	TCCAGCAGTTGTGGAATAATATCG
583	5′-*hilD*_qPCR-60C-fw	ACGCTTGAAGAGGTCAATGG
584	3′-*hilD*_qPCR-60C-rv	TCTTCTGCGCTTTCTCTGTG
716	*gyrB*_qPCR_new-fw	ACGCTCTGTCGCAAAAACTG
717	*gyrB*_qPCR_new-rv	ACCATCGTGCCGGTTTTATC
718	*gmk*_qPCR_new-fw	TTTTGCCGCCGTCAAAGATC
719	*gmk*_qPCR_new-rv	ATGGCTCATTTCTGCAACCG
720	*rpoD*_qPCR_new-fw	ACACCATCAAAGCGAAAGGC
721	*rpoD*_qPCR_new-rv	TCATCACGCGCATACTGTTG
2257	5′-*aer*_qPCR_fw	GCTAAATGAAGGGCGGTGTA
2258	3′-*aer*_qPCR_rv	TTAGCCCCATAATGCTACGC
2259	5′-*csgD*_qPCR_fw	GGTCAGCGGATTACAGGGTA
2260	3′-*csgD*_qPCR_rv	TCGCGATGAGTGAGTAATGC
2261	5′-*dps*_qPCR_fw	ATGAGATGCTGGATGGCTTC
2262	3′-*dps*_qPCR_rv	GCGGATAGCTTTTCAGTGGA
2265	5′-*wzzB*_qPCR_fw	CGATCCGGAACAGATTGATT
2266	3′-*wzzB*_qPCR_rv	AGGTAGCCTACAGCCAGCAA
Labeled oligonucleotides[c]		
455	5′-unspecific DNA-Biotin_53C_fw	gatcatgctgacacgtacggATGAGCGACCTTGCGAGAG
456	3′-unspecific DNA_58C_rv	GCGCACGGCCAACAATGACC
457	5′-Biotin-Primer_54C_fw	/5Biosg/gatcatgctgacacgtacgg
458	5′-*flhDC*_coding-Biotin_50C_fw	gatcatgctgacacgtacggGGAGTTGATTAATCTTGGCG
459	Nr8_*flhDC*_coding_control_rv	GACACTGCTCAAGATAAAGC
460	5′-P_{flhDC}-No1-Biotin_48C_fw	gatcatgctgacacgtacggGCTAAAAGTTAAATCAAATGAGC
461	3′-P_{flhDC}-No1_47C_rv	GTCAACACCAAATTCTTTTTTG
462	5′-P_{flhDC}-No2-Biotin_47C_fw	gatcatgctgacacgtacggCGTTATTTTAACAGAGAGAAAC
463	3′-P_{flhDC}-No2_53C_rv	CATACAACGGAGCGGGAC
464	5′-P_{flhDC}-No3-Biotin_47C_fw	gatcatgctgacacgtacggTCACATATTTTCTAAAATCGCC
465	3′-P_{flhDC}_No3_48C_rv	GAAGCAAAAAGGTCAAATGC

ID	Name	Sequence (5′ to 3′)
468	5′-P_{flhDC}-Motif1+2-Biotin_52C_fw	gatcatgctgacacgtacggTTTAACAGCGGAGGGCGTAT
469	3′-P_{flhDC}-Motif1+2_52C_rv	CATAGCAGCGCTCAGACATT
470	5′-P_{flhDC}-P5-Biotin_50C_fw	gatcatgctgacacgtacggATTCTTATGTAAAGAATCGTGGC
471	3′-P5$_{flhDC}$-P5-Biotin_48C_rv	ATTTTAGAAACGCTTTTATTTTACC
582	3′-P5$_{flhDC}$_47C_DIG_rv	/5DigN/GTCAACACCAAATTCTTTTTTG
675	5′-P1$_{flhDC}$_47C_DIG_fw	/5DigN/TCACATATTTTCTAAAATCGCC
1854	3′-P_{flhDC}_RflMRcsB_rv	TTACAAATGCCTAAGATTTTTCCTAATTCG
2029	5′-Cy5- P_{flhDC} _RflMRcsB_fw	/5Cy5/CGAATTAGGAAAAATCTTAGGCATTTGTAA
gBlocks[b]		
P_{flhDC} (P1+ P2+ P6+)		cataagacacttttacacaccacccggatgcttcatttaaatgggtgaacaaggaa agctaaaagttaaatcaaatgagcttatttttaacagcggagggcg**gttggt**gtgac gagattaattaataacgtttaatatttaagctactgtttactaaaggtaaaataaaagc gtttctaaaatagaaataatagcctgttatctattatcctggcgttattttaacagagag aaacaaaaaagaatttggtgttgacgtacccctattcagcagtg**gttggt**agaaaa agtgaacattaggttattaattaaacaaagtaaaagccatgctgatggttt**gttggt**a agtattccgtTAAAATatgtgatctgcatcacaTATTTTctaaaatcgccgt cccgctccgttgtatgtcacgaagctgacgagTAGAGTtgcgtcgaattagga aaaatcttaggcatttgtaaaaattgatgtaaacgtgtaaggcgaatc
P_{flhDC} (P2+ P5+ P6+)		cataagacacttttacacaccacccggatgcttcatttaaatgggtgaacaaggaa agctaaaagttaaatcaaatgagcttatttttaacagcggagggcgTATGCTgt gacgagattaattaataacgtttaatatttaagctactgtttactaaaggtaaaataaa agcgtttctaaaatagaaataatagcctgttatctattatcctggcgttattttaacaga gagaaacaaaaaagaatttggtgttgacgtacccctattcagcagtg**gttggt**aga aaaagtgaacattaggttattaattaaacaaagtaaaagccatgctgatggttt**gttg gt**aagtattccgtTAAAATatgtgatctgcatcacaTATTTTctaaaatcgc cgtcccgctccgttgtatgtcacgaagctgacgag**gttggt**tgcgtcgaattaggaa aaatcttaggcatttgtaaaaattgatgtaaacgtgtaaggcgaatc

[a] Recognition sites for restriction enzymes are underlined.
[b] Mutated nucleotides are highlighted in bold.
[c] Labels are as follows: /5Biosg/ for 5′-biotin; /5DigN/ for 5′-digoxigenin; /5Cy5/ for 5′-Cy5.

6.5 Software and databases

Following software was used in this study: AmplifX V1.6.2 (Nicolas Jullien; CNRS, Aix-Marseille Université), EnzymeX V3.1 (Mekentosj), GraphPad Prism (GraphPad Software, Inc.), MBCF Oligo Calculator (Paul Morrison, Dana-Farber Cancer Institute and/or Harvard University), Microsoft Excel and PowerPoint for Mac 2011 (Microsoft Corporation), NIH ImageJ64 V1.47/Fiji V2.0 (U.S. National Institutes of Health) Primer3Plus (Untergasser *et al.*, 2007), Serial Cloner V2.6.1 (Franck Perez; Serial Basics), StrainSearch V1.0 (Chris Wozniak). The Nucleotide Database from the National Center for Biotechnology Information (NCBI; www.ncbi.nlm.nih.gov) was used for whole genome sequences of *Salmonella enterica* serovar Typhimurium. Special software and databases are mentioned in the text.

6.6 Microbiological methods

6.6.1 Sterilization techniques

For sterilization, media, buffer, and other consumables were autoclaved 15 min at 121 °C, 1 bar. Heat-sensitive solutions were sterile filtered through 0.22 µm pore size. Glassware was heat-sterilized at 180 °C in a compartment dryer. Surfaces and consumables that were not autoclaved were disinfected with 70 % ethanol.

6.6.2 Cultivation and storage of bacteria

S. Typhimurium and *E. coli* strains were routinely grown aerobically at 37 °C in liquid or on solid media (plates). Strains with temperature-sensitive plasmids pCP20 and pKD46 were grown at 30 °C. Overnight cultures were inoculated from single colonies. Main cultures were diluted 1:100 from overnight cultures and grown 2–3 h to mid exponential growth phase if not stated otherwise. If needed for selection, cultures were supplemented with antibiotics (see Tab. 6.4). For induction of gene expression from the P_{araBAD} or P_{tetA} promoters, cultures were supplemented with arabinose or anhydrotetracycline, respectively (see Tab. 6.4). Bacterial growth was determined by measuring the optical density of liquid cultures at a wavelength of 600 nm (OD_{600}) using an Ultrospec spectrophotometer (Amersham Biosciences). Temporary, bacteria were stored on LB plates at 4 °C. For long-term storage, bacterial overnight cultures were mixed with 10 % DMSO and frozen at - 80 °C.

6.6.3 Preparation of electrocompetent bacteria and electroporation

For electroporation of DNA into bacteria, cells from main cultures were harvested 5 min at 10 000 x*g*, 4 °C and washed twice with ice-cold ddH_2O. 50 µl electrocompetent cells were mixed with up to 5 µl DNA, transferred to electroporation cuvettes (1 mm gap) and pulsed at 1.6 kV, 200 Ω, 25 µF (Eporater, Eppendorf). For phenotypic expression, cells were mixed with 1 ml LB medium and incubated 1 h at 37 °C, before spreading on selective LB plates for incubation.

6.6.4 Homologous recombination with the λ-Red system

Chromosomal mutations of *S.* Typhimurium strains were constructed by homologous recombination using the λ-Red system as described before (Karlinsey, 2007). Briefly, expression of the bacteriophage λ-Red genes (*gam*, *bet*, and *exo*) enabled introduction of linear double-stranded DNA (dsDNA) into target regions via 40 bp homologous flanking

regions. First, to enable selection, a *tetRA* element conferring tetracycline resistance (Tc^R) was PCR amplified from a Tn*10d*Tc template with primers containing 40 bp homology. This PCR product was electroporated into *S.* Typhimurium harboring pKD46, which enabled P_{araBAD}-dependent expression of the λ-Red genes and thereby insertion of the *tetRA* element into the target DNA region. Successful recombination events were selected on LB-Tc^R plates at 37 °C. Next, the *tetRA* element was replaced with a PCR-amplified dsDNA fragment containing the desired mutation using pKD46 as described above. Successful replacement was selected on Tet-sensitive plates, and correct mutations were verified by PCR and sequencing.

In this study, following mutations were constructed. Amino acid mutations in RcsB were constructed with primers 397/398 to amplify the *tetRA* element and primers 400/401 ($RcsB_{D56E}$) or 399/401 ($RcsB_{D56N}$) with *S.* Typhimurium wildtype genomic DNA as template to amplify the mutated dsDNA fragments. Similarly, clean deletions were constructed with primers 986/987 for Δ*rcsB*, primers 967/968 (*tetRA*) and 969/970 for Δ*slyA*, and primers 973/974 (*tetRA*) and 975/976 for Δ*rtsB*. The helix-turn-helix domain of *rflM* under control of the P_{araBAD} promoter was deleted with primers 2304/2305 (*tetRA*), followed by replacement with the mutated dsDNA fragment amplified with primers 927/2306 from genomic DNA of strain TH9386 resulting in P_{araBAD}*1213-rflM*-(ΔHTH). Mutations in the *flhDC* promoter region resulting in P_{flhDC}*22349* (P_{flhDC} P1+ P2+ P6+ (-10 of P3, P4, P5 changed to GTTGGT)) and P_{flhDC}*22350* (P_{flhDC} P2+ P5+ P6+ (-10 of P1, P3, P4 changed to GTTGGT)) were constructed from corresponding gBlocks.

6.6.5 Chromosomal HA- and 3xFLAG-tagging

C-terminal HA- and 3xFLAG-tagging of chromosomal genes was constructed according to the method of Uzzau *et al.* that is based on homologous recombination with the λ-Red system (Uzzau *et al.*, 2001). Briefly, a dsDNA fragment was PCR amplified from the HA-tagging plasmid pSU315 or the 3xFLAG-tagging plasmid pSUB11 with primers containing 40 bp homology preceding the stop codon of the target gene and a downstream region. The PCR products included the HA or 3xFLAG coding sequences, respectively, followed by a kanamycin resistance cassette flanked by FRT sites (FKF). After electroporation into *S.* Typhimurium harboring pKD46, successful recombination events were selected on LB-Km^R plates, and correct tagging was verified by PCR and sequencing.

HA-tagging of *rflM* under control of its native promoter was constructed with primers 1227/1228 resulting in *rflM33*::HA-FKF. Genomic DNA from this strain was used to construct $P_{araBAD1201}$::*rflM*-HA-FKF with primers 927/931. 3xFLAG-tagging of *flhC* was constructed with primers 913/914 resulting in *flhC*::3xFLAG-FKF.

6.6.6 Site-specific recombination with Flp

Chromosomal resistance cassettes flanked by FRT (Flp recombination target) sites (FKF for Km^R or FCF for Cm^R) were removed using the Flp enzyme as described before (Cherepanov and Wackernagel, 1995). Briefly, electroporation of the Flp expression plasmid pCP20 into *S.* Typhimurium strains harboring FKF or FCF enabled homologous recombination between FRT sites after selecting on LB-Amp^R plates at 30 °C. Resulting strains with one FRT scar left were cured from pCP20 by incubating on LB plates at 37 °C.

6.6.7 Transduction with phage P22

In order to transfer chromosomal mutations between *Salmonella* strains, the *S.* Typhimurium generalized transducing phage P22 *HT105/1 int-201* was used in all transductional crosses (Sanderson and Roth, 1988). Phage lysates from *S.* Typhimurium strains were prepared by adding 4 ml P22 broth (2 % Ex50, 0.2 % glucose, 10^8 pfu/ml P22 *HT105/1 int-201*) to 1 ml overnight culture and incubating 8–16 h at 37 °C. Cell debris was removed by centrifugation (10 min at 3 500 x*g*, 4 °C) and residual bacteria were killed by adding 10 % chloroform. Phage lysates were stored at 4 °C.

For transductions, overnight cultures of recipient *S.* Typhimurium strains were mixed 1:1 with phage lysate. As controls, phage lysate and recipient strains only were mixed 1:1 with 1x PBS (8 g/l NaCl, 2.68 g/l Na_2HPO_4 x 7 H_2O, 0.2 g/l KCl, 0.27 g/l KH_2PO_4, pH 7.5). For phenotypic expression, mixtures were incubated 1 h at 37 °C before spreading on selective LB plates for incubation. Phage-free transductants were isolated by streaking on green plates, and white colonies were cross-streaked against the mutant phage P22 H5 to exclude H5 resistant bacteria.

6.6.8 Swimming motility assay

Bacterial swimming motility was determined on motility agar plates. Motility plates were inoculated with overnight cultures by either pipetting 1 µl into the plate or using a pin tool (V&P Scientific). After incubating 3–4 h at 37 °C, diameters of the swimming halos were measured using the software ImageJ/Fiji and normalized to the wildtype control.

6.6.9 Flow cytometry analysis

Expression of e*gfp*$_{LVA}$ fusion constructs from individual cells was determined with flow cytometry analysis. Overnight cultures were diluted in fresh LB-Amp^R medium to an OD_{600} of 0.01 and incubated at 37 °C, 200 rpm. Every hour (1–6 h post inoculation), bacteria were harvested by centrifugation (1 min at 16 873 x*g*, room temperature) and

incubated 20 min in 1 ml 4 % paraformaldehyde (pH 7.5, in ddH_2O) for fixation. Afterwards, cells were washed twice with 1x PBS (8 g/l NaCl, 2.68 g/l Na_2HPO_4 x 7 H_2O, 0.2 g/l KCl, 0.27 g/l KH_2PO_4, pH 7.5), stained at least 15 min at room temperature in 1 ml DAPI solution (1 μg/ml in 1x PBS) and stored at 4 °C until further use. Analysis was performed using the LSR-II SORP flow cytometer (BD Bioscience) and the BD FACSDiva™ software (BD Bioscience) for data acquisition. 100 000 events of DAPI-positive cells were recorded according to the UV-B signal and further processed using the software FlowJo V9.8 (FlowJo, LCC). The gating strategy is exemplified in Fig. S4.

6.6.10 Single-cell time-lapse fluorescence microscopy

Time-lapse fluorescence microscopy on single-cell level was performed at the Institute of Science and Technology Austria in cooperation with Tobias Bergmiller. Strains harboring pEM2055 for monitoring P_{flhDC}-e*gfp*$_{LVA}$ expression and pFS48 for monitoring bacterial cells via constitutive $P_{LtetO\text{-}1}$-*mCherry* expression were analyzed using an inverted fluorescence microscope (Ti-Eclipse, Nikon) with perfect focus system, an automated stage and shutters, and the software NIS-Elements (Nikon). Fluorescence images were acquired with a CCD camera (Orca R2, Hamamatsu) using a 100x 1.4 NA oil immersion objective lens and a LED unit (Lumencore) with ND8 and adjustable light intensities (μW) as light source. mCherry was imaged using a TexasRed HYQ emission filter (LP 596, BP 641/75; Chroma) upon 300 ms exposure with the green LED (549 ± 15 nm) at 320 μW. eGFP$_{LVA}$ was imaged using a GFP emission filter (LP 495, BP 520/35; Chroma) upon 250 ms exposure with the cyan LED (475 ± 28 nm) at 230 μW. Therefore, 1 μl bacteria from main cultures were diluted 1:10 in LB medium and spotted onto 2 % LB-agarose pads (SeaPlaque GTG Agarose, Lonza) that were placed into a Gene Frame® and sealed with a cover slip. Cells were grown under the microscope for 2 h at 37 °C in a custom-made incubator with a temperature controller (Reinach, Life Imaging Services, Switzerland), and pictures were taken every 4 min. Images were further processed using the software ImageJ/Fiji.

6.7 Molecular biological methods

6.7.1 Isolation of DNA from bacteria

Genomic DNA from *S*. Typhimurium was isolated using the DNeasy® Blood & Tissue Kit (Qiagen). 3 ml overnight culture was harvested by centrifugation 2 min at 16 873 x*g* and genomic DNA was prepared according to the manufacturer's instructions.

Plasmid DNA from *E. coli* was isolated using the QIAprep® Spin Miniprep Kit (Qiagen) for small-scale purifications (4–15 ml cultures) or the NucleoBond® Xtra

Midi/Maxi kit (Macherey-Nagel) for medium-scale purifications (100 ml or 200 ml cultures) and low-copy plasmids according to the manufacturers' instructions. For midi-preparations, plasmids were isolated from large overnight cultures that were inoculated 1:100 from pre-cultures, and plasmid DNA was reconstituted in 200–250 µl ddH_2O.

The concentration and purity of isolated genomic and plasmid DNA was determined using a nanospecrophotometer (NanoDrop 1000, Peqlab or NanoPhotometer™ P330, Midsci). Contaminations with proteins or chemicals were excluded according to 260/280 nm and 260/230 nm ratios. DNA was stored at -20 °C.

6.7.2 Polymerase chain reaction

Double stranded DNA fragments were amplified by polymerase chain reaction (PCR) with oligonucleotides listed in Tab. 6.5. Recombinantly produced Phusion DNA polymerase (*pfu-sso7d*; Wang *et al.*, 2004) with proof-reading activity was used with 5x Phusion® HF Reaction Buffer (NEB) in order to amplify DNA fragments for strain constructions, cloning and protein-DNA interaction studies. Recombinantly produced *Taq* DNA polymerase was used with 5x Green GoTaq® Reaction Buffer (Promega) for test or colony PCRs. For colony PCRs, bacteria were lysed by heating 10 min at 95 °C and used directly as template. A standard PCR reaction and cycling conditions for Phusion and *Taq* DNA polymerase are given in Tab. 6.6 and Tab. 6.7.

Tab. 6.6 Standard PCR reaction.

Compound	Final concentration
5x PCR reaction buffer	1x
[For *Taq* polymerase: 25 mM $MgCl_2$	1.5 mM]
20 mM dNTP mix (5 mM each; NEB)	0.8 mM
10 µM oligonucleotide each	0.5 µM each
DNA polymerase	0.5 µl
Template (genomic DNA or plasmid)	1 - 500 ng
ddH_2O	ad 50 µl

Tab. 6.7 PCR cycling conditions for Phusion and *Taq* DNA polymerase.

Cycling conditions[a]	Phusion polymerase	*Taq* polymerase
1. Initial denaturing	2 min at 98 °C	3 min at 95 °C
2. Denaturing	15 sec at 98 °C	15 sec at 95 °C
3. Annealing[b]	30 sec at primer specific annealing temperature	
4. Elongation[c]	30 sec/kb at 72 °C	60 sec/kb at 72 °C
5. Final elongation	5 min at 72°C	
6. Hold at 8 °C		

[a] Steps 2 to 4 were repeated for 35 cycles.
[b] Annealing temperatures were determined using the MBCF Oligo Calculator.
[c] Elongation times were calculated according to the product size and respective DNA polymerase.

6.7.3 Agarose gel electrophoresis

DNA fragments were separated by agarose gel electrophoresis in order to verify successful PCR reactions, for size estimation or preparative purposes. DNA samples were mixed with 6x Purple Gel Loading Dye (NEB), loaded onto a 1 % agarose TAE gel (40 mM Tris, 20 mM acetic acid, 1 mM EDTA), and electrophoresis was performed at 130 V. The 100 bp Low Scale DNA Ladder (Fisher BioReagents) or the *ex*ACTG*ene*™ 1 kb Plus DNA Ladder (Fisher BioReagents) were used as size standard for small or large DNA fragments, respectively. Agarose gels were stained in ethidium bromide solution (1 μg/ml in ddH_2O) and acquired using a Gel Doc™ XR+ documentation system (Bio-Rad) and the Image Lab™ software (Bio-Rad).

6.7.4 Purification of DNA fragments

For purification of DNA fragments from PCR reactions, molecular cloning procedures or agarose gels, the NucleoSpin® Gel and PCR Clean-up kit (Macherey-Nagel) was used according to the manufacturer's instructions. DNA fragments separated by agarose gel electrophoresis and stained in ethidium bromide were excised from the agarose gel using a scalpel and UV transilluminator for visualization. DNA fragments were eluted in 15 μl ddH_2O and stored at -20 °C.

6.7.5 Molecular cloning

New plasmids were constructed by sticky-end cloning with enzymes purchased from NEB according to the manufacturer's protocols. In principle, vectors and PCR amplified inserts were digested with restriction enzymes for 2–3 h at 37 °C producing sticky ends with subsequent vector dephosphorylation using Antarctic Phosphatase. Enzymes were heat-inactivated at enzyme-specific temperatures if needed, followed by vector and insert purification. To get rid of unnecessary fragments, digested vectors were separated by agarose gel electrophoresis prior purification. Purified vectors and inserts with sticky ends were ligated using T4 DNA ligase with 50–100 ng vector DNA and a molar vector-to-insert ratio of 1 to 3 and 1 to 5. After incubating overnight at 4 °C, ligation reactions were purified and electroporated into *E. coli* strains that enabled plasmid propagation. Cells were incubated on selective LB plates and correct cloning was determined by colony PCR and sequencing of isolated new plasmids.

In this study, following plasmids were constructed. For protein purification, plasmid pEM3062 was constructed by cloning *rcsB*, which was PCR-amplified from genomic DNA of strain EM2004 with primers 380/381, into pSUMO via *Bsa*I/*Hind*III. In order to construct pEM4318, *rcsB* with a preceding additional ribosomal binding site (RBS:

AAGAAGGAGATATACAT) was PCR-amplified from *S.* Typhimurium LT2 wildtype genomic DNA with primers 478/479. The insert was cloned into pEM95 via *Hind*III/*Xho*I. pEM4357 was constructed from pEM4318 by replacing *rflM* with *rflM*(ΔHTH), which was amplified from pEM4318 with primers 2255/2256, via *Xba*I/*Hind*III. Fusion plasmids used for bacterial-two-hybrid analyses, pBT and pTRG, were constructed using *Not*I/*Xho*I. Therefore, length variants of *rflM* were PCR-amplified with primer 377 and primers 404–411 for $RflM_{1–15}$ to $RflM_{1–120}$ with 45 bp increments. Translational promoter fusions to $egfp_{LVA}$ were constructed by cloning the respective promoter fragments into pKH70 using *Sal*I/*Eco*RI leading to complete replacement of the original P_{rovA}-*rovA* insert. The P_{flhDC} insert containing -628 to +9 bp relative to the *flhD* start site was PCR-amplified from *S.* Typhimurium LT2 genomic DNA using primers 1218/1219. For pEM2055, pEM2133, pEM2474 and pEM2475, genomic DNA was used from strains TH437, EM1352, EM2370, and EM2371, respectively. The P_{flhDC} region used by Koirala *et al*. (2014) was amplified with primers 1534/1535 from TH437 genomic DNA. The constitutive active promoter $P_{LtetO-1}$ was amplified from pFS48 with primers VI636/2071 and cloned into pKH70 via *Xho*I/*Eco*RI.

6.7.6 DNA sequencing

In order to verify new strains and plasmids, DNA sequencing was performed at the in-house facility of the Helmholtz Centre for Infection Research (Group of Genome Analytics, GMAK). Sequencing results of purified DNA fragments or plasmids were analyzed using the software 4Peaks and SerialCloner.

6.7.7 Isolation and purification of total RNA from bacteria

In order to isolate total RNA from bacteria, main cultures were supplemented with one volume RNAprotect® Bacteria Reagent (Qiagen). Bacteria were lysed enzymatically with lysozyme according to the manufacturer's instructions with subsequent purification of total RNA from bacterial lysates using the RNeasy® Mini Kit (Qiagen). Genomic DNA was removed from isolated RNA using the TUBRO DNA-*free*™ Kit (Ambion) according to the manufacturer's instructions. RNA purity and integrity was determined by PCR and agarose gel electrophoresis upon separation on a 1 % agarose-TAE-formamide gel for 50 min at 80 V. The concentration of purified RNA was measured using a nanospectrophotometer (NanoDrop 1000, Peqlab), and pure RNA was stored at -20 °C.

6.7.8 Quantitative real-time PCR

Quantitative real-time PCR (qRT-PCR) was performed in a Rotor-Gene Q lightcycler (Qiagen) using the SensiFAST™ SYBR® No-ROX One Step Kit (Bioline) that enabled reverse transcription with subsequent qRT-PCR in the same reaction. A standard reaction mix and cycling conditions are shown in Tab. 6.8 and Tab. 6.9, respectively. Purified total bacterial RNA was used as template, and primer efficiencies were determined from a serial dilution of *S.* Typhimurium wildtype genomic DNA using the Rotor-Gene Q software (Qiagen). Transcript levels of target gene mRNA were normalized to the geometric mean of reference genes (*gyrB*, *gmk*, and *rpoD*) as described before (Vandesompele *et al.*, 2002). Relative changes in transcript levels were calculated according to the ΔΔCt method (Pfaffl, 2001).

Tab. 6.8 Standard qRT-PCR reaction mix.

Compound	Volume (10 µl total)	Final concentration
2x SensiFAST SYBR No-ROX One-Step Mix	5.0 µl	1x
10 µM oligonucleotide each	0.4 µl	400 nM
RiboSafe RNase inhibitor	0.2 µl	
Reverse transcriptase	0.1 µl	
RNase-free water	1.9 µl	
RNA template	2.0 µl	

Tab. 6.9 qRT-PCR cycling conditions.

Cycle[a]	Conditions
1. Reverse transcription	20 min at 45 °C
2. Polymerase activation	5 min at 95 °C
3. Denaturing	10 sec at 95 °C
4. Annealing	20 sec at 58 °C
5. Extension	10 sec at 72 °C
6. Final extension	10 min at 72 °C
7. Melting profile analysis	58 °C to 99 °C

[a] Steps 3 to 5 were repeated for 34 cycles.

6.8 Biochemical methods

6.8.1 β-galactosidase assay

The β-galactosidase activity of transcriptional *lacZ* fusions to chromosomal genes of *S.* Typhimurium via the Mu*d*J or Mu*d*A transposon was determined as described before (Zhang and Bremer, 1995) with minor modifications. The OD_{600} of bacterial main cultures was recorded and 80 µl permeabilization solution (100 mM Na_2HPO_4, 20 mM KCl, 2 mM $MgSO_4$, 0.08 % CTAB, 0.04 % sodium deoxycholate, 5.4 µl/ml β-mercaptoethanol) was added to 20 µl cells immediately. The reaction was started by adding 600 µl substrate

solution (60 mM Na_2HPO_4, 40 mM NaH_2PO_4, 1 mg/ml ONPG, 2.7 µg/ml β-mercaptoethanol) and stopped with 700 µl 1 M sodium carbonate after sufficient yellow color had been developed or after 1 h reaction time. Samples were centrifuged 10 min at 16 850 x*g* to remove cell fragments and the absorbance of the supernatant was measured at OD_{420} using a microplate reader (Tecan). Miller units that represent β-galactosidase activity were calculated as described before (Miller, 1972):
Miller units = 1000 x OD_{420} / reaction time [min] x culture volume [ml] x OD_{600}.

6.8.2 Bacterial-two-hybrid assay

Protein-protein interactions were determined in a bacterial-two-hybrid assay according to the method of Dove and Hochschild that is based on transcriptional activation of the *lacZ* reporter gene, whose activity could be determined easily in a β-galactosidase assay (Dove and Hochschild, 2004). Proteins of interest were cloned into the pTRG target and pBT bait plasmids (see Chapter 6.7.5) resulting in N-terminal fusions to the N-terminal domain of the α-subunit of the *E. coli* RNA polymerase and to the phage λcI DNA-binding protein, respectively. Upon induction, interaction between both proteins of interest stabilized binding of the RNA polymerase to a test promoter resulting in *lacZ* transcription. Therefore, *E. coli* BacterioMatch reporter strains harboring pTRG and pBT fusion plasmids were grown overnight in LB medium supplemented with appropriate antibiotics and 20 µM IPTG for induction of fusion proteins. Main cultures were supplemented with antibiotics and 20 µM IPTG, and transcription of *lacZ* was determined in a β-galactosidase assay as described above (Chapter 6.8.1). Empty plasmids served as negative controls, whereas pTRG-Gal11p and pBT-LGF2 served as positive controls.

6.8.3 Luminescence assay

Luminescence activity of the luciferase reporter gene *luxCDABE* was measured using the Varioskan™ microplate reader (Thermo Scientific). Main cultures of strains harboring the P_{flhDC}-*luxCDABE*-Km-P_{flhDC}^+ reporter fusion were grown in white 96-well microtiter plates with clear bottom (Greiner Bio-One) at 37 °C on a shaker. OD_{600} and luminescence were measured every hour for kinetics or after 3 h growth for one-point measurements. The average luminescence of three readings per well was normalized to the bacterial growth (OD_{600}). Throughout the whole experiment, all cultures were supplemented with 25 µg/ml kanamycin in order to retain the *flhDC* promoter duplication that ensures correct *flhDC* transcription.

6.8.4 Flagellar immunostaining

Immunostaining of the flagellar filament protein FliC was performed as described before (Erhardt *et al.*, 2011). Main cultures of strains locked in *fliC* expression (*fliC*^{ON}) were applied to microscopy chambers with 0.1 % poly-L-lysine pre-coated coverslips, fixed with 2 % formaldehyde/0.2 % glutaraldehyde, and blocked with 10 % BSA for at least 10 min. Flagellar filaments were stained for 1 h at room temperature or overnight at 4 °C using the anti-FliC polyclonal rabbit antibody (1:1 000 in 2 % BSA, gift from K. T. Hughes), followed by washing with 1x PBS and another blocking step. Samples were incubated 30 min with the secondary goat-anti-rabbit Alexa Fluor 488 antibody (1:1 000 in 1x PBS, Invitrogen), and bacterial DNA and cell membranes were stained using Fluoroshield™ with DAPI (Sigma) and 5 µg/ml FM® 4-46 Dye (Invitrogen). Images were acquired using an inverted fluorescence microscope (Axio Observer Z1, Zeiss) with an Axiocam HR CCD camera (Zeiss) and the software ZEN 2012 (Zeiss) under 100x magnification. Images were analyzed using the software ImageJ, and the mean flagella number per cell was determined from Gaussian distribution using GraphPad PRISM.

6.8.5 SDS polyacrylamide gel electrophoresis

Denaturing SDS polyacrylamide gel electrophoresis (SDS-PAGE) was performed in order to analyze purified proteins and for subsequent western blot analysis. Samples were either used directly or proteins were enriched by precipitation with TCA. Therefore, bacterial pellets were resuspended in ddH_2O, mixed with 10 % TCA and incubated for at least 5 min at 4 °C. Samples were washed with ice-cold acetone and dried overnight at room temperature. Before loaded on SDS gels (see Tab. 6.10 for composition), samples were mixed with 2x SDS sample buffer (100 mM Tris-HCl pH 6.8, 4 % SDS, 20 % glycerol, 25 mM EDTA, 0.04 % bromophenol blue, 2 % β-mercaptoethanol) and incubated 10 min at 95 °C. In order to load equivalent protein amounts from different bacterial cultures, samples were set to the same OD-units. Electrophoresis was performed for 1 h at 200 V in a Bio-Rad electrophoresis chamber (Mini-PROTEAN® Tetra Cell) with 1x SDS running buffer (Rotiphorese®, Roth). As size standard the Roti®-Mark Standard (Roth) was used for gels that were stained subsequently, and the Fisher's EZ-Run™ Pre-stained *Rec* protein ladder (Fisher BioReagents) was used in case of subsequent western blotting.

SDS gels were routinely stained with coomassie solution (0.1 % brilliant blue R250, 40 % ethanol, 10 % acetic acid) and destained in 20 % ethanol/acetic acid, followed by ddH_2O. Low protein amounts were detected upon staining with the Pierce™ Silver Stain Kit (Thermo Scientific) according to the manufacturer's instructions.

Tab. 6.10 Composition of SDS gels.

Compound	Resolving gel (12 %)	Stacking gel
40 % acrylamide/bis	6.0 ml	1.25 ml
0.5 M Tris pH 6.8	-	3.75 ml
1.5 M Tris pH 8.8	5.0 ml	-
10 % SDS	200 µl	100 µl
10 % APS	200 µl	100 µl
TEMED	15 µl	10 µl
ddH_2O	8.6 ml	4.3 ml

6.8.6 Western blot analysis

Western blotting was performed subsequently after SDS-PAGE using a Bio-Rad wet-blotting tank system (Mini Trans-Blot® Cell). Proteins were transferred 1 h at 100 V in pre-cooled transfer buffer (25 mM Tris base, 192 mM glycine, 20 % methanol) on nitrocellulose or PVDF membranes (Bio-Rad), depending on the primary antibody used. For detection of HA tags, membranes were incubated afterwards in stripping buffer (62.5 mM Tris-HCl pH 6.7, 100 mM β-mercaptoethanol, 2 % SDS) to expose potentially buried epitope tags. Membranes were blocked at least 1 h with 5 % skim milk powder in TBST (20 mM Tris-HCl pH 7.5, 150 mM NaCl, 0.1 % Tween-20) or PBST (1x PBS, 0.1 % Tween-20) depending on the primary antibody that was used afterwards for 1 h incubation at room temperature or overnight at 4 °C. Membranes were washed with the appropriate buffer (TBST or PBST), incubated for at least 45 min with the secondary antibody, and developed using the Clarity™ Western ECL Blotting substrate (Bio-Rad) after another washing. Images were acquired using a ChemiDoc™ XRS+ documentation system (Bio-Rad) and the Image Lab™ software (Bio-Rad). Images were further processed using the software ImageJ/Fiji. Antibodies with corresponding conditions used for western blots are listed in Tab. 6.11.

Tab. 6.11 Antibodies used in this study for western blot analysis.

Antibody	Conditions	Source
Primary antibodies		
Anti-DnaK, monoclonal mouse	Nitrocellulose or PVDF membrane, 1:10 000 in 5 % milk/TBST or PBST	Abcam
Anti-FLAG M2, monoclonal mouse	Nitrocellulose membrane, 1:2 000 in 5 % milk/TBST	Sigma-Aldrich
Anti-GFP, polyclonal rabbit	Nitrocellulose membrane, 1:3 000 in 5 % milk/TBST	antibodies online
Anti-HA.11 clone 16B12, monoclonal mouse	PVDF membrane, 1:1 000 in 5 % milk/PBST	Covance
Secondary antibodies		
Immun-Star™ goat anti-mouse-HRP	1:20 000 in 5 % milk/TBST or PBST	Bio-Rad
Immun-Star™ goat anti-rabbit-HRP	1:20 000 in 5 % milk/TBST	Bio-Rad

6.8.7 Protein stability assay

Protein stability of (P_{araBAD})-RflM-HA or $eGFP_{LVA}$ was analyzed as described before (Aldridge *et al.*, 2006a) with minor modifications. Protein synthesis of bacterial main cultures was stopped by addition of 12.5 µg/ml chloramphenicol and 0.5 mg/ml spectinomycin. At specific time-points after stopping of protein synthesis, total protein extracts were taken from 1 ml culture by centrifugation (1 min at 20 000 x*g*, 4 °C) followed by TCA precipitation as described above (see Chapter 6.8.5). 100 OD-units of HA-tagged RflM or 200 OD units of $eGFP_{LVA}$ samples were subjected to SDS-PAGE and protein levels were visualized upon western blotting as described above (see Chapters 6.8.5 and 6.8.6). Protein bands were quantified using the software ImageJ/Fiji. The half-life of $eGFP_{LVA}$ was determined from linear regression using GraphPad PRISM and the following equation as described before (Andersen *et al.*, 1998): $t_{1/2}$ [min] = - ln2 / slope [min].

6.8.8 Recombinant protein overexpression and purification

N-terminal His_6-SUMO fusion proteins were overexpressed from main cultures of *E. coli* BL21 (λDE3) cells harboring pSUMO fusion plasmids pEM96, pEM775, pEM3062, pEM4318 or pEM4357. Therefore, protein overexpression was induced with 0.2 mM IPTG for 3 h at 37 °C or for 6 h at 18 °C (only pEM96). Afterwards, bacteria were harvested by centrifugation (15 min at 10 000 x*g*, 4 °C) and frozen at -20 °C. Cells were thawed, resuspended in protein buffer (50 mM NaH_2PO_4, 300 mM NaCl, pH 8.0) supplemented with protease inhibitor (cOmplete protease inhibitor cocktail, EDTA-free; Roche) and disrupted using French Press (Heinemann). Soluble fusion proteins were purified under native conditions using Protino® Ni-NTA agarose (Macherey-Nagel) for His_6-SUMO-HilD or Talon® Superflow™ (GE Healthcare) for the other fusion proteins according to the manufacturers' instructions. The N-terminal His_6-SUMO tag was cleaved from His_6-SUMO-HilD, His_6-SUMO-RcsB, and His_6-SUMO-$RcsB_{D56E}$ by supplementing purified proteins with the recombinantly produced SUMO protease His_6-Ulp1. Samples were dialyzed overnight at 4 °C against protein buffer using a Slyde-A-Lyzer™ dialysis cassette (Thermo Scientific) or SnakeSkin™ dialysis tubing (Thermo Scientific). Contaminants (His_6-Ulp1, cleaved His_6-SUMO tags, and uncleaved proteins) were removed by binding to Protino® Ni-NTA agarose. Except for purified HilD, proteins were concentrated using Vivaspin® (Sartorius Stedim) or Amicon® Ultra (Merck) centrifugal concentrator tubes and further purified using gel filtration (Äkta, GE Healthcare) with a Superdex 200 10/300 GL column (GE Healthcare) and the software Unicorn V5.1 (GE Healthcare). Protein concentrations were determined using the Quick Start™ Bradford protein assay (Bio-Rad) with a BSA standard set (Bio-Rad) according to the manufacturer's instructions by measuring absorbance in a microplate reader (Tecan). Pure proteins were stored at 4 °C.

The SUMO protease His_6-Ulp1 was purified from strain EM105 similar to the procedure described above with minor modifications. Instead of protein buffer, lysis buffer (40 mM HEPES pH 7.5, 150 mM KCl, 20 mM β-mercaptoethanol) was used for purification with Protino® Ni-NTA agarose. Purified protein was dialyzed against dialysis buffer (40 mM HEPES pH 7.5, 100 mM KCl, 10 mM β-mercaptoethanol), concentrated to 0.5 mg/ml and stored with 50 % glycerol at -20 °C.

6.8.9 Size exclusion chromatography with multi-angle light scattering

In order to determine the molecular mass of protein complexes, size exclusion chromatography (SEC) in combination with multi-angle light scattering (MALS) was performed at the Centre of Biomolecular Drug Research (BMWZ), Hannover in cooperation with Luca Codutti. First, purified protein was separated using SEC (Äkta Pure, GE Healthcare) with a Superdex 200 Increase 10/300 GL column (GE Healthcare) and 0.5 ml/min flow rate. Subsequently, eluted proteins were analyzed by the on-line miniDAWN TREOS MALS detector (Wyatt Technologies), which contained detectors at three angles, and by the on-line Optilab T-rEX differential refractometer (Wyatt Technologies) that was used to measure the effective complex concentration by assuming a standard protein RI increment value of 0.185 ml/g. Finally, the molecular weight was calculated from MALS and RI signals using the software ASTRA 6 (Wyatt Technologies).

6.8.10 Electrophoretic mobility shift assay

Protein-DNA interactions were studied in electrophoretic mobility shift assays (EMSA). DNA fragments (EMSA probes) were PCR amplified from *S.* Typhimurium LT2 genomic DNA with following primer pairs: 455/456 for *gyrA*, 468/469 for P_{flhDC}, 464/465 for $P1_{flhDC}$, 462/463 for $P4/6_{flhDC}$, 460/461 for $P5_{flhDC}$, 470/471 for $P5'_{flhDC}$, and 458/459 for *flhDC* coding. Positions of the *flhDC* promoter fragments relative to the *flhD* start codon are illustrated schematically in Fig. 2.17 and Fig. 3.4 and are as follows: P_{flhDC} (-560 to -90), $P1_{flhDC}$ (-271 to -71), $P4/6_{flhDC}$ (-431 to -231), $P5_{flhDC}$ (-588 to -388), $P5'_{flhDC}$ (-688 to -462), *flhDC* coding (+403 to +672). A 20 bp overhang in the 5'-region of forward primers allowed labeling of EMSA probes with 5'-biotin in a subsequent PCR using the 5'-biotin primer 457 if needed. Binding reactions were generally performed for 20 min at room temperature in binding buffer (10 mM Tris, 50 mM KCl, 1 mM DTT, pH 7.5). Afterwards, samples were mixed with 6x loading dye (2.5 g/l bromophenol blue, 30 % glycerol) and separated on a native 7 % TBE (90 mM Tris, 90 mM boric acid, 20 mM EDTA, pH 8.3) polyacrylamide gel by gel electrophoresis in 0.5x TBE buffer. DNA was visualized by ethidium bromide staining (see Chapter 6.7.3) or using the LightShift® Chemiluminescent

EMSA kit (Thermo Scientific). For ethidium bromide staining, 100 ng EMSA probes with 100 ng *gyrA* as competitor DNA and increasing amounts of purified protein were used. For analyses with the EMSA kit, 0.01 pmol 5'-biotin labeled EMSA probes with 50 ng/µl poly-(dI-dC) competitor DNA (Sigma) were used with increasing amounts of purified protein. The highest protein concentration was supplemented with a 250x molar excess of the respective unlabeled EMSA probe in order to determine binding specificity. After separation on polyacrylamide gels, samples were transferred on Biodyne™ B nylon membranes (Thermo Scientific) in pre-cooled 0.5x TBE buffer for 30 min at 380 mA constant using a wet-blotting tank system (Bio-Rad). After UV-crosslinking (Stratagene), DNA was visualized using the Chemiluminescence Nucleic Acid Detection Module (Thermo Scientific) according to the manufacturer's instructions and a ChemiDoc™ XRS+ documentation system (Bio-Rad).

6.8.11 DNaseI footprinting

Protein-DNA interaction sites were determined more precisely with DNaseI footprinting. DNA fragments were PCR-amplified from *S.* Typhimurium LT2 genomic DNA with 5'-DIG labeled primers resulting in the $P1_{flhDC}$ EMSA probe DIG labeled on the coding strand (primers 675/465) and a part of the $P5'_{flhDC}$ EMSA probe DIG labeled on the non-coding strand (primers 470/582; -688 to -388 relative to the *flhD* start site). Binding reactions were performed as described above (see Chapter 6.8.10) with 100 ng DIG-labeled DNA fragments instead and increasing amounts of purified protein, followed by treatment with a suitable dilution of DNaseI (Applichem or Roche). After 20 sec incubation, the reaction was stopped with 50 µl stop solution (15 mM EDTA, 10 µg/ml yeast tRNA (Invitrogen)), and DNA was recovered using phenol-chloroform extraction and ethanol precipitation. The USB® Thermo Sequenase™ Cycle Sequencing Kit (Affimetrix) was used for sequencing reactions according to the manufacturer's instructions with P_{flhDC} as template and the DIG-labeled primer. Samples were resuspended in 5 µl blue stop solution (Sequencing Kit) and separated on a 6 % polyacrylamide sequencing gel (1x TBE, 7 M urea) in 0.5x TBE buffer for at least 1.5 h at 60 W. Samples were transferred on a Nytran N nylon membrane (GE Healthcare) by capillary blotting, UV-crosslinked (Stratagene), and DNA was visualized using CDP-*Star* (Roche) and the anti-DIG-alkaline phosphatase antibody (Fab fragments, Roche) according to the manufacturer's instructions with X-ray film development.

6.8.12 Microscale thermophoresis

Binding affinities between proteins and the *flhDC* promoter were determined using microscale thermophoresis (MST). A *flhDC* promoter fragment (-204 to -174 relative to the *flhD* start site) was 5'-Cy5-labeled on the coding strand by annealing a 5'-Cy5 labeled primer with a complementary primer (primers 2029/1853) in duplex buffer (100 mM potassium acetate, 30 mM HEPES, pH 7.5). Purified proteins were centrifuged 10 min at 20 000 x*g* in order to remove potential aggregates. Binding reactions were performed as described above with 100 nM 5'-Cy5 labeled DNA and 1:2 serial dilutions of purified protein with binding buffer instead. After loading into standard capillaries, fluorescence intensities were measured using a Monolith NT.115 MST instrument (Nanotemper Technologies) with 15 % LED and 20 % MST power. Binding-specific fluorescence changes were confirmed by determining fluorescence intensities under denaturing conditions (SD-test). Therefore, samples were mixed with 2x SD mix buffer (4 % SDS, 40 mM DTT), incubated 5 min at 95 °C and fluorescence intensities were measured in standard capillaries as described above. The software MO.Affinity Analysis V2.1.2 (Nanotemper Technologies) was used to calculate dissociation constants (K_D) from fluorescence changes as described before (Baaske *et al.*, 2010). Additionally, MST samples were separated by native PAGE as described above (see Chapter 6.8.10), and DNA was visualized using a Typhoon™ FLA900 Bioscanner (GE Healthcare).

References

Abby, S.S., and Rocha, E.P.C. (2012) The non-flagellar type III secretion system evolved from the bacterial flagellum and diversified into host-cell adapted systems. *PLoS Genet* **8**: e1002983.

Achouri, S., Wright, J.A., Evans, L., Macleod, C., Fraser, G., Cicuta, P., and Bryant, C.E. (2015) The frequency and duration of *Salmonella*-macrophage adhesion events determines infection efficiency. *Philos Trans R Soc Lond B Biol Sci* **370**: 20140033.

Ackermann, M. (2015) A functional perspective on phenotypic heterogeneity in microorganisms. *Nat Rev Microbiol* **13**: 497–508.

Ackermann, M., Stecher, B., Freed, N.E., Songhet, P., Hardt, W.-D., and Doebeli, M. (2008) Self-destructive cooperation mediated by phenotypic noise. *Nature* **454**: 987–990.

Adler, J., and Templeton, B. (1967) The effect of environmental conditions on the motility of *Escherichia coli*. *J Gen Microbiol* **46**: 175–184.

Akbar, S., Schechter, L.M., Lostroh, C.P., and Lee, C.A. (2003) AraC/XylS family members, HilD and HilC, directly activate virulence gene expression independently of HilA in *Salmonella typhimurium*. *Mol Microbiol* **47**: 715–728.

Aldridge, C., Poonchareon, K., Saini, S., Ewen, T., Soloyva, A., Rao, C.V., Imada, K., Minamino, T., and Aldridge, P.D. (2010) The interaction dynamics of a negative feedback loop regulates flagellar number in *Salmonella enterica* serovar Typhimurium. *Mol Microbiol* **78**: 1416–1430.

Aldridge, P., Karlinsey, J., and Hughes, K.T. (2003) The type III secretion chaperone FlgN regulates flagellar assembly via a negative feedback loop containing its chaperone substrates FlgK and FlgL. *Mol Microbiol* **49**: 1333–1345.

Aldridge, P., Karlinsey, J.E., Becker, E., Chevance, F.F.V., and Hughes, K.T. (2006a) Flk prevents premature secretion of the anti-σ factor FlgM into the periplasm. *Mol Microbiol* **60**: 630–643.

Aldridge, P.D., Wu, C., Gnerer, J., Karlinsey, J.E., Hughes, K.T., and Sachs, M.S. (2006b) Regulatory protein that inhibits both synthesis and use of the target protein controls flagellar phase variation in *Salmonella enterica*. *Proc Natl Acad Sci USA* **103**: 11340–11345.

Andersen, J.B., Sternberg, C., Poulsen, L.K., Bjorn, S.P., Givskov, M., and Molin, S. (1998) New unstable variants of green fluorescent protein for studies of transient gene expression in bacteria. *Appl Environ Microbiol* **64**: 2240–2246.

Andréasson, C., Fiaux, J., Rampelt, H., Mayer, M.P., and Bukau, B. (2008) Hsp110 is a nucleotide-activated exchange factor for Hsp70. *J Biol Chem* **283**: 8877–8884.

Angeli, D., Ferrell, J.E., and Sontag, E.D. (2004) Detection of multistability, bifurcations, and hysteresis in a large class of biological positive-feedback systems. *Proc Natl Acad Sci USA* **101**: 1822–1827.

Arnoldini, M., Vizcarra, I.A., Pena-Miller, R., Stocker, N., Diard, M., Vogel, V., Beardmore, R.E., Hardt, W.-D., and Ackermann, M. (2014) Bistable expression of virulence genes in *Salmonella* leads to the formation of an antibiotic-tolerant subpopulation. *PLoS Biol* **12**: e1001928.

Arricau, N., Hermant, D., Waxin, H., Ecobichon, C., Duffey, P.S., and Popoff, M.Y. (1998) The RcsB-RcsC regulatory system of *Salmonella typhi* differentially modulates the expression of invasion proteins, flagellin and Vi antigen in response to osmolarity. *Mol Microbiol* **29**: 835–850.

Avery, S.V. (2006) Microbial cell individuality and the underlying sources of heterogeneity. *Nat Rev Microbiol* **4**: 577–587.

Baaske, P., Wienken, C.J., Reineck, P., Duhr, S., and Braun, D. (2010) Optical thermophoresis for quantifying the buffer dependence of aptamer binding. *Angew Chem Int Ed Engl* **49**: 2238–2241.

Bajaj, V., Hwang, C., and Lee, C.A. (1995) *hilA* is a novel *ompR*/*toxR* family member that activates the expression of *Salmonella typhimurium* invasion genes. *Mol Microbiol* **18**: 715–727.

Bajaj, V., Lucas, R.L., Hwang, C., and Lee, C.A. (1996) Co-ordinate regulation of *Salmonella typhimurium* invasion genes by environmental and regulatory factors is mediated by control of *hilA* expression. *Mol Microbiol* **22**: 703–714.

Balaban, N.Q. (2004) Bacterial persistence as a phenotypic switch. *Science* **305**: 1622–1625.

Baxter, M.A., and Jones, B.D. (2005) The *fimYZ* genes regulate *Salmonella enterica* serovar Typhimurium invasion in addition to type 1 fimbrial expression and bacterial motility. *Infect Immun* **73**: 1377–1385.

Baxter, M.A., and Jones, B.D. (2015) Two-component regulators control *hilA* expression by controlling *fimZ* and *hilE* expression within *Salmonella enterica* serovar Typhimurium. *Infect Immun* **83**: 978–985.

Baxter, M.A., Fahlen, T.F., Wilson, R.L., and Jones, B.D. (2003) HilE interacts with HilD and negatively regulates *hilA* transcription and expression of the *Salmonella enterica* serovar Typhimurium invasive phenotype. *Infect Immun* **71**: 1295–1305.

Bäumler, A.J., Tsolis, R.M., and Heffron, F. (1997) Fimbrial adhesins of *Salmonella typhimurium*. Role in bacterial interactions with epithelial cells. *Adv Exp Med Biol* **412**: 149–158.

Berg, H.C. (2003) The rotary motor of bacterial flagella. *Annu Rev Biochem* **72**: 19–54.

Blair, D.F. (2006) Fine structure of a fine machine. *J Bacteriol* **188**: 7033–7035.

Blocker, A., Komoriya, K., and Aizawa, S.-I. (2003) Type III secretion systems and bacterial flagella: insights into their function from structural similarities. *Proc Natl Acad Sci USA* **100**: 3027–3030.

Boddicker, J.D., Knosp, B.M., and Jones, B.D. (2003) Transcription of the *Salmonella* invasion gene activator, *hilA*, requires HilD activation in the absence of negative regulators. *J Bacteriol* **185**: 525–533.

Brehm-Stecher, B.F., and Johnson, E.A. (2004) Single-cell microbiology: tools, technologies, and applications. *Microbiol Mol Biol Rev* **68**: 538–59.

Bustamante, V.H., Martínez, L.C., Santana, F.J., Knodler, L.A., Steele-Mortimer, O., and Puente, J.L. (2008) HilD-mediated transcriptional cross-talk between SPI-1 and SPI-2. *Proc Natl Acad Sci USA* **105**: 14591–14596.

Campoy, S., Jara, M., Busquets, N., de Rozas, A.M.P., Badiola, I., and Barbé, J. (2002) Intracellular cyclic AMP concentration is decreased in *Salmonella typhimurium fur* mutants. *Microbiology* **148**: 1039–1048.

Cano, D.A., Domínguez-Bernal, G., Tierrez, A., García-del Portillo, F., and Casadesús, J. (2002) Regulation of capsule synthesis and cell motility in *Salmonella enterica* by the essential gene *igaA*. *Genetics* **162**: 1513–1523.

Casadesús, J., and Low, D.A. (2013) Programmed heterogeneity: epigenetic mechanisms in bacteria. *J Biol Chem* **288**: 13929–13935.

Castanié-Cornet, M.-P., Cam, K., Bastiat, B., Cros, A., Bordes, P., and Gutierrez, C. (2010) Acid stress response in *Escherichia coli*: mechanism of regulation of *gadA* transcription by RcsB and GadE. *Nucleic Acids Res* **38**: 3546–3554.

Chadsey, M.S., Karlinsey, J.E., and Hughes, K.T. (1998) The flagellar anti-sigma factor FlgM actively dissociates *Salmonella typhimurium* σ^{28} RNA polymerase holoenzyme. *Genes Dev* **12**: 3123–3136.

Chen, H.-M., Wang, Y., Su, L.-H., and Chiu, C.-H. (2013) Nontyphoid *Salmonella* infection: microbiology, clinical features, and antimicrobial therapy. *Pediatr Neonatol* **54**: 147–152.

Cherepanov, P.P., and Wackernagel, W. (1995) Gene disruption in *Escherichia coli*: Tc^R and Km^R cassettes with the option of Flp-catalyzed excision of the antibiotic-resistance determinant. *Gene* **158**: 9–14.

Chessa, D., Dorsey, C.W., Winter, M., and Bäumler, A.J. (2008) Binding specificity of *Salmonella* plasmid-encoded fimbriae assessed by glycomics. *J Biol Chem* **283**: 8118–8124.

Chessa, D., Winter, M.G., Jakomin, M., and Bäumler, A.J. (2009) *Salmonella enterica* serotype Typhimurium Std fimbriae bind terminal α(1,2)fucose residues in the cecal mucosa. *Mol Microbiol* **71**: 864–875.

Chevance, F.F., and Hughes, K.T. (2008) Coordinating assembly of a bacterial macromolecular machine. *Nat Rev Microbiol* **6**: 455–465.

Chilcott, G.S., and Hughes, K.T. (2000) Coupling of flagellar gene expression to flagellar assembly in *Salmonella enterica* serovar Typhimurium and *Escherichia coli*. *Microbiol Mol Biol Rev* **64**: 694–708.

Chubiz, J.E.C., Golubeva, Y.A., Lin, D., Miller, L.D., and Slauch, J.M. (2010) FliZ regulates expression of the *Salmonella* pathogenicity island 1 invasion locus by controlling HilD protein activity in *Salmonella enterica* serovar Typhimurium. *J Bacteriol* **192**: 6261–6270.

Clark, L., Perrett, C.A., Malt, L., Harward, C., Humphrey, S., Jepson, K.A., Martinez-Argudo, I., Carney, L.J., La Ragione, R.M., Humphrey, T.J., and Jepson, M.A. (2011) Differences in *Salmonella enterica* serovar Typhimurium strain invasiveness are associated with heterogeneity in SPI-1 gene expression. *Microbiology* **157**: 2072–2083.

Clegg, S., and Hughes, K.T. (2002) FimZ is a molecular link between sticking and swimming in *Salmonella enterica* serovar Typhimurium. *J Bacteriol* **184**: 1209–1213.

Cordero-Alba, M., Bernal-Bayard, J., and Ramos-Morales, F. (2012) SrfJ, a *Salmonella* type III secretion system effector regulated by PhoP, RcsB, and IolR. *J Bacteriol* **194**: 4226–36.

Corpet, F. (1988) Multiple sequence alignment with hierarchical clustering. *Nucleic Acids Res* **16**: 10881–10890.

Cox, R.S., Dunlop, M.J., and Elowitz, M.B. (2010) A synthetic three-color scaffold for monitoring genetic regulation and noise. *J Biol Eng* **4**: 10.

Crawford, R.W., Reeve, K.E., and Gunn, J.S. (2010) Flagellated but not hyperfimbriated *Salmonella enterica* serovar Typhimurium attaches to and forms biofilms on cholesterol-coated surfaces. *J Bacteriol* **192**: 2981–2990.

Cummings, L.A., Barrett, S.L.R., Wilkerson, W.D., Fellnerova, I., and Cookson, B.T. (2005) FliC-specific $CD4^+$ T cell responses are restricted by bacterial regulation of antigen expression. *J Immunol* **174**: 7929–7938.

Cummings, L.A., Wilkerson, W.D., Bergsbaken, T., and Cookson, B.T. (2006) *In vivo*, *fliC* expression by *Salmonella enterica* serovar Typhimurium is heterogeneous, regulated by ClpX, and anatomically restricted. *Mol Microbiol* **61**: 795–809.

Darwin, K.H., and Miller, V.L. (1999) InvF is required for expression of genes encoding proteins secreted by the SPI1 type III secretion apparatus in *Salmonella typhimurium*. *J Bacteriol* **181**: 4949–4954.

Darwin, K.H., and Miller, V.L. (2000) The putative invasion protein chaperone SicA acts together with InvF to activate the expression of *Salmonella typhimurium* virulence genes. *Mol Microbiol* **35**: 949–960.

de Jong, H.K., Parry, C.M., van der Poll, T., and Wiersinga, W.J. (2012) Host-pathogen interaction in invasive Salmonellosis. *PLoS Pathog* **8**: e1002933.

Deditius, J.A. (2013) Effect of the *Salmonella* virulence master regulator HilD on flagellar gene expression and motility. *Master's thesis*, Technische Universität Carolo-Wilhemina Braunschweig.

Deiwick, J., Salcedo, S.P., Boucrot, E., Gilliland, S.M., Henry, T., Petermann, N., Waterman, S.R, Gorvel, J.-P., Holden, D.W., and Méresse, S. (2006) The translocated *Salmonella* effector proteins SseF and SseG interact and are required to establish an intracellular replication niche. *Infect Immun* **74**: 6965–6972.

Delgado, M.A., Mouslim, C., and Groisman, E.A. (2006) The PmrA/PmrB and RcsC/YojN/RcsB systems control expression of the *Salmonella* O-antigen chain length determinant. *Mol Microbiol* **60**: 39–50.

Detweiler, C.S., Monack, D.M., Brodsky, I.E., Mathew, H., and Falkow, S. (2003) *virK*, *somA* and *rcsC* are important for systemic *Salmonella enterica* serovar Typhimurium infection and cationic peptide resistance. *Mol Microbiol* **48**: 385–400.

Diard, M., Garcia, V., Maier, L., Remus-Emsermann, M.N.P., Regoes, R.R., Ackermann, M., and Hardt, W.-D. (2013) Stabilization of cooperative virulence by the expression of an avirulent phenotype. *Nature* **494**: 353–356.

Diepold, A., and Wagner, S. (2014) Assembly of the bacterial type III secretion machinery. *FEMS Microbiol Rev* **38**: 802–822.

Dmitrova, M., Younès-Cauet, G., Oertel-Buchheit, P., Porte, D., Schnarr, M., and Granger-Schnarr, M. (1998) A new LexA-based genetic system for monitoring and analyzing protein heterodimerization in *Escherichia coli*. *Mol Gen Genet* **257**: 205–212.

Dorsey, C.W., Laarakker, M.C., Humphries, A.D., Weening, E.H., and Bäumler, A.J. (2005) *Salmonella enterica* serotype Typhimurium MisL is an intestinal colonization factor that binds fibronectin. *Mol Microbiol* **57**: 196–211.

Dove, S.L., and Hochschild, A. (2004) A bacterial two-hybrid system based on transcription activation. *Methods Mol Biol* **261**: 231–246.

Drecktrah, D., Levine-Wilkinson, S., Dam, T., Winfree, S., Knodler, L.A., Schroer, T.A., and Steele-Mortimer, O. (2008) Dynamic behavior of *Salmonella*-induced membrane tubules in epithelial cells. *Traffic* **9**: 2117–2129.

Duan, Q., Zhou, M., Zhu, L., and Zhu, G. (2013) Flagella and bacterial pathogenicity. *J Basic Microbiol* **53**: 1–8.

Dubnau, D., and Losick, R. (2006) Bistability in bacteria. *Mol Microbiol* **61**: 564–572.

Eichelberg, K., and Galán, J.E. (1999) Differential regulation of *Salmonella typhimurium* type III secreted proteins by pathogenicity island 1 (SPI-1)-encoded transcriptional activators InvF and hilA. *Infect Immun* **67**: 4099–4105.

Eisenbach, M. (1996) Control of bacterial chemotaxis. *Mol Microbiol* **20**: 903–910.

Ellermeier, C.D., and Slauch, J.M. (2003) RtsA and RtsB coordinately regulate expression of the invasion and flagellar genes in *Salmonella enterica* serovar Typhimurium. *J Bacteriol* **185**: 5096–5108.

Ellermeier, C.D., Ellermeier, J.R., and Slauch, J.M. (2005) HilD, HilC and RtsA constitute a feed forward loop that controls expression of the SPI1 type three secretion system regulator *hilA* in *Salmonella enterica* serovar Typhimurium. *Mol Microbiol* **57**: 691–705.

Elowitz, M.B. (2002) Stochastic gene expression in a single cell. *Science* **297**: 1183–1186.

Erhardt, M. (2016) Strategies to block bacterial pathogenesis by interference with motility and chemotaxis. *Current Topics in Microbiology and Immunology*. SpringerLink, pp. 1–21.

Erhardt, M., and Dersch, P. (2015) Regulatory principles governing *Salmonella* and *Yersinia* virulence. *Front Microbiol* **6**: 949.

Erhardt, M., and Hughes, K.T. (2010) C-ring requirement in flagellar type III secretion is bypassed by FlhDC upregulation. *Mol Microbiol* **75**: 376–393.

Erhardt, M., Hirano, T., Su, Y., Paul, K., Wee, D.H., Mizuno, S., Aizawa, S.-I., and Hughes, K.T. (2010a) The role of the FliK molecular ruler in hook-length control in *Salmonella enterica*. *Mol Microbiol* **75**: 1272–1284.

Erhardt, M., Mertens, M.E., Fabiani, F.D., and Hughes, K.T. (2014) ATPase-independent type-III protein secretion in *Salmonella enterica*. *PLoS Genet* **10**: e1004800.

Erhardt, M., Singer, H.M., Wee, D.H., Keener, J.P., and Hughes, K.T. (2011) An infrequent molecular ruler controls flagellar hook length in *Salmonella enterica*. *EMBO J* **30**: 2948–2961.

Eriksson, S., Lucchini, S., Thompson, A., Rhen, M., and Hinton, J.C.D. (2003) Unravelling the biology of macrophage infection by gene expression profiling of intracellular *Salmonella enterica*. *Mol Microbiol* **47**: 103–118.

Espinosa, E., and Casadesús, J. (2014) Regulation of *Salmonella enterica* pathogenicity island 1 (SPI-1) by the LysR-type regulator LeuO. *Mol Microbiol* **91**: 1057–1069.

Farizano, J.V., Torres, M.A., Pescaretti, M. de L.M., and Delgado, M.A. (2014) The RcsCDB regulatory system plays a crucial role in the protection of *Salmonella enterica* serovar Typhimurium against oxidative stress. *Microbiology* **160**: 2190–2199.

Farris, C., Sanowar, S., Bader, M.W., Pfuetzner, R., and Miller, S.I. (2010) Antimicrobial peptides activate the Rcs regulon through the outer membrane lipoprotein RcsF. *J Bacteriol* **192**: 4894–4903.

Fass, E., and A Groisman, E. (2009) Control of *Salmonella* pathogenicity island-2 gene expression. *Curr Opin Microbiol* **12**: 199–204.

Fàbrega, A., and Vila, J. (2013) *Salmonella enterica* serovar Typhimurium skills to succeed in the host: virulence and regulation. *Clin Microbiol Rev* **26**: 308–341.

Ferrell, J.E. (2002) Self-perpetuating states in signal transduction: positive feedback, double-negative feedback and bistability. *Curr Opin Chem Biol* **6**: 140–148.

Foster, J.W., and Hall, H.K. (1990) Adaptive acidification tolerance response of *Salmonella typhimurium*. *J Bacteriol* **172**: 771–778.

Francez-Charlot, A., Laugel, B., Van Gemert, A., Dubarry, N., Wiorowski, F., Castanié-Cornet, M.-P., Gutierrez, C., and Cam, K. (2003) RcsCDB His-Asp phosphorelay system negatively regulates the *flhDC* operon in *Escherichia coli*. *Mol Microbiol* **49**: 823–832.

Franchi, L., Amer, A., Body-Malapel, M., Kanneganti, T.-D., Ozören, N., Jagirdar, R., Inohara, N., Vandenabeele, P., Bertin, J., Coyle, A., Grant, E.P., and Núnez, G. (2006) Cytosolic flagellin requires Ipaf for activation of caspase-1 and interleukin 1 beta in *Salmonella*-infected macrophages. *Nat Immunol* **7**: 576–582.

Francis, C.L., Ryan, T.A., Jones, B.D., Smith, S.J., and Falkow, S. (1993) Ruffles induced by *Salmonella* and other stimuli direct macropinocytosis of bacteria. *Nature* **364**: 639–642.

Freed, N.E., Silander, O.K., Stecher, B., Böhm, A., Hardt, W.-D., and Ackermann, M. (2008) A simple screen to identify promoters conferring high levels of phenotypic noise. *PLoS Genet* **4**: e1000307.

Friebel, A., Ilchmann, H., Aepfelbacher, M., Ehrbar, K., Machleidt, W., and Hardt, W.-D. (2001) SopE and SopE2 from *Salmonella typhimurium* activate different sets of RhoGTPases of the host cell. *J Biol Chem* **276**: 34035–34040.

Fu, Y., and Galán, J.E. (1999) A *Salmonella* protein antagonizes Rac-1 and Cdc42 to mediate host-cell recovery after bacterial invasion. *Nature* **401**: 293–297.

Gallegos, M.T., Schleif, R., Bairoch, A., Hofmann, K., and Ramos, J.L. (1997) AraC/XylS family of transcriptional regulators. *Microbiol Mol Biol Rev* **61**: 393–410.

García-Calderón, C.B., Casadesús, J., and Ramos-Morales, F. (2007) Rcs and PhoPQ regulatory overlap in the control of *Salmonella enterica* virulence. *J Bacteriol* **189**: 6635–6644.

García-Calderón, C.B., García-Quintanilla, M., Casadesús, J., and Ramos-Morales, F. (2005) Virulence attenuation in *Salmonella enterica rcsC* mutants with constitutive activation of the Rcs system. *Microbiology* **151**: 579–588.

Garmendia, J., Beuzón, C.R., Ruiz-Albert, J., and Holden, D.W. (2003) The roles of SsrA-SsrB and OmpR-EnvZ in the regulation of genes encoding the *Salmonella typhimurium* SPI-2 type III secretion system. *Microbiology* **149**: 2385–2396.

Golubeva, Y.A., Sadik, A.Y., Ellermeier, J.R., and Slauch, J.M. (2012) Integrating global regulatory input into the *Salmonella* pathogenicity island 1 type III secretion system. *Genetics* **190**: 79–90.

Grantcharova, N., Peters, V., Monteiro, C., Zakikhany, K., and Römling, U. (2010) Bistable expression of CsgD in biofilm development of *Salmonella enterica* serovar Typhimurium. *J Bacteriol* **192**: 456–466.

Graumann, P.L. (2006) Different genetic programmes within identical bacteria under identical conditions: the phenomenon of bistability greatly modifies our view on bacterial populations. *Mol Microbiol* **61**: 560–563.

Grote, J., Krysciak, D., and Streit, W.R. (2015) Phenotypic heterogeneity, a phenomenon that may explain why quorum sensing does not always result in truly homogeneous cell behavior. *Appl Environ Microbiol* **81**: 5280–5289.

Guiney, D.G. (2005) The role of host cell death in *Salmonella* infections. *Curr Top Microbiol Immunol* **289**: 131–150.

Gupte, G., Woodward, C., and Stout, V. (1997) Isolation and characterization of *rcsB* mutations that affect colanic acid capsule synthesis in *Escherichia coli* K-12. *J Bacteriol* **179**: 4328–4335.

Haraga, A., Ohlson, M.B., and Miller, S.I. (2008) Salmonellae interplay with host cells. *Nat Rev Microbiol* **6**: 53–66.

Hautefort, I., Thompson, A., Eriksson-Ygberg, S., Parker, M.L., Lucchini, S., Danino, V., Bongaerts, R.J.M., Ahmad, N., Rhen, M., and Hinton, J.C.D. (2008) During infection of epithelial cells *Salmonella enterica* serovar Typhimurium undergoes a time-dependent transcriptional adaptation that results in simultaneous expression of three type 3 secretion systems. *Cell Microbiol* **10**: 958–984.

Hayashi, F., Smith, K.D., Ozinsky, A., Hawn, T.R., Yi, E.C., Goodlett, D.R., Eng, J.K., Akira, S., Underhill, D.M., and Aderem, A. (2001) The innate immune response to bacterial flagellin is mediated by Toll-like receptor 5. *Nature* **410**: 1099–1103.

Hayward, R.D., and Koronakis, V. (1999) Direct nucleation and bundling of actin by the SipC protein of invasive *Salmonella*. *EMBO J* **18**: 4926–4934.

Henikoff, S., Wallace, J.C., and Brown, J.P. (1990) Finding protein similarities with nucleotide sequence databases. *Meth Enzymol* **183**: 111–132.

Henrichsen, J. (1972) Bacterial surface translocation: a survey and a classification. *Bacteriol Rev* **36**: 478–503.

Herbst, K. (2011) The temperature- and growth-dependent regulation of the global virulence regulator RovA from *Yersinia pseudotuberculosis*. Technische Universität Carolo-Wilhelmina Braunschweig.

Hobbie, S., Chen, L.M., Davis, R.J., and Galán, J.E. (1997) Involvement of mitogen-activated protein kinase pathways in the nuclear responses and cytokine production induced by *Salmonella typhimurium* in cultured intestinal epithelial cells. *J Immunol* **159**: 5550–5559.

Hochschild, A., and Dove, S.L. (1998) Protein-protein contacts that activate and repress prokaryotic transcription. *Cell* **92**: 597–600.

Hohmann, E.L. (2001) Nontyphoidal Salmonellosis. *Clin Infect Dis* **32**: 263–269.

Hoiseth, S.K., and Stocker, B.A. (1981) Aromatic-dependent *Salmonella typhimurium* are non-virulent and effective as live vaccines. *Nature* **291**: 238–239.

Huang, Y.-H., Ferrières, L., and Clarke, D.J. (2006) The role of the Rcs phosphorelay in Enterobacteriaceae. *Res Microbiol* **157**: 206–212.

Hung, C.-C., Garner, C.D., Slauch, J.M., Dwyer, Z.W., Lawhon, S.D., Frye, J.G., McClelland, M., Ahmer, B.M.M., and Altier, C. (2013) The intestinal fatty acid propionate inhibits *Salmonella* invasion through the post-translational control of HilD. *Mol Microbiol* **87**: 1045–1060.

Iino, T. (1969) Genetics and chemistry of bacterial flagella. *Bacteriol Rev* **33**: 454–475.

Ikebe, T., Iyoda, S., and Kutsukake, K. (1999) Promoter analysis of the class 2 flagellar operons of *Salmonella*. *Genes Genet Syst* **74**: 179–183.

Iyoda, S., Kamidoi, T., Hirose, K., Kutsukake, K., and Watanabe, H. (2001) A flagellar gene *fliZ* regulates the expression of invasion genes and virulence phenotype in *Salmonella enterica* serovar Typhimurium. *Microb Pathog* **30**: 81–90.

Jain, S., and Chen, J. (2007) Attachment and biofilm formation by various serotypes of *Salmonella* as influenced by cellulose production and thin aggregative fimbriae biosynthesis. *J Food Prot* **70**: 2473–2479.

Johansson, C., Ingman, M., and Jo Wick, M. (2006) Elevated neutrophil, macrophage and dendritic cell numbers characterize immune cell populations in mice chronically infected with *Salmonella*. *Microb Pathog* **41**: 49–58.

Johnson, R.C., and Simon, M.I. (1985) Hin-mediated site-specific recombination requires two 26 bp recombination sites and a 60 bp recombinational enhancer. *Cell* **41**: 781–791.

Jonas, K., Edwards, A.N., Ahmad, I., Romeo, T., Römling, U., and Melefors, O. (2010) Complex regulatory network encompassing the Csr, c-di-GMP and motility systems of *Salmonella* Typhimurium. *Environ Microbiol* **12**: 524–540.

Jones, B.D., Ghori, N., and Falkow, S. (1994) *Salmonella typhimurium* initiates murine infection by penetrating and destroying the specialized epithelial M cells of the Peyer's patches. *J Exp Med* **180**: 15–23.

Jones, B.D., Lee, C.A., and Falkow, S. (1992) Invasion by *Salmonella typhimurium* is affected by the direction of flagellar rotation. *Infect Immun* **60**: 2475–2480.

Jones, C.J., and Macnab, R.M. (1990) Flagellar assembly in *Salmonella typhimurium*: analysis with temperature-sensitive mutants. *J Bacteriol* **172**: 1327–1339.

Jones, C.J., Homma, M., and Macnab, R.M. (1989) L-, P-, and M-ring proteins of the flagellar basal body of *Salmonella typhimurium*: gene sequences and deduced protein sequences. *J Bacteriol* **171**: 3890–3900.

Kage, H., Takaya, A., Ohya, M., and Yamamoto, T. (2008) Coordinated regulation of expression of *Salmonella* pathogenicity island 1 and flagellar type III secretion systems by ATP-dependent ClpXP protease. *J Bacteriol* **190**: 2470–2478.

Karlinsey, J.E. (2007) *λ*-Red genetic engineering in *Salmonella enterica* serovar Typhimurium. *Methods in Enzymology*. Elsevier Inc, pp. 199–209.

Karlinsey, J.E., Tanaka, S., Bettenworth, V., Yamaguchi, S., Boos, W., Aizawa, S.I., and Hughes, K.T. (2000) Completion of the hook-basal body complex of the *Salmonella typhimurium* flagellum is coupled to FlgM secretion and *fliC* transcription. *Mol Microbiol* **37**: 1220–1231.

Kelly, A., Goldberg, M.D., Carroll, R.K., Danino, V., Hinton, J.C.D., and Dorman, C.J. (2004) A global role for Fis in the transcriptional control of metabolism and type III secretion in *Salmonella enterica* serovar Typhimurium. *Microbiology* **150**: 2037–2053.

Kelm, O., Kiecker, C., Geider, K., and Bernhard, F. (1997) Interaction of the regulator proteins RcsA and RcsB with the promoter of the operon for amylovoran biosynthesis in *Erwinia amylovora*. *Mol Gen Genet* **256**: 72–83.

Kim, T.-J., Young, B.M., and Young, G.M. (2008) Effect of flagellar mutations on *Yersinia enterocolitica* biofilm formation. *Appl Environ Microbiol* **74**: 5466–5474.

Kingsley, R.A., Santos, R.L., Keestra, A.M., Adams, L.G., and Bäumler, A.J. (2002) *Salmonella enterica* serotype Typhimurium ShdA is an outer membrane fibronectin-binding protein that is expressed in the intestine. *Mol Microbiol* **43**: 895–905.

Knodler, L.A., Vallance, B.A., Celli, J., Winfree, S., Hansen, B., Montero, M., and Steele-Mortimer, O. (2010) Dissemination of invasive *Salmonella* via bacterial-induced extrusion of mucosal epithelia. *Proc Natl Acad Sci USA* **107**: 17733–17738.

Koirala, S., Mears, P., Sim, M., Golding, I., Chemla, Y.R., Aldridge, P.D., and Rao, C.V. (2014) A nutrient-tunable bistable switch controls motility in *Salmonella enterica* serovar Typhimurium. *MBio* **5**: e01611-14.

Korhonen, T.K., Lounatmaa, K., Ranta, H., and Kuusi, N. (1980) Characterization of type 1 pili of *Salmonella typhimurium* LT2. *J Bacteriol* **144**: 800–805.

Krin, E., Danchin, A., and Soutourina, O. (2010) RcsB plays a central role in H-NS-dependent regulation of motility and acid stress resistance in *Escherichia coli*. *Res Microbiol* **161**: 363–371.

Kröger, C., Colgan, A., Srikumar, S., Händler, K., Sivasankaran, S.K., Hammarlöf, D.L., Canals, R., Grissom, J.E., Conway, T., Hokamp, K., and Hinton, J.C.D. (2013) An infection-relevant transcriptomic compendium for *Salmonella enterica* serovar Typhimurium. *Cell Host & microbe* **14**: 683–695.

Kröger, C., Dillon, S.C., Cameron, A.D.S., Papenfort, K., Sivasankaran, S.K., Hokamp, K., Chao, Y., Sittka, A., Hébrard, M., Händler, K., Colgan, A., Leekitcharoenphon, P., Landridge, G.C., Lohan, A.J., Loftus, B., Lucchini, S., Ussery, D.W., Dorman, C.J., Thomson, N.R., Vogel, J., and Hinton, J.C.D. (2012) The transcriptional landscape and small RNAs of *Salmonella enterica* serovar Typhimurium. *Proc Natl Acad Sci USA* **109**: E1277–86.

Kukkonen, M., Raunio, T., Virkola, R., Lähteenmäki, K., Mäkelä, P.H., Klemm, P., Clegg, S., and Korhonen, T.K. (1993) Basement membrane carbohydrate as a target for bacterial adhesion: binding of type I fimbriae of *Salmonella enterica* and *Escherichia coli* to laminin. *Mol Microbiol* **7**: 229–237.

Kutsukake, K. (1994) Excretion of the anti-sigma factor through a flagellar substructure couples flagellar gene expression with flagellar assembly in *Salmonella typhimurium*. *Mol Gen Genet* **243**: 605–612.

Kutsukake, K. (1997) Autogenous and global control of the flagellar master operon, *flhD*, in *Salmonella typhimurium*. *Mol Gen Genet* **254**: 440–448.

Kutsukake, K., Minamino, T., and Yokoseki, T. (1994) Isolation and characterization of FliK-independent flagellation mutants from *Salmonella typhimurium*. *J Bacteriol* **176**: 7625–7629.

Kühne, C., Singer, H.M., Grabisch, E., Codutti, L., Carlomagno, T., Scrima, A., and Erhardt, M. (2016) RflM mediates target specificity of the RcsCDB phosphorelay system for transcriptional repression of flagellar synthesis in *Salmonella enterica*. *Mol Microbiol* **101**: 841-855.

Lai, M.A., Quarles, E.K., López-Yglesias, A.H., Zhao, X., Hajjar, A.M., and Smith, K.D. (2013) Innate immune detection of flagellin positively and negatively regulates *Salmonella* infection. *PLos ONE* **8**: e72047.

Lamprokostopoulou, A., Monteiro, C., Rhen, M., and Römling, U. (2010) Cyclic di-GMP signalling controls virulence properties of *Salmonella enterica* serovar Typhimurium at the mucosal lining. *Environ Microbiol* **12**: 40–53.

Latasa, C., García, B., Echeverz, M., Toledo-Arana, A., Valle, J., Campoy, S., García-del Portillo, F., Solano, C., and Lasa, I. (2012) *Salmonella* biofilm development depends on the phosphorylation status of RcsB. *J Bacteriol* **194**: 3708–22.

Lawhon, S.D., Frye, J.G., Suyemoto, M., Porwollik, S., McClelland, M., and Altier, C. (2003) Global regulation by CsrA in *Salmonella typhimurium*. *Mol Microbiol* **48**: 1633–1645.

Le Guyon, S., Simm, R., Rhen, M., and Römling, U. (2014) Dissecting the c-di-GMP signaling network regulating motility in *Salmonella enterica* serovar Typhimurium. *Environ Microbiol* **17**: 1310–1320.

Lehnen, D., Blumer, C., Polen, T., Wackwitz, B., Wendisch, V.F., and Unden, G. (2002) LrhA as a new transcriptional key regulator of flagella, motility and chemotaxis genes in *Escherichia coli*. *Mol Microbiol* **45**: 521–532.

Levine, J.H., Fontes, M.E., Dworkin, J., and Elowitz, M.B. (2012) Pulsed feedback defers cellular differentiation. *PLoS Biol* **10**: e1001252.

Levine, J.H., Lin, Y., and Elowitz, M.B. (2013) Functional roles of pulsing in genetic circuits. *Science* **342**: 1193–1200.

Lin, D., Rao, C.V., and Slauch, J.M. (2008) The *Salmonella* SPI1 type three secretion system responds to periplasmic disulfide bond status via the flagellar apparatus and the RcsCDB system. *J Bacteriol* **190**: 87–97.

Liu, X., and Matsumura, P. (1994) The FlhD/FlhC complex, a transcriptional activator of the *Escherichia coli* flagellar class II operons. *J Bacteriol* **176**: 7345–7351.

Locke, J.C.W., Young, J.W., Fontes, M., Hernández Jiménez, M.J., and Elowitz, M.B. (2011) Stochastic pulse regulation in bacterial stress response. *Science* **334**: 366–369.

López-Garrido, J., and Casadesús, J. (2010) Regulation of *Salmonella enterica* pathogenicity island 1 by DNA adenine methylation. *Genetics* **184**: 637–649.

López-Garrido, J., and Casadesús, J. (2012) Crosstalk between virulence loci: regulation of *Salmonella enterica* pathogenicity island 1 (SPI-1) by products of the *std* fimbrial operon. *PLos ONE* **7**: e30499.

Lucas, R.L., and Lee, C.A. (2001) Roles of *hilC* and *hilD* in regulation of *hilA* expression in *Salmonella enterica* serovar Typhimurium. *J Bacteriol* **183**: 2733–2745.

MacKenzie, K.D., Wang, Y., Shivak, D.J., Wong, C.S., Hoffman, L.J.L., Lam, S., Kröger, C., Cameron, A.D.S., Townsend, H.G.G., Köster, W., and White, A.P. (2015) Bistable expression of CsgD in *Salmonella* connects virulence to persistence. *Infect Immun* **83**: 2312–2326.

Macnab, R.M. (2003) How bacteria assemble flagella. *Annu Rev Microbiol* **57**: 77–100.

Macnab, R.M. (2004) Type III flagellar protein export and flagellar assembly. *Biochim Biophys Acta* **1694**: 207–217.

Majdalani, N., and Gottesman, S. (2005) The Rcs phosphorelay: a complex signal transduction system. *Annu Rev Microbiol* **59**: 379–405.

Mariscotti, J.F., and García-del Portillo, F. (2009) Genome expression analyses revealing the modulation of the *Salmonella* Rcs regulon by the attenuator IgaA. *J Bacteriol* **191**: 1855–1867.

Martin, R.G., Gillette, W.K., Rhee, S., and Rosner, J.L. (1999) Structural requirements for marbox function in transcriptional activation of *mar/sox/rob* regulon promoters in *Escherichia coli*: sequence, orientation and spatial relationship to the core promoter. *Mol Microbiol* **34**: 431–441.

Martinez, L.C., Yakhnin, H., Camacho, M.I., Georgellis, D., Babitzke, P., Puente, J.L., and Bustamante, V.H. (2011) Integration of a complex regulatory cascade involving the SirA/BarA and Csr global regulatory systems that controls expression of the *Salmonella* SPI-1 and SPI-2 virulence regulons through HilD. *Mol Microbiol* **80**: 1637–1656.

Martínez, L.C., Banda, M.M., Fernández-Mora, M., Santana, F.J., and Bustamante, V.H. (2014) HilD induces expression of *Salmonella* pathogenicity island 2 genes by displacing the global negative regulator H-NS from *ssrAB*. *J Bacteriol* **196**: 3746–3755.

McClelland, M., Sanderson, K.E., Spieth, J., Clifton, S.W., Latreille, P., Courtney, L., Porwollik, S., Ali, J., Dante, M., Du, F., Hou, S., Layman, D., Leonard, S., Nguyen, C., Scott, K., Holmes, A., Grewal, N., Mulvaney, E., Ryan, E., Sun, S., Florea, L., Miller, W., Stoneking, T., Nhan, M., Waterston, R., and Wilson, R.K. (2001) Complete genome sequence of *Salmonella enterica* serovar Typhimurium LT2. *Nature* **413**: 852–856.

Méresse, S., Unsworth, K.E., Habermann, A., Griffiths, G., Fang, F., Martínez-Lorenzo, M.J., Waterman, S.R., Gorvel, J.-P., and Holden, D.W. (2001) Remodelling of the actin cytoskeleton is essential for replication of intravacuolar *Salmonella*. *Cell Microbiol* **3**: 567–577.

Miller, J.H. (1972) Assay of β-galactosidase. *Experiments in Molecular Genetics*. Cold Spring Harbor Laboratory Press, Cold Spring Harbor, NY: 352–355.

Minamino, T., and Macnab, R.M. (2000) Domain structure of *Salmonella* FlhB, a flagellar export component responsible for substrate specificity switching. *J Bacteriol* **182**: 4906–4914.

Minamino, T., and Namba, K. (2008) Distinct roles of the FliI ATPase and proton motive force in bacterial flagellar protein export. *Nature* **451**: 485–488.

Misselwitz, B., Barrett, N., Kreibich, S., Vonaesch, P., Andritschke, D., Rout, S., Weidner, K., Sormaz, M., Songhet, P., Horvath, P., Chabria, M., Vogel, V., Spori, D.M., Jenny, P., and Hardt, W.-D. (2012) Near surface swimming of *Salmonella* Typhimurium explains target-site selection and cooperative invasion. *PLoS Pathog* **8**: e1002810.

Mouslim, C., and Groisman, E.A. (2003) Control of the *Salmonella ugd* gene by three two-component regulatory systems. *Mol Microbiol* **47**: 335–344.

Mouslim, C., and Hughes, K.T. (2014) The effect of cell growth phase on the regulatory cross-talk between flagellar and Spi1 virulence gene expression. *PLoS Pathog* **10**: e1003987.

Mouslim, C., Delgado, M., and Groisman, E.A. (2004) Activation of the RcsC/YojN/RcsB phosphorelay system attenuates *Salmonella* virulence. *Mol Microbiol* **54**: 386–395.

Mouslim, C., Latifi, T., and Groisman, E.A. (2003) Signal-dependent requirement for the co-activator protein RcsA in transcription of the RcsB-regulated *ugd* gene. *J Biol Chem* **278**: 50588–50595.

Nachin, L., Nannmark, U., and Nyström, T. (2005) Differential roles of the universal stress proteins of *Escherichia coli* in oxidative stress resistance, adhesion, and motility. *J Bacteriol* **187**: 6265–6272.

Ohnishi, K., Kutsukake, K., Suzuki, H., and Iino, T. (1990) Gene *fliA* encodes an alternative sigma factor specific for flagellar operons in *Salmonella typhimurium*. *Mol Gen Genet* **221**: 139–147.

Olekhnovich, I.N., and Kadner, R.J. (2002) DNA-binding activities of the HilC and HilD virulence regulatory proteins of *Salmonella enterica* serovar Typhimurium. *J Bacteriol* **184**: 4148–4160.

Olekhnovich, I.N., and Kadner, R.J. (2007) Role of nucleoid-associated proteins Hha and H-NS in expression of *Salmonella enterica* activators HilD, HilC, and RtsA required for cell invasion. *J Bacteriol* **189**: 6882–6890.

Ozbudak, E.M., Thattai, M., Kurtser, I., Grossman, A.D., and van Oudenaarden, A. (2002) Regulation of noise in the expression of a single gene. *Nat Genet* **31**: 69–73.

Pannen, D., Fabisch, M., Gausling, L., and Schnetz, K. (2016) Interaction of the RcsB response regulator with auxiliary transcription regulators in *Escherichia coli*. *J Biol Chem* **291**: 2357–2370.

Patel, J.C., and Galán, J.E. (2006) Differential activation and function of Rho GTPases during *Salmonella*-host cell interactions. *J Cell Biol* **175**: 453–463.

Paul, K., Erhardt, M., Hirano, T., Blair, D.F., and Hughes, K.T. (2008) Energy source of flagellar type III secretion. *Nature* **451**: 489–492.

Pescaretti, M. de L.M., Farizano, J.V., Morero, R., and Delgado, M.A. (2013) A novel insight on signal transduction mechanism of RcsCDB system in *Salmonella enterica* serovar Typhimurium. *PLos ONE* **8**: e72527.

Pfaffl, M.W. (2001) A new mathematical model for relative quantification in real-time RT-PCR. *Nucleic Acids Res* **29**: 2002–2007.

Ramsden, A.E., Holden, D.W., and Mota, L.J. (2007) Membrane dynamics and spatial distribution of *Salmonella*-containing vacuoles. *Trends Microbiol* **15**: 516–524.

Rappleye, C.A., and Roth, J.R. (1997) A Tn*10* derivative (T-POP) for isolation of insertions with conditional (tetracycline-dependent) phenotypes. *J Bacteriol* **179**: 5827–5834.

Rescigno, M., Urbano, M., Valzasina, B., Francolini, M., Rotta, G., Bonasio, R., Granucci, F., Kraehenbuhl, J.-P., and Ricciardi-Castagnoli, P. (2001) Dendritic cells express tight junction proteins and penetrate gut epithelial monolayers to sample bacteria. *Nat Immunol* **2**: 361–367.

Rhee, S., Martin, R.G., Rosner, J.L., and Davies, D.R. (1998) A novel DNA-binding motif in MarA: the first structure for an AraC family transcriptional activator. *Proc Natl Acad Sci USA* **95**: 10413–10418.

Robert Koch Institut: Infektionsepidemiologisches Jahrbuch für 2015, Berlin, 2016.

Rocco, C.J., Dennison, K.L., Klenchin, V.A., Rayment, I., and Escalante-Semerena, J.C. (2008) Construction and use of new cloning vectors for the rapid isolation of recombinant proteins from *Escherichia coli*. *Plasmid* **59**: 231–237.

Rossez, Y., Wolfson, E.B., Holmes, A., Gally, D.L., and Holden, N.J. (2015) Bacterial flagella: twist and stick, or dodge across the kingdoms. *PLoS Pathog* **11**: e1004483.

Ruiz-Albert, J., Yu, X.-J., Beuzón, C.R., Blakey, A.N., Galyov, E.E., and Holden, D.W. (2002) Complementary activities of SseJ and SifA regulate dynamics of the *Salmonella typhimurium* vacuolar membrane. *Mol Microbiol* **44**: 645–661.

Rydstrom, A., and Wick, M.J. (2007) Monocyte recruitment, activation, and function in the gut-associated lymphoid tissue during oral *Salmonella* infection. *J Immunol* **178**: 5789–5801.

Saini, S., Brown, J.D., Aldridge, P.D., and Rao, C.V. (2008) FliZ is a posttranslational activator of $FlhD_4C_2$-dependent flagellar gene expression. *J Bacteriol* **190**: 4979–4988.

Saini, S., Ellermeier, J.R., Slauch, J.M., and Rao, C.V. (2010a) The role of coupled positive feedback in the expression of the SPI1 type three secretion system in *Salmonella*. *PLoS Pathog* **6**: e1001025.

Saini, S., Koirala, S., Floess, E., Mears, P.J., Chemla, Y.R., Golding, I., Aldridge, C., Aldridge, P.D., and Rao, C.V. (2010b) FliZ induces a kinetic switch in flagellar gene expression. *J Bacteriol* **192**: 6477–6481.

Saini, S., Slauch, J.M., Aldridge, P.D., and Rao, C.V. (2010c) Role of cross talk in regulating the dynamic expression of the flagellar *Salmonella* pathogenicity island 1 and type 1 fimbrial genes. *J Bacteriol* **192**: 5767–5777.

Salscheider, S.L., Jahn, A., and Schnetz, K. (2014) Transcriptional regulation by BglJ-RcsB, a pleiotropic heteromeric activator in *Escherichia coli*. *Nucleic Acids Res* **42**: 2999–3008.

Samatey, F.A., Matsunami, H., Imada, K., Nagashima, S., Shaikh, T.R., Thomas, D.R., Chen, J.Z., DeRosier, D.J., Kitao, A., and Namba, K. (2004) Structure of the bacterial flagellar hook and implication for the molecular universal joint mechanism. *Nature* **431**: 1062–1068.

Sanderson, K.E., and Roth, J.R. (1988) Linkage map of *Salmonella typhimurium*, Edition VII. *Microbiol Rev* **52**: 485–532.

Sano, G.-I., Takada, Y., Goto, S., Maruyama, K., Shindo, Y., Oka, K., Matsui, H., and Matsuo, K. (2007) Flagella facilitate escape of *Salmonella* from oncotic macrophages. *J Bacteriol* **189**: 8224–8232.

Sansonetti, P. (2002) Host-pathogen interactions: the seduction of molecular cross talk. *Gut* **50**: iii2–iii8.

Sato, Y., Takaya, A., Mouslim, C., Hughes, K.T., and Yamamoto, T. (2014) FliT selectively enhances proteolysis of FlhC subunit in $FlhD_4C_2$ complex by an ATP-dependent protease, ClpXP. *J Biol Chem* **289**: 33001–33011.

Schechter, L.M., and Lee, C.A. (2001) AraC/XylS family members, HilC and HilD, directly bind and derepress the *Salmonella typhimurium hilA* promoter. *Mol Microbiol* **40**: 1289–1299.

Schleif, R. (2010) AraC protein, regulation of the L-arabinose operon in *Escherichia coli*, and the light switch mechanism of AraC action. *FEMS Microbiol Rev* **34**: 779–796.

Schultz, M. (2008) Theobald Smith. *Emerging Infectious Diseases* **14**: 1940–1942.

Schuster, F. (2015) Underlying principles of bistability in the expression of the pivotal virulence regulator RovA of *Yersinia pseudotuberculosis* and its role for virulence. Technische Universität Carolo-Wilhelmina Braunschweig.

Singer, H.M., Erhardt, M., and Hughes, K.T. (2013) RflM functions as a transcriptional repressor on the autogenous control of the *Salmonella* flagellar master operon *flhDC*. *J Bacteriol* **195**: 4274–5382.

Singer, H.M., Kühne, C., Deditius, J.A., Hughes, K.T., and Erhardt, M. (2014) The *Salmonella* Spi1 virulence regulatory protein HilD directly activates transcription of the flagellar master operon *flhDC*. *J Bacteriol* **196**: 1448–1457.

Sledjeski, D.D., and Gottesman, S. (1996) Osmotic shock induction of capsule synthesis in *Escherichia coli* K-12. *J Bacteriol* **178**: 1204–1206.

Smith, C., Stringer, A.M., Mao, C., Palumbo, M.J., and Wade, J.T. (2016) Mapping the regulatory network for *Salmonella enterica* serovar Typhimurium invasion. *MBio* **7**: e01024-16.

Stecher, B., Barthel, M., Schlumberger, M.C., Haberli, L., Rabsch, W., Kremer, M., and Hardt, W.-D. (2008) Motility allows *S*. Typhimurium to benefit from the mucosal defence. *Cell Microbiol* **10**: 1166–1180.

Stecher, B., Robbiani, R., Walker, A.W., Westendorf, A.M., Barthel, M., Kremer, M., Chaffron, S., Macpherson, A.J., Buer, J., Parkhill, J., Dougan, G., von Mering, C., and Hardt, W.-D. (2007) *Salmonella enterica* serovar Typhimurium exploits inflammation to compete with the intestinal microbiota. *PLoS Biol* **5**: 2177–2189.

Steele-Mortimer, O. (2008) The *Salmonella*-containing vacuole: moving with the times. *Curr Opin Microbiol* **11**: 38–45.

Stewart, M.K., and Cookson, B.T. (2014) Mutually repressing repressor functions and multi-layered cellular heterogeneity regulate the bistable *Salmonella fliC* census. *Mol Microbiol* **94**: 1272–1284.

Stewart, M.K., Cummings, L.A., Johnson, M.L., Berezow, A.B., and Cookson, B.T. (2011) Regulation of phenotypic heterogeneity permits *Salmonella* evasion of the host caspase-1 inflammatory response. *Proc Natl Acad Sci USA* **108**: 20742–20747.

Stout, V., and Gottesman, S. (1990) RcsB and RcsC: a two-component regulator of capsule synthesis in *Escherichia coli*. *J Bacteriol* **172**: 659–669.

Stout, V., Torres-Cabassa, A., Maurizi, M.R., Gutnick, D., and Gottesman, S. (1991) RcsA, an unstable positive regulator of capsular polysaccharide synthesis. *J Bacteriol* **173**: 1738–1747.

Stratmann, T., Pul, Ü., Wurm, R., Wagner, R., and Schnetz, K. (2012) RcsB-BglJ activates the *Escherichia coli leuO* gene, encoding an H-NS antagonist and pleiotropic regulator of virulence determinants. *Mol Microbiol* **83**: 1109–1123.

Sturm, A., Heinemann, M., Arnoldini, M., Benecke, A., Ackermann, M., Benz, M., Dormann, J., and Hardt, W.-D. (2011) The cost of virulence: retarded growth of *Salmonella typhimurium* cells expressing type III secretion system 1. *PLoS Pathog* **7**: e1002143.

Su, L.-H., and Chiu, C.-H. (2007) *Salmonella*: clinical importance and evolution of nomenclature. *Chang Gung Med J* **30**: 210–219.

Takaya, A., Erhardt, M., Karata, K., Winterberg, K., Yamamoto, T., and Hughes, K.T. (2012) YdiV: a dual function protein that targets FlhDC for ClpXP-dependent degradation by promoting release of DNA-bound FlhDC complex. *Mol Microbiol* **83**: 1268–1284.

Takaya, A., Kubota, Y., Isogai, E., and Yamamoto, T. (2005) Degradation of the HilC and HilD regulator proteins by ATP-dependent Lon protease leads to downregulation of *Salmonella* pathogenicity island 1 gene expression. *Mol Microbiol* **55**: 839–852.

Takaya, A., Matsui, M., Tomoyasu, T., Kaya, M., and Yamamoto, T. (2006) The DnaK chaperone machinery converts the native $FlhD_2C_2$ hetero-tetramer into a functional transcriptional regulator of flagellar regulon expression in *Salmonella*. *Mol Microbiol* **59**: 1327–1340.

Takeda, S., Fujisawa, Y., Matsubara, M., Aiba, H., and Mizuno, T. (2001) A novel feature of the multistep phosphorelay in *Escherichia coli*: a revised model of the RcsC → YojN → RcsB signalling pathway implicated in capsular synthesis and swarming behaviour. *Mol Microbiol* **40**: 440–450.

Teixidó, L., Carrasco, B., Alonso, J.C., Barbé, J., and Campoy, S. (2011) Fur activates the expression of *Salmonella enterica* pathogenicity island 1 by directly interacting with the *hilD* operator *in vivo* and *in vitro*. *PLos ONE* **6**: e19711.

Teplitski, M., Goodier, R.I., and Ahmer, B.M.M. (2003) Pathways leading from BarA/SirA to motility and virulence gene expression in *Salmonella*. *J Bacteriol* **185**: 7257–7265.

Thijs, I.M., De Keersmaecker, S.C., Fadda, A., Kristof, E., Zhao, H., McClelland, M., Marchal, K., and Vanderleyden, J. (2007) Delineation of the *Salmonella enterica* serovar Typhimurium HilA regulon through genome-wide location and transcript analysis. *J Bacteriol* **189**: 4587–4596.

Toker, A.S., and Macnab, R.M. (1997) Distinct regions of bacterial flagellar switch protein FliM interact with FliG, FliN and CheY. *J Mol Biol* **273**: 623–634.

Torres-Cabassa, A.S., and Gottesman, S. (1987) Capsule synthesis in *Escherichia coli* K-12 is regulated by proteolysis. *J Bacteriol* **169**: 981–989.

Troxell, B., Sikes, M.L., Fink, R.C., Vazquez-Torres, A., Jones-Carson, J., and Hassan, H.M. (2011) Fur negatively regulates *hns* and is required for the expression of HilA and virulence in *Salmonella enterica* serovar Typhimurium. *J Bacteriol* **193**: 497–505.

Uchiya, K., Barbieri, M.A., Funato, K., Shah, A.H., Stahl, P.D., and Groisman, E.A. (1999) A *Salmonella* virulence protein that inhibits cellular trafficking. *EMBO J* **18**: 3924–3933.

Uchiya, K.-I., Sugita, A., and Nikai, T. (2009) Involvement of SPI-2-encoded SpiC in flagellum synthesis in *Salmonella enterica* serovar Typhimurium. *BMC Microbiol* **9**: 179.

Uchiya, K.I., and Nikai, T. (2008) *Salmonella* virulence factor SpiC is involved in expression of flagellin protein and mediates activation of the signal transduction pathways in macrophages. *Microbiology* **154**: 3491–3502.

Untergasser, A., Nijveen, H., Rao, X., Bisseling, T., Geurts, R., and Leunissen, J.A.M. (2007) Primer3Plus, an enhanced web interface to Primer3. *Nucleic Acids Res* **35**: W71–74.

Uzzau, S., Figueroa-Bossi, N., Rubino, S., and Bossi, L. (2001) Epitope tagging of chromosomal genes in *Salmonella*. *Proc Natl Acad Sci USA* **98**: 15264–15269.

van Gestel, J., Vlamakis, H., and Kolter, R. (2015) Division of labor in biofilms: the ecology of cell differentiation. *Microbiol Spectr* **3**: MB–0002–2014.

Vandesompele, J., De Preter, K., Pattyn, F., Poppe, B., Van Roy, N., De Paepe, A., and Speleman, F. (2002) Accurate normalization of real-time quantitative RT-PCR data by geometric averaging of multiple internal control genes. *Genome Biol* **3**: research0034.1–0034.11.

Veening, J.-W., Smits, W.K., and Kuipers, O.P. (2008a) Bistability, epigenetics, and bet-hedging in bacteria. *Annu Rev Microbiol* **62**: 193–210.

Veening, J.-W., Stewart, E.J., Berngruber, T.W., Taddei, F., Kuipers, O.P., and Hamoen, L.W. (2008b) Bet-hedging and epigenetic inheritance in bacterial cell development. *Proc Natl Acad Sci USA* **105**: 4393–4398.

Venkatesh, G.R., Kembou Koungni, F.C., Paukner, A., Stratmann, T., Blissenbach, B., and Schnetz, K. (2010) BglJ-RcsB heterodimers relieve repression of the *Escherichia coli bgl* operon by H-NS. *J Bacteriol* **192**: 6456–6464.

Vijay-Kumar, M., Wu, H., Jones, R., Grant, G., Babbin, B., King, T.P., Kelly, D., Gewirtz, A.T., and Neish, A.S. (2006) Flagellin suppresses epithelial apoptosis and limits disease during enteric infection. *Am J Pathol* **169**: 1686–1700.

Virlogeux, I., Waxin, H., Ecobichon, C., Lee, J.O., and Popoff, M.Y. (1996) Characterization of the *rcsA* and *rcsB* genes from *Salmonella typhi*: *rcsB* through *tviA* is involved in regulation of Vi antigen synthesis. *J Bacteriol* **178**: 1691–1698.

Wada, T., Morizane, T., Abo, T., Tominaga, A., Inoue-Tanaka, K., and Kutsukake, K. (2011) EAL domain protein YdiV acts as an anti-$FlhD_4C_2$ factor responsible for nutritional control of the flagellar regulon in *Salmonella enterica* serovar Typhimurium. *J Bacteriol* **193**: 1600–1611.

Wada, T., Tanabe, Y., and Kutsukake, K. (2011) FliZ acts as a repressor of the *ydiV* gene, which encodes an anti-$FlhD_4C_2$ factor of the flagellar regulon in *Salmonella enterica* serovar Typhimurium. *J Bacteriol* **193**: 5191–5198.

Wagner, C., Barlag, B., Gerlach, R.G., Deiwick, J., and Hensel, M. (2014) The *Salmonella enterica* giant adhesin SiiE binds to polarized epithelial cells in a lectin-like manner. *Cell Microbiol* **16**: 962–975.

Walthers, D., Carroll, R.K., Navarre, W.W., Libby, S.J., Fang, F.C., and Kenney, L.J. (2007) The response regulator SsrB activates expression of diverse *Salmonella* pathogenicity island 2 promoters and counters silencing by the nucleoid-associated protein H-NS. *Mol Microbiol* **65**: 477–493.

Wang, H., Liu, B., Wang, Q., and Wang, L. (2013) Genome-wide analysis of the *Salmonella* Fis regulon and its regulatory mechanism on pathogenicity islands. *PLos ONE* **8**: e64688.

Wang, Q., and Harshey, R.M. (2009) Rcs signalling-activated transcription of *rcsA* induces strong anti-sense transcription of upstream *fliPQR* flagellar genes from a weak intergenic promoter: regulatory roles for the anti-sense transcript in virulence and motility. *Mol Microbiol* **74**: 71–84.

Wang, Q., Zhao, Y., McClelland, M., and Harshey, R.M. (2007) The RcsCDB signaling system and swarming motility in *Salmonella enterica* serovar Typhimurium: dual regulation of flagellar and SPI-2 virulence genes. *J Bacteriol* **189**: 8447–8457.

Wang, S., Fleming, R.T., Westbrook, E.M., Matsumura, P., and McKay, D.B. (2006) Structure of the *Escherichia coli* FlhDC complex, a prokaryotic heteromeric regulator of transcription. *J Mol Biol* **355**: 798–808.

Wang, Y., Prosen, D.E., Mei, L., Sullivan, J.C., Finney, M., and Vander Horn, P.B. (2004) A novel strategy to engineer DNA polymerases for enhanced processivity and improved performance *in vitro*. *Nucleic Acids Res* **32**: 1197–1207.

Waterman, S.R., and Holden, D.W. (2003) Functions and effectors of the *Salmonella* pathogenicity island 2 type III secretion system. *Cell Microbiol* **5**: 501–511.

Wee, D.H., and Hughes, K.T. (2015) Molecular ruler determines needle length for the *Salmonella* Spi-1 injectisome. *Proc Natl Acad Sci USA* **112**: 4098–4103.

Weening, E.H., Barker, J.D., Laarakker, M.C., Humphries, A.D., Tsolis, R.M., and Bäumler, A.J. (2005) The *Salmonella enterica* serotype Typhimurium *lpf, bcf, stb, stc, std*, and *sth* fimbrial operons are required for intestinal persistence in mice. *Infect Immun* **73**: 3358–3366.

Wehland, M., and Bernhard, F. (2000) The RcsAB box. Characterization of a new operator essential for the regulation of exopolysaccharide biosynthesis in enteric bacteria. *J Biol Chem* **275**: 7013–7020.

Wiedemann, A., Virlogeux-Payant, I., Chaussé, A.-M., Schikora, A., and Velge, P. (2014) Interactions of *Salmonella* with animals and plants. *Front Microbiol* **5**: 791.

Williams, A.W., Yamaguchi, S., Togashi, F., Aizawa, S.I., Kawagishi, I., and Macnab, R.M. (1996) Mutations in *fliK* and *flhB* affecting flagellar hook and filament assembly in *Salmonella typhimurium*. *J Bacteriol* **178**: 2960–2970.

Wilmes-Riesenberg, M.R., Foster, J.W., and Curtiss, R. (1997) An altered *rpoS* allele contributes to the avirulence of *Salmonella typhimurium* LT2. *Infect Immun* **65**: 203–210.

Wilson, R.L., Libby, S.J., Freet, A.M., Boddicker, J.D., Fahlen, T.F., and Jones, B.D. (2001) Fis, a DNA nucleoid-associated protein, is involved in *Salmonella typhimurium* SPI-1 invasion gene expression. *Mol Microbiol* **39**: 79–88.

Winter, S.E., Winter, M.G., Thiennimitr, P., Gerriets, V.A., Nuccio, S.-P., Rüssmann, H., and Bäumler, A.J. (2009) The TviA auxiliary protein renders the *Salmonella enterica* serotype Typhi RcsB regulon responsive to changes in osmolarity. *Mol Microbiol* **74**: 175–193.

Wood, T.K., González Barrios, A.F., Herzberg, M., and Lee, J. (2006) Motility influences biofilm architecture in *Escherichia coli*. *Appl Microbiol Biotechnol* **72**: 361–367.

Wozniak, C.E., Lee, C., and Hughes, K.T. (2009) T-POP array identifies EcnR and PefI-SrgD as novel regulators of flagellar gene expression. *J Bacteriol* **191**: 1498–508.

Yamamoto, S., and Kutsukake, K. (2006a) FljA-mediated post-transcriptional control of phase 1 flagellin expression in flagellar phase variation of *Salmonella enterica* serovar Typhimurium. *J Bacteriol* **188**: 958–967.

Yamamoto, S., and Kutsukake, K. (2006b) FliT acts as an anti-$FlhD_4C_2$ factor in the transcriptional control of the flagellar regulon in *Salmonella enterica* serovar Typhimurium. *J Bacteriol* **188**: 6703–6708.

Yanagihara, S., Iyoda, S., Ohnishi, K., Iiono, T., and Kutsukake, K. (1999) Structure and transcriptional control of the flagellar master operon of *Salmonella typhimurium*. *Genes Genet Syst* **74**: 105–111.

Yang, X., Thornburg, T., Suo, Z., Jun, S., Robison, A., Li, J., Lim, T., Cao, L., Hoyt, T., Avci, R., and Pascual, D.W. (2012) Flagella overexpression attenuates *Salmonella* pathogenesis. *PLos ONE* **7**: e46828.

Yonekura, K., Maki-Yonekura, S., and Namba, K. (2003) Complete atomic model of the bacterial flagellar filament by electron cryomicroscopy. *Nature* **424**: 643–650.

Zhang, X., and Bremer, H. (1995) Control of the *Escherichia coli rrnB* P1 promoter strength by ppGpp. *J Biol Chem* **270**: 11181–11189.

Zhao, Y., Yang, J., Shi, J., Gong, Y.-N., Lu, Q., Xu, H., Liu, L., and Shao, F. (2011) The NLRC4 inflammasome receptors for bacterial flagellin and type III secretion apparatus. *Nature* **477**: 596–600.

Zhou, D., Mooseker, M.S., and Galán, J.E. (1999) Role of the *S. typhimurium* actin-binding protein SipA in bacterial internalization. *Science* **283**: 2092–2095.

Supplemental Material

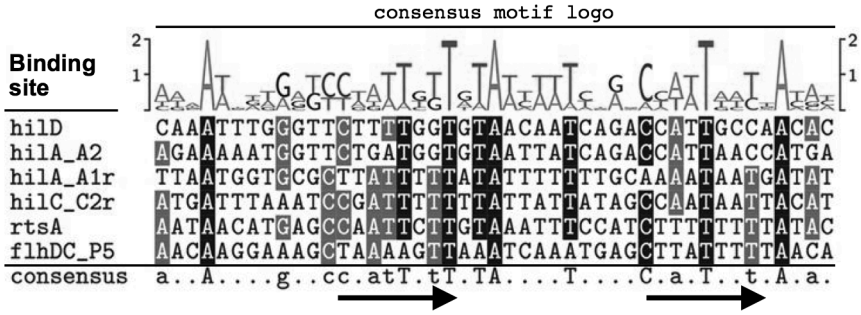

Fig. S1 Alignment of HilD bindings sites in target promoters.
Multiple sequence alignment of experimentally validated HilD binding sites in the *hilD, hilA, hilC, rtsA,* and *flhDC* promoters according to previous studies (Olekhnovich and Kadner, 2002; Olekhnovich and Kadner, 2007) and this thesis. The consensus sequence is shown as motif logo on top and below the binding sites. Predominant nucleotides (> 80 % conserved) are highlighted in black and shown in uppercase letters. Conserved nucleotides (> 60 % conserved) are highlighted in gray and shown in lowercase letters. Arrows indicate the two imperfect direct repeats with CNATTNTT. Figure modified from Singer, Kühne *et al.*, 2014 with permission from ASM.

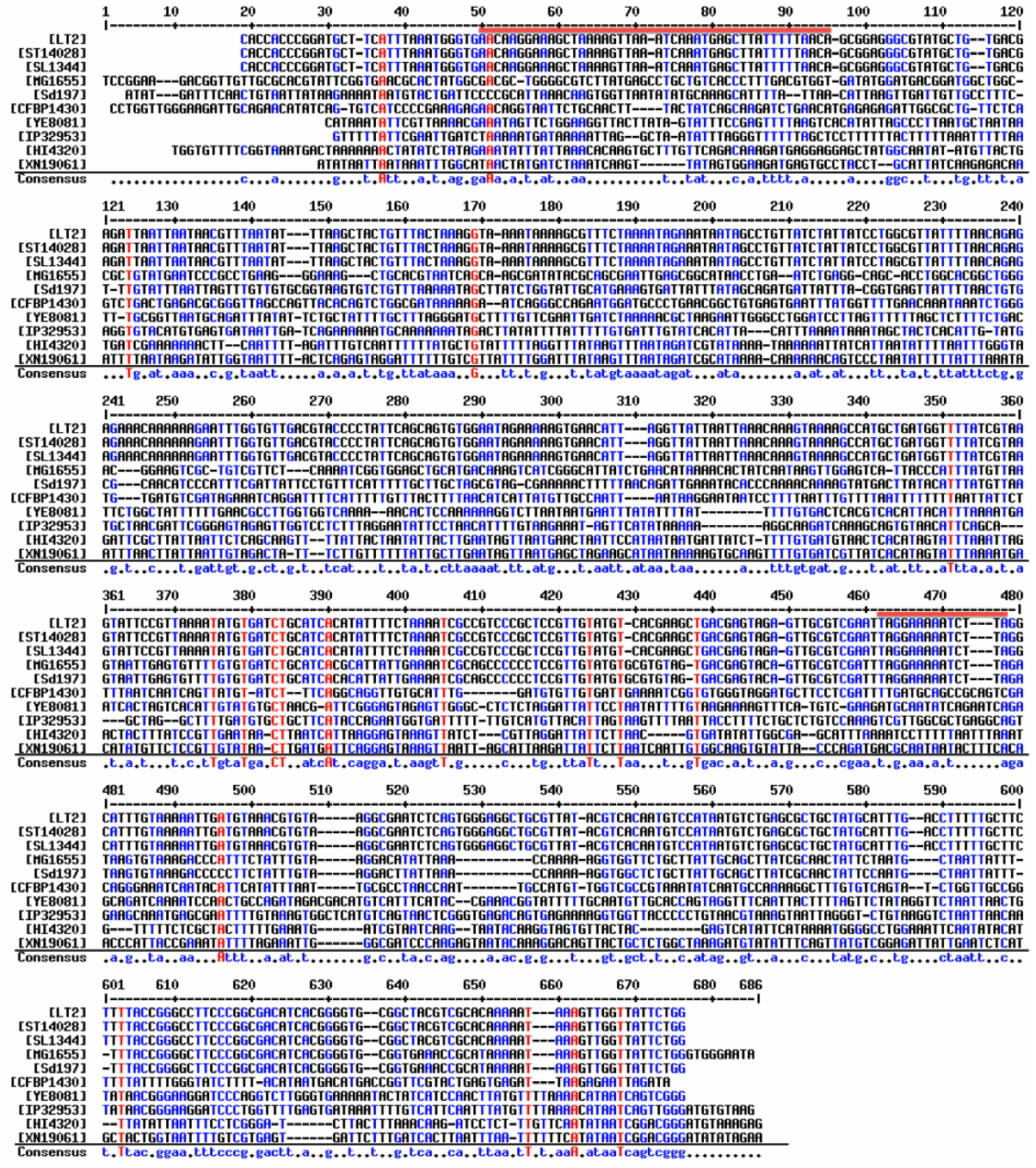

Fig. S2 Multiple sequence alignment of the *flhDC* promoter region.
The *flhDC* promoter sequences upstream of the *flhD* start codon (628 nucleotides) were taken from the nucleotide database from the National Center for Biotechnology Information (NBCI) and compared by multiple sequence alignment using MultAlin (Corpet, 1988). Following Enterobacteriaceae species with strain specifications in brackets were analyzed: *S.* Typhimurium (LT2, ST14028, and SL1344), *E. coli* (MG1655), *Shigella dysenteriae* (Sd197), *Erwinia amylovora* (CFBP1430), *Yersinia enterocolitica* (YE8081), *Yersinia pseudotuberculosis* (IP32953), *Proteus mirabilis* (HI4320), and *Xenorhabdus nematophila* (XN19061). Homologous sequences are highlighted in color (red > 90 % homolog; blue > 50 % homolog) and the consensus sequence is shown below. Horizontal red bars above the LT2 sequence indicate the HilD binding site (nucleotides 598–554 upstream of the *flhD* start codon) and the RcsB/RflM binding site (nucleotides 202–177 upstream of the *flhD* start codon).

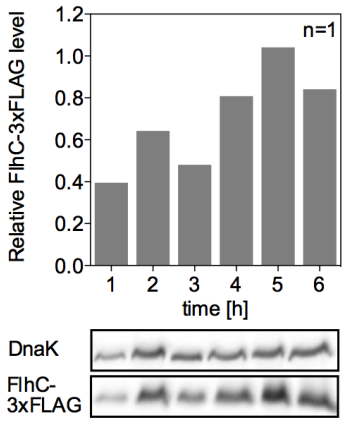

Fig. S3 FlhC protein levels reflect the growth phase-dependent P$_{flhDC}$-*egfp*$_{LVA}$ expression profile.
Protein levels of chromosomal, epitope-tagged FlhC-3xFLAG were determined 1–6 h post inoculation from a batch culture of ST14028 harboring pKH70-P$_{flhDC}$-*egfp*$_{LVA}$. Top: FlhC-3xFLAG levels are shown relative to the corresponding DnaK control and bars represent initial results from one biological replicate. Bottom: Western-blots of DnaK and FlhC-3xFLAG protein levels. It is important to note that the employed C-terminal, 3xFLAG-tagged version of FlhC is non-motile and presumably unfunctional.

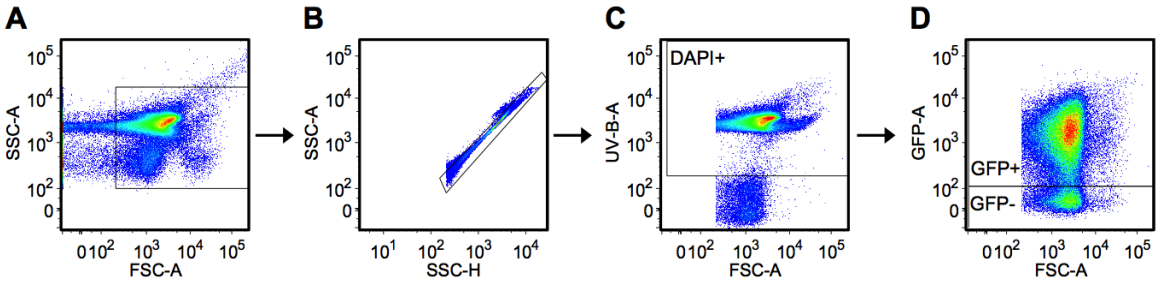

Fig. S4 Gating strategy for flow cytometry analyses of bacteria.
Bacterial samples that have been recorded by flow cytometry as described in Material and Methods (see Chapter 6.6.9) were further processed using the software FlowJo V9.8. **(A)** First, cells were gated according to their size and granularity using FSC-A and SSC-A, respectively. **(B)** Next, doublets were excluded (SSC-H vs. SSC-A), followed by **(C)** gating of DAPI-positive cells (DAPI+) according to UV-B signals, which enabled an exact identification of bacterial cells. **(D)** Finally, eGFP$_{LVA}$-positive (GFP+) and eGFP$_{LVA}$-negative (GFP-) cells were gated according to their fluorescence intensities. **(C+D)** Gates were applied according to positive and negative controls and are shown as gray boxes.

Declaration of Author Contributions

Kühne C., Singer H. M., Grabisch E., Codutti L., Carlomagno T., Scrima A., and Erhardt M. (2016): RflM mediates target specificity of the RcsCDB phosphorelay system for transcriptional repression of flagellar synthesis in *Salmonella enterica*. In: *Molecular Microbiology* vol. 101(5) pp. 841–855, doi: 10.1111/mmi.13427.

I wrote the paper and contributed to the experimental design. I performed all experiments and analyzed all data except the following. T-POP transposon mutagenesis and expression studies of *rflM* and *rcsB* were done by HMS. Bacterial-two-hybrid assays were done by ME. The cooperativity of RcsB and RflM in repression of *flhDC* was analyzed by EG under my supervision. For SEC-MALS analyses, I prepared the protein samples and performed the experiment together with LC at the Centre for Biomolecular Drug Research in the group of TC. SEC-MALS data were analyzed by LC. Overall, experiments were designed and supervised by ME, LC (only SEC-MALS), and AS (only MST). Editorial changes of the paper were done by ME and LC (only SEC-MALS parts).

Singer H. M., **Kühne C.**, Deditius J. A., Hughes K. T., and Erhardt M. (2014): The *Salmonella* Spi1 virulence regulatory protein HilD directly activates transcription of the flagellar master operon *flhDC*. In: *Journal of Bacteriology* vol. 196(7) pp. 1448-1457, doi: 10.1128/JB.01438-13.

I wrote the figure legends and Materials and Methods sections of the paper concerning HilD protein purification, EMSA, and DNaseI footprinting. I contributed to the experimental design, performed experiments and analyzed data regarding effects of HilA on flagellar gene expression, dominant effects of RtsB and HilD on *flhDC* expression, HilD protein purification, EMSAs and DNaseI footprinting. JAD contributed to experimental design, performed experiments, analyzed data and wrote the figure legends regarding effects of HilD and its DNA-binding domain on flagellar gene expression. The residual parts of the paper were designed, performed, analyzed and written by HMS. Overall, experiments were designed and supervised by KTH and ME. Editorial changes of the paper were done by KTH and ME.

Danksagung

Mein größter Dank gilt Dr. Marc Erhardt für die Möglichkeit, meine Arbeit über dieses sehr interessante Thema in seiner Nachwuchsforschungsgruppe „Infektionsbiologie von Salmonellen“ am Helmholtz-Zentrum für Infektionsforschung anzufertigen. Danke für die gute Betreuung, die vielen konstruktiven und motivierenden Gespräche, das Vertrauen in meine Arbeit und die Unterstützung in vielerlei Hinsicht.

Gleichzeitig danke ich meiner Mentorin Prof. Dr. Petra Dersch für die Übernahme des Hauptreferates, die Teilnahme an meinem Thesis Committee und die konstruktiven Diskussionen in den Meetings.

Prof. Dr. Susanne Engelmann danke ich für die Übernahme des Koreferates und die damit verbundene Begutachtung meiner Dissertation. Zudem danke ich Prof. Dr. Michael Hust für die Übernahme des Prüfungsvorsitzes.

Weiterhin danke ich Prof. Dr. Emmanuelle Charpentier für die Teilnahme an meinem Thesis Committee.

Der „HZI International Graduate School for Infection Research“ danke ich für die Finanzierung der Teilnahme an Weiterbildungen, externen Forschungsaufenthalten und Konferenzen im In- und Ausland.

Darüber hinaus danke ich allen internen und externen Kooperationspartnern. Dr. Andrea Scrima danke ich für die Bereitstellung des MST Messgerätes und die Unterstützung bei den MST Versuchen. Ich danke Ass. Prof. Dr. Calin Guet und Dr. Tobias Bergmiller vom Institute of Science and Technology Austria für meinen einwöchigen Forschungsaufenthalt und die dabei entstandenen fluoreszenzmikroskopischen Aufnahmen. Dr. Luca Codutti danke ich für die tatkräftige Unterstützung bei den SEC-MALS-Versuchen am Biomolekularen Wirkstoffzentrum Hannover.

Ein großer Dank geht an alle derzeitigen und ehemaligen Mitglieder der IBIS Gruppe für die großartige Unterstützung, die tolle Arbeitsatmosphäre sowie für die schönen Momente auch außerhalb der Arbeitszeit, insbesondere an Imke Spöring, Julia Horstmann, Florian Fabiani, Nadine Körner und Eva Grabisch. Zudem danke ich Dr. Hanna Singer für ihre Arbeit, auf der Teile meiner Dissertation erst aufbauen konnten.

Ebenfalls danken möchte ich der MIBI Gruppe für die schöne Zeit, die konstruktiven Diskussionen in den Meetings und für die jederzeit offenen Türen bei Fragen und Problemen, insbesondere Dr. Franziska Schuster in Bezug auf meine Footprint- und Durchflusszytometrie-Versuche. Darüber hinaus danke ich Dr. Hagen Richter für die Einweisung an der Äkta.

Meiner Familie danke ich von ganzem Herzen für die bedingungslose Unterstützung und den Glauben an mich und meine Fähigkeiten. Danke, dass ich immer auf euch zählen kann, ihr mir Rückhalt gebt und immer für mich da seid.